

Electropolishing in Deep Eutectic Solvents

Thesis submitted for the degree of

Doctor of Philosophy

At the University of Leicester

By

Saima Saleem

Department of Chemistry

University of Leicester

December 2012



Electropolishing in Deep Eutectic Solvents

Saima Saleem

University of Leicester

2012

Abstract

A fundamental study of electropolishing of stainless steel and nickel based single crystal superalloy CMSX-4 in type III deep eutectic solvent based on choline chloride and hydrogen bond donor i.e. mixture of choline chloride with ethylene glycol in a 1:2 molar ratio was carried out and had been found to be competitive with the current concentrated mixture of inorganic acid electrolytes.

Life cycle study was conducted to define the key process controlling factors like electrochemical stability, current efficiency, effect of history of electrolyte, recycling of ionic liquid and its reuse for electropolishing. The electrochemical techniques like linear sweep anodizing curves, chronoamperometry and galvanostatic studies revealed that electropolishing in 1:2 ChCl:EG proceeded through the formation of viscous layer on the surface of the substrate similar to electropolishing in inorganic acid electrolytes. The optimization of electropolishing process was carried out using the experimental design strategies, Fractional Factorial Design (FFD) and found that electropolishing variables like addition of water, oxalic acid, electropolishing bath temperature, time and potential had positive impact on the surface finish.

Surface texture measurements such as surface roughness and surface overlayer morphology of electropolished stainless steel and CMSX-4 was carried out using the microscopic techniques, atomic force microscopy (AFM), scanning electron microscopy (SEM), field emission scanning electron microscopy (FE-SEM) and digital holographic microscopy (DHM) and found to be the function of electropolishing time. Effect of electropolishing on corrosion behaviour of stainless steel was studied using the electrochemical techniques like open circuit potential measurements (OCP), potentiodynamic polarization curves and gravimetric method showed improvement in the general or pitting corrosion of the workpiece. Nickel based superalloy was also successfully electropolished to remove the casting scales. The dissolution of two phases was found to be the function of electrochemical regime i.e. applied potential and current density.

Acknowledgement

I would like to express my gratitude to a few people who helped me all the way through my studies and made this dissertation possible. Firstly I am extremely thankful to my supervisor Dr. Karl Ryder whose encouragement, support, guidance, useful comments, flexibility of working, patience with the timelines always gave me strength and enthusiasm to work. I feel myself really lucky and blessed to have him as my supervisor.

I am also thankful to Prof. Andrew P. Abbott for his insightful feedback and comments during the group presentations which helped me a lot to improve my work and understand different concepts.

I would also like to thank all the Scionix lab group members, past and present who were always there to help me at any stage of my studies where I found any difficulty.

Lastly I am grateful to my family members especially my parents and my son whose patience gave me strength to work with a peaceful mind. I am extremely grateful to my husband as well without whose support, love and help, this would have never been possible.

Table of Contents

| | |
|--|----------|
| Abstract | ii |
| Acknowledgement | iii |
| Table of Contents | iv |
| List of Abbreviations | ix |
| | |
| Chapter 1 : New system for electrolytic surface finishing | 1 |
| 1.1 Surface finishing techniques | 2 |
| 1.2 Metal finishing processes | 3 |
| 1.2.1 <i>Mechanical surface finishing processes</i> | 3 |
| 1.2.2 <i>Non-mechanical surface finishing processes</i> | 4 |
| 1.2.3 <i>Electropolishing vs. mechanical polishing</i> | 5 |
| 1.2.4 <i>Characteristics of electropolished surface</i> | 5 |
| 1.2.5 <i>Applications of electropolishing process</i> | 6 |
| 1.3 New system for electropolishing | 8 |
| 1.4 Ionic liquids | 9 |
| 1.5 Ionic liquids and future electrochemical challenges | 10 |
| 1.5.1 <i>Electrodeposition</i> | 11 |
| 1.5.1.1 <i>Water sensitive metals</i> | 11 |
| 1.5.1.2 <i>Deposition of reactive metals</i> | 13 |
| 1.5.1.3 <i>Nanoparticles</i> | 13 |
| 1.5.1.4 <i>Nanowires</i> | 14 |
| 1.5.1.5 <i>Semiconductors</i> | 15 |
| 1.5.2 <i>Energy Management</i> | 17 |
| 1.5.3 <i>Biomechanics</i> | 18 |
| 1.5.4 <i>Biosensing</i> | 20 |
| 1.6 Metal finishing in eutectic based ionic liquids | 21 |
| 1.6.1 <i>Electroplating of Chromium</i> | 22 |
| 1.6.2 <i>Electrodeposition of Zinc and its alloys</i> | 23 |
| 1.6.3 <i>Deposition of other metals and alloys</i> | 24 |
| 1.6.4 <i>Electroless deposition of metals</i> | 25 |
| 1.6.5 <i>Electropolishing in deep eutectic solvents</i> | 25 |
| 1.7 Summary | 28 |
| 1.8 References | 29 |

| | | |
|--------------------|--|-----------|
| Chapter 2 : | Experimental Procedures | 36 |
| 2.1 | Materials | 37 |
| 2.2 | Stainless steel samples | 37 |
| 2.3 | Preparation of solutions | 38 |
| | 2.3.1 <i>Deep Eutectic solvents</i> | 38 |
| | 2.3.2 <i>Oxalic acid solution</i> | 38 |
| 2.4 | Physical properties | 38 |
| | 2.4.1 <i>Viscosity measurements</i> | 38 |
| | 2.4.2 <i>Surface tension measurements</i> | 39 |
| | 2.4.3 <i>Density measurements</i> | 39 |
| | 2.4.4 <i>Conductivity measurements</i> | 39 |
| 2.5 | Electrochemical study | 39 |
| | 2.5.1 <i>Linear sweep polarization curves</i> | 39 |
| | 2.5.2 <i>Potential step experiments</i> | 40 |
| | 2.5.3 <i>Galvanostatic measurements</i> | 40 |
| | 2.5.4 <i>Electropolishing</i> | 40 |
| | 2.5.5 <i>Open circuit potential (OCP) measurements</i> | 40 |
| | 2.5.6 <i>Anodic polarization curves (corrosion curves)</i> | 41 |
| 2.6 | Surface analysis | 41 |
| | 2.6.1 <i>AFM</i> | 41 |
| | 2.6.2 <i>SEM and EDAX</i> | 41 |
| | 2.6.3 <i>DHM</i> | 41 |
| 2.7 | Analysis of Data | 42 |
| | 2.7.1 <i>Electrochemical data</i> | 42 |
| 2.8 | Scanning electron microscope (SEM) | 42 |
| | 2.8.1 <i>Working of SEM</i> | 42 |
| | 2.8.2 <i>Everhart thornley detector</i> | 43 |
| | 2.8.3 <i>X-rays detectors</i> | 44 |
| 2.9 | Atomic force microscope (AFM) | 45 |
| | 2.9.1 <i>Modes of operation</i> | 46 |
| 2.10 | Digital holographic microscope (DHM) | 47 |
| | 2.10.1 <i>Working of DHM</i> | 49 |
| | 2.10.2 <i>Reconstruction of hologram</i> | 50 |
| | 2.10.3 <i>Phase images</i> | 50 |
| 2.11 | References | 51 |
| Chapter 3 : | Electropolishing of Austenitic Steel in Deep Eutectic Solvent | 52 |
| 3.1 | Introduction | 53 |

| | | |
|-------------------------------|---|----|
| 3.1.1 | <i>Electropolishing</i> | 54 |
| | 3.1.1.1 <i>Electropolishing Process</i> | 54 |
| 3.1.2 | <i>Mechanism of Electropolishing</i> | 56 |
| | 3.1.2.1 <i>Duplex salt film model</i> | 56 |
| | 3.1.2.2 <i>Adsorbate acceptor mechanism</i> | 57 |
| | 3.1.2.3 <i>Preferential adsorption of shielding molecules</i> | 58 |
| Results and Discussion | | |
| 3.2 | Physical Properties of 1:2ChCl:EG | 61 |
| | 3.2.1 <i>Viscosity and conductivity</i> | 61 |
| | 3.2.2 <i>Surface tension</i> | 63 |
| 3.3 | Life Cycle Studies | 65 |
| | 3.3.1 <i>Drag out</i> | 65 |
| | 3.3.2 <i>Characteristics of electropolishing solution</i> | 66 |
| | 3.3.2.1 <i>Appearance of solution</i> | 67 |
| | 3.3.2.2 <i>Concentration of metal ions</i> | 68 |
| | 3.3.2.3 <i>De-alloying effect</i> | 69 |
| | 3.3.3 <i>Electrochemical Studies</i> | 71 |
| | 3.3.3.1 <i>Variation of potential and current</i> | 71 |
| | 3.3.3.2 <i>Weight loss</i> | 72 |
| | 3.3.4 <i>Recycling of liquid</i> | 73 |
| 3.4 | Electrochemistry | 75 |
| | 3.4.1 <i>Potentiodynamic study</i> | 75 |
| | 3.4.1.1 <i>Electrochemical window of 1:2 ChCl:EG</i> | 75 |
| | 3.4.1.2 <i>Anodic linear sweep voltammetry</i> | 76 |
| | 3.4.1.3 <i>Effect of scan rate</i> | 78 |
| | 3.4.1.4 <i>Effect of temperature</i> | 79 |
| | 3.4.1.5 <i>Effect of additives</i> | 80 |
| | 3.4.2 <i>Chronoamperometry</i> | 81 |
| | 3.4.2.1 <i>Effect of temperature</i> | 82 |
| | 3.4.2.2 <i>Effect of additives</i> | 84 |
| | 3.4.3 <i>Galvanostatic study</i> | 85 |
| 3.5 | Optimization of electropolishing process – Experimental design strategies | 86 |
| | 3.5.1 <i>Fractional Factorial Design (FFD)</i> | 88 |
| | 3.5.2 <i>Contour plot</i> | 94 |
| | 3.5.3 <i>The steepest ascent path</i> | 95 |
| 3.6 | Summary | 97 |
| 3.7 | References | 98 |

| | | |
|-------------------------------|---|------------|
| Chapter 4 : | Surface texture of Electropolished Stainless Steel | 102 |
| 4.1 | Introduction | 103 |
| | 4.1.1 <i>Types of stainless steel</i> | 107 |
| | 4.1.2 <i>Structure of stainless steel</i> | 108 |
| Results and Discussion | | |
| 4.2 | Nanostructuring of electropolished surface | 109 |
| 4.3 | Surface finish of electropolished surface | 112 |
| | 4.3.1 <i>Surface roughness</i> | 113 |
| | 4.3.1.1 <i>Surface roughness parameters</i> | 114 |
| | 4.3.2 <i>Surface roughness measurement</i> | 117 |
| | 4.3.2.1 <i>Profile (2D) measurements</i> | 118 |
| | 4.3.2.2 <i>Surface (3D) measurements</i> | 119 |
| | 4.3.3 <i>Effect of electropolishing time on surface roughness</i> | 120 |
| | 4.3.4 <i>Surface finish in recycled liquid</i> | 122 |
| | 4.3.5 <i>Amount of material etched</i> | 124 |
| | 4.3.6 <i>Surface roughness measurements by DHM</i> | 126 |
| 4.4 | Corrosion behaviour of austenitic steel | 128 |
| | 4.4.1 <i>Types of corrosion</i> | 129 |
| | 4.4.2 <i>Corrosion resistance measurements</i> | 129 |
| | 4.4.2.1 <i>Open circuit potential (OCP) measurements</i> | 130 |
| | 4.4.2.2 <i>Weight loss measurements</i> | 132 |
| | 4.4.2.3 <i>Potentiodynamic polarization curves</i> | 136 |
| 4.5 | Summary | 142 |
| 4.6 | References | 143 |
| | | |
| Chapter 5 : | Electrofinishing of nickel based superalloy | 145 |
| 5.1 | Introduction | 146 |
| | 5.1.1 <i>Superalloys</i> | 147 |
| | 5.1.2 <i>Nickel based superalloys</i> | 150 |
| | 5.1.2.1 <i>Microstructure of nickel based superalloys</i> | 151 |
| | 5.1.3 <i>Processing of superalloys</i> | 154 |
| | 5.1.4 <i>Applications of nickel based superalloys</i> | 156 |
| Results and Discussion | | |
| 5.2 | Surface morphology of CMSX-4 | 157 |
| | 5.2.1 <i>Topography of unpolished CMSX-4</i> | 157 |
| | 5.2.2 <i>Surface morphology of electropolished CMSX-4</i> | 158 |
| | 5.2.2.1 <i>Controlled potential electropolishing</i> | 159 |

| | | | |
|--------------------|---------|---|------------|
| | 5.2.2.2 | <i>Galvanostatically electropolishing</i> | 161 |
| 5.3 | | Surface roughness of electropolished CMSX-4 | 163 |
| | 5.3.1 | <i>Surface roughness of potentiostatically electropolished CMSX-4</i> | 164 |
| | 5.3.2 | <i>Surface roughness of galvanostatically electropolished CMSX-4</i> | 167 |
| 5.4 | | Material etch rate of CMSX-4 | 168 |
| | 5.4.1 | <i>Extended time scale electropolishing</i> | 169 |
| | 5.4.2 | <i>Anodic dissolution rate</i> | 171 |
| 5.5 | | Surface composition | 175 |
| 5.6 | | Summary | 177 |
| 5.7 | | References | 178 |
| Chapter 6 : | | | 179 |
| | | Summary and Future Directions | |
| 6.1 | | Summary | 180 |
| | 6.1.1 | <i>Electropolishing of austenitic steel in deep eutectic solvent</i> | 180 |
| | 6.1.2 | <i>Surface texture of electropolished stainless steel</i> | 181 |
| | 6.1.3 | <i>Electropolishing of nickel based superalloys</i> | 182 |
| 6.2 | | Future Directions | 182 |
| 6.3 | | References | 184 |

List of Abbreviations

| | |
|---|---|
| DES | Deep Eutectic Solvents |
| 1:2 ChCl:EG | 1:2 ChCl:Ethylene glycol / Ethaline |
| [C ₄ mim][PF ₆] | 1-butyl-3-methylimidazolium hexafluorophosphate |
| [C ₄ mim][BF ₄] | 1-butyl-3-methylimidazolium tetrafluoroborate |
| [C ₄ mim][OTf] | 1-butyl-3-methylimidazolium trifluoromethylsulfonate |
| [C ₄ mim][NO ₃] | 1-butyl-3-methylimidazolium nitrate |
| [C ₄ mim][Cl] | 1-butyl-3-methylimidazolium chloride |
| [C ₄ mim][H ₂ PO ₄] | 1-butyl-3-methylimidazolium dihydrogenphosphate |
| [C ₄ mim][CF ₃ CO ₂] | 1-butyl-3-methylimidazolium trifluoroacetate |
| [C ₄ mim][HSO ₄] | 1-butyl-3-methylimidazolium hydrogensulfate |
| [Bu ₄ N][NO ₃] | Bis(tetrabutylammonium) nitrate |
| [H _x ₃ (C ₁₄ H ₂₉)P][NO ₃] | Trihexyl(tetradecyl)phosphonium nitrate |
| [Py _{1,4}][Tf ₂ N] | 1-butyl-1-methylpyrrolidinium bis(trifluoromethylsulfonyl) amide |
| SEM | Scanning Electron Microscope |
| AFM | Atomic Force Microscope |
| DHM | Digital Holographic Microscope |
| EDX | Energy Dispersive X-ray |
| FE-SEM | Field Emission Scanning Electron Microscope |

| | | |
|--------------------|---|----------|
| Chapter 1 : | New system for electrolytic surface finishing | 1 |
| 1.1 | Surface finishing techniques | 2 |
| 1.2 | Metal finishing processes | 3 |
| | 1.2.1 <i>Mechanical surface finishing processes</i> | 3 |
| | 1.2.2 <i>Non-mechanical surface finishing processes</i> | 4 |
| | 1.2.3 <i>Electropolishing vs. mechanical polishing</i> | 5 |
| | 1.2.4 <i>Characteristics of electropolished surface</i> | 5 |
| | 1.2.5 <i>Applications of electropolishing process</i> | 6 |
| 1.3 | New system for electropolishing | 8 |
| 1.4 | Ionic liquids | 9 |
| 1.5 | Ionic liquids and future electrochemical challenges | 10 |
| | 1.5.1 <i>Electrodeposition</i> | 11 |
| | 1.5.1.1 <i>Water sensitive metals</i> | 11 |
| | 1.5.1.2 <i>Deposition of reactive metals</i> | 13 |
| | 1.5.1.3 <i>Nanoparticles</i> | 13 |
| | 1.5.1.4 <i>Nanowires</i> | 14 |
| | 1.5.1.5 <i>Semiconductors</i> | 15 |
| | 1.5.2 <i>Energy Management</i> | 17 |
| | 1.5.3 <i>Biomechanics</i> | 18 |
| | 1.5.4 <i>Biosensing</i> | 20 |
| 1.6 | Metal finishing in eutectic based ionic liquids | 21 |
| | 1.6.1 <i>Electroplating of Chromium</i> | 22 |
| | 1.6.2 <i>Electrodeposition of Zinc and its alloys</i> | 23 |
| | 1.6.3 <i>Deposition of other metals and alloys</i> | 24 |
| | 1.6.4 <i>Electroless deposition of metals</i> | 25 |
| | 1.6.5 <i>Electropolishing in deep eutectic solvents</i> | 25 |
| 1.7 | Summary | 28 |
| 1.8 | References | 29 |

Surface finishing is a process that alters the surface of a material either by applying a thin complementary layer to its surface or the removal of the surface layer for aesthetic or functional purposes. The material may be any material (a metal, a plastic, concrete and a ceramic) used for engineering or decorative purposes. Finishing processes may be employed to improve appearance, adhesion, wettability, solderability, corrosion resistance, tarnish resistance, chemical resistance, wear resistance, hardness, modify electrical conductivity, remove burrs and other surface flaws like faults in casting and control the surface friction¹.

1.1 Surface finishing techniques

Surface finishing dates back from stone ages (cutting edges and spear points by splintering stone) to today's modern world where not a single activity of mankind that does not include surface finishing ranging from daily uses to a sophisticated equipment. A variety of materials and processes are being used to create a workpiece with desired surface characteristics by either cleaning or etching the metallic and non metallic surfaces.

Figure 1.1 shows some of the processes used for surface finishing.

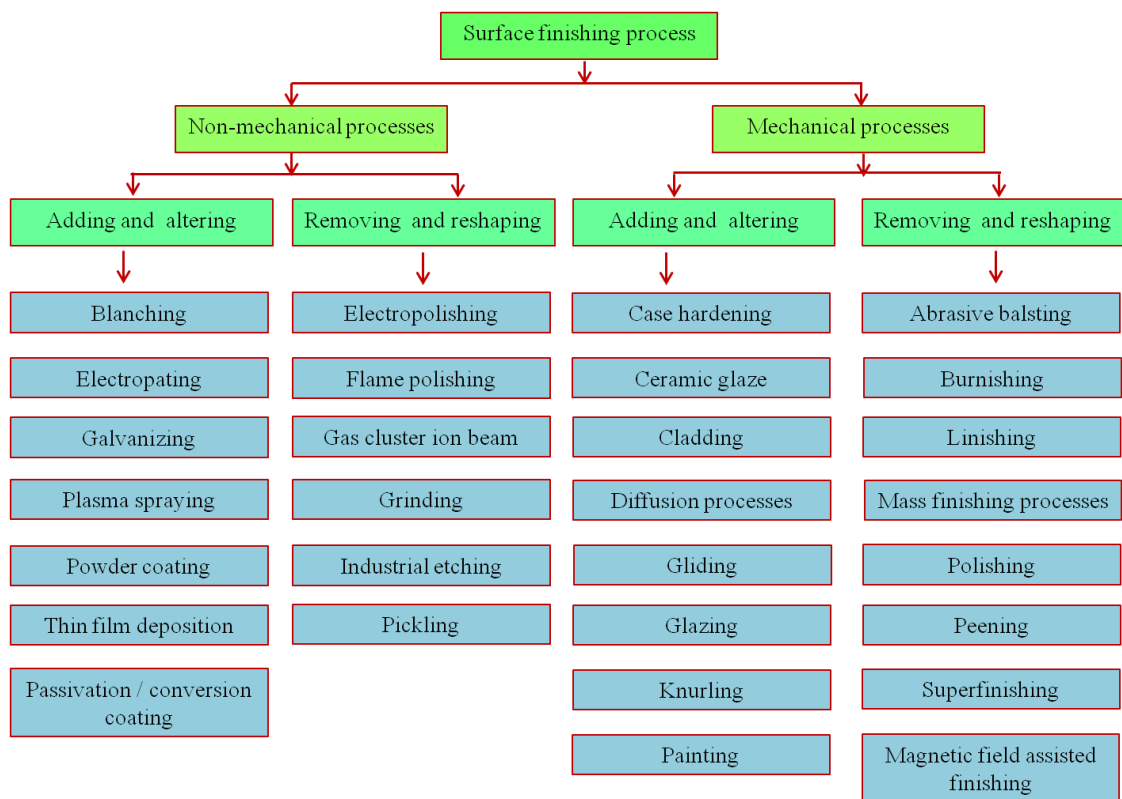


Figure 1.1 :

Surface finishing processes

1.2 Metal finishing processes

Metal finishing of the engineering components / products enhances the life span which otherwise may last only a fraction of their present life span by changing the attributes of corrosion and wear. Typically the metal finishing is conducted after the metal part has been formed. Many techniques are used for metal finishing which can be categorised broadly as follows.

1.2.1 Mechanical surface finishing processes

These processes use abrasive or cutting tools to change the micro shape of the metal surface.

Sand blasting – it involves the propelling of abrasive material such as sand into a substrate under high pressure. It is usually applied to get uniform matte texture particularly for soft metals.

Brushed metal – it involves the use of abrasive belt (120 -180 grit) or wire brush followed by softening with greaseless compound or medium non-woven abrasive belt (80 -120 grit). It produces the smooth, unidirectional, uniform and parallel grain texture.

Buff polishing - it involves the use of loose abrasive applied to the cloth wheel starting with rough and progressively finer until the desired surface finish is achieved. It produces smooth, not-textured highly glossy surface.

Metal grinding – uses friction, attrition and / or compression to smooth metal surface. It is used for high surface quality and high accuracy of shape and dimension (dimension accuracy of the order of 25 µm). In most applications it is a surface finishing process and removes comparatively little metal about 0.25 to 0.50 mm.

Metal vibratory finishing – uses the abrasive action of the abrasive media combined with the tumbling vibration. It is used to deburr products and remove sharp edges as well as descale and texture the surface. It creates smoother surfaces and can abrade inside deep cavities or tubular parts. It can also finish the fragile or extra large parts.

Burnishing – Sliding contact with other object which may be ball or roller plastically deforming the surface. It improves the size, shape, surface finish and surface hardness of the work piece and smears the texture of rough surface and makes it shinier.

Shot peening – cold working process and involves the bombardment of surface of work piece with particles (round metallic, glass or ceramic) propelled by an air blast system and centrifugal blast wheels. Each particle acts as a ball peen hammer. It produces the compressive residual stress layer and modifies mechanical properties of metals such as fatigue strength and resistance to stress corrosion cracking.

1.2.2 Non-mechanical surface finishing processes

These processes use heat or chemistry is being employed to alter the attributes of the metal surface.

Industrial etching – chemical milling processes using acids, bases or other chemicals to dissolve unwanted material such as metals, semiconductor material or glass. It can remove metals to a depth of about 12 mm (0.5 inches). Masking is used to control the differential dissolution of material. It produces much finer details than can be achieved by simple engraving. Mostly it is used in printed circuit board (PCB), semiconductor fabrication and may be used to produce plaques, house signs, name plates, ID tags and graduation scales. The most common etchants used are Keller's reagent (Al), HCl + HNO₃, FeCl₃ (stainless steel), cupric chloride, FeCl₃, ammonia (copper), hydrofluoric acid (silica).

Pickling – removes the thin surface layer and impurities such as stains, inorganic contaminants, rust or scale from heat tint and welding from ferrous metals. It is commonly used to descale or clean steel in various steel making processes. Strong acids such as HCl, H₂SO₄ and phosphoric acid are mostly used for pickling.

Gas cluster ion beam (GCIB) – a novel technique for nano scale modification of surface and smooth the surface within an angstrom of roughness without damaging the subsurface. It utilizes the energetic ionized gas cluster ion beam of any gas but usually argon gas is used due to its inertness. For maximum smoothness the high energy GCIB treatments are followed by low energy GCIB.

Electropolishing – There are different descriptions for electropolishing like electro-brightening, electrochemical polishing, reverse plating and de-plating. It is the electrochemical removal of surface layer producing micro-smooth, contaminant free surface without producing any thermal or physical distortion. It is similar to electroplating except the difference in polarity of the work piece (positively charged). In electropolishing the metal is preferentially removed from high current density areas such as edges of

components or any high spots or peaks on the surface. Generally small amount of material 10-40 microns are removed therefore it does not remove scratches or heavy scuff marks.

Electropolishing is mainly confined to various grades of stainless steel i.e. over 95%. The metals such as titanium or nitinol are also processed by electropolishing but it is mainly restricted to the medical industries.

1.2.3 Electropolishing vs. Mechanical polishing

| Mechanical polishing | | Electropolishing |
|----------------------|---|--|
| 1. | Mechanical polished surface has an abundance of scratches, strains, metal debris and embedded abrasives. | Electropolished surfaces are extremely smooth, macroscopically flat and microscopically featureless. |
| 2. | Surface finishing by mechanical methods using abrasive, cutting or burnishing action distorts the metal surface regardless of how small the amount of work is. | It reveals the true crystal structure without distortion. |
| 3. | In spite of the topographical distortion, the damages accompanied with cold working penetrate deep into the metal which significantly reduces the mechanical strength of the surface. | Electropolishing substantially reduces the surface area available for contamination pick up and eliminates all micro-cracks and internal crevices. |

1.2.4 Characteristics of electropolished surface

The characteristics of surface obtained by electropolishing process are significantly different from that of mechanically finished surface. In electropolishing, the peaks are preferentially removed resulting in micro-smooth, reflective, contaminant free surface without any thermal or physical distortion. The electropolished surface has the following beneficial characteristics.

- Highly lustrous with decoratively appealing surface.
- Removes the surface contamination and produces the surfaces with critical cleanliness requirement.
- Electropolished surface is easier to clean and maintain.
- Increases the corrosion resistance by improving the passive oxide layer.
- Fine deburring of precision components.
- Microsmooth surface reduces the bacterial growth.

- Decrease in micro-roughness reduces the friction for contact surfaces.
- Controlled metal removal on complex shaped components to attain precision fit.
- Hole size may be increased by controlled dissolution around holes, slots etc.
- Material control by detection of micro cracks, porosity etc.
- Sealed and micro smooth surface finish reduces the radiation ingress.

1.2.5 Applications of electropolishing process

Electropolished finished surfaces find applications ranging from aesthetic, decorative or functional purposes. Some of the major sectors using electropolished surface finished components are given below.

Automotive industry – in the automobile industry, electropolishing is used to enhance decorative appeal and corrosion resistance. Typical automotive components treated with electropolishing are exhaust pipes, radiator grilles, loud speaker bezel, bull- bar and car trim.

Pharmaceutical – electropolishing is extensively used for sterile equipment, water storage tanks, vessels and processing equipment for powders and gels. Electropolishing reduces the chances for bacterial growth on product contact surfaces and in crevices and slow down the ‘roughing’.

Process equipment – in processing of adhesive products such as latex, polymeric products and plastics etc. the microsmooth surface eases the deattachment of the product materials and eliminates the chances of interaction of occluded gases in metal surfaces and the product. Complex process equipments like pumps, vessels, valves, pipe work etc. are electropolished.

Medical – medical devices whether used for external or internal purposes, surgical instruments, dental appliances, sterile handling equipment, hypodermic needles and body implants are most frequently treated by electropolishing. The microsmooth surfaces reduce the risk of pathogen and pyrogen growth, easy to clean and can be repeatedly sterilised without the fear of corrosion.

Food and beverages – Food processing (food and drink preparation) requires the hygienic and anti-stick surfaces. The internal surfaces of food mixing vessels, mixer shaft and

blades, hot water tanks for vending machine for prevention of lime scale build up and containers for storing acidic drinks such as colas are treated by electropolishing.

Pulp and Paper – In pulp and paper industry electropolishing is applied for critical components such as head box to prevent the building up of pulp fibres ('snow balling'), the removal of snow balling is costly and time consuming. Holes and slots in screen cylinders can be enlarged with precision to accommodate the grade of paper being produced and simultaneously prevent clogging.

Semi conductor – During the production of micro-chips gases are employed which are transported through a maze of small bore pipework and fittings. Minutest traces of contamination disrupt the production and therefore the inner surface of the pipes and fittings is electropolished to give clean and particle free finish.

Architectural – In architecture electropolishing is employed for complex pattern decorative purposes, ease of cleaning, corrosion resistance and durability. Complex pattern gates, durbar plate, flooring, doors, street furniture and handrailing etc. is being electropolished.

Sculptures – sculptures are electropolished for uniform bright finish and corrosion free appearance for out of doors sculptures. Electropolishing provides the great flexibility (complex creation) and is cost effective than hand polishing.

Leisure – Chlorine whether in air borne or as liquid is detrimental for stainless steel. Electropolishing forms the passive layer on the surface and can withstand the chlorine environment for extended time than mechanically finished surfaces. Tubular ladders, storage cabinets, tubular pulpits, boat fittings are electropolished to meet the hostile chlorine borne and marine environment.

Textiles – In textile processing, snagging of synthetic material is the major problem which damages the fabric. Microsmooth electropolished surfaces alleviate this problem significantly.

High vacuum and nuclear – The occluded gases in stainless steel surfaces slow down the process of achieving the desired vacuum conditions. Electropolishing seals the surface pores and removes bulk of these gases and the desired vacuum conditions are obtained in shorter time.

Electropolished surface absorbs lesser amount of radioactivity due to microsmoothness and sealed pores and more receptive to decontamination. Electropolished stainless steel plants in secured places have been employed for decontamination of radio-active tools and components.

1.3 New system for electropolishing

In 1930, French scientist Dr Jacquet, reported first time the electropolishing of copper². In 1950s, Gmbh successfully marketed the electropolishing plant, chemicals for electropolishing of copper and its alloys. In 1960s, stainless steel, in all its forms was electropolished and it attained the significant importance and many concoctions for electropolishing of these metals were developed. A volatile electrolyte based on perchloric acid was developed for electropolishing by a French company but it has the problem that it becomes explosive when comes in contact with organic material.

In 1970s and 1980s, efforts were continued for development of safer and more effective electrolytes for electropolishing. New electrolytes were developed with greater throwing power for achieving highly reflective, bright polished surfaces. Now a days different electrolytes are used for electropolishing of stainless steel and its different alloys. All these electrolytes consist of mixtures of acids which are highly corrosive and hazardous for workers and environment inspite of the fact that polishing quality is good. Currently there is great emphasis on 'green' processes for minimizing the waste and toxic effects of organic solvents. The discovery of room temperature ionic liquids (RTIL) proved to be the green alternative to the existing volatile organic solvents^{3,4} and a vast variety of reactions including nanomaterial fabrication, polymerization and catalysis can be conducted in ionic liquids. The archetypal properties like high thermal stability, non-volatility, high polarity, large viscosity, high intrinsic conductivity and wide electrochemical widows⁵⁻⁷ make them successful for electrochemical applications. A new alternative for electropolishing of stainless steel based on choline chloride and ethylene glycol, type III deep eutectic solvent namely Ethaline 200 was introduced by Abbott et al.⁸ The raw materials are readily available and biodegradable. The major advantages over the commercial process are high current efficiency, negligible gas evolution at anode / solution interface and benign liquid compared to acid mixture solution.

1.4 Ionic Liquids

Ionic liquids are the neoteric solvents comprised entirely of ions⁹ and fluid at around or below 100°C (100°C is merely a convenient marker). This is a class of novel solvents with remarkable new properties which ‘break new ground’ and have huge potential for industrial applications. They offer the promising new solvent system for cleaning up the modern chemical industry along with the supercritical fluids.

Earlier on, the chemistry had only been confined in aqueous media. In the nineteenth century, with the use of molecular solvents the reactive chemistry expanded dramatically. Organic solvents such as alcohols, chlorinated hydrocarbons, arenes, nitriles etc. caused a blossoming in the organic chemistry. Liquid ammonia, nitrogen(IV) oxide and bromine(III) fluoride allowed the exploration in low oxidation and high oxidation state chemistry respectively while the use of acids, hydrochloric acid and sulphuric acid combined high solvation with acid catalysis.

The ionic liquids have the potential to act as the solvent for a broad range of chemical processes and recent reports / reviews¹⁰ revealed the promising environmental benefits and represented innovative approach to green chemistry. All these features of ionic liquids are attracting increasing attention from industry. The proposed applications of ionic liquids ranging from fuel desulfurization¹¹, petrochemical industry¹² via heavy chemicals, fine chemicals, agrochemicals and pharmaceuticals¹³ to organic synthesis to catalysis to electrochemistry to precious metal processing¹⁴ and nuclear industry. The use of ionic liquids show many advantages over conventional organic solvents but very few have come to practical fruition although several are at pilot scale.

Room temperature ionic liquids (RTIL) may potentially provide environmental friendly solvent medium for chemical and pharmaceutical industries and one do not have the concern which may be present in case of volatile organic solvents that can contribute to the air pollution. Thermodynamically and kinetically ionic liquids environment for a chemical reaction is different from the normal polar and non-polar organic solvents and therefore the outcome of the reaction may also be different. Many organic reactions such as Friedel-Crafts¹⁵, Diels-Alder¹⁶, Heck catalysis¹⁷, chlorination¹⁸, enzyme catalysis¹⁹, polymerization²⁰, cracking²¹, oxidation²² and hydrogenation²³ have successfully been studied in ionic liquids. A recent review on Heck chemistry²⁴ concluded with these remarks

‘the ionic liquid process appears as one of the cleanest recyclable procedures so far described for the Heck reaction’.

The ionic liquids are not ‘one size fits all’ products but can be tailored to meet the criteria for a specific application by selecting suitable cations and anions or their physicochemical properties can be fine-tuned by modifying a single cation class by changing the nature of one or more substituent alkyl chains. So they are termed as ‘designer’ solvents²⁵. So there is an implication (implicit rather than explicit) that for every chemical reaction of interest, it is possible to design or tailor a solvent to optimize that reaction²⁶. Currently chemical industry uses almost six hundred molecular solvents but with claim of ‘designer’ solvents for ionic liquids there are possibilities to prepare ionic liquids, by orders of magnitude than are currently available for conventional solvents and at least one million of simple ionic liquids can easily be prepared in the laboratory²⁶. Some examples of the different combinations of the ionic liquid are shown in **Figure 1.2**.

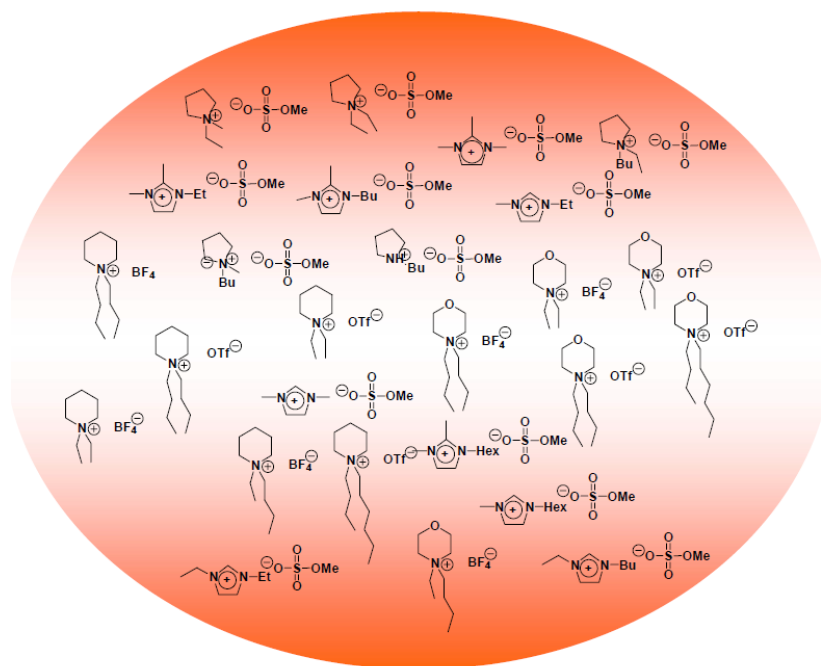


Figure 1.2 : An example of different combinations of cations and anions to form ionic liquids²⁶

1.5 Ionic liquids and future electrochemical challenges

The scientific and technological importance of ionic liquids is due to their unique solvent potential which has made many processes viable that are impossible or fail in the conventional solvents like electrodeposition of water sensitive metal / semiconductors,

energy devices such as polymer, electrolyte membrane fuel cells and super capacitors exploiting their low vapour pressure and non-flammability. In bioscience ionic liquids open a vast field for bio-inspired catalysis and bio-fuel cells due to remarkable enzyme activity. The advent of ionic liquids spans a wide range of applications like new types of lubricants, seals, fluids for thermal engines and adsorption refrigeration.

1.5.1 Electrodeposition

Ionic liquids have wide electrochemical windows spanning up to 6V (**Figure 1.3**) and extremely low vapour pressure which make them promising media for electrodeposition of metals and semi-conductors. They have revolutionized the electroplating process and make the deposition of many metals possible which are impossible in the aqueous media.

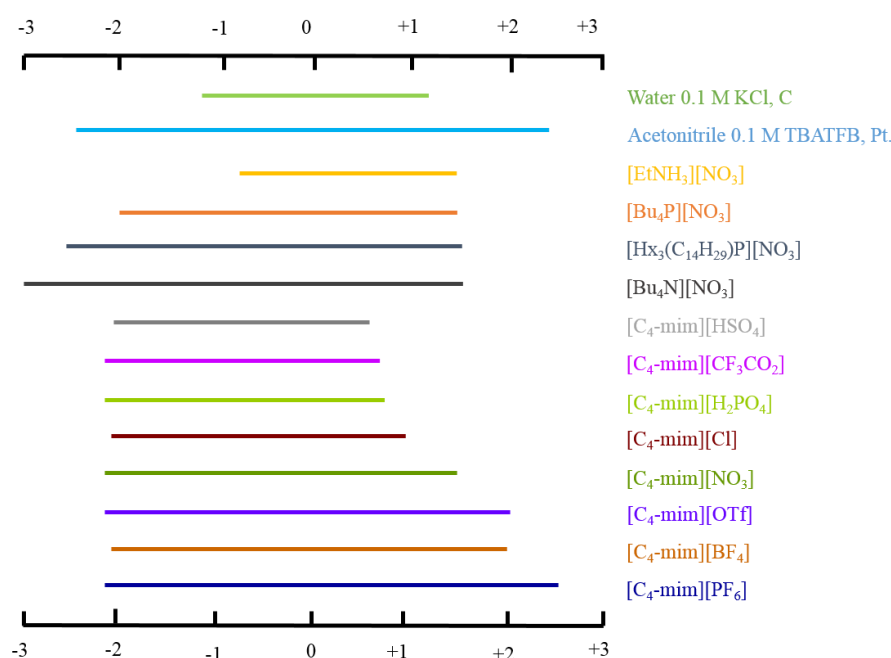


Figure 1.3 : Electrochemical window of some typical ionic liquids.²⁷ The names of these ionic liquids are given in the **list of abbreviations**.

1.5.1.1 Water sensitive metals

Water sensitive metals like aluminium, magnesium etc. or metals having the deposition potential overlapping with decomposition of water like titanium, tantalum, silicon and germanium etc. can be directly electroplated using the ionic liquids. Aluminium is industrially important for the protection of steel from corrosion due to its self passivation in air. Aluminium ($E^{\circ} = -1.67\text{V}$ vs. NHS) is very difficult to deposit from aqueous medium and is deposited by the SIGAL process^{28,29} using alkylaluminium compounds in organic

solvents. The SIGAL required the strict exclusion of oxygen owing to the high flammability of aluminium precursor.

Aluminium deposition from chloroaluminate ionic liquids was intensively studied. Nano crystalline aluminium can be deposited from a lewis acidic ionic liquid based on AlCl_3 and 1-ethyl-3-methylimidazolium chloride ($[\text{EMIm}]^+\text{Cl}^-$) while the addition of nicotinic acid as an additive reduces the crystal size from 100 nm to 10 nm³⁰. These chloroaluminate ionic liquids are hygroscopic in nature which was the major hindrance in the commercialization of this process. The electrodeposition of aluminium from water and air stable ionic liquids has been studied^{31,32} and the process is at sufficiently advance stage and may be commercialized in next few years.

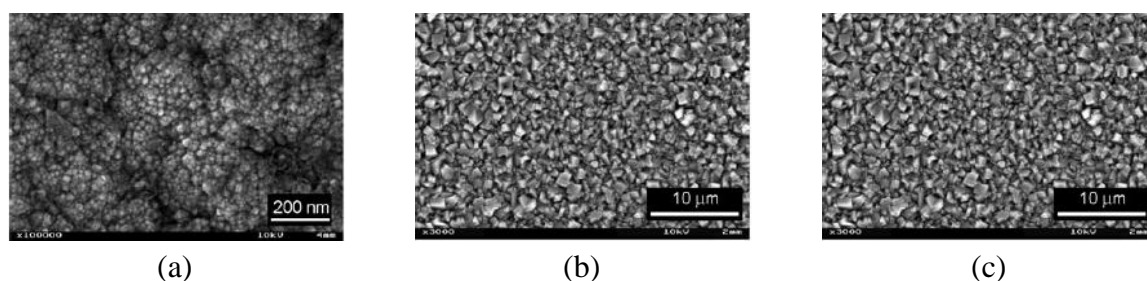


Figure 1.4 : SEM micrographs of potentiostatically electrodeposited Al films on gold substrate for one hour at 25°C (a) shiny, dense and adherent Al deposit with nanometer crystallites at -1.7 V from 1-butyl-1-methylpyrrolidinium-bis(trifluoromethylsulfonyl) amide (b) coarse, cubic shaped micrometer Al particles at -0.3 V from 1-ethyl-3-methylimidazolium-bis(trifluoromethylsulfonyl) amide (c) thin, mirror like Al film with average size of crystallite 20 nm at -1.1 V from trihexyl-tetradecyl phosphonium-bis(trifluoromethylsulfonyl) amide³³

Nano and microcrystalline aluminium can be successfully electrodeposited from the air and water stable ionic liquids (2nd and 3rd generation) namely 1-butyl-1-methylpyrrolidinium-bis(trifluoromethylsulfonyl) amide, 1-ethyl-3-methylimidazolium-bis(trifluoromethylsulfonyl) amide and trihexyltetradecylphosphonium-bis(trifluoromethylsulfonyl) amide³³ shown in **Figure 1.4**. Interestingly the morphology and grain size of Al can be influenced by the choice of the ionic liquid. The use of air and water stable ionic liquids is very interesting for Al electrodeposition. Firstly they can easily be made water free and secondly the morphology and grain size of Al deposit can be tailored by changing the ionic liquid.

1.5.1.2 Deposition of reactive metals

The wide electrochemical window of ionic liquids allows the electrodeposition of reactive elements such as titanium, tantalum, molybdenum or other transition metals which should be reduced at electrode potential similar to Al or even less negative from thermodynamic point of view. The multiplicity of redox states of these metals is the major difficulty which results in the electrochemical equivalent of short circuits. Titanium can be deposited from titanium (II) at a deposition potential very close to lithium. A thin layer of tantalum has been successfully deposited from ionic liquid at elevated temperature e.g. coated biomedical implants^{34,35}. **Figure 1.5** shows the SEM of Tantalum deposited on NiTi alloy.

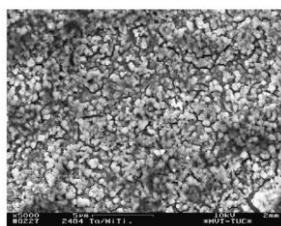


Figure 1.5 : SEM micrograph of potentiostatically deposited tantalum on NiTi alloy substrate at -2 V for one hour at 200°C from [BMP]Tf₂N containing 0.25M TaF₅ and 0.25 M LiF³⁴

1.5.1.3 Nanoparticles

Transition metals nanoparticles (nanoalloys materials) are of utmost interest in many areas of science particularly in catalysis as they exhibit a high surface to bulk metal ratio and control over the composition and size^{36,37}. The stability of the nanoparticles is key for controlling the activity and the performance of nanoparticles as catalyst. The nanoparticles are kinetically very unstable and tend to agglomerate to the bulk metal thus requiring the stabilization which may be achieved either by surface ligating anions or other ligands³⁶. Ionic liquids are effective in screening the charged layer on the metal nanoparticles thus stabilizing them³⁸ and preventing the aggregation due to the ionic charge, high polarity, high dielectric constant and supramolecular network with high degree of self-organization and weak interactions^{39,40}. The stability, size and solubility of nanoparticles can be tailored by tuning the composition of the ionic liquids⁴¹. Moreover the use of ionic liquids also facilitate the inorganic synthesis of the nanoparticles from highly polar starting materials under the ambient and anhydrous conditions thus suppressing the formation of hydroxide or oxy-hydrate³⁶. In ionic liquids metal nanoparticles are synthesized through the reduction of

metal salts by hydrogen gas^{42,43}, thermal / photochemical decomposition⁴⁴ or electroreduction/electrodeposition⁴⁵⁻⁴⁷. Stable metals (Cr, Mo, W) or metal oxide nanoparticles dispersions are obtained through thermal / photochemical decomposition of respective metal carbonyls in n-butyl-methyl-imidazolium tetrafluoroboron, n-butyl-methyl-imidazolium trifluoromethane sulfonate and n-butyl-trimethyl-ammonium bis(trifluoromethyl sulfonyl) amide⁴⁸. Novel small size (1-1.5 nm) nanoparticles of Cr, Mo and W in BMim⁺BF₄⁻ are obtained while large nanoparticles (70-150 nm) are obtained in BtMA⁺Tf₂N⁻. The size of the metal nanoparticles show correlation with the molecular volume of ionic liquid anion and it increases with the increase in the volume of the ionic liquid anion⁴⁸⁻⁵⁰.

1.5.1.4 Nanowires

The unique physical, chemical, electronic and optical properties of nanomaterial have attracted much interest from the perspective of both basic science and applied research. Nanowires are of particular interest for applications such as magnetic sensor, electronic and optoelectronic devices⁵¹⁻⁵³. Iron, cobalt and nickel nanowires due to their ferromagnetic properties are of very much interest in fundamental research. Nanowires obtained from aqueous media are of limited quality due to the co-evolution of hydrogen. Compact nanowires mat of template assisted deposit of silver⁵⁴, cobalt⁵⁵, germanium and silicon⁵⁶ from ionic liquid has been reported. Semiconductor nanowires are of particular importance as they exhibit quantum confinement effect⁵⁷, quasi one dimensional structures that confer the tuneable features depending on their size and structural characteristics and high carrier mobility compared to the bulk materials. All these features give them promising potential for fabrication of nanowire field effect transistors⁵⁸, solar cells, nanomagnets⁵⁹ and higher capacity anodes for Li-ion batteries⁶⁰. Template fabrication of a number of metals and alloy nanowires like Cu, Ni, Au, Zn, Co, Gd, CoPt and semiconductors like ZnO and CdSe from aqueous solutions have been reported. Nanowires obtained from aqueous media are of limited quality due to the co-evolution of hydrogen.

Schwarzacher et al.⁶¹ has reported the electrodeposition of Ag nanowires using a commercial polycarbonate nanoporous membrane (pore diameter 30 nm) from 1-butyl-3-methyl imidazolium hexfluorophosphate ([BMIM]⁺[PF₆]⁻). Semiconductor (germanium and silicon) nanowires can be potentiostatically electrodeposited on polycarbonate nanoporous membrane from air and water stable ionic liquid 1-butyl-1-methylpyrrolidinium

bis(trifluoromethylsulfonyl) amide ($[Py_{1,4}]Tf_2N^{56}$ and are shown in **Figure 1.6**. Previously metal nanoclusters were synthesized by vapour-liquid-solid (VLS) process, pulsed laser deposition and molecular epitaxy which required the constraining conditions of high vacuum and high temperature.

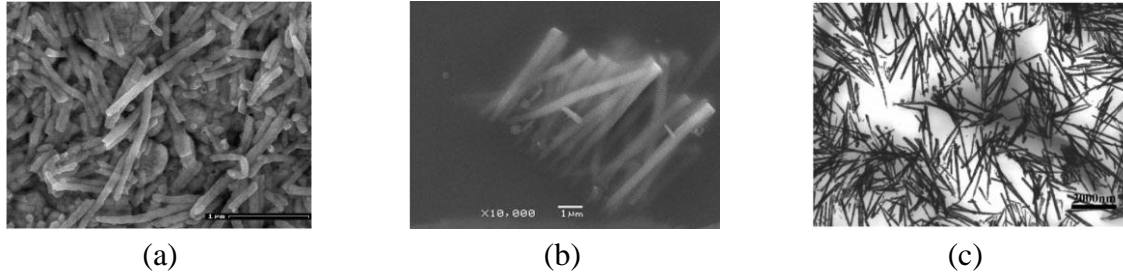


Figure 1.6 : (a) HR SEM image of Ge nanowires (approx. $2\mu m$ long and $80 - 130$ nm diameter) after dissolution of M90 PC membrane at -1.86 V from $[Py_{1,4}]Tf_2N$ (b) Si nanowires ($4-6 \mu m$ long and 400 nm diameter) after dissolution of M400 PC membrane at -2.8 V from $[Py_{1,4}]Tf_2N$ (c) TEM bright field image of Ag nanowires ($5 \mu m$ long and 80 nm diameter) at -1.2 V from 1-butyl-3-methylimidazolium hexafluorophosphate ($BMIMPF_6$)⁶¹

1.5.1.5 Semiconductors

Silicon and Germanium have similar chemical and physical properties which make the manufacturing of 'SiGe' comparatively simple than the other high speed semiconductors⁶². Si-Ge alloy may act as the bridge between low cost, low frequency silicon chips and high cost, high frequency chips from class III – V semiconductors^{63,64}. Low base resistance and high current gain makes SiGe of particular interest for the manufacturing of heterojunction bipolar transistors (HBT) for radio frequency (RF) applications^{64,65}. SiGe HBTs can also be used as bipolar complementary metal oxide semiconductor (BiCMOS) applications^{66,67} and make it an attractive material for dual use applications such as wireless communications and advanced radar systems⁶⁸ due to its high operating frequency (up to 120 GHz). SiGe can also be used in a variety of devices such as solar cells⁶⁹, resonating tunnelling diodes (RTD)⁷⁰⁻⁷², modulation doped field effect transistors (MODFET)^{73,74}, infra-red detectors⁷⁵ and light emitting diodes⁷⁶.

Si_xGe_{1-x} alloys are normally made by means of molecular beam epitaxy (MBE) and chemical vapour deposition (CVD). These techniques may be technologically disadvantageous due to the requirement of high or ultra-high vacuum and make it preferable to prepare it by simple electrodeposition. Si, Ge and Si_xGe_{1-x} cannot be

electrodeposited from aqueous media. Material absorbs visible light and may open the way to a simple electrochemical fabrication of inexpensive solar cells.

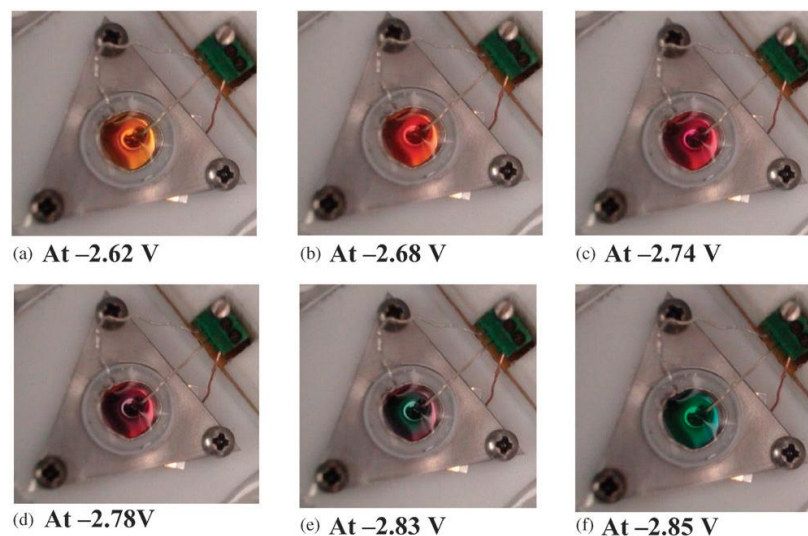


Figure 1.7 :

In situ optical photographs of electrochemical cell showing photoluminescent deposits of $\text{Si}_x\text{Ge}_{1-x}$ semiconductor during the cyclic voltammetric scan, the observed colors are due to the quantum size effects of nanometer range particles. (a , b) orange red color due to the absorption of light with wavelength of roughly 380 – 560 nm, (c , d) dark red color is due to the absorption of light between 380 and 650 nm, (e , f) green / blue green color is due to the absorption of light between 380 – 450 and 560 – 700 nm.⁶²

Ionic liquids allow the pure deposit so that photoluminescence effect can be seen. Photoluminescent $\text{Si}_x\text{Ge}_{1-x}$ with a band gap of at least 1.5 – 3.2eV can be made by electrodeposition from an ultrapure ionic liquid containing silicon and germanium halides. During deposition different colours ranging from orange to green are observed in the visible spectrum, due to a quantum size effect of the semiconductor particles ranging from 2-20 nm⁶².

The $\text{Si}_x\text{Ge}_{1-x}$ alloy can be successfully electrodeposited from 1-butyl-1-methylpyrrolidinium bis(trifluoromethylsulfonyl) amide ($[\text{Py}_{1,4}]\text{Tf}_2\text{N}$)⁶². The $\text{Si}_x\text{Ge}_{1-x}$ deposit showed a strong color change (red – blue) during the electrodeposition probably due to the quantum size effect and is indicative of band gaps between at least 1.5 – 3.2 eV⁶² as shown in **Figure 1.7**. Electrodeposition of metals and semiconductors from ionic liquids has been demonstrated in a variety of cases but the fundamental electrochemistry aspects of the process are still to be explored. The double layer structure at the electrode - liquid interface owing to the formation of solvation layers in ionic liquids still needs to be

investigated. Similarly the effect of large ions on the diffusion kinetics and mechanism of nucleation and growth of the electrodeposition of metals require thorough investigations.

1.5.2 Energy Management

The major emphasis of the present energy policy is to shift or increase the use of renewable energy sources in household and industry and use of vehicles with zero or low emissions due to economic and ecological problems. Batteries are the ideal electrochemical systems both for storing the energy obtained by harnessing intermittent sources such as solar or wind and are used to power electric or hybrid vehicles⁷⁷. Lithium batteries, the most efficient and technologically at advanced stage of development may be the best choice. Lithium batteries used the commercial electrolyte consisting of ethylcarbonate (EC), dimethylcarbonate (DMC) and diethylcarbonate (DEC) with lithium hexafluorophosphate as lithium salt⁷⁸. EC / DMC / DEC electrolyte has excellent charge / discharge cycles without losing significant capacity but their thermal stability is an issue at 60°C or above owing to volatility and flammability of DEC and DMC. The large scale use of lithium cells suffer owing to the hazards of fire or explosion due to undesirable reactions between battery components triggered by short circuits or local overheating leading to an exothermic reaction of the electrolyte with the electrode material.

The promising characteristics of ionic liquids like negligible vapour pressure, non-flammability, high thermal stability, intrinsic ionic conductivity and good electrochemical stability range (4 -5.7 V) make them appealing alternative electrolyte for Li batteries⁷⁹. The biggest disadvantage in their application is their high viscosity which in turn limits ionic mobility hence ionic conductivity.

The RTILs based on pyrrolidinium cation group (1-n-butyl-3-methylpyrrolidinium bis-(trifluoromethanesulfonyl) amide, Py_{1,4} TFSI) complexed with Li salt for Li batteries showed promising results for ionic liquid based electrolyte having ionic conductivity of the order of 10⁻³ Scm⁻¹ and lithium transference number 0.4 and is suitable for electrolyte in advance lithium batteries⁸⁰. A prototype battery consisting of lithium iron phosphate as cathode showed good performance in terms of charge / discharge efficiency and rate capability. In case of pyrrolidinium based ionic liquid electrolyte, solid electrolyte interface (SEI) is formed which prevents the undesirable reactions between ionic liquid electrolyte and the electrode material but at the same time increases the resistance and decreases the capacity due to the consumption of lithium^{81,82}.

3-methyl-1-propylimidazolium bis-trifluoromethylsulfonyl) imide (PMIM TFSI) complexed with Li-TFSI (1:1) for lithium battery electrolyte showed very good results due to low viscosity, good Li salt solvation and electrochemical stability avoiding the undesirable reactions between electrode and electrolyte in comparison to Py_{1,4} TFSI – Li TFSI electrolyte. Li TFSI / PMIM TFSI electrolyte have conductivity above $\sim 10^{-4} \text{ Scm}^{-1}$ at 0°C, value proposed for large batteries for EV's or HEV's⁷⁹. A coin cell constructed by ionic liquid gel electrolyte (soaking fibrous membrane of electrospun poly(vinylidene fluoride–co-hexafluoropropylene) in the Li TFSI/PMIM TFSI electrolyte) and Li/ LiFePO₄ electrode showed the excellent charge / discharge capacity with a retention of >96% after 50 cycles ($\sim 146 \text{ mAhg}^{-1}$) and good interfacial stability⁷⁹.

The probable next generation of power sources for portable electronic devices and electric vehicles, rechargeable lithium metal polymer electrolyte batteries (LMPBs) have limited performance owing to low ionic conductivity of poly(ethylene oxide) (PEO) based electrolytes. PEO has good thermal properties and interfacial stability with Li electrode. The addition of molecular solvents enhances the ionic conductivity⁸³ but at the same time reduces the interfacial stability with Li electrode and its volatile nature may cause battery to explode due to overheating as a result of short circuits⁸⁴. The addition of RTILs to PEO-LiX electrolyte improves the ionic conductivity without having the detrimental effects of molecular solvents. The addition of N-methyl-N-propylpyrrolidinium bis-(trifluoromethanesulfonyl) amide to P(EO)₂₀ – LiTFSI polymer electrolyte in solid state Li/V₂O₅ batteries were investigated. The incorporation of Py_{1,4}TFSI showed the promising improvement in the performance and electrolyte showed excellent reversible cyclability with a capacity fading of 0.04% per cycle over several hundred cycles at 60°C⁸⁵.

1.5.3 Biomechanics

Electrochemical actuators are intensively studied for their biomimetic capability. Actuators may be based either on metal coated ion exchange polymer or intrinsically electron conducting polymer. The device is based on a membrane coated with a metal layer on both sides, each of which act as an electrode and their operation requires humidification for ion conduction in the polymer and water is usually used as a solvent. High levels of strain can be produced by using intrinsically conducting polymers, electrodes of polypyrrole or polyaniline that show volume change when cycled between their oxidised and reduced states. Conventionally aqueous or aprotic solvents are used which limit the performance

and life time of the device owing to their potential for evaporation and limited electrochemical stability window.

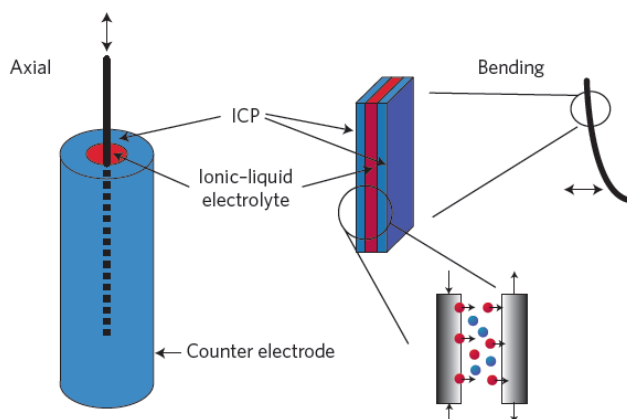


Figure 1.8 : *Electrochemical actuator produces a mechanical bending or axial motion in response to an electrical stimulus⁵⁵*

Ionic liquids are the materials of choice for electrolytes of biomimetic actuator devices having the required strain, life time and rate capability⁵⁵. The use of ionic liquids as an electrolyte in these electrochemical actuators considerably increase their performance and operational life (approximately 10^6 cycles) because of their high electrochemical stability⁵⁵ and allows the redox cycling process without any diffusion limit in the electrolyte as the counter ions in the conducting polymers are the same as that of anions of ionic liquids (PF_6 , BF_4 , CF_3SO_3 or $(\text{CF}_3\text{SO}_2)_2\text{N}$)⁸⁶.

A solid state actuator can be fabricated by gelling the ionic liquid in cross linked polymer component (polymer in ionic liquid, (PILE)). The schematic representation of the accuator is shown in **Figure 1.8**. Ionic liquids, 1-ethyl-3-methylimidazolium bis(trifluoromethyl sulfonyl) amide (EMIMTFSa), and 1-butyl-3-methylimidazolium (BMIMPF_6) were used in synthesizing PILEs. The PILEs have wider electrochemical windows as compared to the conventional liquid electrolytes. The shelf life of a PPy/ PF_6 /Pt/PVDF/PILE electromechanical actuator is at least several months and the system can be subjected to continuous pulsing for more than 3600 cycles without degradation⁸⁷. Axial geometry actuators based on polyaniline yarn and hollow fibres with ionic liquid as electrolyte can generate stresses (0.85 mPa) exceeding that of skeletal muscles. This ‘yarn in fibre’ approach allows the creation of multifibre device with required stress capability by simple

combination of a sufficient number of fibres⁸⁸. Similarly Carbon nanotubes based actuators with ionic liquid as electrolyte have been reported recently⁸⁹.

1.5.4 Biosensing

Immobilization of electron transfer mediators to electrode surface is a key step for design, fabrication and performance of the sensors and biosensors⁹⁰. The conventional electrodes show quasi reversible electrochemical behaviour and low electrocatalytic activity. Specific characteristics of room temperature ionic liquids like good electronic and mechanical properties, electric conductivity and good compatibility with biomolecules and enzymes make them good choice for applications in the field of electroanalysis⁹¹. RTILs can be used as the supporting electrolyte or binder in the carbon paste electrode or modifier on the chemically modified electrodes⁹².

DNA modified carbon paste electrode (DNACPIE) using ionic liquid binder (mixture of ionic liquid 1-butyl-3-methylimidazolium hexafluorophosphate and paraffin oil) shows higher sensitivity and better selectivity than electrode with organic binder for voltammetric sensing of adenine⁹¹. The electrode showed good results when applied to the milk samples with good stability and selectivity.

Third generation reagent less biosensor, multiwalled carbon nanotubes and carbon ionic liquid electrode (MWCNTs / CILE) was fabricated using the hydrophilic ionic liquid, EMIMBF₄ as the modifier for electrochemical detection of organophosphates in pesticides (paraoxon, parathion, sarin, soman etc.)⁹². Reagent less biosensor, carbon nanotubes ionic liquid and chlorpromazine modified electrode for the determination of nicotinamide adenine dinucleotide (NADH) and ethanol was fabricated⁹⁴. This nanocomposite modified electrode exhibits excellent electrocatalytic activity towards oxidation of NADH and **Figure 1.9** shows its morphology and mode of action. It shows high sensitivity (0.5835 A M^{-1}), low detection limit (80 nM) at concentration range up to 20 μM for NADH while the concentration range 40 μM – 1.5 mM with detection limit 5 μM and sensitivity $1.97 \mu\text{A mM}^{-1}$ for ethanol⁹⁰.

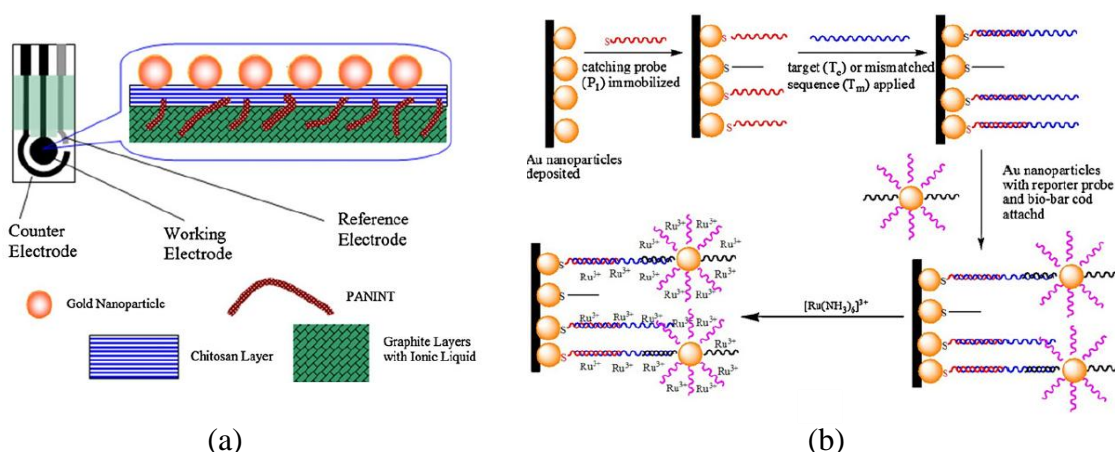


Figure 1.9 : (a) The pattern of the PANINT – IL / chitosan / AuNP SPE and the structure of the working electrode (b) Procedure for the detection of DNA with RuHex as electrochemical probe⁹³.

Recently screen printed electrodes (SPEs) have gained much interest due to their low cost (disposable) owing to the requirement of tiny amount of ink and other materials. SPEs can be used for detection of DNA sequence, DNA damage and other biomolecules⁹³. Due to their versatile applications, their performance need to be modified by modifying the electrode surface. A SPE was constructed using chitosan, polyaniline nanotubes (PANINTs) and ionic liquid (1-dodecyl-3-methylimidazolium hexafluorophosphate). Ionic liquid and PANINTs were doped into commercial graphite ink while chitosan and gold nanoparticles were covered on the electrode surface to get homogeneous, stable and highly conductive electrode surface. It is capable of detecting the complementary target DNA at low concentration (1.0×10^{-16} M to 1.0×10^{-14} M and detection limit of 8.0×10^{-17} M) from three base mismatched DNA at higher concentration.

1.6 Metal finishing in eutectic based ionic liquids

Ionic liquids based on cations (imidazolium, pyridinium or pyrrolidinium) have potential for many diversified synthetic and electrochemical applications including lithium batteries, photoelectrochemical cells, fuel cells and capacitors etc^{6,47,95,96}. This revolutionary technology also permeate into the metal finishing industry, over 35 pure metals and alloys including those which are very difficult or impossible to deposit from aqueous electrolytes or to deposit metals on water sensitive substrates (Al, Mg, Ti etc.) can be deposited using ionic liquids. Unfortunately no electrolytic coating using ionic liquid electrolyte has yet

been commercialized on large scale due to issues like cost, registration and handling associated with ionic liquids⁹⁷.

Eutectic based ionic liquid having the general formula $\text{cat}^+\text{X}^- z\text{Y}$ can be formed by mixing the cations (ammonium, phosphonium or sulfonium) with either a Lewis or Bronsted acid. The complex anionic species are formed between X^- (usually Cl^-) and either a Lewis or Bronsted acid, Y and z refers to the number of molecules which interact with the anion⁹⁸⁻¹⁰⁰. They are based on equilibria set up between X^- and Y. The ionic liquids described can be subdivided into three types

Eutectic Type I $\text{Y} = \text{MCl}_x$, $\text{M} = \text{Zn}^{101}$, Sn^{102} , Fe^{103} , Al^{104} , Ga^{105}

Eutectic Type II $\text{Y} = \text{MCl}_x \cdot y\text{H}_2\text{O}$, $\text{M} = \text{Cr}^{106}$, Co , Cu , Ni , Fe

Eutectic Type III $\text{Y} = \text{RZ}$, $\text{Z} = \text{CoNH}_2^{107}$, COOH^{108} , OH

The relative proportions of anionic species depend on the ionic liquid composition. The ability to vary the composition of Lewis or Bronsted acid adds an additional dimension to the tuneability of the eutectic-based ionic liquids. The anionic species have been identified for Type I, II and III based eutectics where Al^{109} , Sn^{99} , Zn^{99} , Cr^{106} and urea¹⁰⁷ are the complexing agents and some studies have quantified the proportion of species present^{99,109}. These eutectic based ionic liquids are probably the possible alternative for metal finishing industry from cost, registration and handling perspective⁹⁷. Abbott et al. used the choline chloride $[\text{HOC}_2\text{H}_4\text{N}(\text{CH}_3)_3\text{Cl}]$ as the quaternary ammonium component which is classified as provitamin and is produced on mega ton scale as an animal feed supplement. These deep eutectic solvents are air and water stable, easy to handle, prepare, less toxic and biodegradable.

These deep eutectic solvents have a number of applications in metal finishing including electrolytic and electroless deposition and electrodisolution of metals.

1.6.1 Electroplating of Chromium

Hard / decorative chromium can be deposited from aqueous bath containing the hexavalent chromium but the toxicity of the hexavalent chromium and recent environment legislation has urged to search for alternative bath for chromium deposition.

Crack free metallic chromium on steel substrate can be deposited by using the type II deep eutectic solvents ($\text{ChCl}:\text{CrCl}_3 \cdot 6\text{H}_2\text{O}$) with a high current density (>90%)¹⁰⁶. The addition of

lithium chloride as an additive enables to deposit crack free, nanocrystalline black chromium film with an excellent corrosion resistance properties¹¹⁰. Benaben et al.¹¹¹ optimized the bath composition and operating conditions for the deposition of hard and bright chromium layer. The hardness of the layer can be improved by heat treatment (400°C / 1 h, under nitrogen atmosphere) from 700 to 1400-1500 HV which may be attributed to the evolution of the structure between simple cubic to FCC structure⁹⁷. **Figure 1.10** shows the decorative chromium deposit on steel substrate from liquids developed by Fundacion Inasmet (San Sebastian, Spain).



Figure 1.10 : Photographs of potentiostatic deposition of hard chromium film (25-30 μm) from $\text{ChCl}:\text{CrCl}_3\cdot\text{H}_2\text{O}$ on XC38 steel (left) and SS304 (right)⁹⁷

1.6.2 Electrodeposition of Zinc and its alloys

Zinc coatings are technologically important due to its environmental compatibility, cost and corrosion resistance properties. The zinc deposition from aqueous bath is very well developed. The study of zinc deposition in ionic liquid is an important stepping stone for the production of zinc alloys⁹⁷. Silver colored smooth zinc deposits were obtained in 7:3 EMIMBr: ZnBr_2 with ethylene glycol (>45 mol %) as a diluent at current densities 100-150 $\text{A}\cdot\text{m}^{-2}$ while at current densities higher than 150 $\text{A}\cdot\text{m}^{-2}$, the deposit turned grey. The deposit was also found sensitive to water contents in the electrolyte^{112,113}.

Zinc was successfully deposited from 1:2 $\text{ChCl}:\text{ZnCl}_2$ eutectic mixture with current efficiency of 100%¹¹⁴. The good deposit was obtained at current density of 2-5 $\text{A}\cdot\text{m}^{-2}$ at 60°C while higher current densities led to powdery and non-adherent coating owing to the low conductivity and higher viscosity of the liquid. Zinc deposition from type III deep eutectic solvents using different hydrogen bond donors such as urea and a number of dihydric alcohols was studied⁹⁷. The deposit was found to be sensitive to the type of hydrogen bond donor. Uniform, dense and free of defects zinc coatings were obtained on

Mg-RE alloy from 1:2 ChCl:urea which were extremely difficult as Mg and its alloys react with water to form loose corrosion layers. **Figure 1.11 (c)** shows the morphology of Zn deposited on Mg-RE¹¹⁵.

Zn-Sn alloys coating on mild steel substrates have been prepared by using type III deep eutectic solvent electrolyte (ChCl : urea / glycol). A range of compositions with high zinc contents (>80 mol %) have been obtained which have potential applications in aeronautic applications with good co-efficient of friction. **Figure 1.11 (a & b)** shows the photographs and morphology of Zn/Sn prepared from type III deep eutectic solvents¹¹⁴.

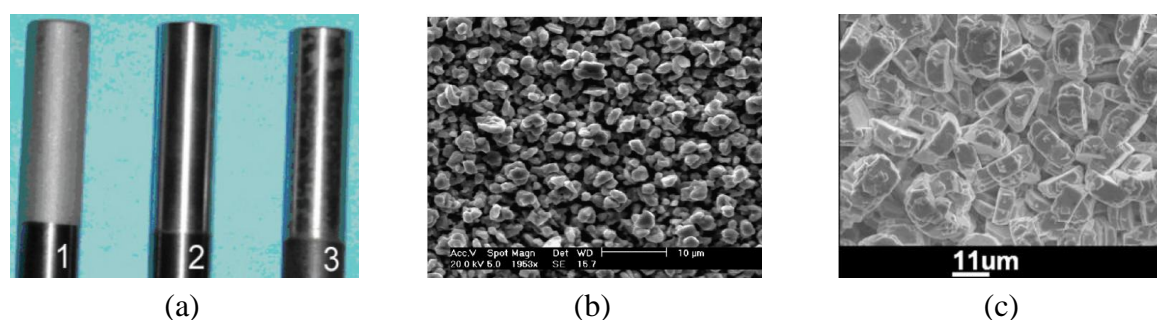


Figure 1.11 : (a) Zn/Sn alloy (1 - 15% Zn-85% Sn 5 µm thickness, 2 & 3- with diluent and brightner, 5 µm & 6.7 µm thickness respectively) deposition on XC38 steel from ChCl:EG eutectic mixture at 60°C⁹⁷ (b) SEM micrograph of Zn/Sn alloy from 0.5M ZnCl₂ / 0.5 M SnCl₂ in 1:2 ChCl:EG at current density of 10 mA-cm⁻²¹¹⁴ (c) SEM of galvanostatically deposited Zn onto Mg-RE alloy from 1:2 ChCl:urea⁹⁷

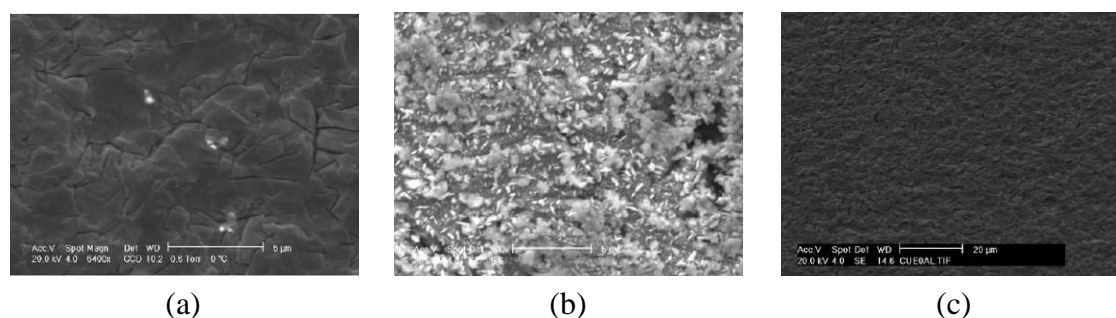


Figure 1.12 : SEM images of copper and Al₂O₃ composites from 1:2 ChCl:EG containing 0.02 M CuCl₂.2H₂O and different concentrations of Al₂O₃ at -0.8 V (a) 5 wt % 0.05 mM Al₂O₃ (3 wt% in film), (b) 10 wt % 0.005 mM Al₂O₃ (27 wt% in film), (c) no Al₂O₃¹¹⁷

1.6.3 Deposition of other metals and alloys

Abbott et al. studied the deposition of nickel on copper and aluminium substrates from 1:2 ChCl:EG and studied the influence of brighteners on the morphology of the deposits¹¹⁶.

Bright copper and uniformly distributed composite of pure copper and Al_2O_3 were obtained from type III deep eutectic solvents i.e. choline chloride / ethylene glycol and choline chloride / urea. **Figure 1.12** shows the pure copper and Al_2O_3 composite coatings deposited from solutions with particulate loadings of 3%, 5% and 10% (w/w). Other metals and alloys such as iron, nickel/molybdenum, nickel/tin alloy and tellurium and its binary compounds with bismuth and antimony were also electroplated from the deep eutectic solvents¹¹⁷.

1.6.4 Electroless deposition of metals

Thick, bright, adherent and porous nanocrystalline silver layer on copper substrate can be efficiently deposited by simple drop-in technology (immersion plating) from 1:2 $\text{ChCl}:\text{EG}$ mixture^{118,119}. The plating bath is non-toxic (cyanide free), less light sensitive and allows uniform deposition rate. A silver coated PCB from type III deep eutectic solvent is shown in **Figure 1.13 (a)**.

Similarly copper can be deposited on to aluminium substrate⁹⁷. The thickness of the layer depends on the immersion time and typically thin, adherent and homogeneous films can be deposited in few minutes. This process allows easy electrolytic deposition of other metals on top of copper ad-layers. Good adherent Ni (10 μm) coating on electroless copper plated Al rod from aqueous Watt bath is shown in **Figure 1.13 (b)**.



Figure 1.13 : (a) Immersion silver coating on multitrack circuit board from 1:2 $\text{ChCl}:\text{EG}$ ⁹⁷ (b) Photograph of electrolytically deposited Ni from aqueous Watt nickel bath on immersion plated Cu Al rod⁹⁷

1.6.5 Electropolishing in deep eutectic solvents

The commercial electropolishing processes of stainless steel mainly based on a mixture of inorganic acids (phosphoric acid and sulphuric acid mixture) are under serious discussion due to major technological issues such as highly corrosive liquids and current efficiency (extensive gassing at anode). In the last three decades ionic liquids are extensively studied

for metal finishing processes¹²⁰. Air and moisture stable ionic liquids based on quaternary ammonium salts (choline chloride) mixed with anhydrous / hydrated metal salts can be used for metal electrodeposition^{100,106,110}. Deep eutectic ionic liquids analogues can also be formed by mixing choline chloride with hydrogen bond donors like amides, carboxylic acids and alcohols instead of metal salts.

Abbott et al. at university of Leicester, first time used choline chloride and ethylene glycol based eutectic solvent as an alternate electrolyte for electropolishing of stainless steel in place of aqueous acidic mixture¹²¹. The electropolishing of stainless steel in 1:2 ChCl:EG is more efficient with current efficiency of 92% and current density 53-71 mA-cm⁻² with no gas evolution at anode suggesting lack of appreciable side processes while in phosphoric/sulphuric acid mixture the current efficiency is approximately 30% and the typical current density is 100 mA-cm⁻² with a considerable evolution of gas at anode¹²². The electropolishing of stainless steel in ionic liquid involves the simple dissolution of metals forming complexes of the form $M^+_x Cl_y Gly_z$ and UV studies showed that iron and nickel are present in +2 oxidation states while Cr is present in +3 oxidation state¹²¹.

Both voltammetric and impedance studies of electropolishing of stainless steel in 1:2 ChCl:EG showed that the mechanism of electropolishing of stainless steel in ionic liquid is different from that of acidic mixture. In 1:2 ChCl:EG, removal of the surface oxide layer is a rate determining step and after the removal of the surface oxide layer the polishing process is mass transport controlled and the diffusion of the chloride ions to the electrode surface may be rate limiting factor. The etching is anisotropic i.e there is no differential etching at different crystal faces¹²³.

As the deep eutectic solvents are air and water stable, they allow the electropolishing process to be conducted in an open atmosphere where moisture absorbance may be up to 5 weight %. The presence of water (up to 10 wt %) in 1:2 ChCl:EG had no detrimental effect upon the polishing process but the presence of water in the deep eutectic solvent electropolishing bath widened the current density window over which mirror finish of stainless steel was obtained and this beneficial effect may be attributed to the possible decrease in viscosity and increase in the conductivity of the ionic liquid¹²³.

The primary purpose of the electropolishing of stainless steel is to enhance the corrosion resistance of the substrate therefore it is important that there is no change in surface composition. The analysis of the electropolishing solution after bulk electropolishing of the

stainless steel substrate¹²¹, the energy dispersive X-ray analysis (EDAX) at the interface of the polished and unpolished surfaces (outermost surface) and the X-ray photoelectron spectroscopy (XPS) of the subsurface volume showed negligible change in the elemental composition of the stainless steel substrate suggesting no dealloying effect of the steel during the electropolishing of stainless steel in ionic liquid^{8,123}.

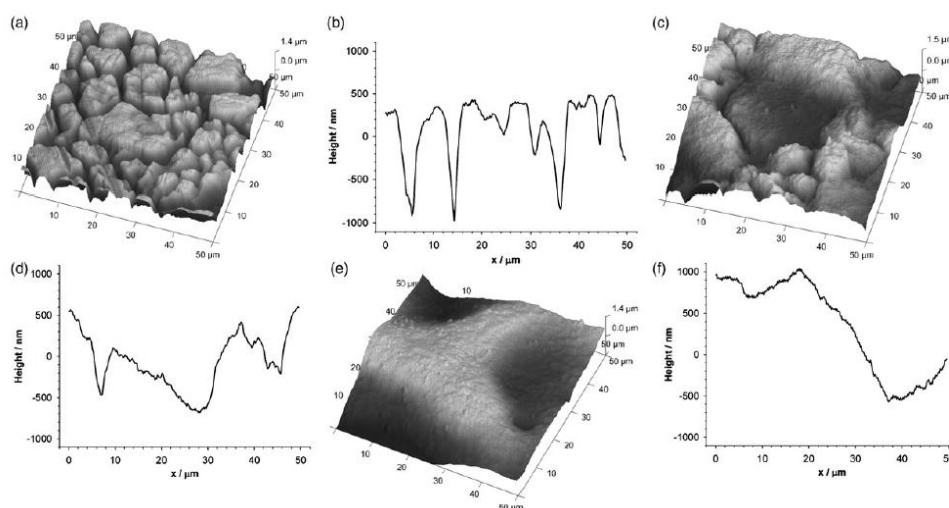


Figure 1.14: *AFM images with single line trace of stainless steel electropolished at 25 mA-cm⁻², (a), (b) unpolished (c), (d) electropolished for 10 min (e, f) electropolished for 25 min. The single line traces were taken laterally across the centres of the images⁸.*

Abbott et al.⁸ attempted the in situ liquid AFM to study the surface transformation of the steel substrate during the electropolishing in ionic liquid. Owing to the difficulties such as laser light scattering and loss of feedback control due to diffusion of small fragments and particles of the dissolved metal, the surface was imaged at discrete intervals i.e. before polishing, part way through and at the end of polishing and is shown in **Figure 1.14**. To ensure the imaging of the same area the tip of AFM was not fully withdrawn from the surface. The qualitative transition from the unpolished to polished surface was observed with the initial erosion at the prominent features of the surface where presumably current density was the highest. The polished surface was smooth and bright and micro-roughness was reduced to less than 100 nm^{8,121,123}.

1.7 Summary

Surface finishing is a range of processes to change the surface attributes of the manufactured item either for enhancing the substrate's appearance by removing burrs and

other surface flaws and improve the aesthetic appeal of a casting by changing its gloss, shininess and color or for functional treatments like to improve corrosion protection, abrasion, wear resistance and wettability. Surface finishing processes for metals are mainly divided into two groups on the basis of their effect on the workpiece (i) removing or reshaping finishing (ii) adding or altering finishing. Each of the above division is further subdivided into two groups on the basis of how the surface finishing is being achieved (a) Mechanical surface finishing processes (b) Non-mechanical surface finishing processes.

Surfaces finished with mechanical processes have abundance of scratches, strains, metal debris and embedded abrasives while electropolished surfaces have lustrous, smooth, reflective and microscopically featureless appearance.

Electropolishing is the most economical and most widely used technique for surface finishing of stainless steel. Presently the whole sector relies on the electropolishing bath consisting of concentrated sulphuric acid and phosphoric acid. This can be associated with hazardous vapours and highly corrosive and toxic with extensive gas evolution and have negative impact on the environment. The stringent legislation shifts the focus to find alternative electropolishing bath to achieve more environmentally compatible deposition systems. Ionic liquids have the potential to replace the current electropolishing bath due to their unique electrochemical properties like negligible vapour pressure, wide liquid range, high thermal stability, large electrochemical window and intrinsic electrical conductivity. A lot of issues have not been addressed yet such as life cycle analysis and their greenness, electropolishing qualities and variables, economic impacts and improved quality over the existing techniques.

In the present work, fundamental aspects of the electropolishing of austenitic stainless steel and nickel based superalloy CMSX-4 in novel electrolyte, deep eutectic solvent based on choline chloride and hydrogen bond donor (1:2 ChCl:EG) has been carried out. Electrochemical techniques like linear sweep voltammetry, chronoamperometry and galvanostatic studies have been used to study the effect of temperature, potential and water contents of 1:2 ChCl:EG on the electropolishing quality of 300 series stainless steel. Fractional factorial design experimental strategies has been used to optimize the process variables. Surface characterization of electropolished stainless steel i.e. surface over layer morphology and surface roughness has also been studied using metrology techniques namely atomic force microscopy (AFM), scanning electron microscopy (SEM), field

emission scanning electron microscopy (FE-SEM) and digital holographic microscopy (DHM). Open circuit potential measurements (OCP), potentiodynamic polarization curves and gravimetric methods have been used to investigate the effect of electropolishing on the corrosion behaviour of stainless steel. Similarly electropolishing of second generation single crystal nickel based superalloy (CMSX-4) in deep eutectic solvent has also been carried out to remove the casting scales on turbine blades and the surface texture of electropolished work piece has been investigated by using the microscopic techniques, AFM, SEM and DHM.

1.8 References

- (1) Degarmo, E. P.; T, B. J.; A, K. R. *Materials and processes in Manufacturing*; 9th ed.; Wiley, **2003**.
- (2) H.Figous; Jacquet, P. A. In *French Patent*, **1930**; Vol. 707526.
- (3) Welton, T. *Chemical Reviews* **1999**, 99, 2071-2083.
- (4) Blanchard, L. A.; Hancu, D.; Beckman, E. J.; Brennecke, J. F. *Nature* **1999**, 399, 28-29.
- (5) Abbott, A. P.; McKenzie, K. J. *Physical Chemistry Chemical Physics* **2006**, 8, 4265-4279.
- (6) Buzzeo, M. C.; Evans, R. G.; Compton, R. G. *Chemphyschem* **2004**, 5, 1106-1120.
- (7) Endres, F. *Chemphyschem* **2002**, 3, 144-154.
- (8) Abbott, A. P.; Capper, G.; McKenzie, K. J.; Glidle, A.; Ryder, K. S. *Physical Chemistry Chemical Physics* **2006**, 8, 4214-4221.
- (9) Wassersheid, P.; Welton, T. *Ionic liquid in synthesis*; Wiley VCH: Weinheim, **2003**.
- (10) Rooney, D. W.; R, S. K. *Handbook of Solvents*; Chem Tech Publishing: Toronto, **2001**.
- (11) Whitehead, J. A.; Lawrance, G. A.; McCluskey, A. *Green Chemistry* **2004**, 6, 313-315.
- (12) Rogers, R. D.; Seddon, K. R. ACS Symp. series Vol. 856, American Chemical Society, Washington D.C., **2003**.
- (13) Earle, M. J.; Seddon, K. R.; McCormac, P. B. *Green Chemistry* **2000**, 2, 261-262.
- (14) A.Noda; M.Watanabe *Electrochemistry (Tokyo, Jpn)* **2002**, 70, 140.
- (15) Seddon, K. R.; Hardacre, C.; McCauley, B. J. In *World Patent*; 1, Ed.; 1222, **2003**; Vol. WO 03 028883.
- (16) Earle, M. J.; McCormac, P. B.; Seddon, K. R. *Green Chemistry* **1999**, 1, 23-25.

- (17) Carmichael, A. J.; Earle, M. J.; Holbrey, J. D.; McCormac, P. B.; Seddon, K. R. *Organic Letters* **1999**, *1*, 997-1000.
- (18) Winterton, N.; Seddon, K. R.; Patell, Y., **2000**, World Patent, WO 0037400.
- (19) Sheldon, R. A.; Lau, R. M.; Sorgedragger, M. F.; Seddon, K. R. *Green Chemistry* **2002**, *4*, 147-151.
- (20) Hardacre, C.; Holbrey, J. D.; Datdare, S. P.; Seddon, K. R. *Green Chemistry* **2002**, *4*, 143-146.
- (21) Adam, C. J.; Earle, M. J.; Seddon, K. R. *Green Chemistry* **2000**, *2*, 21-24.
- (22) Seddon, K. R.; Stark, A. *Green Chemistry* **2002**, *4*, 119-123.
- (23) J. Dyson, P.; J. Ellis, D.; Welton, T.; G. Parker, D. *Chemical Communications* **1999**, 25-26.
- (24) Beletskaya, I. P.; Cheprakov, A. V. *Chemical Reviews* **2000**, *100*, 3009-3066.
- (25) Zhang, S.; Conrad Zhang, Z. *Green Chemistry* **2002**, *4*, 376-379.
- (26) Fitzwater, G.; Geissler, W.; Moulton, R.; Plechkova, N. V.; Robertson, A.; Seddon, K. R.; Wsindall, J.; Wan Joo, K. "Ionic liquids : Sources of Innovation," *QUILL*, **2005**.
- (27) Plechkova, N. V.; Seddon, K. R. *Chemical Society Reviews* **2008**, *37*, 123-150.
- (28) Ziegler, K.; Lehmkuhl, H. *Zeitschrift für anorganische und allgemeine Chemie* **1956**, *283*, 414-424.
- (29) Kautek, W.; Birkle, S. *Electrochimica Acta* **1989**, *34*, 1213-1218.
- (30) Endres, F.; Bukowski, M.; Hempelmann, R.; Natter, H. *Angewandte Chemie-International Edition* **2003**, *42*, 3428-3430.
- (31) Caporali, S.; Fossati, A.; Lavacchi, A.; Perissi, I.; Tolstogouzov, A.; Bardi, U. *Corrosion Science* **2008**, *50*, 534-539.
- (32) Liu, Q. X.; El Abedin, S. Z.; Endres, F. *Surface and Coatings Technology* **2006**, *201*, 1352-1356.
- (33) Zein El Abedin, S.; Moustafa, E. M.; Hempelmann, R.; Natter, H.; Endres, F. *Chemphyschem* **2006**, *7*, 1535-1543.
- (34) Zein El Abedin, S.; Welz-Biermann, U.; Endres, F. *Electrochemistry Communications* **2005**, *7*, 941-946.
- (35) Arnould, C.; Delhalle, J.; Mekhalif, Z. *Electrochimica Acta* **2008**, *53*, 5632-5638.
- (36) Parvulescu, V. I.; Hardacre, C. *Chemical Reviews* **2007**, *107*, 2615-2665.
- (37) Braunstein, P.; Rose, J. *Metal Clusters in Chemistry*; P. Braunstein, L.A. Oro and P.R. Raithby ed.; Wiley - VCH: Weinheim, **2001**.

- (38) Dyson, P. J. *Coordination Chemistry Reviews* **2004**, *248*, 2443-2458.
- (39) Consorti, C. S.; Suarez, P. A. Z.; de Souza, R. F.; Burrow, R. A.; Farrar, D. H.; Lough, A. J.; Loh, W.; da Silva, L. H. M.; Dupont, J. *The Journal of Physical Chemistry B* **2005**, *109*, 4341-4349.
- (40) Dupont, J. *Journal of Brazilian Chemical Society* **2004**, *15*, 341.
- (41) Astruc, D.; Lu, F.; Aranzaes, J. R. *Angewandte Chemie International Edition* **2005**, *44*, 7852-7872.
- (42) Fonseca, G. S.; Machado, G.; Teixeira, S. R.; Fecher, G. H.; Morais, J.; Alves, M. C. M.; Dupont, J. *Journal of Colloid and Interface Science* **2006**, *301*, 193-204.
- (43) Migowski, P.; Machado, G.; Texeira, S. R.; Alves, M. C. M.; Morais, J.; Traverse, A.; Dupont, J. *Physical Chemistry Chemical Physics* **2007**, *9*, 4814-4821.
- (44) Zhu, J.; Shen, Y.; Xie, A.; Qiu, L.; Zhang, Q.; Zhang, S. *The Journal of Physical Chemistry C* **2007**, *111*, 7629-7633.
- (45) Endres, F.; Bukowski, M.; Hempelmann, R.; Natter, H. *Angewandte Chemie International Edition* **2003**, *42*, 3428-3430.
- (46) Kim, K.; Lang, C.; Kohl, P. A. *Journal of the Electrochemical Society* **2005**, *152*, E9-E13.
- (47) Abbott, A. P.; Dalrymple, I.; Endres, F.; Macfarlane, D. R. In *Electrodeposition from Ionic Liquids*; Wiley-VCH Verlag GmbH & Co. KGaA, **2008**.
- (48) Redel, E.; Thomann, R.; Janiak, C. *Chemical Communications* **2008**, 1789-1791.
- (49) Jin, H.; O'Hare, B.; Dong, J.; Arzhantsev, S.; Baker, G. A.; Wishart, J. F.; Benesi, A. J.; Maroncelli, M. *The Journal of Physical Chemistry B* **2007**, *112*, 81-92.
- (50) Machado, G.; Scholten, J. D.; Vargas, T. d.; Teixeira, S. R.; Ronchi, L. H.; Dupont, J. *Int. J. of Nanotechnology*, **2007**, *4*, 541.
- (51) Yanson, A. I.; Bollinger, G. R.; van den Brom, H. E.; Agrait, N.; van Ruitenbeek, J. M. *Nature* **1998**, *395*, 783-785.
- (52) Ge, Y.; Walther, S. *Applied Physics Letters* **1999**, *74*, 1746-1748.
- (53) Liu, K.; Chien, C. L.; Searson, P. C.; Yu-Zhang, K. *Applied Physics Letters* **1998**, *73*, 1436-1438.
- (54) Kazeminezhad, I.; Barnes, A. C.; Holbrey, J. D.; Seddon, K. R.; Schwarzacher, W. *Applied Physics A* **2007**, *86*, 373-375.
- (55) Armand, M.; Endres, F.; MacFarlane, D. R.; Ohno, H.; Scrosati, B. *Nat Mater* **2009**, *8*, 621-629.

- (56) Al-Salman, R.; Mallet, J.; Molinari, M.; Fricoteaux, P.; Martineau, F.; Troyon, M.; El Abedin, S. Z.; Endres, F. *Physical Chemistry Chemical Physics* **2008**, *10*, 6233-6237.
- (57) Bruno, M.; Palummo, M.; Ossicini, S.; Del Sole, R. *Surface Science* **2007**, *601*, 2707-2711.
- (58) Wang, D.; Wang, Q.; Javey, A.; Tu, R.; Dai, H.; Kim, H.; McIntyre, P. C.; Krishnamohan, T.; Saraswat, K. C. *Applied Physics Letters* **2003**, *83*, 2432-2434.
- (59) Alguno, A.; Usami, N.; Ujihara, T.; Fujiwara, K.; Sazaki, G.; Nakajima, K.; Shiraki, Y. *Applied Physics Letters* **2003**, *83*, 1258-1260.
- (60) Chan, C. K.; Peng, H.; Liu, G.; McIlwrath, K.; Zhang, X. F.; Huggins, R. A.; Cui, Y. *Nat Nano* **2008**, *3*, 31-35.
- (61) Kazeminezhad, I.; Barnes, A. C.; Holbrey, J. D.; Seddon, K. R.; Schwarzacher, W. *Applied Physics A: Materials Science & Processing* **2007**, *86*, 373-375.
- (62) Al-Salman, R.; El Abedin, S. Z.; Endres, F. *Physical Chemistry Chemical Physics* **2008**, *10*, 4650-4657.
- (63) Senapati, B.; Maiti, C. K. *Solid-State Electronics* **2001**, *45*, 1905-1908.
- (64) Paul, D. J. *Thin Solid Films* **1998**, *321*, 172-180.
- (65) Behammer, D.; Albers, J. N.; Konig, U.; Temmler, D.; Knoll, D. *Solid-State Electronics* **1996**, *39*, 471-480.
- (66) Jain, S. C.; Decoutere, S.; Willander, M.; Maes, H. E. *Semiconductor Science and Technology* **2001**, *16*, R67.
- (67) Jain, S. C.; Decoutere, S.; Willander, M.; Maes, H. E. *Semiconductor Science and Technology* **2001**, *16*, R51.
- (68) Gaucher, B.; Floyd, B.; Reynolds, S.; Pfeiffer, U.; Grzyb, J.; Joseph, A.; Mina, E.; Orner, B.; Ding, H.; Wachnik, R.; Walter, K. *Semiconductor Science and Technology* **2007**, *22*, S236.
- (69) Said, K.; Poortmans, J.; Caymax, M.; Loo, R.; Daami, A.; Bremond, G.; Kruger, O.; Kittler, M. *Thin Solid Films* **1999**, *337*, 85-89.
- (70) Chern, C. H.; Tijero, J. M. G.; Wang, K. L.; Wang, S. J. *Journal of vacuum science and technology B*, **1992**, *10*, 937-939.
- (71) Rommel, S. L.; Dillon, T. E.; Dashiell, M. W.; Feng, H.; Kolodzey, J.; Berger, P. R.; Thompson, P. E.; Hobart, K. D.; Lake, R.; Seabaugh, A. C.; Klimeck, G.; Blanks, D. K. *Applied Physics Letters* **1998**, *73*, 2191-2193.

- (72) Ferland, B.; Akyuz, C. D.; Zaslavsky, A.; Sedgwick, T. O. *Physical Review B* **1996**, *53*, 994-997.
- (73) Ismail, K.; Meyerson, B. S.; Wang, P. J. *Applied Physics Letters* **1991**, *58*, 2117-2119.
- (74) Hackbarth, T.; Hoeck, G.; Herzog, H. J.; Zeuner, M. *Journal of Crystal Growth* **1999**, *201-202*, 734-738.
- (75) People, R.; Bean, J. C.; Bethea, C. G.; Sputz, S. K.; Peticolas, L. J. *Applied Physics Letters* **1992**, *61*, 1122-1124.
- (76) Tang, Y. S.; Ni, W. X.; Torres, C. M. S.; Hansson, G. V. *Electronics Letters* **1995**, *31*, 1385-1386.
- (77) Howlett, P. C.; MacFarlane, D. R.; Hollenkamp, A. F. *Electrochemical and Solid-State Letters* **2004**, *7*, A97-A101.
- (78) Geoffroy, I.; Willmann, P.; Mesfar, K.; Carre, B.; Lemordant, D. *Electrochimica Acta* **2000**, *45*, 2019-2027.
- (79) Kim, J. K.; Matic, A.; Ahn, J. H.; Jacobsson, P. *Journal of Power Sources* **2010**, *195*, 7639-7643.
- (80) Fernicola, A.; Croce, F.; Scrosati, B.; Watanabe, T.; Ohno, H. *Journal of Power Sources* **2007**, *174*, 342-348.
- (81) Sato, T.; Maruo, T.; Marukane, S.; Takagi, K. *Journal of Power Sources* **2004**, *138*, 253-261.
- (82) Lewandowski, A.; Swiderska-Mocek, A. *Journal of Power Sources* **2009**, *194*, 601-609.
- (83) Chintapalli, S.; Frech, R. *Solid State Ionics* **1996**, *86-88, Part 1*, 341-346.
- (84) Bandara, L. R. A. K.; Dissanayake, M. A. K. L.; Mellander, B. E. *Electrochimica Acta* **1998**, *43*, 1447-1451.
- (85) Shin, J.-H.; Henderson, W. A.; Passerini, S. *Journal of the Electrochemical Society* **2005**, *152*, A978-A983.
- (86) MacFarlane, D. R.; Pringle, J. M.; Johansson, K. M.; Forsyth, S. A.; Forsyth, M. *Chemical Communications* **2006**, 1905-1917.
- (87) Zhou, D.; Spinks, G. M.; Wallace, G. G.; Tiyapiboonchaiya, C.; MacFarlane, D. R.; Forsyth, M.; Sun, J. *Electrochimica Acta* **2003**, *48*, 2355-2359.
- (88) Xi, B.; Truong, V.-T.; Whitten, P.; Ding, J.; Spinks, G. M.; Wallace, G. G. *Polymer* **2006**, *47*, 7720-7725.

- (89) Barisci, J. N.; Wallace, G. G.; MacFarlane, D. R.; Baughman, R. H. *Electrochemistry Communications* **2004**, *6*, 22-27.
- (90) Liu, Y. S.; Pan, G. B. In *Ionic liquids : Applications and Perspective*; Kodorin, P. A., Ed.; InTech, **2011**.
- (91) Xi, M.; Duan, Y.; Li, X.; Qu, L.; Sun, W.; Jiao, K. *Microchimica Acta* **2010**, *170*, 53-58.
- (92) Choi, B. G.; Park, H.; Park, T. J.; Kim, D. H.; Lee, S. Y.; Hong, W. H. *Electrochemistry Communications* **2009**, *11*, 672-675.
- (93) Ren, R.; Leng, C.; Zhang, S. *Biosensors and Bioelectronics* **2010**, *25*, 2089-2094.
- (94) Salimi, A.; Lasghari, S.; Noorbakhash, A. *Electroanalysis* **2010**, *22*, 1707-1716.
- (95) Ohno, H. *Electrochemical aspects of ionic liquids*; Hoboken, N.J. Wiley-Interscience, **2005**.
- (96) Endres, F.; Zein El Abedin, S. *Physical Chemistry Chemical Physics* **2006**, *8*, 2101-2116.
- (97) Abbott, A. P.; Ryder, K. S.; Konig, U. *Transactions of the Institute of Metal Finishing* **2008**, *86*, 196-204.
- (98) Abbott, A. P.; Capper, G.; Davies, D. L.; Munro, H. L.; Rasheed, R. K.; Tambyrajah, V. *Chemical Communications* **2001**, 2010-2011.
- (99) Abbott, A. P.; Capper, G.; Davies, D. L.; Rasheed, R. *Inorganic Chemistry* **2004**, *43*, 3447-3452.
- (100) Abbott, A. P.; Capper, G.; Davies, D. L.; Rasheed, R. K.; Tambyrajah, V. *Transactions of the Institute of Metal Finishing* **2001**, *79*, 204-206.
- (101) Chen, P. Y.; Lin, M. C.; Sun, I. W. *Journal of the Electrochemical Society* **2000**, *147*, 3350-3355.
- (102) Golding, J.; Forsyth, S.; MacFarlane, D. R.; Forsyth, M.; Deacon, G. B. *Green Chemistry* **2002**, *4*, 223-229.
- (103) Sitze, M. S.; Schreiter, E. R.; Patterson, E. V.; Freeman, R. G. *Inorganic Chemistry* **2001**, *40*, 2298-2304.
- (104) Wilkes John, S. In *Ionic Liquids*; American Chemical Society, **2002**; Vol. 818.
- (105) Yang, J. Z.; Jin, Y.; Xu, W. G.; Zhang, Q. G.; Zang, S. L. *Fluid Phase Equilibria* **2005**, *227*, 41-46.
- (106) Abbott, A. P.; Capper, G.; Davies, D. L.; Rasheed, R. K. *Chemistry-a European Journal* **2004**, *10*, 3769-3774.

- (107) Abbott, A. P.; Capper, G.; Davies, D. L.; Rasheed, R. K.; Tambyrajah, V. *Chemical Communications* **2003**, 70-71.
- (108) Abbott, A. P.; Boothby, D.; Capper, G.; Davies, D. L.; Rasheed, R. K. *Journal of the American Chemical Society* **2004**, *126*, 9142-9147.
- (109) Heerman, L.; Dolieslager, W. *Inorganic Chemistry* **1985**, *24*, 4704-4707.
- (110) Abbott, A. P.; Capper, G.; Davies, D. L.; Rasheed, R. K.; Archer, J.; John, C. *Transactions of the Institute of Metal Finishing* **2004**, *82*, 14-17.
- (111) Haerens, K. Ph.D thesis, Katholieke Universiteit Leuven, **2011**.
- (112) Iwagishi, T.; Yamamoto, H.; Koyama, K.; Shirai, H.; H.Kobayashi; *Electrochemistry*, **2002**, *70*, 671-674.
- (113) Koyama, K.; Iwagishi, T.; Yamamoto, H.; Shirai, H.; Kobayashi, H. *Electrochemistry*, **2002**, *70*, 178.
- (114) Abbott, A. P.; Capper, G.; McKenzie, K. J.; Ryder, K. S. *Journal of Electroanalytical Chemistry* **2007**, *599*, 288-294.
- (115) Bakkar, A.; Neubert, V. *Electrochemistry Communications* **2007**, *9*, 2428-2435.
- (116) Abbott, A. P.; El Ttaib, K.; Ryder, K. S.; Smith, E. L. *Transactions of the Institute of Metal Finishing* **2008**, *86*, 234-240.
- (117) Abbott, A. P.; El Ttaib, K.; Frisch, G.; McKenzie, K. J.; Ryder, K. S. *Physical Chemistry Chemical Physics* **2009**, *11*, 4269-4277.
- (118) Abbott, A. P.; Griffith, J.; Nandhra, S.; O'Connor, C.; Postlethwaite, S.; Ryder, K. S.; Smith, E. L. *Surface and Coatings Technology* **2008**, *202*, 2033-2039.
- (119) Smith, E. L.; Abbott Andrew, P.; Griffith, J.; Harris, R. C.; O'Connor, C.; Ryder, K. S. *Circuit World*, **2010**, *36*, 3-9.
- (120) Zhao, Y.; VanderNoot, T. J. *Electrochimica Acta* **1997**, *42*, 1639-1643.
- (121) Abbott, A. P.; Capper, G.; Swain, B. G.; Wheeler, D. A. *Transactions of the Institute of Metal Finishing* **2005**, *83*, 51-53.
- (122) Lee, S. J.; Lai, J. J. *Journal of Materials Processing Technology* **2003**, *140*, 206-210.
- (123) Abbott, A. P.; Capper, G.; McKenzie, K. J.; Ryder, K. S. *Electrochimica Acta* **2006**, *51*, 4420-4425.

| | | |
|--------------------|--|-----------|
| Chapter 2 : | Experimental Procedures | 36 |
| 2.1 | Materials | 37 |
| 2.2 | Stainless steel samples | 37 |
| 2.3 | Preparation of solutions | 38 |
| | 2.3.1 <i>Deep Eutectic solvents</i> | 38 |
| | 2.3.2 <i>Oxalic acid solution</i> | 38 |
| 2.4 | Physical properties | 38 |
| | 2.4.1 <i>Viscosity measurements</i> | 38 |
| | 2.4.2 <i>Surface tension measurements</i> | 39 |
| | 2.4.3 <i>Density measurements</i> | 39 |
| | 2.4.4 <i>Conductivity measurements</i> | 39 |
| 2.5 | Electrochemical study | 39 |
| | 2.5.1 <i>Linear sweep polarization curves</i> | 39 |
| | 2.5.2 <i>Potential step experiments</i> | 40 |
| | 2.5.3 <i>Galvanostatic measurements</i> | 40 |
| | 2.5.4 <i>Electropolishing</i> | 40 |
| | 2.5.5 <i>Open circuit potential (OCP) measurements</i> | 40 |
| | 2.5.6 <i>Anodic polarization curves (corrosion curves)</i> | 41 |
| 2.6 | Surface analysis | 41 |
| | 2.6.1 <i>AFM</i> | 41 |
| | 2.6.2 <i>SEM and EDAX</i> | 41 |
| | 2.6.3 <i>DHM</i> | 41 |
| 2.7 | Analysis of Data | 42 |
| | 2.7.1 <i>Electrochemical data</i> | 42 |
| 2.8 | Scanning electron microscope (SEM) | 42 |
| | 2.8.1 <i>Working of SEM</i> | 42 |
| | 2.8.2 <i>Everhart thornley detector</i> | 43 |
| | 2.8.3 <i>X-rays detectors</i> | 44 |
| 2.9 | Atomic force microscope (AFM) | 45 |
| | 2.9.1 <i>Modes of operation</i> | 46 |
| 2.10 | Digital holographic microscope (DHM) | 47 |
| | 2.10.1 <i>Working of DHM</i> | 49 |
| | 2.10.2 <i>Reconstruction of hologram</i> | 50 |
| | 2.10.3 <i>Phase images</i> | 50 |
| 2.11 | References | 51 |

This chapter contains the standard experimental conditions and protocols used throughout this thesis. The working principle and underlying theories of surface characterization techniques scanning electron microscope, atomic force microscope and digital holographic microscope are briefly described.

2.1 Materials

| Table 2.1: | | <i>List of compounds used in the project. All the chemicals were used as obtained.</i> | |
|-------------------------|--|--|--------------------------------------|
| Compound | Abbreviation | Molecular Weight | Purity |
| Choline chloride (ChCl) | $\text{HOC}_2\text{H}_4\text{N}(\text{CH}_3)^+\text{Cl}^-$ | 139.63 | Aldrich, >98% |
| Ethylene glycol (EG) | $\text{C}_2\text{H}_4(\text{OH})_2$ | 62.07 | Aldrich, >99% |
| Oxalic acid (OA) | $\text{HO}_2\text{CCO}_2\text{H}$ | 90.03 | Aldrich, >99% |
| Iron (III) chloride | $\text{FeCl}_3 \cdot 6\text{H}_2\text{O}$ | 270.3 | Aldrich, >98% |
| Nickel (II) chloride | NiCl_2 | 129.60 | Aldrich, >98% |
| Chromium (III) chloride | $\text{CrCl}_3 \cdot 6\text{H}_2\text{O}$ | 266.45 | Aldrich, >96% |
| Sodium chloride | NaCl | 58.44 | Aldrich, >99.5% |
| Sulphuric acid | H_2SO_4 | 98.08 | ACS reagent, 98% |
| Phosphoric acid | H_3PO_4 | 98 | Aldrich, 85% in H_2O |

2.2 Stainless steel samples

Austenitic stainless steel ss304 and ss316 used in this study were obtained from ABS metals Ltd. Tregonigge Estate, Falmouth, Cornwall UK. The samples ss316 and ss304 obtained in the form of sheets (100 mm x 150 mm x 1 mm) from the supplier were further cut into pieces of 20 x 50 mm for electropolishing. The ss 316 tubes ((25 mm OD x 6 mm wall) x 120 mm) were further cut into pieces of length 30 mm for electropolishing. The grades ss304 and ss316 were selected due to their versatility and in a wide variety of home and commercial applications ranging from food, dairy, pharmaceutical, cryogenic, chemical industries, cookware, sinks, table tops and architectural applications because of their durability, excellent resistance to oxidation and corrosion and immunity from sensitisation (grain boundary carbide precipitates). The typical composition of these grades is tabulated in **Table 2.2**. The addition of molybdenum

and higher nickel contents give ss316 greater corrosion resistance in many aggressive environments than ss304.

| Table 2.2 | | <i>Chemical composition of ss304 and ss316</i> | | | | | | |
|------------------|-------------|--|-------------|-------------|------------|------------|-------------|------------|
| Grade | Cr % | Ni % | Mn % | Mo % | C % | S % | Si % | P % |
| ss304 | 18 - 20 | 8 - 10 | 2 max | - | 0.08 max | 0.03 max | 1 max | 0.045 max |
| ss316 | 16 - 18 | 10 - 14 | 2 max | 2 -3 | 0.08 max | 0.03 max | 1 max | 0.045 max |

2.3 Preparation of solutions

2.3.1 Deep eutectic solvents

The ionic liquids used in this study was 1:2 ChCl:EG. The H-bond donor for the complex anions of the liquid was ethylene glycol (EG). The deep eutectic mixtures were formed by continuous stirring of the two components at 60°C until a homogeneous, colourless liquid was formed.

2.3.2 Oxalic acid solution

Oxalic acid solution 3% W/V was prepared by dissolving 3 grams of anhydrous oxalic acid in 1:2 ChCl:EG at 50°C.

2.4 Physical properties

The physical properties of 1:2 ChCl:EG i.e conductivity, viscosity, surface tension and density were measured.

2.4.1 Viscosity measurements

The viscosity of eutectic mixtures was measured using a Brookfield DV-E Viscometer fitted with a thermostated jacket. The viscometer jacket was connected to a thermostated water bath. The readings were taken at different temperatures ranging from 25 to 50 °C with an increment of 5 °C after 15-20 min. The measurements were conducted using the spindle attachment and spindles S61 was used for viscosity measurements of 1:2 ChCl:EG.

2.4.2 Surface tension measurements

The surface tension of 1:2 ChCl:EG was measured using a Kruss Tensiometer K9 with a platinum plate. The plate was thoroughly washed with deionised water followed by heating to red heat in a Bunsen flame to ensure the removal of any adherent material and then cooled to room temperature. Readings were taken at 25 °C.

2.4.3 Density measurements

The density of the system was also measured on the Kruss Tensiometer K9 using the density probe. The density probe was submerged into the liquid for 5 minutes so that the apparatus reach equilibrium and then the reading on the tentiometer was taken at 25 °C.

2.4.4 Conductivity measurements

The conductivity of 1:2 ChCl:EG was measured using a Jenway 4071 conductivity meter probe. The conductivity values were measured at temperatures ranging from 25 to 70 °C with an increment of 10 °C. The temperature was controlled by using the jacket connected to the water bath. Readings were taken after 25-30 min. for each temperature to ensure good equilibration of temperature between the water bath and the sample.

2.5 Electrochemical Study

All electrochemical procedures e.g. linear sweep voltammetry, galvanometry and chronoamperometry were carried out using an Autolab PGSTAT20 potentiostat (Ecochemie, Holland) controlled by GPES software. A 3-electrode system consisting of a working electrode, counter electrode (platinum flag; area 2cm²) and pseudo-reference electrode (silver wire or Ag/AgCl) was used. The working electrode was first washed with soap to remove the dirt and grease and then mechanically polished with 600 grit silicon carbide paper followed by rinsing with deionised water and dried before each measurement. The measurements were carried out at 30 °C or otherwise mentioned.

2.5.1 Linear sweep polarization curves

Linear sweep anodizing curves were conducted in the potential window of -0.3 to +3 V, at scan rate 1, 2, 5, 10, 20 mVs⁻¹. The sweep potential was initiated at -0.3 V and proceeded in the positive direction. Each time a fresh ss304 coupon with an area of 0.5 cm² was used as was fresh electrolyte (1:2 ChCl:EG).

2.5.2 Potential step experiments

The chronoamperometric data have been obtained by stepping the potential of the austenitic steel (1 cm^2) working electrode from (0 V) to sufficiently positive values (0.7, 1.4, 2.3 V) in different regions of the anodic polarization curve against the silver wire quasi reference. Each experiment was conducted with a fresh piece of austenitic steel (ss304) as the working electrode. The working electrode was degreased and mechanically polished with 600 grit silicon carbide paper. The experiments were conducted in fresh electrolytes every time to avoid the effect of the dissolved metals.

2.5.3 Galvanostatic measurements

The galvanostatic study was conducted at current densities of 2, 10, 25 and 50 mA cm^{-2} at 30°C . Fresh ss304 sheet having an area of 1 cm^2 and fresh electrolyte (40 ml) was used everytime.

2.5.4 Electropolishing

Electropolishing of stainless steel coupons (ss304 & ss316) was conducted both potentiostatically and galvanostatically in 1:2 ChCl:EG containing oxalic acid (3% W/V). Electropolishing of steel samples was carried out using a two electrode assembly using the Thurbly Thander instrument (TTi) EX355P power supply. Carbon mesh was used as the cathode and electropolishing was conducted at 40°C . The steel samples were pre-treated (degreased and pickled) prior to electropolishing. After electropolishing, the samples were removed from the electrolyte, rinsed with tap water and washed on ultrasonic bath at 30°C in deionised water for ten minutes and then dried under air.

2.5.5 Open circuit potential (OCP) measurements

Open circuit potential measurements of unpolished and electropolished ss304 and ss316 for varying time periods (5, 10, 20, 30 minutes) were carried out in aqueous sodium chloride (3%), diluted sulphuric acid (2%), tap water, 1:2 ChCl:EG and 1:2 ChCl:EG with oxalic acid as an additive for 14 hours using an Autolab PGSTAT20 potentiostat (Ecochemie, Holland) controlled by GPES software. Ag/AgCl was used as the reference electrode in aqueous solutions while Ag wire quasi electrode was used as the reference in deep eutectic solvent.

2.5.6 Anodic polarization curves (corrosion curves)

Potentiodynamic polarization experiments were conducted in NaCl (3%), H₂SO₄ (2%) and aerated tap water. The potentiodynamic curves of unpolished and electropolished samples of ss304 were measured against Ag / AgCl after immersion for 30 minutes using an Autolab PGSTAT20 potentiostat (Ecochemie, Holland). The anodic polarization curves were obtained by scanning the potential at 5 mV sec⁻¹ in the potential range of -1.5 V to +1 V with an exposed area of 0.5 cm² of working electrode (ss304) in 100 ml of electrolyte each time.

2.6 Surface Analysis

The surface analysis involving the topography, morphology, surface roughness and chemical composition of the unpolished and electropolished samples were carried out using a digital holographic microscope (DHM), atomic force microscope (AFM) and scanning electron microscope (SEM).

2.6.1 AFM

Atomic force micrographs were acquired using a Digital Instrument (DI) Nanoscope IV, Dimension 3100 instrument using resonant tapping mode and the controlling software was nanoscope version 6.13.

2.6.2 SEM and EDAX

Surface analysis with SEM and elemental analysis by EDAX were carried out using a Phillips XL30 ESEM instrument with an accelerating voltage between 20 and 25 keV, giving an average beam current of ca. 120 μA.

2.6.3 DHM

A digital holographic microscope of R1000 series Lyncee Tec SA controlled by Koala V4 software was used.

A brief description of principle and operation of these techniques is given in sections 2.8, 2.9 and 2.10.

2.7 Analysis of data

2.7.1 Electrochemical data

The peak analysis of the anodic polarization curves, current time transients, potential time transients, rate of corrosion and Tafel fitting of the corrosion curves was performed by using the GPES software version 4.95.

2.8 Scanning electron microscope (SEM)

A scanning electron microscope produces strikingly clear images of a sample by scanning over it with a focused beam of high energy electrons scanned in a raster pattern. The incident electrons interact with electrons in the sample, producing secondary electrons, back scattered electrons and characteristic X-ray that reveal information about the topography, chemical composition, crystal structure and orientation of the building material of the sample. The first SEM image was obtained by Max Knoll in 1935 while the first SEM was marketed as 'Stereoscan' by Cambridge Scientific Instrument Company in 1965.

SEM has the following advantages over traditional optical microscopes

- Large depth of field – enables to focus more of the sample at one time.
- Higher resolution (spatial resolution of 50 – 100 nm) – enables to magnify clearly packed specimens to higher levels.
- Electromagnets – give much control in the degree of magnifications (ranging from 20X to 30,000X)

Limitations of SEM

- SEM requires a vacuum for imaging to avoid the interference of electrons with air particles.
- Samples should be conducting to avoid the accumulation of charge on the surface, non conducting samples are coated with the ultra thin coating of metal.

2.8.1 Working of SEM

In a typical SEM, an electron beam having energy in the range of 0.2 keV to 40 keV is emitted either by thermionic gun (under applied thermal energy usually a tungsten filament) or field emission gun (under applied strong electrical field) located either at the

top or at the very bottom of the SEM. The emitted electron beam is focused by one or two condenser lenses (made of magnets) to a spot about 0.4 nm to 5 nm in diameter. After passing through pairs of scanning coils or pairs of deflector plates in the electron column, the electron beam is deflected in the x and y axes i.e. in a raster fashion over a rectangular area of the sample by the final lens and schematic representation of the working of SEM is shown in **Figure 2.1**.

The interaction of the primary electrons (incident beam) with the sample electrons results in (i) the reflection of high energy electrons by elastic scattering which gives insight into the spatial distribution and orientation of different elements in the sample (ii) emission of secondary electrons by inelastic scattering gives information about the surface morphology and topography. (iii) electromagnetic radiation (x-rays) produced as a result of the relaxation of excited electrons from higher orbitals to lower orbitals gives information about the chemical composition of the samples.

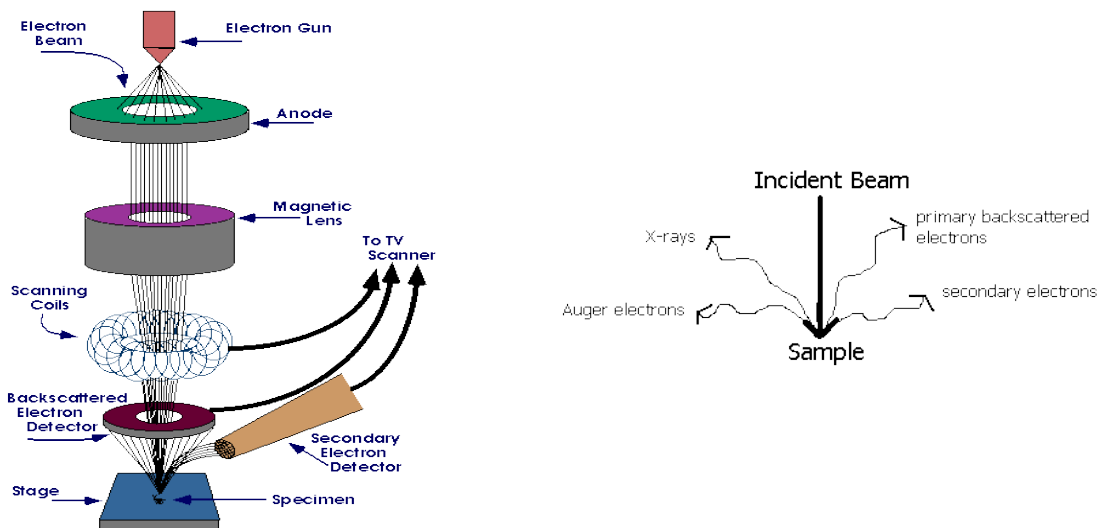


Figure 2.1: Working of the scanning electron microscope¹

2.8.2 Everhart thornley detector

It is used to detect the low energy secondary electrons produced as a result of interaction of incident electrons with the sample and is positioned at one side of the specimen and **Figure 2.2** shows the schematic representation of its working. The secondary electrons are collected by a collector grid biased from -50 to +300 V and draws electrons towards the scintillator coated with phosphor which converts the electron energy to light energy. The outer layer of the scintillator is coated with a thin layer of aluminium which is biased at

approximately 10 KeV and it accelerates the electrons towards the scintillator and also reflects the photons produced down the light pipe consisting of Plexiglas or polished quartz. The emitted photons are converted into electronic signals by photocathode and photomultiplier tube. Electronic amplifiers of various types are used to amplify the signals which are displayed as variation in brightness on a computer monitor. Each pixel of the computer video memory is synchronised with the position of the beam on the specimen in the microscope and the resulting image is therefore a distribution map of the intensity of the signal being emitted from the scanned area of the specimen.

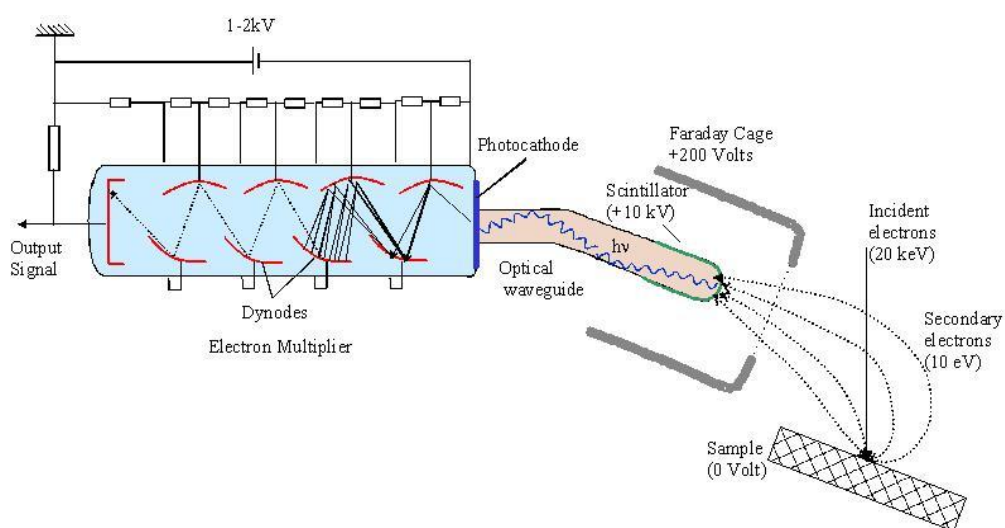


Figure 2.2: *Everhart – Thornley detector for secondary electrons²*

Back scattered electrons are collected by detectors which are either scintillators or of semiconductor type and positioned above the sample concentric with the incident electron beam. A negative potential is applied on the collector to filter the back scattered electrons from the secondary electrons.

2.8.3 X-ray detectors

It is composed of a thin silicon crystal doped with lithium and the central intrinsic region is sandwiched between a thin p-type layer and thin n-type layer. Thin gold electrodes are deposited on both crystal surfaces and a potential is applied to make the p-i-n junction reversed biased. A large number of electrons and holes in the Si(Li) region are produced as a result of X-ray photon hitting the detector. A pulse of current is produced by accelerating the electrons to the positive side and holes to the negative side and its magnitude is proportional to the X-ray energy.

Each current pulse is analysed to determine the energy of incident photons and the photons count is stored in one channel of a multichannel analyzer for a predetermined time and the number of accumulated X-rays counts constitute an X-ray spectrum.

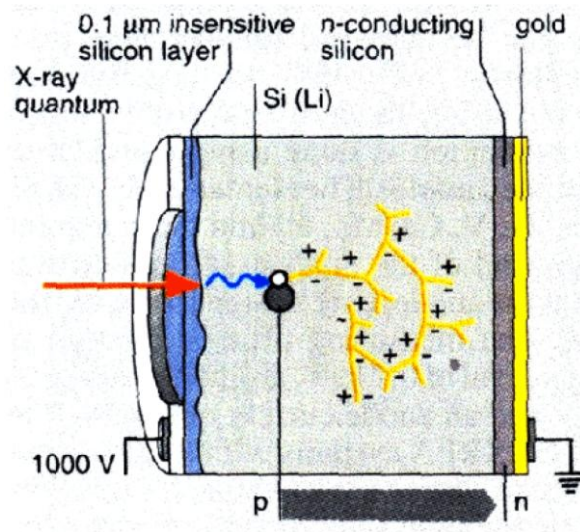


Figure 2.3: *Electron dispersive X-ray spectrometer³*

2.9 Atomic force microscope (AFM)

Atomic force microscopy is a very high resolution scanning probe microscopy and is one of the foremost tools for imaging, measuring and manipulating matter of the order of a fraction of a nanometer. The lateral resolution of AFM is low (~30 nm) due to convolution while the vertical resolution can be up to 0.1 nm. The working principle of AFM is similar to that of a scanning tunnel microscope (STM) and earlier stylus profiler devices. It was invented in 1986 by Binnig, Quate and Gerber at the IBM Zurich Research laboratory while the first commercial AFM was introduced in 1989. The advantage of the AFM over the STM is that it can be used for the imaging of any type of surface including polymers, ceramics, composites, glass and biological samples. A block diagram of AFM is shown in **Figure 2.4**.

AFM images the surface by ‘feeling’ the surface with mechanical probe. The probe consists of typically a silicon or silicon nitride cantilever with a sharp tip which is a 3-6 μm tall pyramid usually having a radius of curvature of the order of 15 – 40 nm. Accurate and precise movement of the tip is controlled by piezoelectric elements.

The deflection of the tip is measured using a laser spot reflected from the top surface of the cantilever into an array of photodiodes which control through the feedback mechanism of the piezoelectric elements. As the tip is brought into the close proximity of the sample surface, the forces that may be mechanical contact force, van der Waals forces or electrostatic forces between the tip and sample are measured. These forces result in vertical and lateral deflection of the cantilever according to Hook's law. The deflection of the tip is measured by an optical lever. A laser spot is reflected from the top surface of the cantilever into a position sensitive detector - an array of photodiodes (usually four) which control the z movement of the tip through the feedback mechanism of the piezoelectric elements.

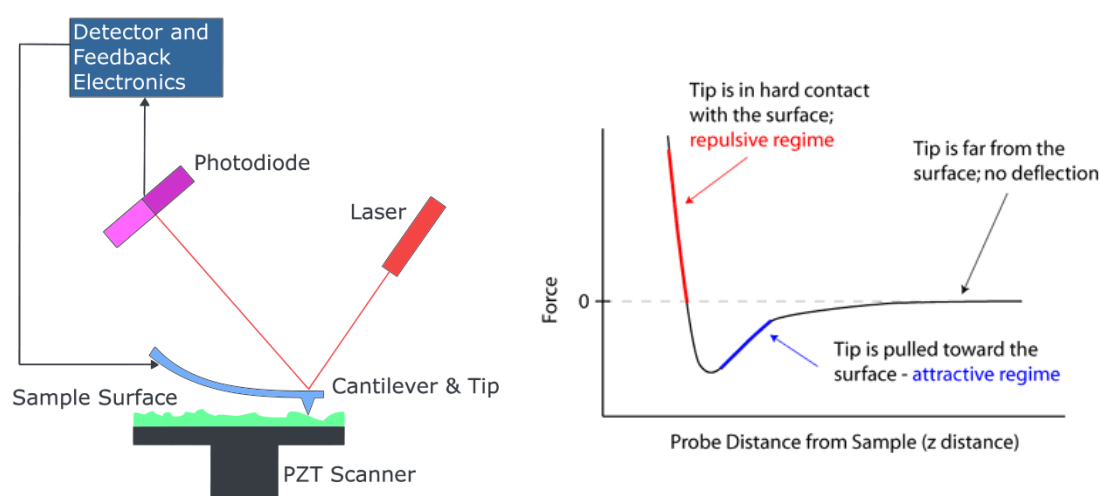


Figure 2.4: *Block diagram of Atomic Force Microscope⁴*

The feedback loop consists of the tube scanner that controls the height of the tip, the cantilever and the optical lever. A feedback circuit attempts to keep the height of the cantilever constant by adjusting the applied voltage.

2.9.1 Modes of operation

AFM can be operated in both static and dynamic mode. In static mode the stationary cantilever is moved across the sample surface and the contours of the surface are measured directly using the deflection of the cantilever. In dynamic mode of operation, the cantilever oscillates at or close to its fundamental resonance frequency. The tip and sample interaction forces modify the amplitude, phase and resonance frequency of cantilever and the changes in oscillation provide information about the surface of the sample.

In contact mode of operation, the static tip deflection is used as a feedback signal. The contact mode is always done in the regime of repulsive force to avoid the 'snap in' of the tip to the surface as a result of the attractive force due to close proximity to the sample surface. Cantilevers of low stiffness are used to avoid the noise and drift in measuring of the signal.

In non contact mode, the tip of the cantilever is not in contact with the sample surface but instead it oscillates at slightly above its resonant frequency, typically the amplitude of oscillation is a few nanometres (< 10 nm). The van der Waals forces or any other long range force that extends above the surface, changes the oscillation amplitude of the cantilever. The change in oscillation amplitude combined with the feedback loop system maintains the constant distance between the tip and the sample surface. The measurement of the tip to sample surface distance at each point (x, y) constructs the topographic images of the sample surface. Non contact mode does not suffer from tip or sample degradation effects and also enables for measuring soft samples.

In tapping mode, also known as 'intermittent contact mode' the cantilever is driven to oscillate up and down at near its resonance frequency with amplitude of typically in the range of 100 – 200 nm by a small piezoelectric element mounted in the AFM tip holder similar to non contact mode. The interaction of forces like van der Waals force, dipole - dipole interaction or electrostatic forces. cause the change in the amplitude of oscillation. An electronic servo uses the piezoelectric actuator to control the constant height of the cantilever above the surface. In tapping mode the topographic image of the surface is produced by measuring the force of the intermittent contacts of the tip with the sample surface⁴.

2.10 Digital holographic microscope (DHM)

Digital Holographic Microscopy is a fast, non-destructive and non-contact surface metrology technique which allows high frequency measurements at interferometric resolution and provides quantitative phase contrast imaging. DHM has the following advantages (i) Quantitative 3D information (ii) Nanometric vertical resolution (iii) Non invasive and non contact measurement (iv) Rapid acquisition (v) Ease of use (vi) Robustness and stability

Light interaction with a sample modifies two fundamental characteristics, intensity and phase of the illuminating wave. The detector, usually a camera, is only sensitive to the intensity of the light therefore a part of the information carried by the light is lost. Gabor invented in 1948 a way to encode the phase modifications as an intensity variation: the “hologram”⁵.

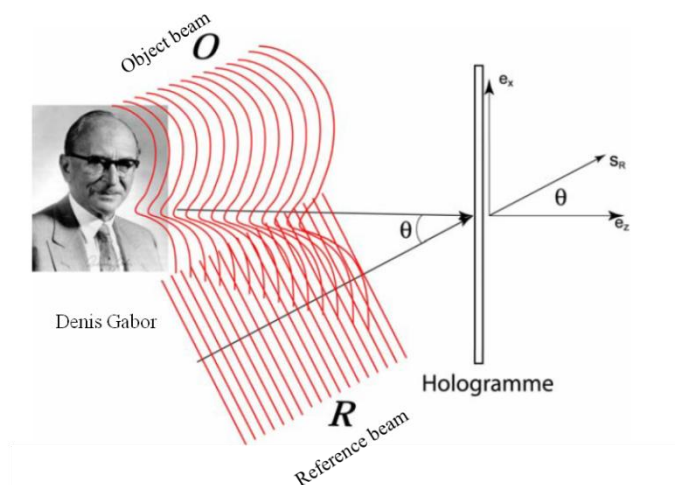


Figure 2.5: Principle of the formation of a hologram using off axis

DHM uses the principle of classical holography.^{5, 7, 8} **Figure 2.5** shows the principle of formation of hologram. Holograms are generated by combining a coherent reference wave with the wave received from a specimen that compresses complete 3D information of the object. The holograms are recorded by a video camera and transmitted to a computer for real time numerical reconstruction. DHM software allows computation by numerical algorithms by a computer⁹ of the complete wave front emanating from an object. The reconstruction of a digital hologram gives two images (i) amplitude of light (intensity images) with the same contrast as classical optical microscopy. (ii) phase changes of light (phase images) provide quantitative data used for accurate and stable measurements and reveal the object surface with vertical resolution below 1° of the wave phase (the nanometre scale for homogeneous samples). In reflection, the phase image reveals directly the surface topography with a sub nanometre vertical resolution. In transmission, the phase image reveals the phase shift induced by a transparent specimen that depends on its thickness and refractive index.

The strength of DHM lies in off-axis configuration by which the whole information about the surface can be retrieved by a single image acquisition ‘hologram’ within a few micron seconds. The extremely short acquisition time makes the system insensitive to the vibrations and ambient light, hence very stable and robust. DHM can be used for shape and surface characterization of high aspect ratio micro optics, surface nanostructures and surface roughness.

2.10.1 Working of DHM

A basic digital holographic microscopy setup consists of an illumination source, an interferometer, a digitizing camera and a computer with necessary program. Usually a laser is used as an illumination source (HeNe lasers, diode lasers, double YAG laser, argon laser, tuneable dye lasers). In multiwavelength techniques, two or more different lasers can be coupled into the interferometer. The optical setup, the Michelson interferometer and Mach-Zehnder interferometer are used for reflective and transmission DHM respectively. The Michelson interferometer is shown in **Figure 2.6**.

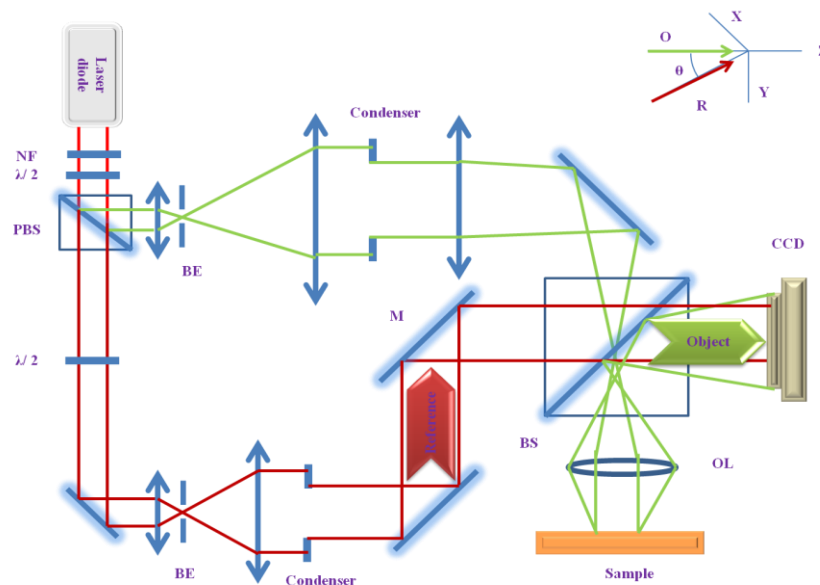


Figure 2.6: *The Michelson interferometer for reflective digital holographic microscope¹⁰*

The collimated source beam (from a laser diode) is separated into two coherent beams with slightly different propagation directions (i) a ‘reference beam’ and (ii) an ‘object beam’ with the polarization separator. The object beam illuminates the sample via the condenser and mirrors and the retro-diffused beam is collected by objective of the microscope. The objective and reference beams are recombined to generate the ‘hologram’. There are a few

degrees (angle θ) between the reference (R) and the object beams (O). This off axis configuration enables the reconstruction of information using a single hologram acquisition while on-axis holography (i.e. $\theta = 0$) requires acquisition of several holograms.

2.10.2 Reconstruction of Hologram

The reconstruction of the hologram involves ‘apodization’, removal of ‘zeroth order’ and the ‘twin’ images by the process filtration in the Fourier plane. The resulting hologram is multiplied by a digital reference wave ‘ R_D ’ that simulates an illumination wave and a propagation calculation in the Fresnel approximation is applied to reconstruct a focused image of the specimen.

2.10.3 Phase images

Figure 2.7 illustrates the principle of phase measurement by a DHM configured in reflection. The homogeneous reflective sample is lit by a monochromatic plane wave of wavelength (λ). The deformation of the reflected wave is measured in degrees of dephasing ($\Delta\varphi$) and directly connected to the 3D topology of the sample by

$$\Delta h = \frac{\lambda \Delta\varphi}{4\pi n} \quad (2.1)$$

where ‘ Δh ’ is the height of the sample and ‘ n ’ is the refractive index of the immersion medium ($n = 1$ in air, 1.33 in water).

For non-homogeneous samples the physical characteristics of the surface must be taken into account when calculating its height as a function of dephasing during reflection. However, a DHM does not measure the real dephasing but the modulo 2π

$$\varphi_{DHM} = \left[\frac{\Delta h 2\pi (n_2 - n_1)}{\lambda} \right] \text{Mod} 2\pi \quad (2.2)$$

This is a representation that is similar to that of the topography as described by the contour lines on a geographic map. In this case the equidistance is 360° (2π), where :

$$\text{equidistance} = \frac{\lambda}{(n_2 - n_1)} \quad (2.3)$$

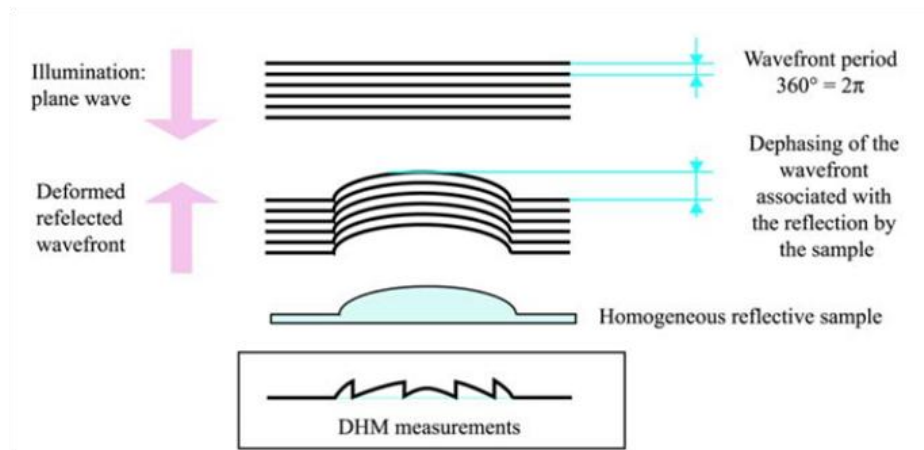


Figure 2.7: Principle of phase measurements by DHM in reflection mode.⁶

2.11 References

1. J. Schweitzer, <http://www.purdue.edu/rem/rs/sem.htm>, Accessed 02/10/2012.
2. E. d. Chambost, http://upload.wikimedia.org/wikipedia/commons/0/09/Everhart-Thornley_detector.JPG, Accessed 07/12/2012, 2012.
3. R. E. Lee, *Scanning electron microscopy and X-rays microanalysis*, Prentice Hall, **1993**.
4. N. A. Geisse, *Materials Today*, **2009**, 12, 40-45.
5. D. Gabor, *Nature (London)*, **1948**, 161, 777.
6. *DHM 1000 Family - User Operating Manual*, Lyncee tec.
7. M. Wolfke, *Phys. Zeits.*, **1920**, 21, 495.
8. D. Gabor, *Proceedings of the Royal Society*, **1949**, 197, 454.
9. E. Cucho, F. Bevilacqua and C. Depeursinge, *Opt. Lett.*, **1999**, 24, 291-293.
10. Florian Charriere, J. Kuhn, T. Colomb, F. Montfort and E. Cucho, *Applied Optics*, **2006**, 45, 829.

| | | |
|-------------------------------|---|-----------|
| Chapter 3 : | Electropolishing of Austenitic Steel in Deep Eutectic Solvent | 52 |
| 3.1 | Introduction | 53 |
| | 3.1.1 <i>Electropolishing</i> | 54 |
| | 3.1.1.1 <i>Electropolishing Process</i> | 54 |
| | 3.1.2 <i>Mechanism of Electropolishing</i> | 56 |
| | 3.1.2.1 <i>Duplex salt film model</i> | 56 |
| | 3.1.2.2 <i>Adsorbate acceptor mechanism</i> | 57 |
| | 3.1.2.3 <i>Preferential adsorption of shielding molecules</i> | 58 |
| Results and Discussion | | |
| 3.2 | Physical Properties of 1:2ChCl:EG | 61 |
| | 3.2.1 <i>Viscosity and conductivity</i> | 61 |
| | 3.2.2 <i>Surface tension</i> | 63 |
| 3.3 | Life Cycle Studies | 65 |
| | 3.3.1 <i>Drag out</i> | 65 |
| | 3.3.2 <i>Characteristics of electropolishing solution</i> | 66 |
| | 3.3.2.1 <i>Appearance of solution</i> | 67 |
| | 3.3.2.2 <i>Concentration of metal ions</i> | 68 |
| | 3.3.2.3 <i>De-alloying effect</i> | 69 |
| | 3.3.3 <i>Electrochemical Studies</i> | 71 |
| | 3.3.3.1 <i>Variation of potential and current</i> | 71 |
| | 3.3.3.2 <i>Weight loss</i> | 72 |
| | 3.3.4 <i>Recycling of liquid</i> | 73 |
| 3.4 | Electrochemistry | 75 |
| | 3.4.1 <i>Potentiodynamic study</i> | 75 |
| | 3.4.1.1 <i>Electrochemical window of 1:2 ChCl:EG</i> | 75 |
| | 3.4.1.2 <i>Anodic linear sweep voltammetry</i> | 76 |
| | 3.4.1.3 <i>Effect of scan rate</i> | 78 |
| | 3.4.1.4 <i>Effect of temperature</i> | 79 |
| | 3.4.1.5 <i>Effect of additives</i> | 80 |
| | 3.4.2 <i>Chronoamperometry</i> | 81 |
| | 3.4.2.1 <i>Effect of temperature</i> | 82 |
| | 3.4.2.2 <i>Effect of additives</i> | 84 |
| | 3.4.3 <i>Galvanostatic study</i> | 85 |
| 3.5 | Optimization of electropolishing process – Experimental design strategies | 86 |
| | 3.5.1 <i>Fractional Factorial Design (FFD)</i> | 88 |
| | 3.5.2 <i>Contour plot</i> | 94 |
| | 3.5.3 <i>The steepest ascent path</i> | 95 |
| 3.6 | Summary | 97 |
| 3.7 | References | 98 |

3.1 Introduction

Surface finishing has been utilized as the main technique for enhancing or changing a substrate's appearance and / or attributes such as abrasion and wear resistance, corrosion protection, lubricity, improvement of aesthetic qualities for a surface lacking that property¹. It is the subject of significant interest in modern electrochemistry due to its technological importance, particularly for the coatings and microelectronics industries, mainly for corrosion protection and to produce integrated circuitry.

Corrosion and cavitation erosion are the common problems in engineering parts made of stainless steel when they come in contact with a liquid. As corrosion and cavitation occurs at the solid: liquid interface, therefore the properties of the surface layer are more important than the bulk material to prevent the corrosion and cavitation erosion of a solid. The most important surface property that contributes to these problems is the surface roughness. Therefore surface modification is the most important tool to combat these problems. Surface modification techniques have immense attractions in engineering applications as they only consume a small amount of precious materials on the surface while retaining the bulk properties of the treated parts. These techniques are cost effective and at the same time provide combinations of surface and bulk properties which may be tailored for specific purposes.

Various techniques and materials have been used to improve the surface properties of the engineering materials made of stainless steel to increase their resistance to corrosion over the past two decades. In the conventional regime, techniques including nitriding², carbonitriding, hard chromium coating, electroless nickel coating³, electroplating⁴, ion implantation^{5,6}, ion-plating⁷, explosive welding⁸, thermal spraying^{9,10}, chemical vapour deposition¹¹, diamond-like coating¹², laser surface melting (LSM) of iron and steel^{13,14}, bronze¹⁵ etc, have been attempted with varying degrees of success.

Although these techniques prove to be very effective in achieving the desired improvement, some of them suffer from several limitations in engineering applications. In ion plating, ion implantation and chemical vapour deposition, a vacuum or controlled atmosphere is required. Therefore bulky engineering parts like turbines are difficult to process by these methods. Welding, on the other hand, would induce a large heat-affected zone and thus change the microstructure and properties of the treated part in an undesirable way. Mechanical polishing may result in surface hardening, inducing a degree of residual tension and oxide incorporation, introducing scratch marks and damaged layers¹⁶.

3.1.1 Electropolishing

Electropolishing is the electrochemical dissolution (ECM) based on the controlled dissolution of a metal surface around 20 to 40 microns approximately, which removes not only the deformed layer, optimize corrosion resistance by reduction in surface roughness, increase optical reflectivity and also forms a very effective, thin chemically homogeneous passive film on the surface. Other metals like copper, nickel and titanium and high strength and high melting point alloys can also be electropolished but majority of the research has been conducted on stainless steel. Major benefits of electropolishing are; (1) Improvement of corrosion resistance (2) Improvement of surface reflectivity (3) Removal of machining burrs (4) Improved surface cleansability compared to mechanically finished surfaces (5) Lower rate of bacterial growth in food industry applications (6) Lower surface stresses in machined components. (7) Removal of deformations in metallic surfaces e.g. non metallic inclusions (8) Produces a chemically passivated layer (surface oxide layer) that other mechanically polishing processes cannot produce^{17,18}.

3.1.1.1 Electropolishing process

Electropolishing is an anodic process used for the surface finishing of metals or alloys. The electropolishing produces microscopically smooth and bright surfaces that are free of defects, stress¹⁷ and contamination and is a function of many interconnected events occurring during the electropolishing process and schematic representation is shown in **Figure 3.1**. The bright surface of the electropolished workpiece generally results from the effective combination of three surface phenomena namely anodic levelling, anodic brightening and passivation

(a) Anodic levelling

It results from the different dissolution rates of peaks and valleys of the rough metal/alloy surface. It is achieved under the ohmic (primary current distribution), activation and mass transport controlled metal dissolution reactions^{19,20}. It is associated with a decrease in roughness in micrometre or larger range²¹.

(b) Anodic brightening

It is due to the suppression of the effect of crystallographic orientation related to the metal microstructure on the dissolution rate^{19,20,22,23}. It takes place under the tertiary current distribution only²¹ and shifting of metal dissolution rate from surface kinetic control to mass transport controlled regime²⁴ and the precipitated salt layer on the electrode

(metal/alloy) surface may be the course of this crystallographic insensitive phenomenon. Anodic brightening improves surface roughness at the submicron scale and specular reflectivity of metals/alloys can be obtained.

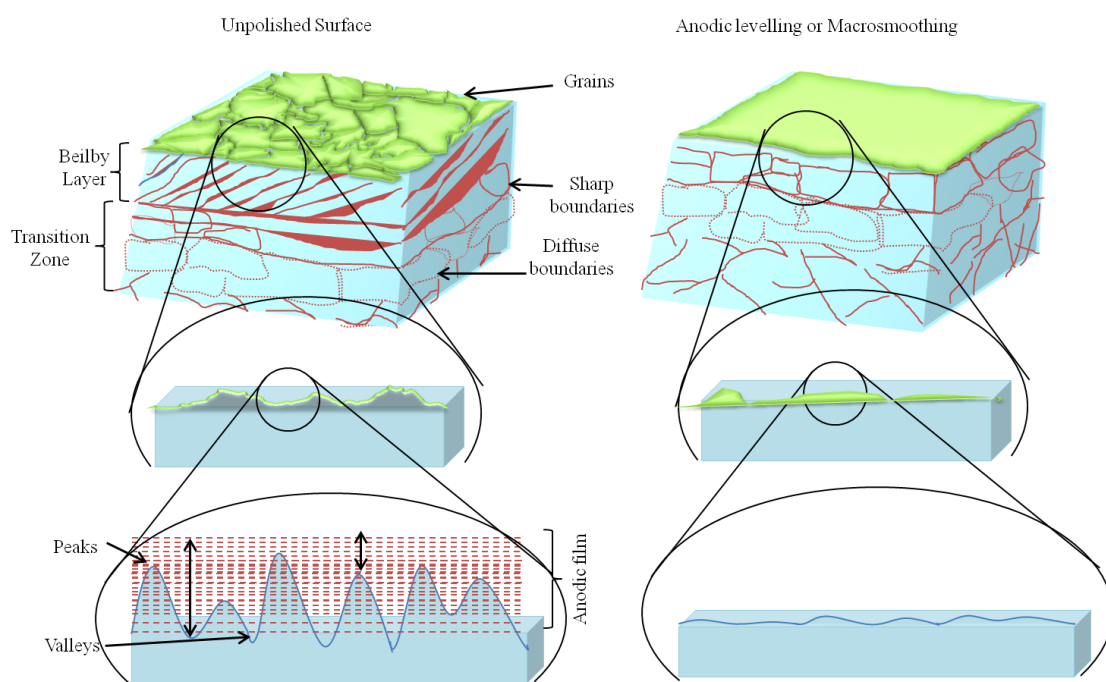


Figure 3.1 : Schematic presentation of the anodic levelling or macrosmoothing of the metal surface

(c) Passivation

Passivation results from the formation of chemically inert surface due to the selective dissolution. The metallurgical compositions of the passive film may be different from the bulk substrate in which anodic oxides / hydroxides are the most important and has higher chromium to iron ratio. This film is very thin of the order of 1-5 nm. The passivity of the given material is a function of electropolishing parameters such as applied current, voltage, temperature, composition and concentration of the electrolyte bath. This compact and dense surface texture of the passive film enhances the corrosion resistance and reduces the wettability of the substrate (hydrophilic to hydrophobic)²⁵.

The electropolishing process is governed by many different mechanisms and depends on many parameters²⁵. Due to its variability, no single theory for attaining the best electropolishing covers all the complexities. In general several mechanisms of anodic dissolution have been proposed in literature; (1) Duplex salt film model^{21,26} (2) Adsorbate acceptor mechanism²⁶ (3) Preferential adsorption of the shielding molecules^{24,27}

3.1.2 Mechanism of Electropolishing

3.1.2.1 Duplex salt film model

This model was proposed by Grimm et al²⁸ and represent a dynamic process with constant salt film thickness. The constant thickness of the film is maintained by continuous renewal beneath the pores and the dissolution at the outer edge along the film / electrolyte interface. The potential drop along the limiting current plateau is increased by the thickening of the salt layer. The potential drop along the limiting current plateau is increased by the thickening of the salt layer. **Figure 3.2** shows the schematic representation of duplex salt film model and the corresponding potential drop in this model.

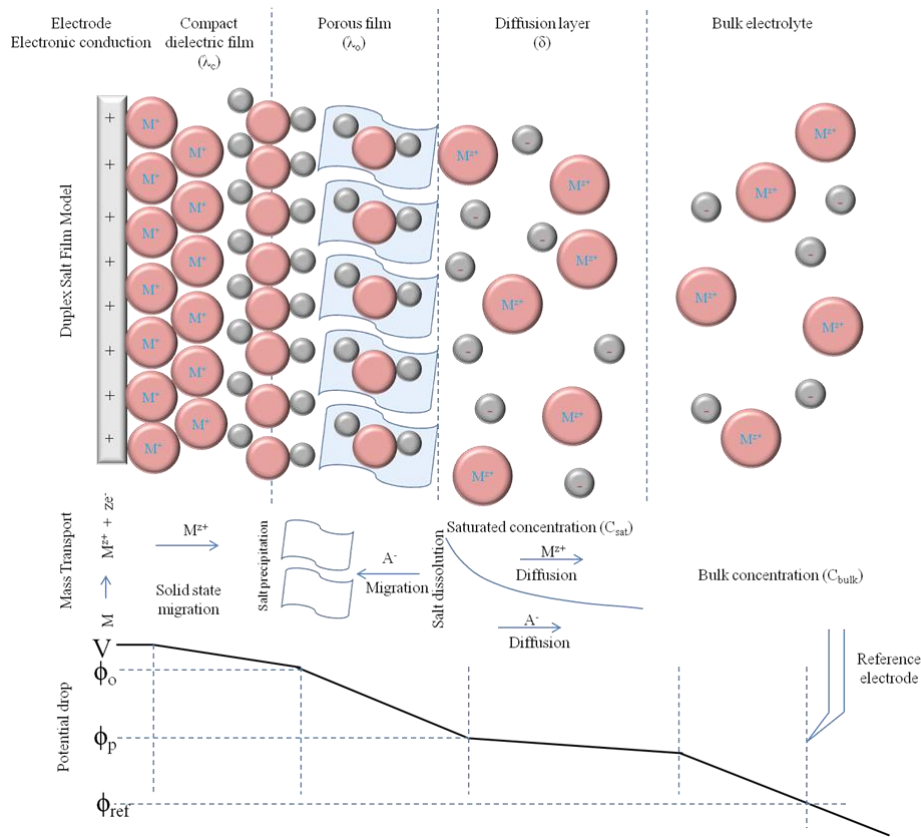


Figure 3.2 : Schematic illustration of Duplex salt film model and the source of the potential drops in salt film system

The salt film formed on the surface of the anode is composed of two regions. The inner region in the immediate vicinity of the anode is compact and forms a solid dielectric barrier through which metal cations are transported by solid state ionic conduction in the presence of higher electric field. The thickness of the film is of the order of 10 nm.

The outer region at the interface of the electrolyte is porous and the pores are filled with electrolyte and the concentration of anions and cations is the same throughout the length of the pores. The metal cations move outward while anions move inward under the influence of the electric field. There is no net inward movement of the anions into the dissolving electrode and all the anions transported into the film are precipitated as metal salt beneath the pores. For constant porosity of the film, its thickness should be constant and is the order of several microns. Therefore the precipitation of freshly formed salt beneath the pores is compensated by equivalent dissolution at the outer edge / electrolyte interface.

The concentration of the metal cations at the interface with the electrolyte is at its saturation value and the metal anions move away to the bulk electrolyte through diffusion. Hence the dissolution of the salt film is limited by the diffusion of the cations and the origin of the anodic limiting current.

3.1.2.2 Adsorbate Acceptor Mechanism

This model was proposed by Matlosz et al.²⁹ **Figure 3.3** represents the schematic illustration of the uniform anodic dissolution of metal in an electrolyte containing a small amount of the acceptor species. The oxidized metal cations adsorb on the anode surface to form an adsorbate layer followed by the solvation by the acceptor species. The adsorbate layer increases the overpotential of metal dissolution and hinders the solvation of metal ions with acceptors.

According to this model acceptors (e.g water or water related species) are the key factor for starting the effective electropolishing process²⁶. The diffusion of the acceptor species control the dissolution of the metal at the anode surface and hence the limiting current is observed when its concentration reaches zero at the electrode surface similar to the cathodic deposition of metals.

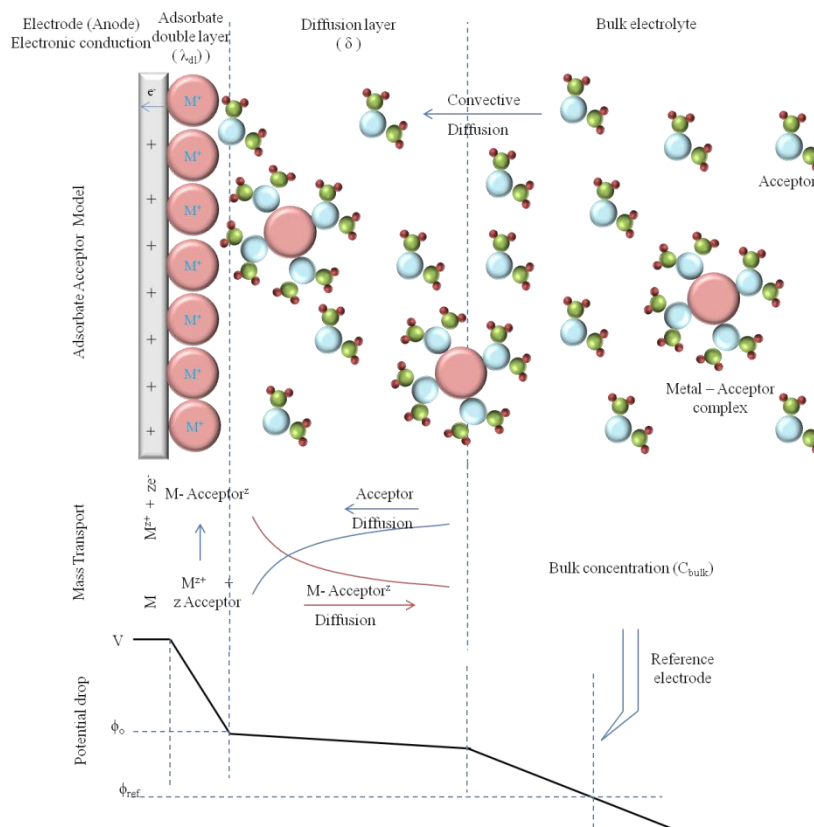


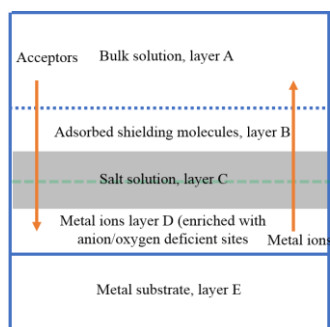
Figure 3.3: Schematic presentation of the adsorbate acceptor model and subsequent potential drop in the system.

3.1.2.3 Preferential adsorption of shielding molecules

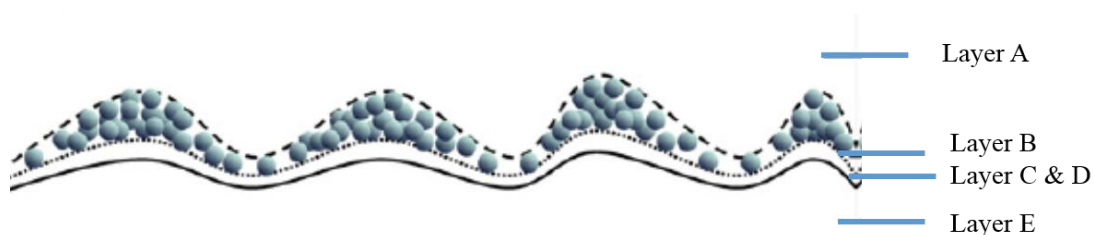
This model was proposed by Chang et al.^{30,31} to explain the pattern formation during the electropolishing. **Figure 3.4 (a)** shows the schematic representation of this model. The bulk polishing solution (acceptors, acids, organic additives) forms the top most layer (layer A). Layer B is formed by the adsorbed molecules including acceptors or other adsorbed organic molecules. It is relatively compact layer and is the Helmholtz layer. Salt solution formed by the electrolyte and the dissolved metal ions forms the salt solution layer C. Layer D is composed of the precipitated dissolved metal ions formed by the dissolution of the metal or alloy substrate. The bulk metal or alloy substrate forms the layer E. The dissolution of the metal substrate and the mass transport of the acceptors and dissolved metal ions is determined by the microstructure of the layer B, C and D which depends on the electropolishing solution.

Adsorbed organic molecules change the surface energies of the metal/substrate atoms and also induce the atomic rearrangement. The shielding molecules may be the same ones that

pack the surface to produce the double layer. If the packing species are not involved in the dissolution reaction, they result in the enhanced packing. The shielding species may be polar or polarizable molecules so that their adsorption rate is enhanced by the electric field, therefore the shielding molecules readily adsorb on the maxima due to the higher electric field than the minima with negative electric field.



(a)



(b)



(c)

Figure 3.4 : (a) Schematic model for the electropolishing of metal substrate showing the movement of acceptors and metal ions. Surface morphologies of the finished surface dominated by the microstructure of layer B (b) small or weak aggregates of polymeric structure (c) large or strong aggregates of polymeric structure.³²

The adsorbate and metal interactions (electrostatic or chemisorbed) may stabilize the surface atoms and hence reduce the dissolution rate. Secondly they may shield the surface resulting in the reduction of the transport rate of the ions / acceptor molecules involved in

the dissolution reaction. Therefore less dissolution rate because of the relatively strong hindrance of the shielding molecules results in the peak formation. The less compact nature of layer B i.e. the shielding molecules offer weak hindrance to the ion flux and favours the diffusion of acceptors and dissolved products resulting in the relatively faster rate of dissolution and ascribes the evolution of valleys. **Figure 3.4 (b & c)** shows the different schematic surface morphologies of the electropolished surface obtained as a result of the weak and strong interaction of the shielding molecules.

A second possible scenario is that water can appear within complexes of solvated ions that have been speculated to be the packing species for the double layer. As these symmetric polar complexes have fewer degrees of freedom than water or other organic additives so they can reach the anode more readily. The water in these complexes is chemically stable so it does not participate in the dissolution reaction. If the Helmholtz layer is composed of solvated ions, then water or other organic additives may compete for the metal surface with solvated ions. As a result the packing will have defects at location where these molecules are either electrostatically adsorbed or site specifically chemisorbed. Chemisorbed shielding molecules can stabilize surface atoms against dissolution. The short hydrophobic tail of chemisorbed molecules may repel the solvated ions (OH^-) and hence reduces its flux to the surface to participate in the dissolution.

Since the patent in 1930³³, mixtures of concentrated sulphuric and phosphoric acids are used for electropolishing of stainless steel on a commercial scale worldwide. Although the polishing quality of this process is very good, the major disadvantages are that the solution used is highly corrosive and hazardous for both environment and workers involved and extensive gas evolution associated with low current efficiency.

A current research focus is on the use of 'green' processes to reduce the environmental impact of existing technologies by waste minimisation and replacement of highly toxic and polluting organic solvents. With the advent of air and moisture stable room temperature ionic liquids (RTILs), a variety of reactions related to organic and inorganic syntheses, nano-material fabrication, polymerization and catalysis have recently been so extensively investigated in RTILs that they are considered to be one of the most promising greener alternative to the current volatile organic solvents³⁴. From an electrochemical perspective, many RTILs possess the archetypal properties such as high thermal stability, non-volatility, high polarity, large viscosity, high intrinsic conductivity and wide

electrochemical windows³⁵⁻³⁷. These properties of RTILs commend their use for electrochemical processes. Abbott et al.¹ introduced the new alternative for electropolishing based on the mixture of choline chloride and ethylene glycol, type III deep eutectic solvent called 1:2 ChCl:EG which was used for electropolishing of stainless steel. The raw materials used were cheap, readily available and biodegradable. This process revealed considerable advantages over the commercial process, among those are high current efficiency, negligible gas evolution at anode / solution interface and benign liquid compared to the acid mixture solution.

This chapter focuses on the studies of the electropolishing of stainless steel in type III choline chloride based deep eutectic solvent 1:2 ChCl:EG. The fundamental aspects of the electropolishing of austenitic stainless steel using the electrochemical techniques i.e. linear sweep voltammetry, chronoamperometry and galvanostatic techniques and the optimization of the electropolishing process using the experimental design strategies (Fractional Factorial Design) are studied. The life cycle analysis of the electropolished liquid is also carried out.

3.2 Physical Properties of 1:2 ChCl:EG

The thermophysical properties of ionic liquids are the key parameters for the complete design of industrial processes. Densities, viscosities and surface tensions are very important for the process operations like rates of liquid-liquid phase separation, mass transfer and power requirements of mixing and pumping etc. The physical properties of 1:2 ChCl:EG such as viscosity, conductivity, density and surface tension are measured as a function of temperature. The viscosity and electrical conductivity of this system may be explained in terms of the hole theory proposed for the high temperature molten salts³⁸.

3.2.1 Viscosity and Conductivity

The viscosity and conductivity of the 1:2 ChCl:EG is 60 cP and 2000 μ S at 25 °C respectively. The variation of conductivity and the viscosity with temperature over the range of 25 - 70 °C and 25 - 50 °C respectively are shown in **Figure 3.5 (a)**. The viscosity and conductivity are affected significantly with temperature. The viscosity is decreased 60 % at 50 °C as compared to room temperature in 1:2 ChCl:EG while the increase in conductivity at 70 °C is twice as compared to room temperature. The conductivity of 1:2 ChCl:EG is increased about two fold at 70 °C.

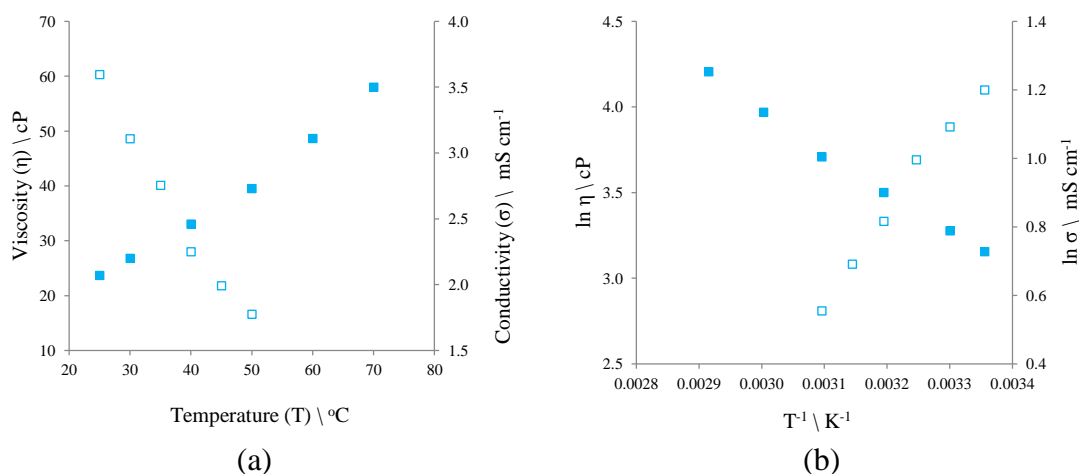


Figure 3.5 : The viscosity (open symbols) and conductivity (solid symbols) (a) as a function of temperature (b) vs. reciprocal of temperature of 1:2 ChCl:EG

The viscosity and the conductivity of the solvents are related to the temperature by the equations 3.1 and 3.2 respectively³⁹.

$$\ln \eta = \ln \eta_o + \frac{E_\eta}{RT} \quad (3.1)$$

$$\ln \sigma = \ln \sigma_o - \frac{E_\Lambda}{RT} \quad (3.2)$$

Where η_o and σ_o are constants, E_η is the energy of activation of viscous flow and E_Λ is the energy of activation for conduction.

Figure 3.5(b) shows that the data fits well to the equation 3.1 and equation 3.2 in both cases and the energy of activation for viscous flow (E_η) and conductivity (E_Λ) are calculated using the slope of these graphs and found to be 34.97 and 10.43 kJ mol⁻¹ respectively. These values are comparable to that of the high temperature molten salts (typically group I halides have the values of 5-20 kJ mol⁻¹)⁴⁰.

A model which has been demonstrated to accurately predict the viscosities and conductivities of ionic liquids and deep eutectic solvents is the hole theory^{38,41,42}. The central assumption of the hole theory is that as a solid melts, voids of random size and orientations are formed. The ability of an ion to move is therefore considered to be dependent upon the presence of an adjacent void of an equal or greater size than the ion. The probability of ion motion can therefore be considered to be dependent on the size of the ions in consideration and the relative density of suitable sized holes.

The mass transport properties of a range of ionic liquids and deep eutectic solvents have been calculated using the hole theory and show a strong degree of correlation with experimentally obtained values⁴¹. This correlation suggests that mass transport in ionic liquids, which contain bulky asymmetric ions, is primarily controlled by the availability of suitably sized holes. This is in contrast to the classical high temperature molten salts which are generally composed of small symmetric ions, where mass transport is principally controlled by the concentration of charge carriers⁴¹.

A strong linear correlation between conductivity and the reciprocal of viscosity (**Figure 3.6**) indicates that the conductivity is governed by the ionic mobility rather than the number of charge carriers.

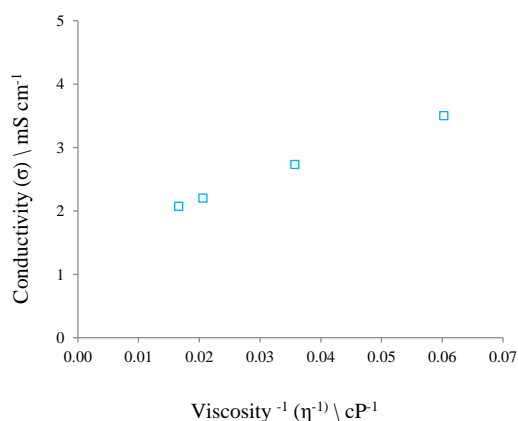


Figure 3.6: Conductivity as a function of fluidity of 1:2 ChCl:EG

3.2.2 Surface tension

The interfacial tension (air-liquid) of 1:2 ChCl:EG was measured using a Kruss Tensiometer K9 with a platinum plate (2 cm) and was measured over the temperature range 298 K to 353 K. At each temperature the measurements were triplicate and the average value was used. A correction factor was determined by measuring the surface tension of DI water at 298 K and was divided by the value reported in literature and then each measured value was multiplied with this correction factor.

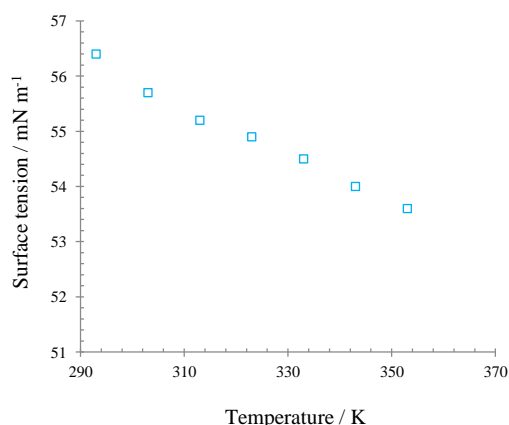


Figure 3.7: Variation of surface tension as a function of temperature of 1:2 ChCl:EG.

| Table 3.1: Comparison of the surface tension, density and thermodynamic functions of 1:2 ChCl:EG, organic solvents and other ionic liquids at 298K | | | | |
|---|---|---|---|--|
| | Surface tension (γ) mN m ⁻² | Density (ρ) g cm ⁻³ | Surface entropy (S^γ) x 10 ⁻⁵ J m ⁻² K ⁻¹ | Surface enthalpy (H^γ) x 10 ⁻² J m ⁻² |
| 1:2 ChCl:EG | 55.9 | 1.106 | 4.46 | 6.92 |
| [BMIM][I] | 53.3 ⁴³ | | 8.16 | 7.75 |
| [BMMIM][PF ₆] | 44.80 ⁴⁴ | | 6.9 | 6.57 |
| [BMIM][BF ₄] | 44.81 ⁴⁴ | 1.198 | 6.35 | 6.34 |
| [BMPyrr]DCA | 55.8 ⁴⁵ | 1.118 | 8.897 | 8.28 |
| [BMIM]DCA | 48.6 ⁴⁵ | 1.062 | 7.75 | 7.19 |
| H ₂ O | 73 ⁴⁶ | - | - | - |
| Methanol | 22.07 ⁴⁷ | - | - | - |
| Acetone | 23.5 ⁴⁷ | - | - | - |
| Hexane | 18 ⁴⁶ | - | - | - |
| Toluene | 32 ⁴⁶ | - | - | - |

The surface tension of 1:2 ChCl:EG is found to be 56.3 mN m⁻¹ at 298 K which is less than water but larger than the organic solvent and is comparable to the imidazolium based ionic liquids as shown in **Table 3.1**. The variation of the surface tension as a function of temperature is shown in **Figure 3.7** which shows a linear relationship with a linear correlation coefficient of 0.99. This linear relation is used to study the surface

thermodynamic properties like surface entropy and surface enthalpy which are derived using **equations 3.3 and 3.4**⁴⁷ and are reported in **Table 3.1** at 298K.

$$S^\gamma = -\frac{d\gamma}{dT} \quad (3.3)$$

$$H^\gamma = \gamma - T \left(\frac{d\gamma}{dT} \right) \quad (3.4)$$

The surface entropy of 1:2 ChCl:EG is remarkably low as compared to other organic compounds but these values are comparable to the imidazolium based ionic liquids. The low value of surface entropy of 1:2 ChCl:EG indicates high surface organization.

3.3 Life cycle studies

3.3.1 Drag out

Drag out is the amount of liquid lost from the processing tank as a result of the adhering film of liquid associated with the immersed part. It depends on the physical properties of the liquid like viscosity, density and surface tension and also a function of the temperature as these properties are linked to the temperature. Drag out is crucial in the surface finishing processes (electroplating or electropolishing) as it has both economic as well as environmental factors and it removes the process chemicals from the processing tank which should be replenished to keep the electrolyte composition constant and it also requires the processing of the rinsing tank water prior to the disposal. The loss of chemicals from the processing tank is equal to the mass of the drag out and hence the amount of the pollutants in the rinsing tank. The electrolyte used in this study is 1:2 ChCl:EG which is composed of choline chloride and ethylene glycol which are biodegradable and not harmful for the environment⁴⁸ but the heavy metals as a result of dissolution of the metal are the real threat for the environment.

In the present study the mass of the drag out was quantified by immersing the plane piece of stainless steel (4 x 5 cm) in the electropolishing solution and drained for varying time periods ranging from 10 to 60 seconds. The maximum draining time was selected keeping in view the actual process as the process operator can not wait longer than this for draining. The experiment for selected delay time was repeated thrice and conducted at two temperatures, room temperature (23°C) and the process temperature (43°C). The findings are presented in **Figure 3.8**. Surprisingly the drag-out is not a strong function of temperature although the range is very small. Most significant is the time delay.

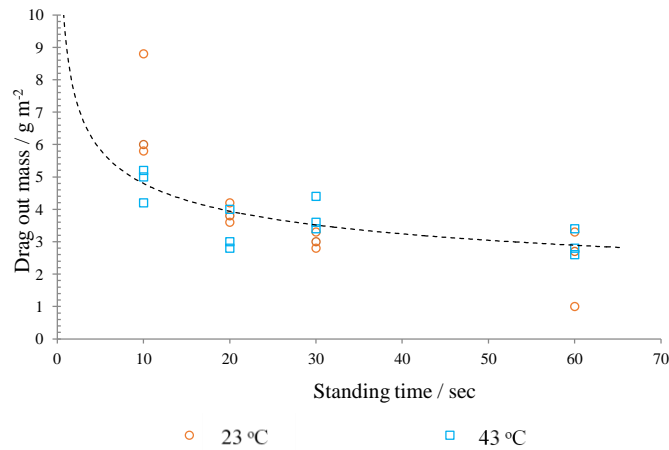


Figure 3.8 : Drag out data for the electropolishing liquid (1:2 ChCl:EG) at room temperature and operating temperature. Dotted line shows the first order fit from which the minimum drag out figures have been

Fitting of the drag out mass – time function to an exponential function typical for a first order process gives the function below.

$$m = Ae^{-kt} + c \quad (3.5)$$

Where, m , is the drag-out mass at time, t ; here, k , A and C are constants. This is useful because minimum drag-out can be determined from the value of C in this function because at infinite time the exponential term of the expression tends to zero. Numerical iterative fitting gave the following values; $A = 8.46 \text{ g m}^{-2}$, $k = 88.5 \times 10^{-3} \text{ s}^{-1}$ and $C = 2.18 \text{ g m}^{-2}$. Consequently the minimum drag-out is estimated to be at 2 g m^{-2} at process temperature of *ca.* $40 \text{ }^\circ\text{C}$. This is comparable and slightly better than corresponding figures for one commercial aqueous alternative electrolyte (Anopol 66 $\text{H}_2\text{SO}_4 / \text{H}_3\text{PO}_4$). The values of K and k are also interesting in terms of the interaction between the substrate and the liquid and they represent collectively a combination of dripping frequency, surface tension and viscosity effects.

3.3.2 Characteristics of electropolishing solution

The life cycle study of deep eutectic solvent 1:2 ChCl:EG with oxalic acid as an additive for the electropolishing of stainless steel 316 was carried out at constant voltage (6 V) and constant current (600 mA) and was conducted for short time scale of one hour and extended time scale of 10 hours. Data for variation in voltage, current density, conductivity, colour and concentration of the electrolyte as well as the weight loss of the electropolished ss316 piece at different time intervals over the entire time scale of the

experiment were collected. The spent liquid was recycled and the electropolishing of ss316 was studied again in the same manner and the results were compared with the virgin liquid. The experiments were modelled in such a way that each experiment was started with the fresh liquid (500 ml) and the fresh ss316 pipe piece (25.434 cm²) and then subsequently used for rest of the experiments. The voltage or current readings as the case may be were taken after every 15 minutes.

Short time scale electropolishing of the stainless steel piece was conducted separately for one hour at constant current ca 600 mA and voltage ca 6 V in 500 ml 1:2 ChCl:EG. Samples of liquid (10 ml) were taken out after every three minutes without stopping the experiment. These samples were analysed by UV-Vis and ICP-MS.

Long time scale electropolishing of stainless steel pieces were carried out separately for 10 hrs and 7 hrs at constant current ca. 600 mA and constant voltage ca. 6 V starting with 500ml of electrolyte respectively. The experiments were stopped after every hour and the steel pieces were taken out, washed with water, air dried and weighed. Every time the solution was stirred for five minutes and liquid samples (10 ml) were taken out. Same stainless steel pieces were further electropolished in the same solution without degreasing and pickling. The collected solution samples were analysed by UV-Vis and ICP-MS. The voltage and current reading as the case may be were taken after every 15 minutes.

3.3.2.1 Appearance of solution

The electrolyte turned dark green as the electropolishing proceeded. Deconvolution of the UV-Vis spectra, together with spectral convolution fitting of standard solution spectra for the pure metal ions showed that the dark green colour of the electrolyte was due to the combination of Cr³⁺ and Fe²⁺ ions. The time dependant UV-Vis spectra from one such experiment are presented in **Figure 3.9**. The optical absorbance of the liquid gradually increases over the period of 1 hour as the colour develops into a dark green indicating that the electropolishing process occurs via dissolution of the metals to form complexes of the form M^{x+}Cl_yGly_z.

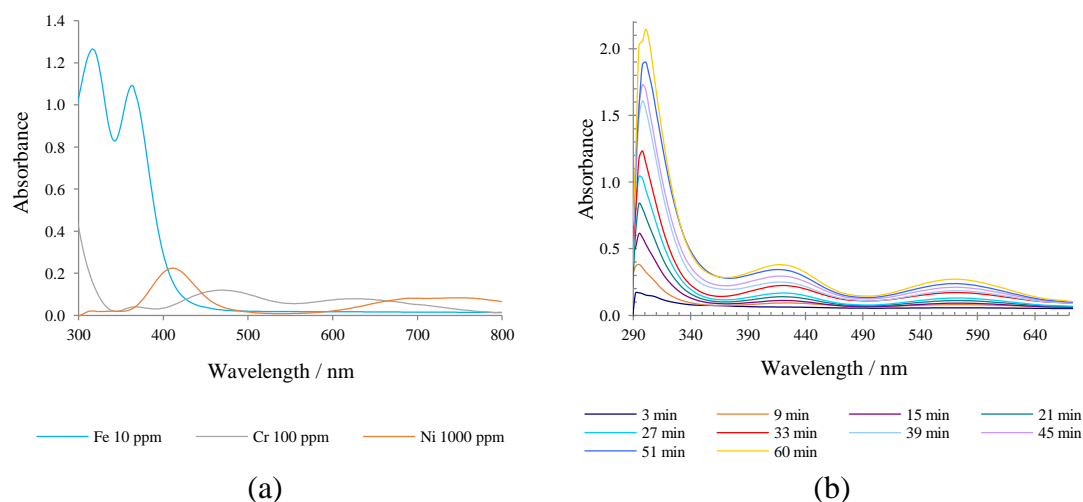


Figure 3.9: *UV-Vis spectra of (a) standard solutions of iron, nickel and chromium (b) electropolishing liquid as a function of electropolishing time during one hour*

3.3.2.2 Concentration of metal ions

ICP-MS determination was carried out for quantitative estimation of iron, nickel and chromium in the electropolishing solution for short and extended time scale experiments. Before proceeding to ICP-MS determination of metal concentrations, a series of blind calibration trials for each of the three metal systems were performed twice in order to establish the appropriate conditions for sample digestion and analysis. **Figure 3.10** shows a good correlation between known concentrations and measured values except a little deviation in the case of nickel.

Figure 3.11 (a) and (b) shows the concentration profiles of three metals iron, nickel and chromium at constant voltage and constant current as a function of charge passed during the course of one hour. In both cases the concentration profiles match well unlike for the extended time scale experiment. **Figure 3.12 (a) and (b)** present the variation in concentration of three metals as a function of charge passed during the course of 7 hours of electropolishing. The concentration of the three metals in galvanostatic experiment is twice that from the cell voltage controlled experiment.

This difference in concentration may be attributed to the smaller amount of the metal dissolution which is due to fall of the current as a result of the changes in the metal concentration of the solution and the passivation layer geometry. This is consistent with qualitative analysis in that finish is not generally effected – except in some circumstances

where polishing pieces of particular geometry may occasionally benefit from one or other method. The other feature of the plots is that the metal ion concentrations have still not reached saturation limits even after 10 hours of electropolishing.

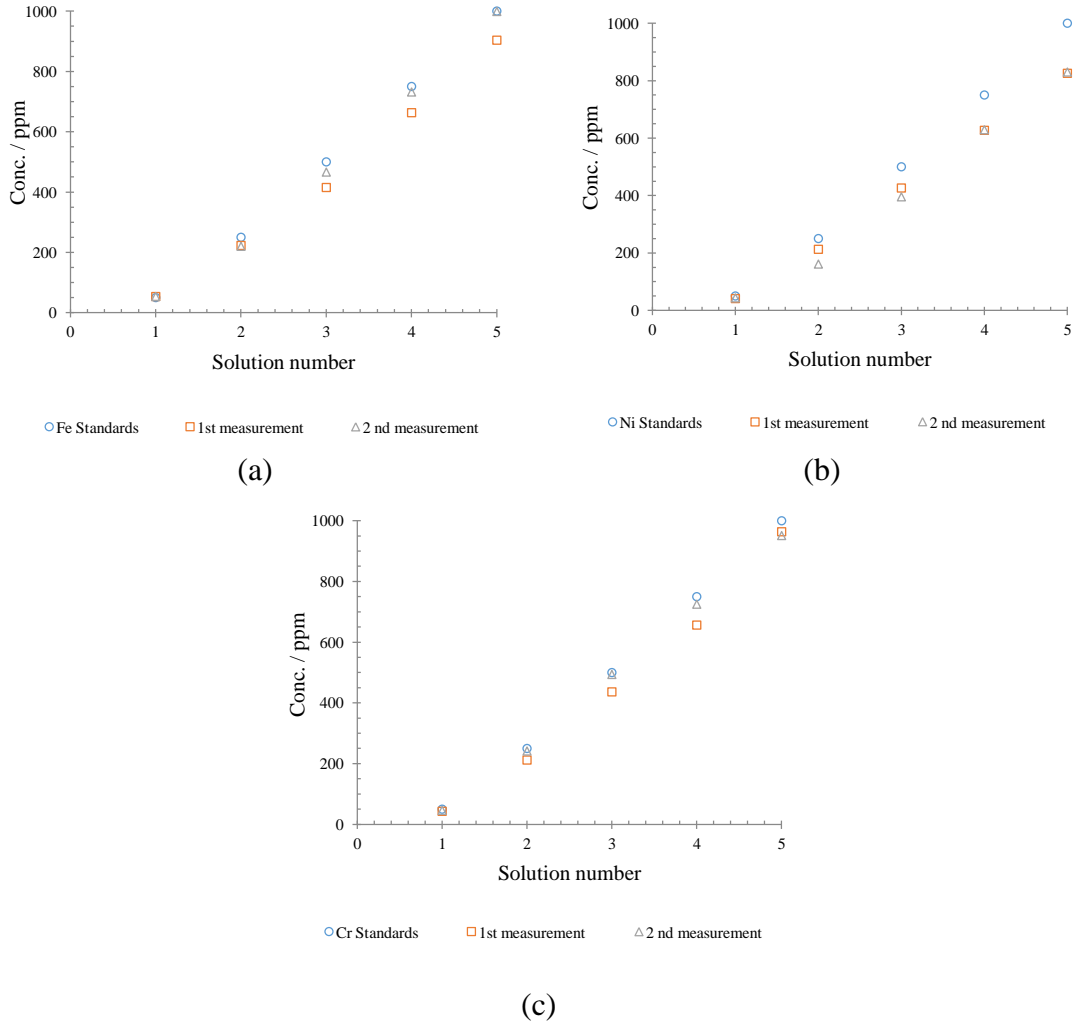


Figure 3.10: Repeat calibration data for metal ion concentrations determined in 1:2 ChCl:EG by ICP-MS for (a) Iron (b) Nickel (c) Chromium

3.3.2.3 De-alloying effect

The ratio of the metal ions in the liquid is also of special importance since it provides bulk evidence for the homogeneous dissolution (or otherwise) of the stainless steel alloy. The data presented in **Figure 3.13** show the concentration ratio for Fe and Cr in the liquid at short and extended time scale experiments.

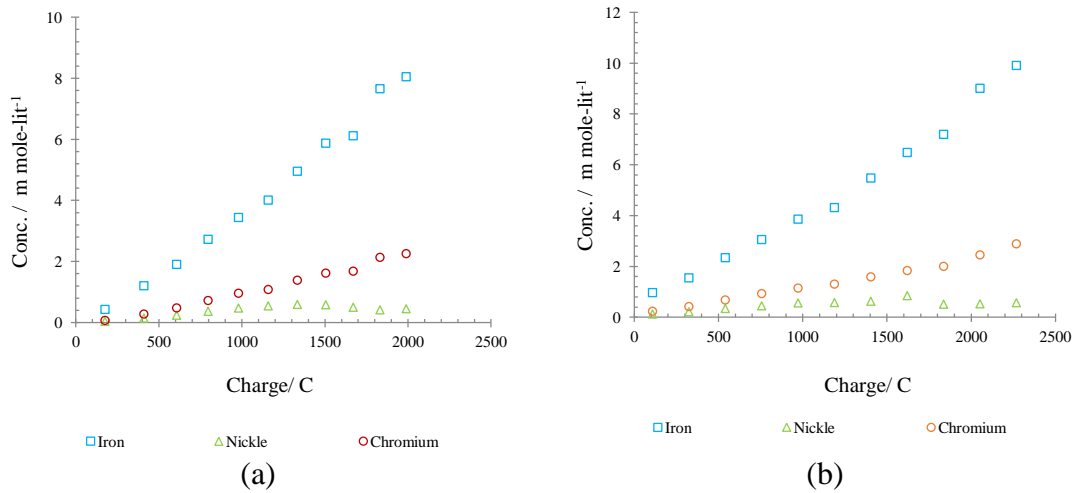


Figure 3.11: Metal ion concentration plotted as a function of total charge passed during the course of one hour (a) at constant voltage (b) at constant current

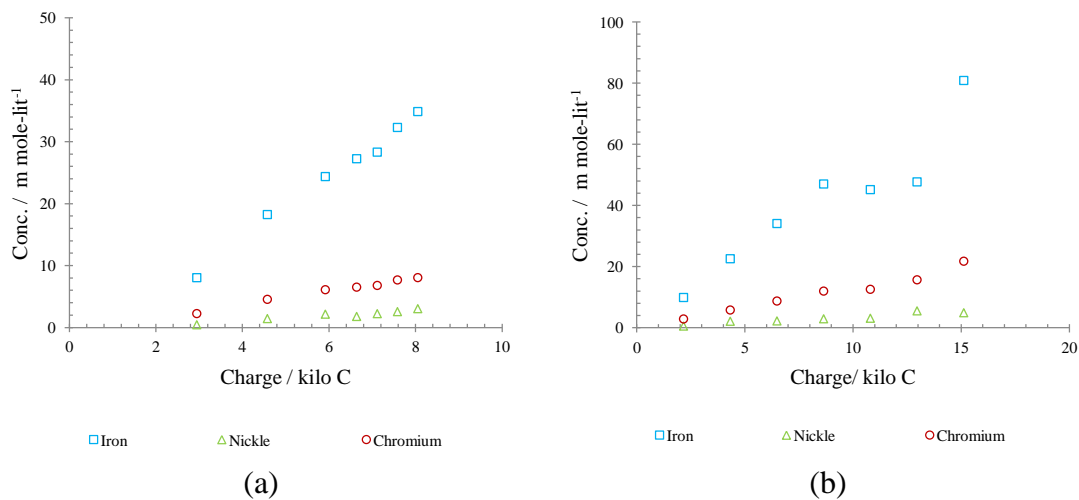


Figure 3.12: Metal ion concentration plotted as a function of total charge passed during the course of 7 hours (a) at constant voltage (b) at constant current

During the controlled potential experiment the relative Fe concentration increases slightly but the corresponding ratio in the controlled current experiment remains essentially constant. Within experimental error these data indicate that no dealloying of the steel is occurring on these time scales and this is consistent with previous observations and surface analysis of samples^{1,49}.

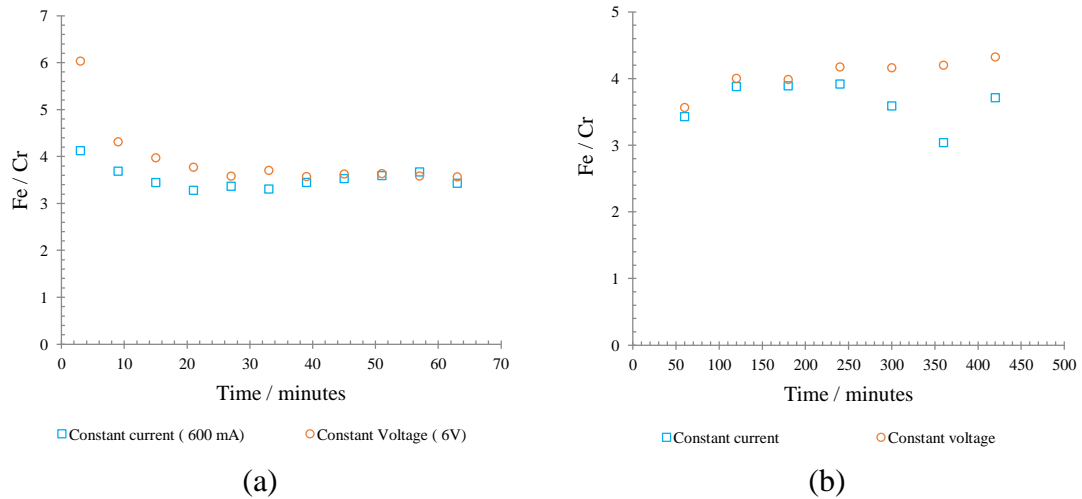


Figure 3.13 : Concentration ratios of Fe and Cr plotted as a function of electropolishing time of ss316 under potentiostatic and galvanostatic control (a) one hour (b) 7 hours

3.3.3 Electrochemical studies

3.3.3.1 Variation of potential and current

The variation of the cell voltage in controlled current experiment is shown in **Figure 3.14 (a)**. During the first 7 hours the cell voltage fluctuated around 5 V while later on it increased to 6 V. This increase in the cell voltage value may be related to the increase in the metal concentration in the bulk solution which slows down the diffusion of the dissolved metals from the vicinity of the dissolving metal to the bulk electrolyte in the absence of the stirring. The slight variation in cell voltage was also observed during each hour. This may be attributed to the thick salt film on the surface of the metal which hinders the movement of the metal ions in the solution and the formation of the passive layer at the cathode surface during the experiment.

Figure 3.14 (b) represents the current density profile of the electropolishing of SS316 at 6 V for the time period of 7 hours. The gradual decrease in current density was observed for the first three hours and then the value fluctuate around 3 A cm^{-2} for the rest of the experiment. This decrease can be explained in terms of the solution resistance and the passivation layer.

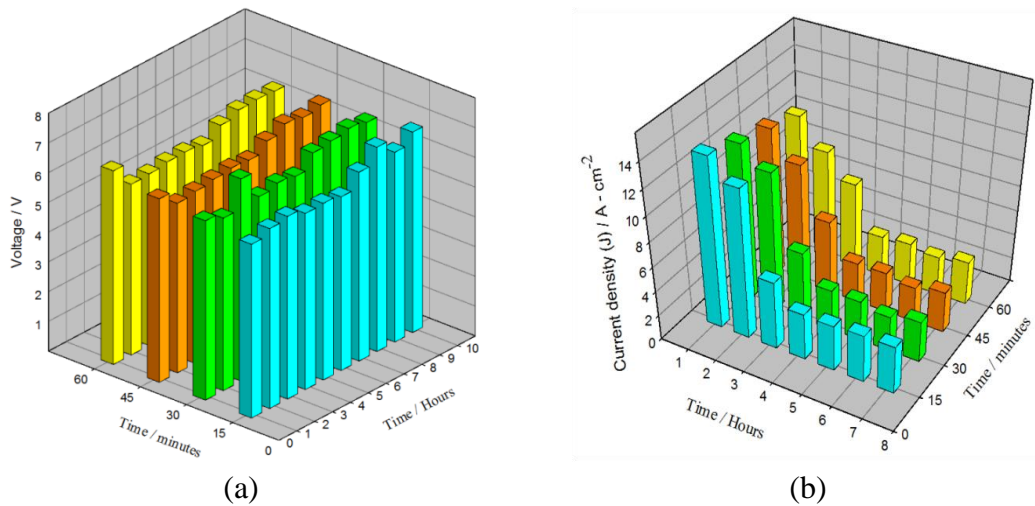


Figure 3.14: (a) Variation of the cell voltage at constant current (600 mA) (b) fluctuation of current density at fixed voltage (6 V) as a function of time.

3.3.3.2 Weight loss

The comparative weight loss for extended time scale electropolishing experiments both at controlled potential and controlled current is depicted in **Figure 3.15**. In case of constant current experiment, the weight loss is more or less the same throughout the experimental period but in the case of the potentiostatic experiment the weight loss is the strong function of time linked with the decrease in current density, but in both cases the weight loss is a linear function of the charge passed.



Unpolished



10 minutes electropolishing at 6 V



10 hours electropolishing at 6 V



13 hours electropolishing at 6 V



16 hours electropolishing at 6 V

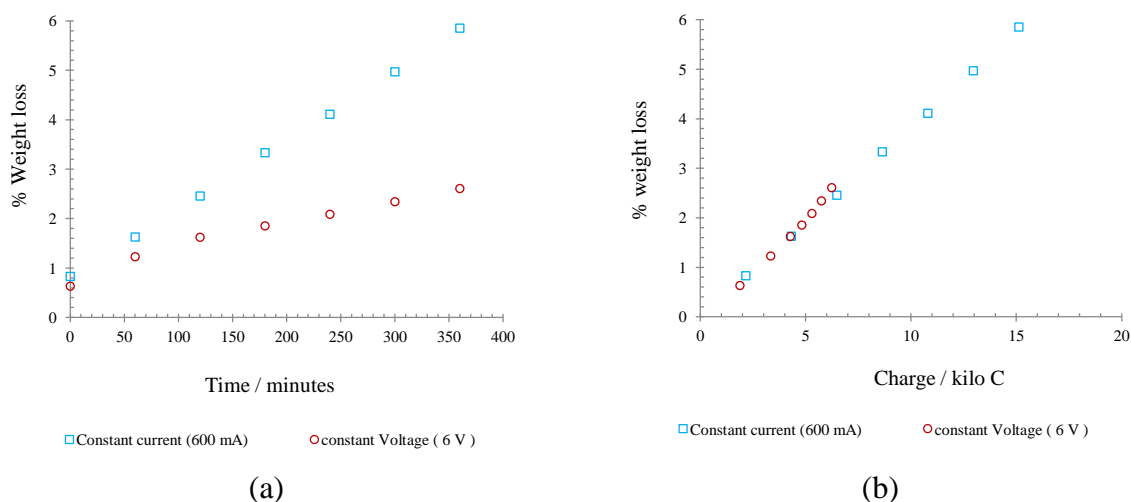


Figure 3.15: *Photographs of the potentiostatically electropolished ss316 pieces. Comparative % weight loss of ss316 at constant current and controlled potential for 7 hours as a function of (a) time (b) charge passed.*

3.3.4 Recycling of liquid

The recycling study of the solution, firstly electropolishing of freshly degreased and pickled stainless steel piece was conducted in 500 ml solution for 16 hrs at a constant current of 600 mA. The electropolishing was stopped after every hour. The steel piece was removed from the solution, washed, air dried and weighed. The conductivity of the solution was measured. The same piece was electropolished again in the same solution without degreasing and pickling.

Spent liquid from the above experiment was recycled. Spent liquid was mixed with an equal volume of de-ionised water and allowed to stand for one day to allow settlement of the precipitates. The dissolved metals were precipitated due to change in the solubility constant. The liquid was then centrifuged. Precipitates were separated out and water was removed by gentle heating at 60°C until the volume of the starting liquid was reached. The recycled liquid was not fortified with ethylene glycol.

In this recycled unfortified liquid, electropolishing of the freshly pickled stainless steel pieces was conducted at a constant current of 600 mA in the same way as was carried out in the virgin solution for 7 hours and potential, weight and conductivity data were collected.

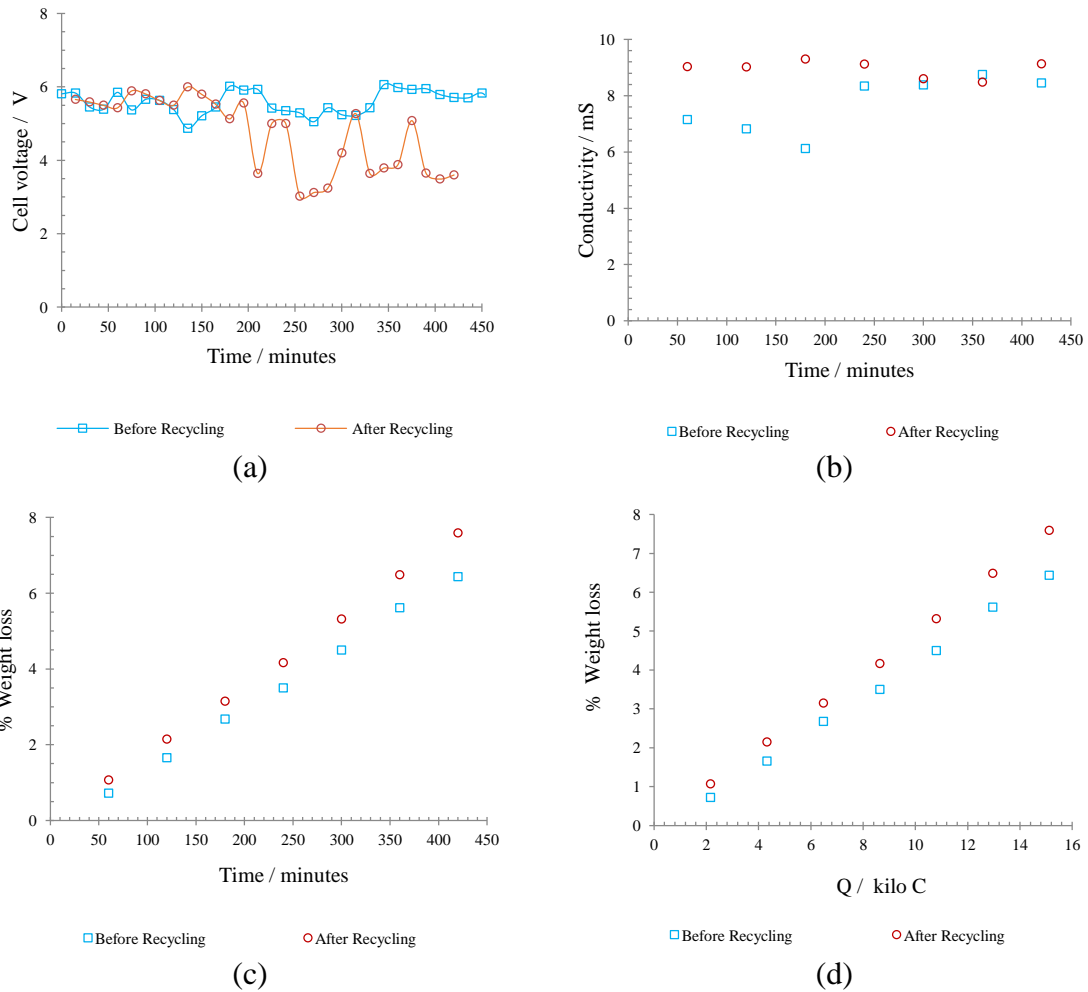
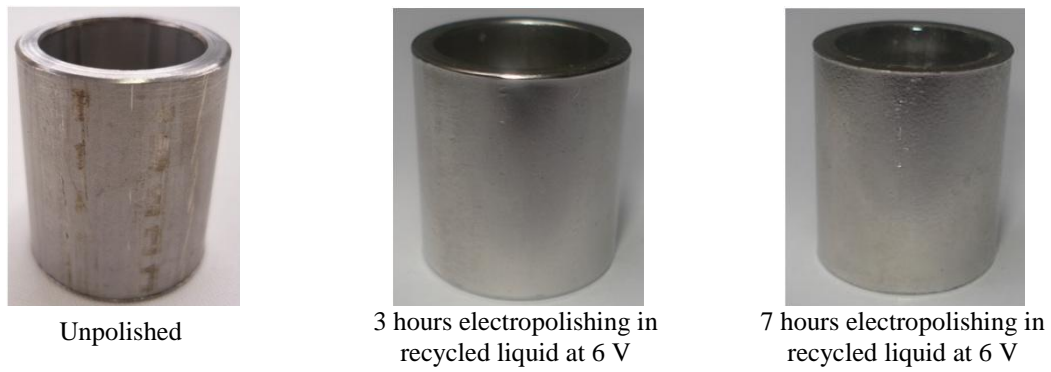


Figure 3.16: Photographs of the potentiostatically electropolished ss316 piece in recycled liquid and comparative study of the recycled and virgin liquid in current controlled experiment (a) variation of cell voltage (b) conductivity (c) weight loss as a function of time (d) weight loss as a function of charge

Unfortified recycled liquid performed well in qualitative tests by visual assessment of the polish. Quantitative tests like potential variation, weight loss and conductivity of the native and recycled solutions are compared in **Figure 3.16**. The potential variation for the first

three hours is comparable with the native solution but later on it fluctuated around to 3.5 V as in **Figure 3.16 (a)**. This decrease may be attributed to the change in viscosity and passivation layer. The bump in the recycled curve at the start of each hour may be due to washing off the thick viscous liquid layer as the piece is removed after each hour.

In another test the conductivity of the liquids was measured during a polishing experiment and the data for native and recycled liquids are presented in **Figure 3.16 (b)**. Apart from small variations at early times the two data sets are essentially indistinguishable. The difference at the early stages may be due to the presence of some water left during the recycling process and the presence of the metal ions in the recycled liquid.

The weight loss data are plotted as function of time and charge passed in **Figure 3.16 (c & d)** and show that there is slightly more weight loss observed in recycled liquid as compared to the native solution and is a linear function of the charge passed and time. This difference in weight loss may be linked with the presence of the water in the recycled liquid. These quantitative and qualitative assessments have confirmed that the recycled liquids perform at a comparable level to the original formulations.

3.4 Electrochemistry

3.4.1 Potentiodynamic study

3.4.1.1 Electrochemical window of 1:2 ChCl:EG

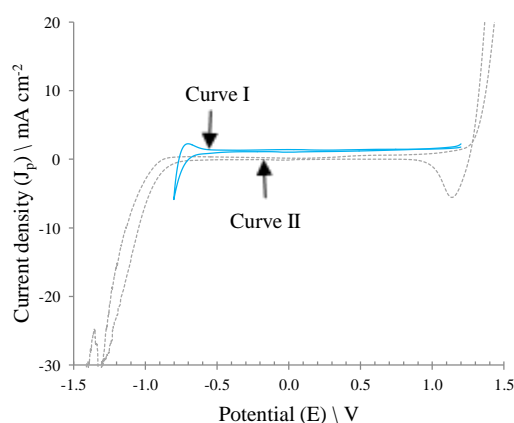


Figure 3.17 : *Cyclic voltammograms of the neat DES 1:2 ChCl:EG at a scan rate of 10 mV sec⁻¹*

The electrochemical window is defined as the two intersection points between the zero line and the tangents to the reduction and oxidation potential limits, where the current increased

strongly and continuously, indicating the decomposition of the ILs. The electrochemical window is determined by cyclic voltammetry at a scan rate of 10 mV s^{-1} at a platinum disc electrode. **Figure 3.17** exhibits that the electrochemical window of 1:2 ChCl:EG is about 2 volts extending from $+1.3 \text{ V}$ to -0.8 V vs. silver wire as quasi reference. The cut off current density arbitrarily used here is the potential at which the current density reaches 0.1 mA cm^{-2} (usually the cut off current density is selected between $0.1 - 1 \text{ mA cm}^{-2}$ ^{50,51} but it is more common to select the cut off current density below 0.1 mA cm^{-2}). The cathodic and anodic limits probably correspond to the reduction of the hydrogen bond donor and oxidation of Cl^- respectively. In 1:2 ChCl:EG zero current is observed throughout the cathodic scan. On the anodic scan in curve I, the presence of the anodic wave at -0.75V is due to the oxidation of the products formed during the cathodic scan.

3.4.1.2 Anodic linear sweep voltammetry

Linear sweep voltammetry was conducted to define the potential regions for polishing of stainless steel in the diffusion controlled regime and the influence of electrolyte temperature, composition and the effect of different additives on the polishing of stainless steel. The experiments were conducted at 30°C with an electrolyte solution of 40 ml in the absence of agitation. The three electrode system consisting of platinum flag counter electrode (2 cm^2), a silver wire quasi reference electrode and the stainless steel sheet plate (0.5 cm^2) was used. Each experiment was conducted with the fresh stainless sheet plate and the fresh electrolyte. The electropolishing by linear sweep voltammetry was initiated at -0.3 V and anodically swept up to 3 V .

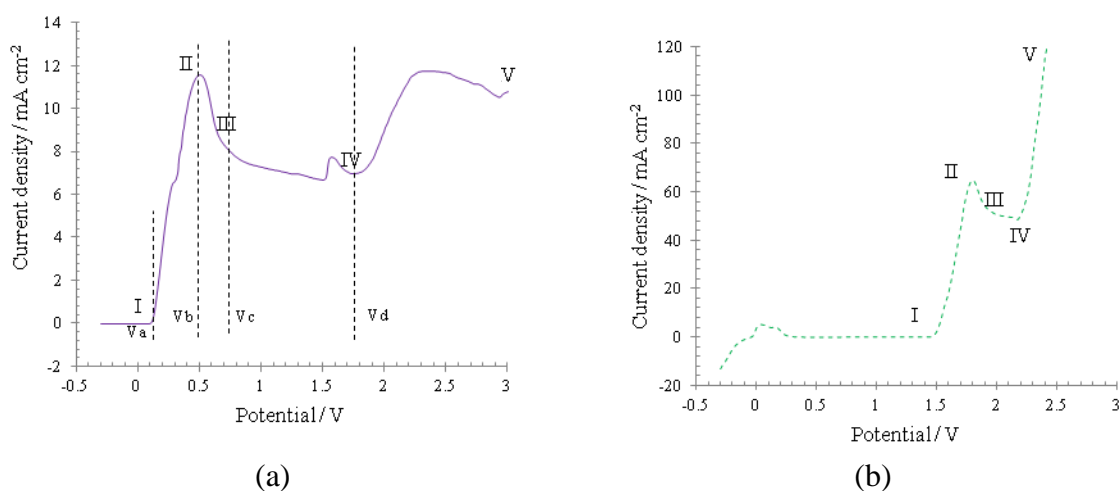


Figure 3.18 Anodic linear sweep voltammograms of ss304 at 30°C at scan rate of 2 mV sec^{-1} (a) 1:2 ChCl:EG (b) $\text{H}_3\text{PO}_4:\text{H}_2\text{SO}_4:\text{H}_2\text{O}$ (3:2:1)

Figure 3.18 (a) shows the linear sweep voltammogram of ss304 in 1:2 ChCl:EG electrolyte at a scan rate of 2 mV sec^{-1} . The anodic curve has four distinct regions: the active dissolution region (I-II), the passive region (II-III), the diffusion controlled current region (III-IV) and the pitting region (IV-V). The anodic curves of stainless steel in 1:2 ChCl:EG exhibit same behaviour as those obtained in $\text{H}_3\text{PO}_4:\text{H}_2\text{SO}_4:\text{H}_2\text{O}$ (3:1:1) (**Figure 3.18 (b)**) and reported in the literature⁵²⁻⁵⁴. The I-V in 1:2 ChCl:EG differs from the acidic solution in the following manner (i) the anodic dissolution peak is cathodically shifted to 0.5 V while in acidic solution it is around 1.8 V. (ii) the LSV curve has wider diffusion limited plateau extending from 0.9 V to 1.9 V while in acidic solution it is narrow (2.1-2.2 V).

In the active dissolution region, the current rises steeply upto V_b due to breakdown of the surface oxide layer and aggressive etching of the surface. The surface conserves its mechanically worked appearance and show some signs of pitting (**Figure 3.19 (b)**). In the passive region, there is simultaneous drop in current density due to the formation of new oxide layer and build up of thin solid green film of dissolved oxides. This film offers the greatest ohmic resistance. The surface is still rough and semi bright in appearance in this region (**Figure 3.19 (c)**). The third region is technically very important. The current decreases slowly due to the mass transfer control of anodic metal dissolution up to V_d . In this region a gradual transition to the fully electropolished surface is apparent and bright smooth surface is obtained (**Figure 3.19 (d)**). In IV-V region, the current rises again, this may be due to dissociation of the small amount of water present in the 1:2 ChCl:EG or the rupture of the thin solid film on the anode surface at certain point under the influence of the high applied potential and results in the pitting of the surface due to the faster rate of dissolution of the stainless steel at the point of the ruptured film. The surface is bright with etching pits (**Figure 3.19 (e)**).

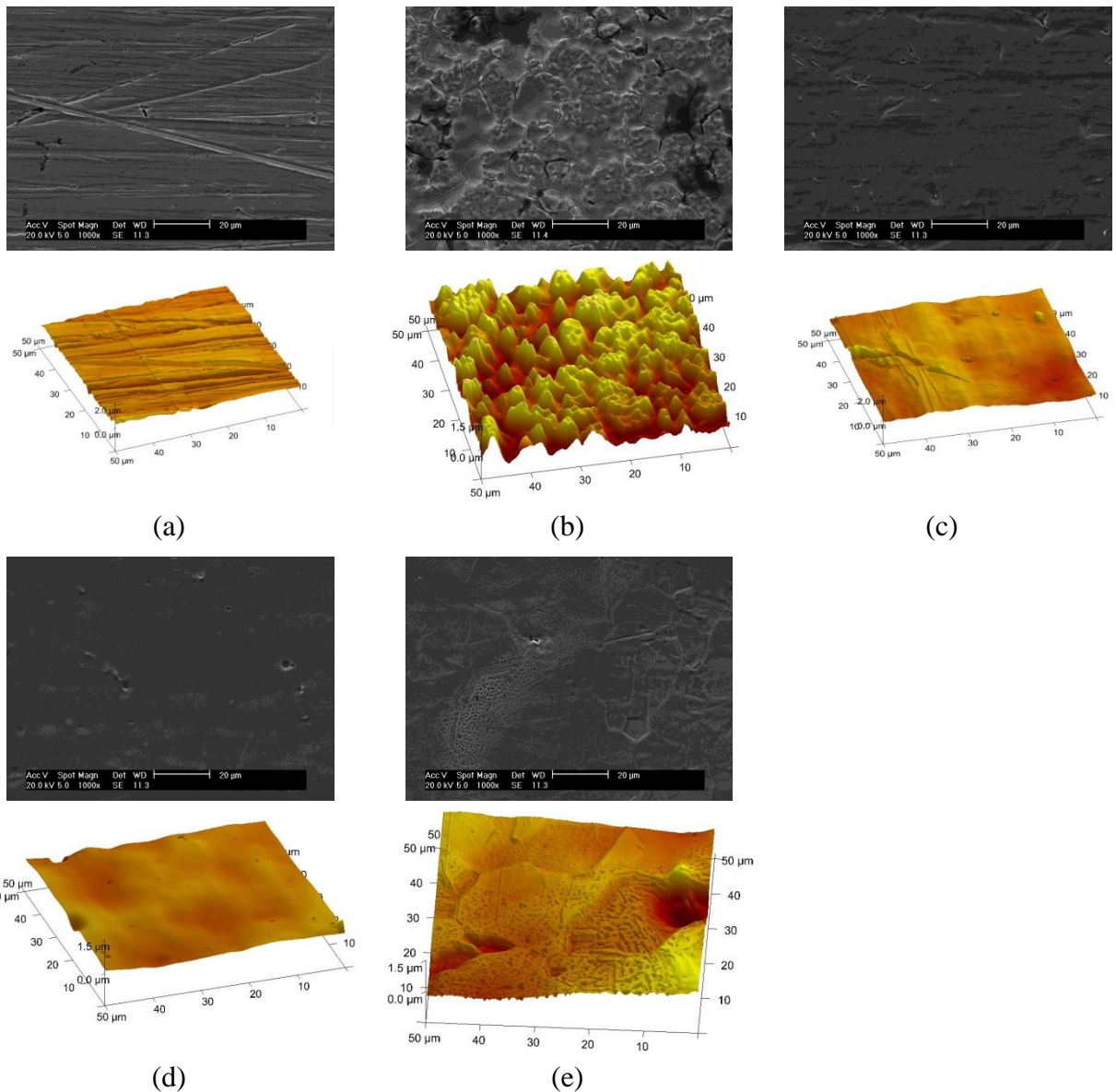


Figure 3.19 : SEM and AFM images of the electropolished ss304 at scan rate of 2 mV sec^{-1} at 30°C in 1:2 ChCl:EG obtained by stopping the scan at different potentials (a) unpolished (b) 0.7 V (c) 1V (d) 1.7 V (e) 3V

3.4.1.3 Effect of scan rate

The dependence of the electropolishing behaviour of ss304 on scan rate is investigated at different scan rates 1, 2, 5, 10, 15 and 20 mV sec^{-1} and is presented in **Figure 3.20**. The peak current density increases and peak potential is shifted towards more positive values with increasing scan rate. The shift in peak potential may be due to uncompensated resistance or electrode kinetics and at 20 mV Sec^{-1} no diffusion control regime is obtained.

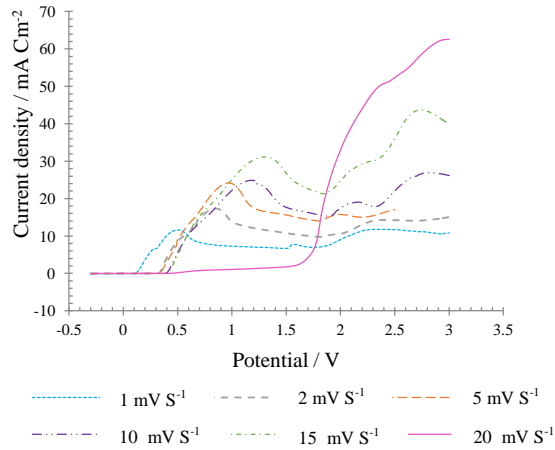


Figure 3.20: Linear sweep voltammograms of ss304 in 1:2 ChCl:EG at 30°C at different scan rates.

3.4.1.4 Effect of Temperature

The influence of the temperature of the electrolyte on the electropolishing of ss304 is shown in **Figure 3.21**. The experiments were conducted at bath temperatures 20, 30, 40 and 50 °C under unstirred conditions at a scan rate of 2 mV sec⁻¹. The peak current density increases with the rise in temperature and at 50°C the current rises initially and then fluctuates around the plateau value. The linear relationship between the peak current density and the temperature suggests that the anodic dissolution in 1:2 ChCl:EG is diffusion controlled process as for the other electrolytes^{22,52,55-57}.

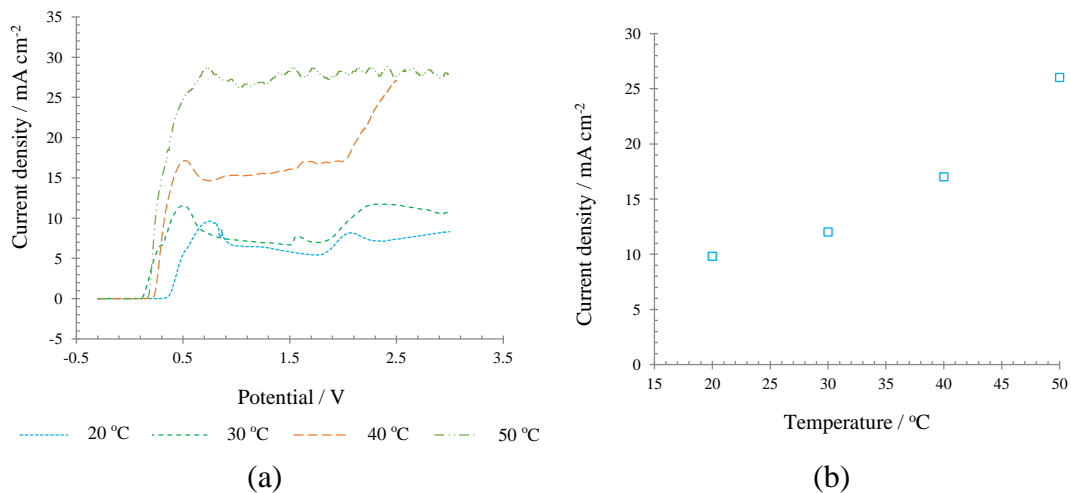


Figure 3.21 : (a) Influence of the temperature on the linear sweep voltammogram of electropolishing of ss304 in 1:2 ChCl:EG at 2 mV sec⁻¹ (b) dependence of the peak current density as a function of temperature.

3.4.1.5 Effect of additives

Figure 3.22 (a) & (b) depict the effect of additives (water & oxalic acid) in 1:2 ChCl:EG on the anodic dissolution curve of stainless steel respectively. The experiments were performed in 1:2 ChCl:EG containing different amounts of water (5%, 10% and 20%) and oxalic acid (3%). The presence of water shifts the peak current density to high values and interestingly the pitting region is not observed in the presence of water and the electropolished surface is smooth and even unlike in 1:2 ChCl:EG (**Figure 3.23 (a) & (b)**). This beneficial effect may be due to the decrease in the viscosity and increase in the conductivity of the 1:2 ChCl:EG or it can be involved in the dissolution mechanism.

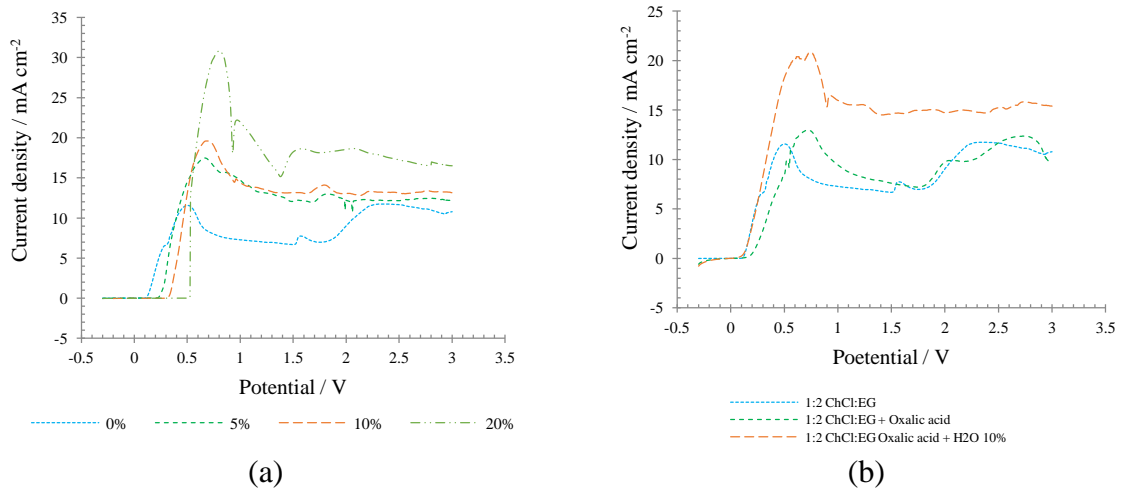


Figure 3.22 : Effect of additives on the linear sweep voltammogram in 1:2 ChCl:EG at scan rate of 2 mV sec⁻¹(a) water (b) oxalic acid

The addition of the oxalic acid in 1:2 ChCl:EG does not effect the behaviour of the anodic curve but the addition of water along with oxalic acid has the similar effect on the anodic curve as in the case of 1:2 ChCl:EG + H₂O system (**Figure 3.23 (c)**).

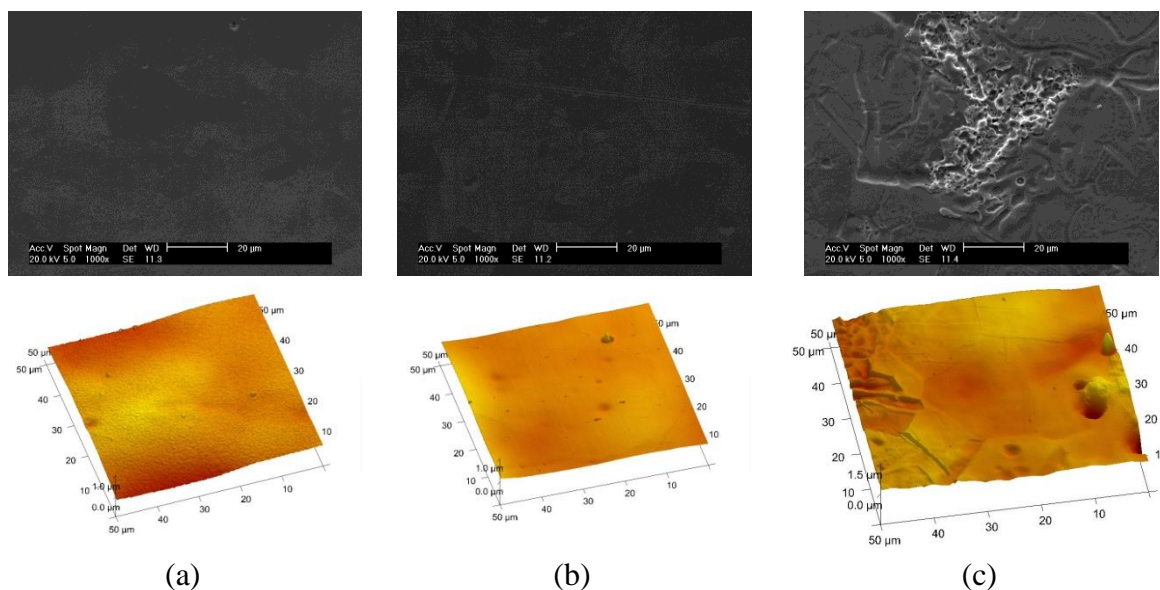


Figure 3.23 : SEM and AFM images of the anodic linear sweep electropolished ss304 of Figure 3.21 (a) 5% H₂O (b) 10% H₂O (c) 3% oxalic acid

3.4.2 Chronoamperometry

Chronoamperometry was conducted to investigate the polishing quality of stainless steel at different potentials regions of the anodic linear sweep voltammogram. Each experiment was conducted at 30°C in 1:2 ChCl:EG at each potential for 15 minutes. A freshly abraded stainless steel sheet (1 cm²) was used each time and to avoid the effect of the dissolved metals fresh electrolyte (40 ml) was used in each electropolishing procedure. A platinum flag (2 cm²) and silver wire were used as counter and quasi reference electrode.

Figure 3.24 shows the current time transients of the electropolishing of ss304 obtained by applying the potential pulse from 0 to 0.7, 1.4 and 2.3 V and the surface topography at these potentials. These potentials are chosen for the three regions of the linear sweep voltammogram namely active dissolution, diffusion controlled and the pitting regions respectively.

The current transients obtained at overpotential of 0.7 V shows the initial rise in the current and then it reaches the steady state value. The electropolished surface obtained at this potential is milky and very rough due to aggressive etching. The current time curves at higher over potentials (1.4 V & 2.3 V) show the initial anodic dissolution followed by the mass transfer controlled decay current. The electropolished surface obtained at the overpotential of 1.4 V is bright and smooth in agreement with the various studies which

proposed that the best results of electropolishing are obtained at potential in the limiting current region^{21,56}. At an overpotential of 2.3 V, the surface with pits around the grain boundaries is obtained.

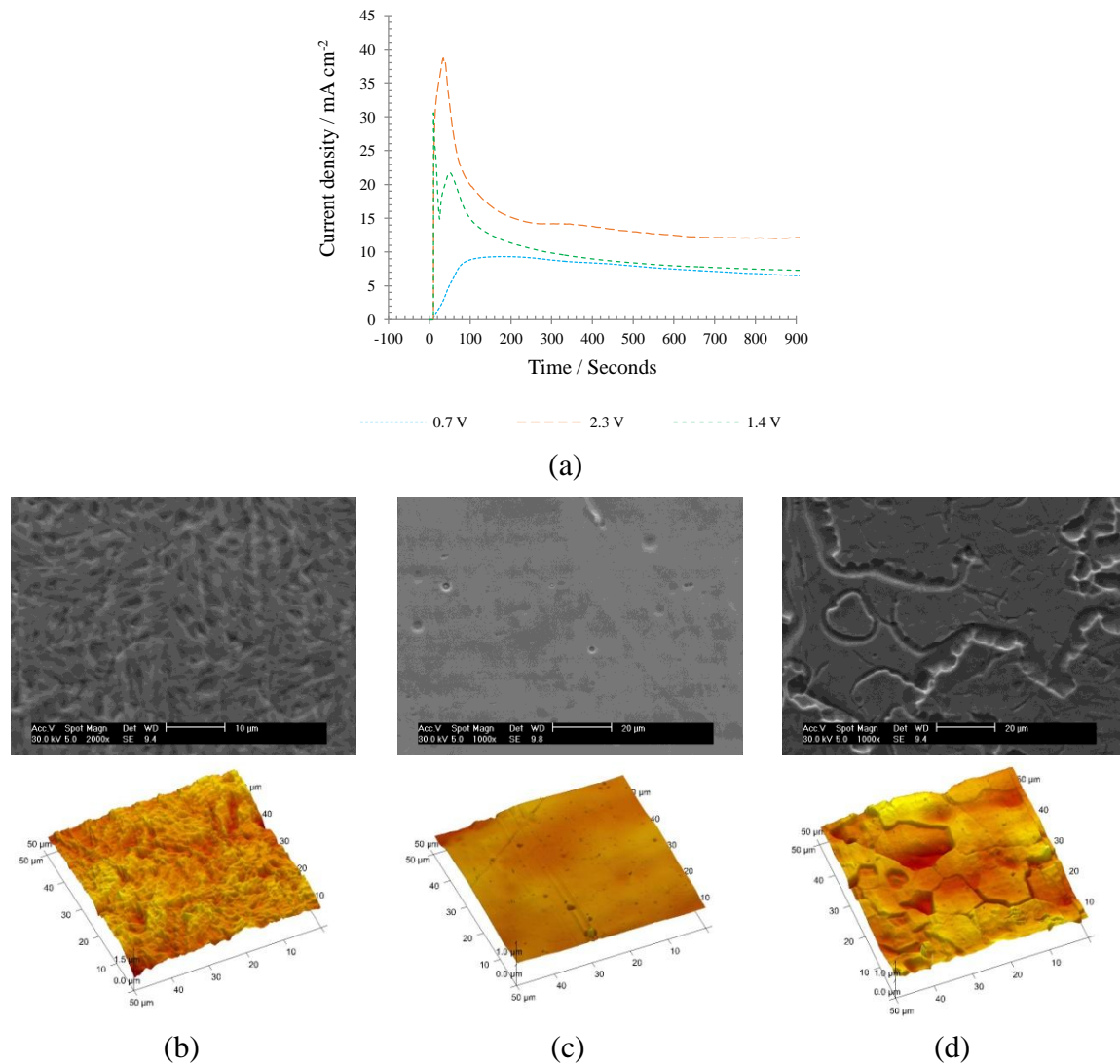
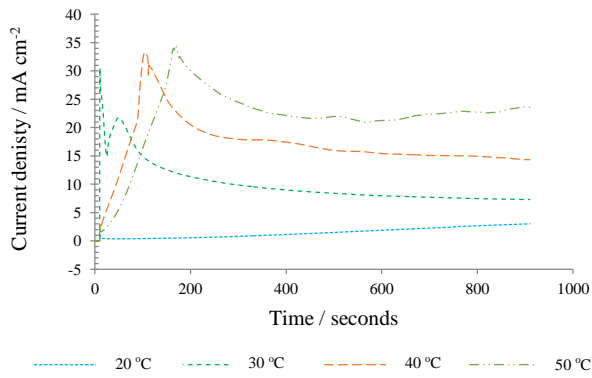


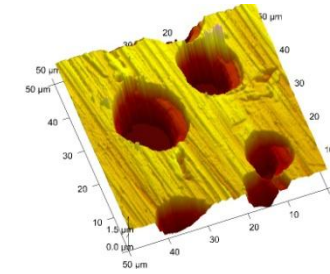
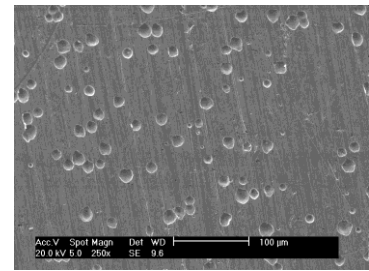
Figure 3.24 : (a) Current time transients of the electropolishing of ss304 at different potentials. SEM and AFM images of the electropolished ss304 for these current-time transients at (b) 0.7 V (c) 1.4 V (d) 2.3 V

3.4.2.1 Effect of temperature

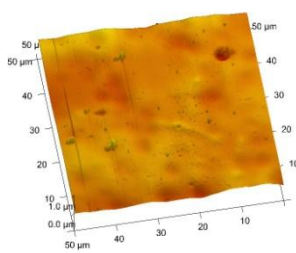
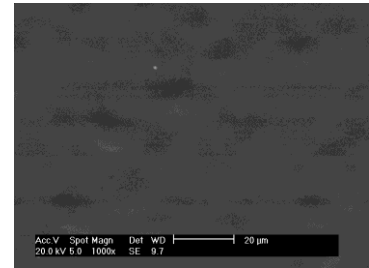
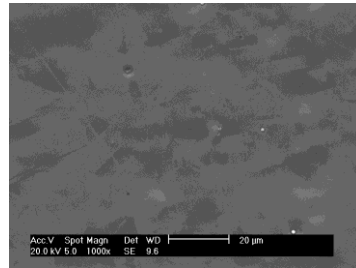
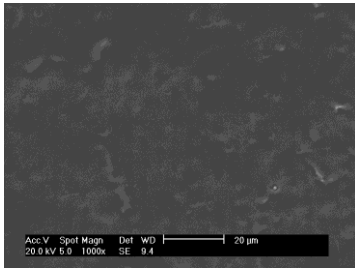
The effect of electropolishing temperature on the current time transients obtained at overpotential of 1.4 V along with the finished surface topography are shown in **Figure 3.25**.



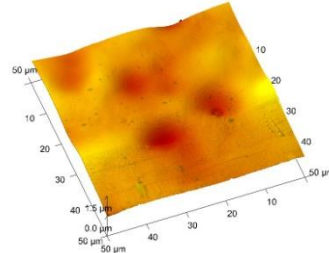
(a)



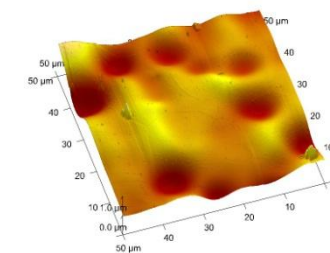
(b)



(c)



(d)



(e)

Figure 3.25 : (a) Current transients of ss304 electropolishing in 1:2 ChCl:EG at overpotential of 1.4 V at 20, 30, 40 and 50 °C. Surface morphologies of finished surface from these current time curves (b) 20 °C (c) 30 °C (d) 40 °C (e) 50 °C

Both anodic dissolution peak and the diffusion limited current plateau are shifted to higher values as the electrolyte temperature is increased from 20 °C to 50 °C. At 20 °C no dissolution peak is observed and pitted surface is obtained due to the partial dissolution of the oxide film. At higher temperatures (40 °C, 50 °C) the viscous thick film on the anode surface become unstable indicated by fluctuation of the current in the mass transfer control region which results in the crystallographic etching or pitting.

3.4.2.2 Effect of Additives

The presence of water in 1:2 ChCl:EG shifts the current time response to higher value due to an increase in conductivity and decrease in the viscosity while the addition of oxalic acid does not affect the current time response. At higher water contents (10 % - 20 %) the finished surface starts to become rough (**Figure 3.26 & 3.27**).

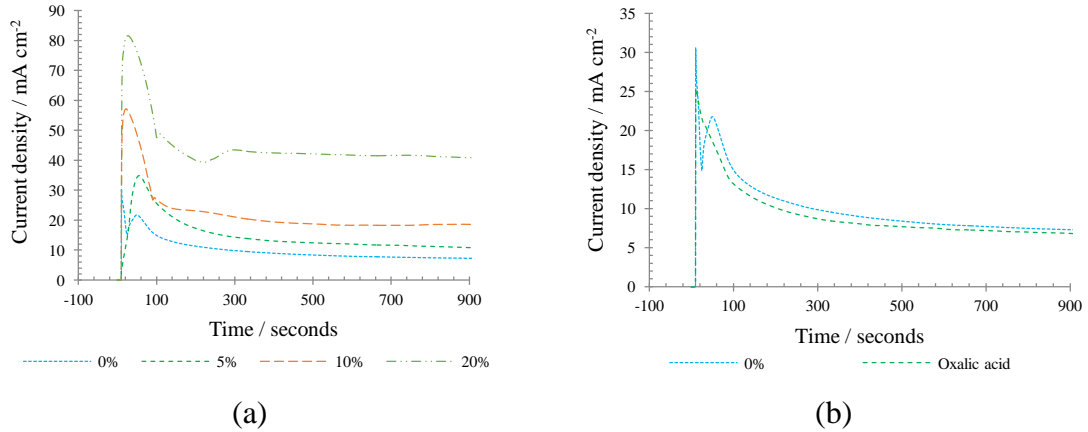


Figure 3.26: Current transients obtained at an overpotential of 1.4 V in 1:2 ChCl:EG (a) different water contents (b) 3% oxalic acid

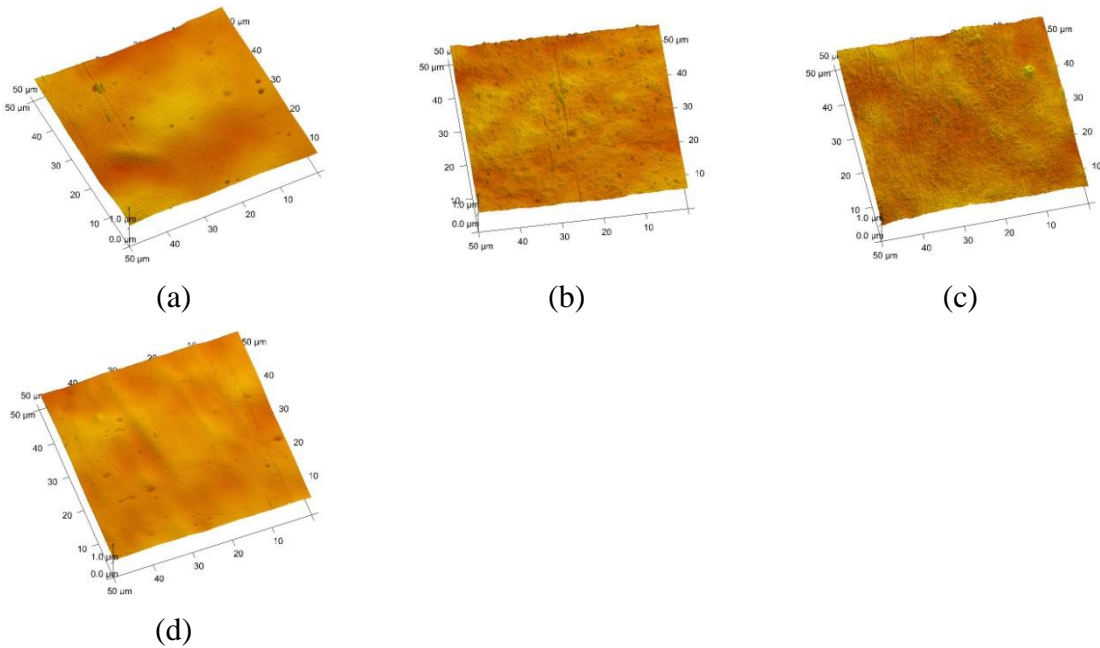


Figure 3.27: Surface morphologies of ss304 for current transients in **Figure 3.26** (a) 5 % H₂O (b) 10 % H₂O (c) 20 % H₂O (d) 3 % oxalic acid

3.4.3 Galvanostatic study

The galvanostatic study was conducted to investigate the variation in cell voltage during the electropolishing of ss304 at current densities of 2, 10, 25 and 50 mA cm⁻² at 30 °C. Fresh ss304 sheet, having an area of 1 cm² and fresh electrolyte (40 ml) was used every time. A three electrode configuration similar to the potentiostatic experiment was used.

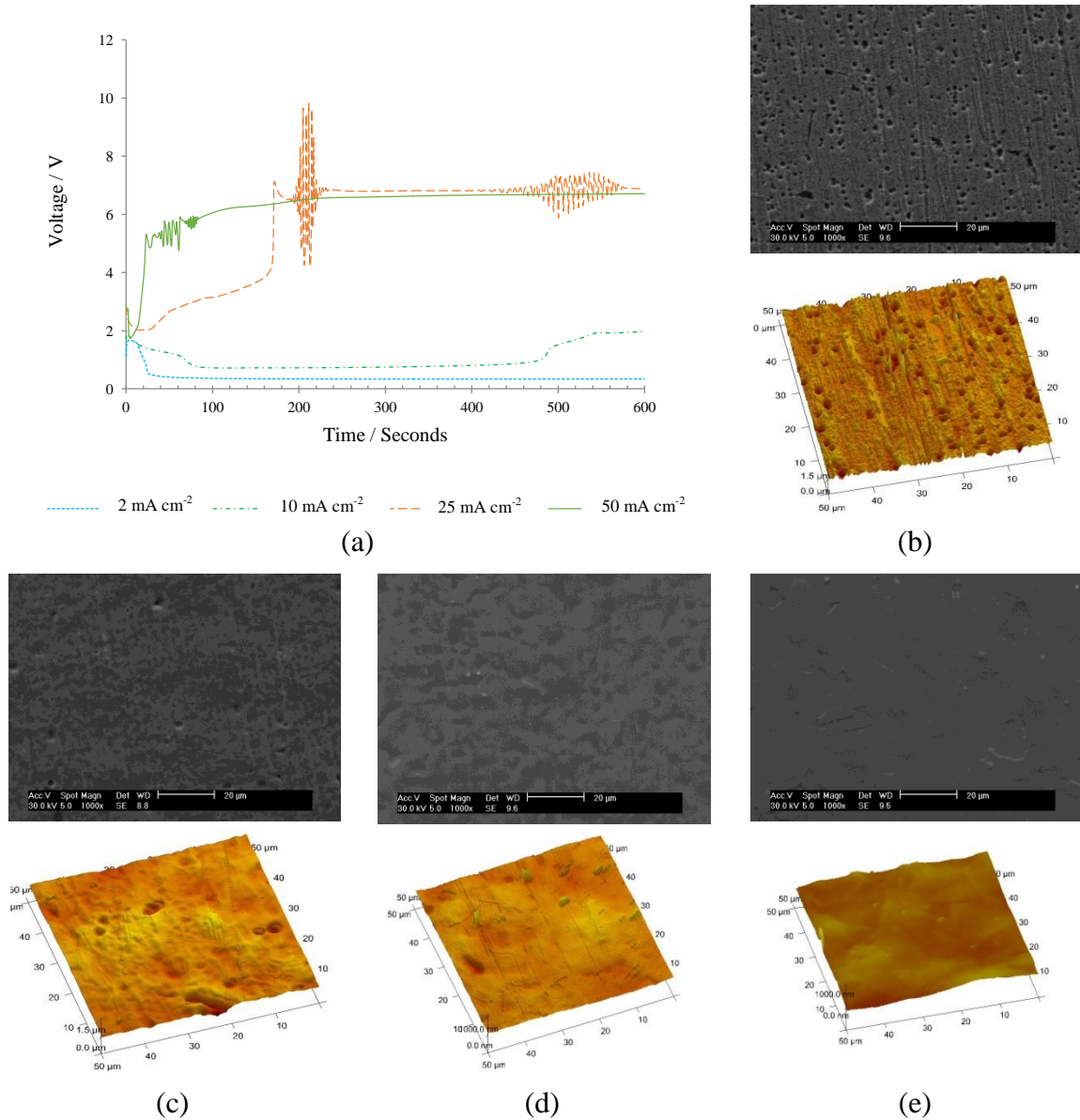


Figure 3.28 : (a) Galvanostatic transients in 1:2 ChCl:EG at 2 mA cm⁻², 10 mA cm⁻², 25 mA cm⁻² and 50 mA cm⁻²
SEM and AFM images of the polished surface in these transients
(b) 2 mA cm⁻² (c) 10 mA cm⁻² (d) 25 mA cm⁻² (e) 50 mA cm⁻²

The galvanostatic transients along with the finished surface topography are shown in **Figure 3.28**. At lower current density than the critical value, the cell voltage initially decreases and then becomes stable showing the absence of the thick viscous layer on anode surface and pitting of the surface is observed due to the partial breakdown of the surface oxide layer. In the E-t curve at 10 mA cm^{-2} , a rise in cell voltage around 460 seconds indicates the beginning of the formation of the thick viscous film. The surface finish is better than at 2 mA cm^{-2} though it still has pits.

The galvanostatic transients at 25 and 50 mA cm^{-2} show the characteristic rise in the cell voltage due to the formation of a high ohmic resistant thick viscous film and is found to be a function of the current density. In both cases the cell voltage rises from the initial value and then become stable around 6 V . The fluctuation in cell voltage at the stable cell voltage indicates the high ohmic resistance of the thick viscous film.

3.5 Optimization of electropolishing process – Experimental design strategies

Electropolishing is the anodic dissolution process for surface finishing of metals / alloys. It is widely used in the industry to obtain smooth and bright surfaces free of defects, contamination and stress. The surface finish is the function of different electropolishing variables and their interactions such as electrolyte composition, bath temperature, applied potential / current density and the electropolishing time. A sequential procedure was used to screen out the key factors or their interactions to find the robust operation conditions using the experimental design strategy i.e. fractional factorial design (FFD). The same strategies are used to study the composition control of Ni-P⁵⁸ and Fe-Ni⁵⁹ in electrodeposition. The main aim of this study is to construct a mathematical model for the controlled variable (surface roughness, Ra) based on the key influential electropolishing factors to control or predict Ra of the ss304. The key factors / their interactions obtained from the FFD study were further examined in the study of the steepest path to confirm the trend of Ra variations by simultaneously varying these variables.

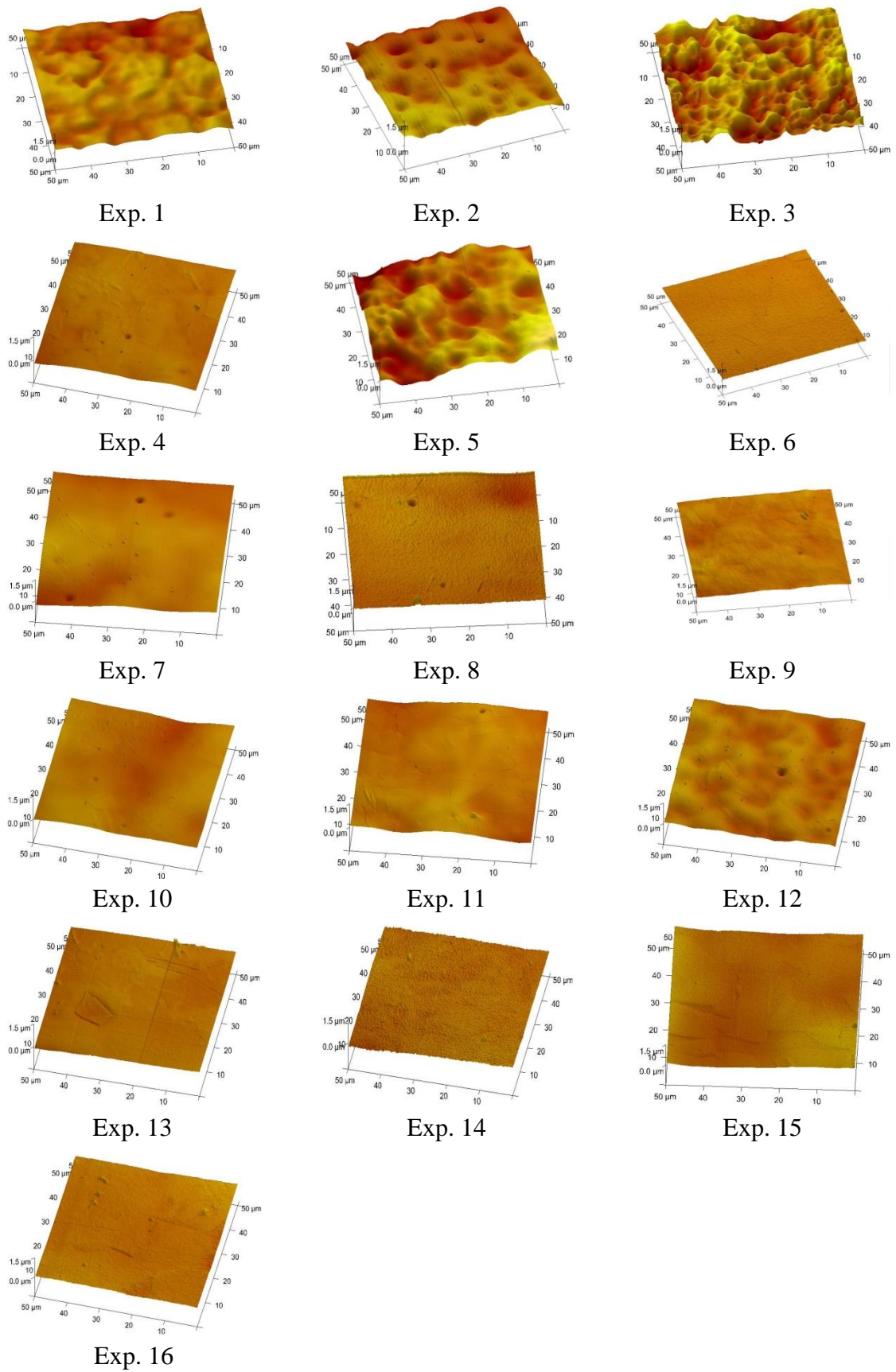


Figure 3.29 : *Topography of the electropolished ss304 for different experiments of FFD analysis. (Exp. represent the experiment sequence in Table 3.3)*

For fractional factorial analysis the electropolishing was performed on ss304 sheets with an exposed surface area of 4.2 cm^2 . Prior to the electropolishing the stainless steel sheets were degreased in soap and pickled in HCl solution (3%) for 5 minutes followed by thorough rinsing with deionised water. The electropolishing was conducted in 50 ml of 1:2 ChCl:EG electrolyte. A carbon mesh having surface area of $3 \times 8 \text{ cm}$ fully immersed in the solution and surrounding the substrate was used as cathode. The temperature was controlled by thermostating in a water bath. The electropolishing was conducted under various conditions designed in the FFD and the path of steepest ascent studies. After electropolishing the stainless steel sheets were thoroughly rinsed under tap water and then dipped in deionized water at 30°C in an ultrasonic oscillation bath for 10 minutes and dried under nitrogen.

The surface topography of the electrofinished surfaces were studied by atomic force microscope (AFM) and scanning electron microscope (SEM). The surface roughness was measured at two points with an area of $40 \times 40 \mu\text{m}$ and presented in **Figure 3.29**. The measured roughness values are used in the fractional factorial design to evaluate the effect of the different variables on the electropolishing quality.

3.5.1 Fractional Factorial Design (FFD)

Factorial design is an experimental strategy consisting of two or more factors, each having the discrete levels and studies all possible combination of these levels across all such factors. This design allows the study of the effect of each factor on the response variable as well as the effects of interactions between factors on the response variable. Mostly each factor has two levels and has 2^k treatment combinations. In case of large number of combinations, a fractional factorial design is adopted and this reduces the number of combinations to half at least.

Fractional factorial design is an experimental design consisting of a carefully chosen subset of the experiment runs of full factorial design exploiting the sparsity of effects principle which refers to the idea that only a few effects in a factorial experiment are statistically significant⁶⁰. Usually the system is dominated by the main effects (single factor) and low order interactions, two factor interactions are the most significant while three order interactions are very rare. Fractional factorial design is expressed by using the notation 1^{k-p} where '1' is the number of levels in each factor, 'K' is the number of factors investigated and 'p' describe the size of the fraction of the full factorial.

2^{k-1} fractional factorial design matrix can be constructed by writing down full factorial design matrix for factors 'k-1'. The kth factor is added by identifying its '+' and '-' levels by higher order interactions of 'k-1' factors. For example 2^{5-1} fractional factorial design is constructed by writing the full design matrix of 2^4 and the factor 'E' is added by defining the relation $I = ABCD$ i.e. the '+' and '-' of factor 'E' is determined by the interactions of A,B,C and D ($E = A \times B \times C \times D$)⁶⁰. Therefore the main effect of factor 'E' and the interaction effect of ABCD are confounded^{59,61} and according to the principle of the sparsity of effects⁶¹ the main effect of factor 'E' can be isolated using FFD experiment.

In fractional factorial design study, the following electropolishing parameters were investigated (a) volume content of water in 1:2 ChCl:EG (b) addition of oxalic acid (c) electrolyte temperature (d) electropolishing potential (e) electropolishing time. The low ('-') and high ('+') levels of these variables are given in **Table 3.2**.

| Table 3.2 : | | <i>Factors with their levels for 2^{5-1} fractional factorial design</i> | |
|--------------------|-----------------------------|---|----|
| Factors | | Levels | |
| | | - | + |
| A | 1:2 ChCl:EG + Water / vol % | 0 | 10 |
| B | Oxalic acid / weight % | 2 | 5 |
| C | Temperature / °C | 30 | 60 |
| D | Applied potential / V | 4 | 6 |
| E | Time / minutes | 5 | 10 |

Fractional factorial design (2^{5-1}) matrix is used to investigate the effect of these variables on electropolishing quality and is tabulated in **Table 3.3** along with the surface roughness values (R_a). The contrast coefficient of factor 'E' is generated from the contrast coefficient of the factors A, B, C and D using the **equation 3.6**^{60,61}

$$E = EI = EABCDE = E^2ABCD = ABCD \quad (3.6)$$

The inspection of the topographical images and the roughness values shows that certain factors and/or interactions have significant effect on surface finish; hence analysis of variance (ANOVA) was carried out.

| Table 3.3 : | | <i>The matrix design for 2^{5-1} fractional factorial design with the defining relation $I = ABCDE$ with the experimental data of R_a in nm</i> | | | | |
|--------------------|---------|--|---|---|---|----------------------------------|
| Experiment | Factors | | | | | Surface roughness (R_a) / nm |
| | A | B | C | D | E | |
| 1 | - | - | - | - | + | 66.75 |
| 2 | + | - | - | - | - | 47.50 |
| 3 | - | + | - | - | - | 86.50 |
| 4 | + | + | - | - | + | 15.30 |
| 5 | - | - | + | - | - | 81.25 |
| 6 | + | - | + | - | + | 8.68 |
| 7 | - | + | + | - | + | 33.98 |
| 8 | + | + | + | - | - | 15.25 |
| 9 | - | - | - | + | - | 38.75 |
| 10 | + | - | - | + | + | 34.35 |
| 11 | - | + | - | + | + | 27.58 |
| 12 | + | + | - | + | - | 23.68 |
| 13 | - | - | + | + | + | 20.65 |
| 14 | + | - | + | + | - | 16.18 |
| 15 | - | + | + | + | - | 23.33 |
| 16 | + | + | + | + | + | 22.00 |

The analysis of variance is based on partitioning of total variability (SST) into its component parts namely model sum of square (SS_{model}) and error sum of square (SS_{error})⁶⁰ and are calculated using **equations 3.7, 3.8, and 3.9**⁵⁹.

$$SST = \sum_{i=1}^{2^{k-1}} (Y_i - \bar{Y})^2 \quad (3.7)$$

where Y_i is the indicative of i_{th} response and \bar{Y} is the grand average of all the observations.

$$SS_i = \frac{(C_i)^2}{2^{k-1}} \quad (3.8)$$

SS_i is the sum of square corresponding to factor or interaction ‘i’, ‘C_i’ is the indicative of the contrast of factor or interaction ‘i’ which is the sum of multiplying all the observations with the corresponding signs in the appropriate column of the design matrix.

$$SS_{error} = SST - SS_{model} \quad (3.9)$$

Where SS_{error} is the sum of SS_i with the statistical insignificance while SS_{model} is the sum of SS_i with the statistical significance.

The results of the statistical analysis along with calculated ‘F’ value are tabulated in **Tables 3.4 and 3.5.**

| Table 3.5: | | <i>ANOVA results for surface roughness(Ra) from fractional factorial design matrix 2⁵⁻¹</i> | | |
|--------------------------------|---------|--|-------------------------|-------|
| Source | SS | d.f. | MS | F |
| A | 2397.33 | 1.00 | 2397.33 | 81.03 |
| B | 276.39 | 1.00 | 276.39 | 9.34 |
| C | 886.55 | 1.00 | 886.55 | 29.96 |
| D | 1381.98 | 1.00 | 1381.98 | 46.71 |
| E | 665.00 | 1.00 | 665.00 | 22.48 |
| AD | 1756.66 | 1.00 | 1756.66 | 59.37 |
| AE | 214.62 | 1.00 | 214.62 | 7.25 |
| DE | 735.09 | 1.00 | 735.09 | 24.84 |
| Error | 177.52 | 6.00 | 29.59 | |
| Total | 8491.13 | 15.00 | 566.08 | |
| $R^2 = 1 - (SSE / SST) = 0.98$ | | | $F_{0.05} (1,6) = 5.99$ | |

| Table 3.4 : | | <i>SSi calculation of factors and their interactions for 2^{5-1} fractional factorial design matrix</i> | | | | | | | | | | | | | |
|--------------------|---------|--|---------|---------|---------|---------|---------|---------|---------|---------|---------|---------|---------|---------|---------|
| | A | B | C | D | E | AB | AC | AD | AE | BC | BD | BE | CD | CE | DE |
| 1 | -66.75 | -66.75 | -66.75 | -66.75 | 66.75 | 66.75 | 66.75 | 66.75 | -66.75 | 66.75 | 66.75 | -66.75 | 66.75 | -66.75 | -66.75 |
| 2 | 47.5 | -47.5 | -47.5 | -47.5 | -47.5 | -47.5 | -47.5 | -47.5 | -47.5 | 47.5 | 47.5 | 47.5 | 47.5 | 47.5 | 47.5 |
| 3 | -86.5 | 86.5 | -86.5 | -86.5 | -86.5 | -86.5 | 86.5 | 86.5 | 86.5 | -86.5 | -86.5 | -86.5 | 86.5 | 86.5 | 86.5 |
| 4 | 15.3 | 15.3 | -15.3 | -15.3 | 15.3 | 15.3 | -15.3 | -15.3 | 15.3 | -15.3 | -15.3 | 15.3 | 15.3 | -15.3 | -15.3 |
| 5 | -81.25 | -81.25 | 81.25 | -81.25 | -81.25 | 81.25 | -81.25 | 81.25 | 81.25 | -81.25 | 81.25 | 81.25 | -81.25 | -81.25 | 81.25 |
| 6 | 8.675 | -8.675 | 8.675 | -8.675 | 8.675 | -8.675 | 8.675 | -8.675 | 8.675 | -8.675 | 8.675 | -8.675 | -8.675 | 8.675 | -8.675 |
| 7 | -33.975 | 33.975 | 33.975 | -33.975 | 33.975 | -33.975 | -33.975 | 33.975 | -33.975 | 33.975 | -33.975 | 33.975 | -33.975 | 33.975 | -33.975 |
| 8 | 15.25 | 15.25 | 15.25 | -15.25 | -15.25 | 15.25 | 15.25 | -15.25 | -15.25 | 15.25 | -15.25 | -15.25 | -15.25 | -15.25 | 15.25 |
| 9 | -38.75 | -38.75 | -38.75 | 38.75 | -38.75 | 38.75 | 38.75 | -38.75 | 38.75 | 38.75 | -38.75 | 38.75 | -38.75 | 38.75 | -38.75 |
| 10 | 34.35 | -34.35 | -34.35 | 34.35 | 34.35 | -34.35 | -34.35 | 34.35 | 34.35 | 34.35 | -34.35 | -34.35 | -34.35 | -34.35 | 34.35 |
| 11 | -27.575 | 27.575 | -27.575 | 27.575 | 27.575 | -27.575 | 27.575 | -27.575 | -27.575 | -27.575 | 27.575 | 27.575 | -27.575 | -27.575 | 27.575 |
| 12 | 23.675 | 23.675 | -23.675 | 23.675 | -23.675 | 23.675 | -23.675 | 23.675 | -23.675 | -23.675 | 23.675 | -23.675 | -23.675 | 23.675 | -23.675 |
| 13 | -20.65 | -20.65 | 20.65 | 20.65 | 20.65 | 20.65 | -20.65 | -20.65 | -20.65 | -20.65 | -20.65 | -20.65 | 20.65 | 20.65 | 20.65 |
| 14 | 16.175 | -16.175 | 16.175 | 16.175 | -16.175 | -16.175 | 16.175 | 16.175 | -16.175 | -16.175 | -16.175 | 16.175 | 16.175 | -16.175 | -16.175 |
| 15 | -23.325 | 23.325 | 23.325 | 23.325 | -23.325 | -23.325 | -23.325 | -23.325 | 23.325 | 23.325 | 23.325 | -23.325 | 23.325 | -23.325 | -23.325 |
| 16 | 22 | 22 | 22 | 22 | 22 | 22 | 22 | 22 | 22 | 22 | 22 | 22 | 22 | 22 | 22 |
| SSi | 2397.33 | 276.39 | 886.55 | 1381.98 | 665.00 | 1.93 | 0.17 | 1756.66 | 214.62 | 0.28 | 99.00 | 0.70 | 75.26 | 0.19 | 735.09 |

MS_i is the mean square of factor or interaction ‘i’ and is given by

$$MS_i = \frac{SS_i}{df_i} \quad (3.10)$$

MS_E is the mean square of factor or interactions with statistical insignificance and is calculated by

$$MS_E = \frac{SS_E}{df_E} \quad (3.11)$$

Where SS_i and SS_E are the sum of squares of factors/interactions of statistical significance and statistical insignificance respectively, df_i and df_E are the respective degrees of freedom.

The statistic ‘F’ is defined by⁵⁹

$$F = \frac{MS_i}{MS_E} \quad (3.12)$$

‘F’ value is used to judge the statistical significance of the factor or interaction, if at certain probability level (usually $\alpha = 0.05$) the calculated ‘F’ value for a factor or interaction is greater than the theoretical tabulated value then that factor or interaction is statistical significance otherwise it is pooled in error.

In this study main factors A (volume % age of water), B (weight % age of oxalic acid), C (electropolishing temperature), D (electropolishing potential) and E (Electropolishing time) and interactions AD, AE and DE are of statistical significance with the multiple correlation co-efficient (R^2) 0.98 indicating the good fit of the experimental data. The effect of all factors and interactions are shown in **Figure 3.30**.

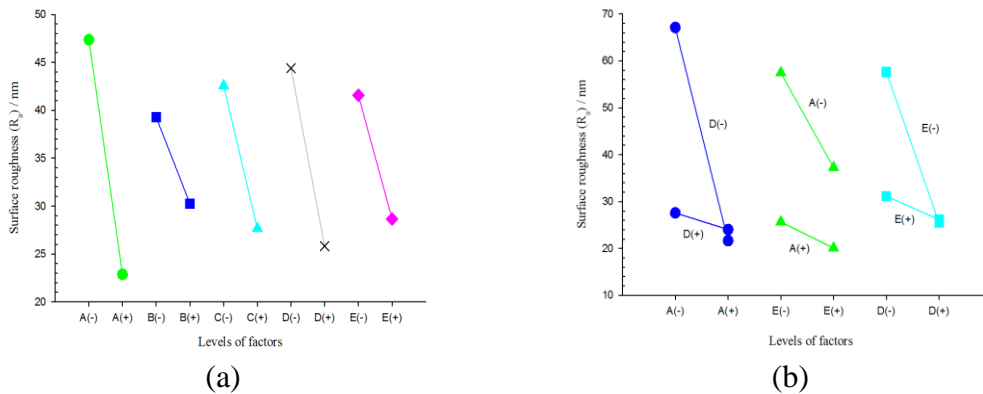


Figure 3.30 : Effects of (a) main factors A, B, C, D, E (b) interactions AD, AE, DE on the surface roughness of electropolished ss304. (+) and (-) signs indicate the high and low levels of factors respectively.

The factors / interactions have the following sequence in their decreasing order of influence $A > AD > D > C > DE > E > B > AE$. All the main factors have the positive impact on the roughness of electropolished ss304 with factor A is the most influential while the factor B is the least. Addition of water to the electropolishing bath decreases the viscosity of the 1:2 ChCl:EG and increase the conductivity of the solution. The decrease in the viscosity increases the diffusion rate of the anodically dissolved metals hence a smoother surface is obtained. This concept is supported by the complex interaction AD and AE. In interaction AD, when D (applied potential) is kept at its low level (4 V) the addition of water markedly decrease the Ra value indicating that addition of water increases the conductivity and decreases the viscosity of the solution which results in increase in current density at the applied potential and hence increase the rate of anodic dissolution and a better surface finish is obtained. Interaction AE further supports this argument that high level of A does not effect the surface finish while at low level, factor E (electropolishing time) has a strong influence on the R_a value.

From the analysis of variance and regression analysis in **Table 3.5**, a fitted polynomial model can be generated which quantitatively elucidates the effects of all the electropolishing variables and their interactions with statistical significance.

$$Y = 35.11 - 12.24x_A - 4.16x_B - 7.44x_C - 9.29x_D - 6.45x_E + 10.48x_Ax_D + 3.66x_Ax_E + 6.78x_Dx_E \quad (3.13)$$

where 'x_i' are the coded variables for factors A-E and defined as follows⁶²

$$x_i(\text{high}) = \frac{x_i(\text{high}) - x_i(\text{mean})}{S_i} = +1 \quad (3.14)$$

$$x_i(\text{low}) = \frac{x_i(\text{low}) - x_i(\text{mean})}{S_i} = -1 \quad (3.15)$$

$$x_i(\text{mean}) = \frac{1}{2}(x_i(\text{high}) + x_i(\text{low})) \quad (3.16)$$

$$S_i = \frac{1}{2}(x_i(\text{high}) - x_i(\text{mean})) \quad (3.17)$$

3.5.2 Contour plot

The contour plot for the dependence of the surface roughness of ss304 on factor C (temperature) and E (electropolishing time) is constructed by using the regression model in **equation 3.13 (Figure 3.31)**. The synergistic effect on decreasing the surface roughness

occurs when simultaneously increasing the factors C and E while keeping all other factors at their high level. The R_a values decrease from 19 nm to 10 nm in the investigation range. The minimum value is obtained when the temperature is 50°C and the electropolishing time is 10 minutes i.e. both are at their high levels. This is further confirmed by the steepest ascent path that the minimum roughness values are obtained when all the factors are at their highest level.

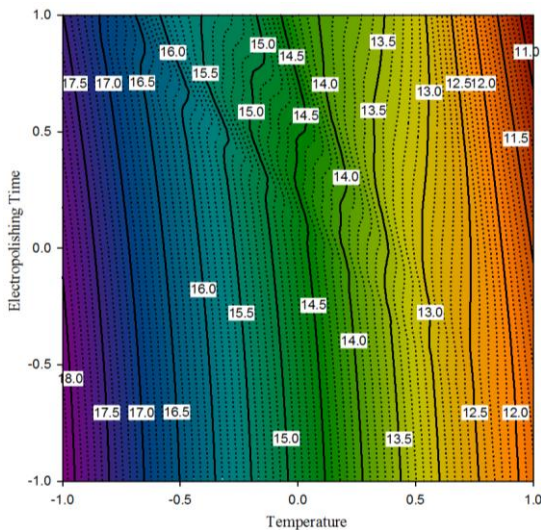


Figure 3.31 : A contour plot for contrast surface roughness against bath temperature and electropolishing time

3.5.3 The steepest ascent path

The steepest ascent path is the direction in which the response variable/s increase most rapidly⁶². It is directly proportional to the regression coefficients of the control variables in the **equation 3.13**. Therefore the step size along the steepest ascent path is approximately directly proportional to the first order regression coefficients⁶⁰.

The factors A, C, D and E are considered in the steepest ascent path and from the discussion in the previous section, the synergistic effect on decreasing the surface roughness of ss304 occurs by simultaneously moving A, C, D and E in the positive direction by $+12.24S_A$, $-7.44S_C$, $-9.29S_D$ and $-6.54S_E$. The corresponding step size comes out to be 2.5 vol %, 4 °C, 0.5 V and 1.25 minute respectively. Typical points on the path of the steepest ascent study with the corresponding results (R_a values) are tabulated in **Table 3.6** and their morphologies are shown in **Figure 3.32**. With experimental conditions of experiment 3, the optimal surface finish is obtained. The steepest ascent path and the

contour plot show the ability of the fitted regression model of the FFD study to explain the dependence of surface roughness.

| Table 3.6 : | | <i>Points on the path of steepest ascent with the corresponding surface roughness</i> | | | | |
|--------------------|-----------|---|--------|-------|-------------|---------------------|
| Experiment | A / % vol | B / % wt | C / °C | D / V | E / minutes | R _a / nm |
| 1 | 5.00 | 5.00 | 40.00 | 5.00 | 7.50 | 24.05 |
| 2 | 7.50 | 5.00 | 44.00 | 5.50 | 8.75 | 14.90 |
| 3 | 10.00 | 5.00 | 48.00 | 6.00 | 10.00 | 11.07 |
| 4 | 12.50 | 5.00 | 52.00 | 6.50 | 11.25 | 23.70 |
| 5 | 15.00 | 5.00 | 56.00 | 7.00 | 11.85 | 32.45 |

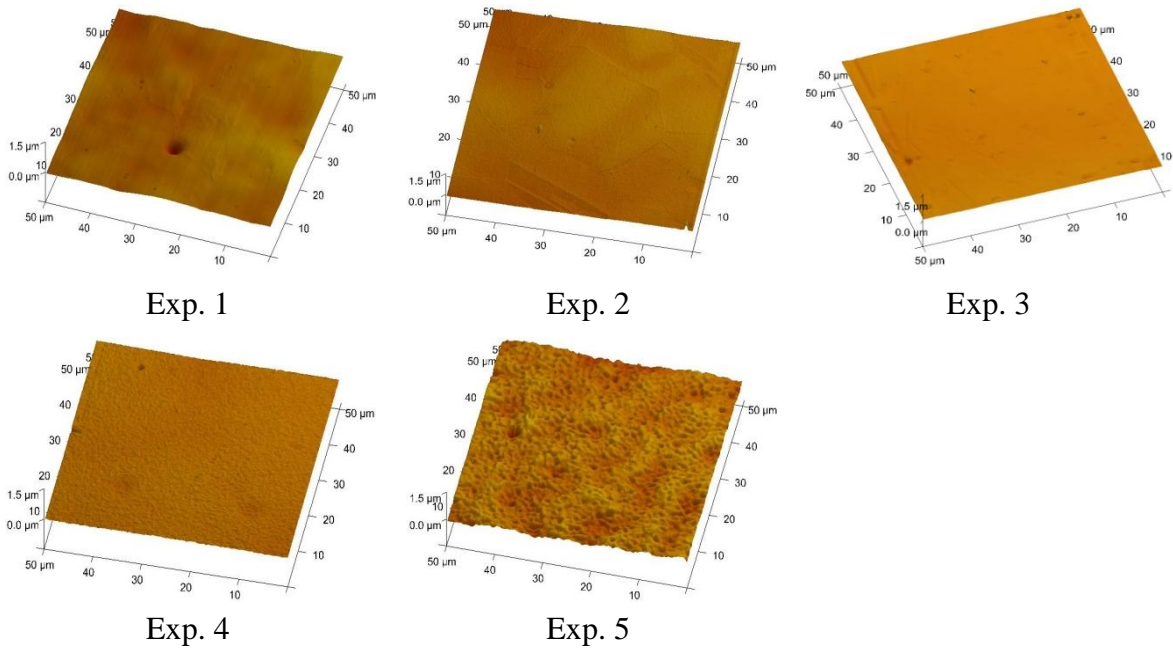


Figure 3.32: *AFM topographical images of electropolished ss304 at conditions described in Table 3.6.*

The sequential experiment strategies i.e. the fractional factorial design and the study of the steepest ascent path has demonstrated that volume content of water, electropolishing temperature, electropolishing voltage and time are the important factors and no strong interaction is found between these variables. All these electropolishing variables have positive effect on the quality of the surface finish. The study of the path of the steepest

ascent has shown that the model **equation 3.13** established in FFD study has the ability to predict precisely the effect of different electropolishing variables on the surface finish.

3.6 Summary

The electropolishing of stainless steel (ss304, ss316) had been studied in 1:2 ChCl:EG using the electrochemical techniques and the experimental design strategies for the process optimization. The physical properties and life cycle study have also been conducted to probe into the fundamentals of the electropolishing process.

The electropolishing of ss304 was carried out successfully in 1:2 ChCl:EG. The physical properties viscosity, conductivity and surface tension showed the strong dependence on temperature. Surface tension of 1:2 ChCl:EG was comparable to imidazolium based ionic liquids. Large values of surface entropy indicated a high level of surface organization due to the strong hydrogen bonding. The life cycle studies revealed that the history of the liquid had no effect on the quality of surface finish and the recycled liquid worked well similar to the virgin liquid. With potentiostatic electropolishing, the rate of anodic dissolution slightly decreased with aging of the solution that might be attributed to slow migration of the dissolved metal ions due to build up of a high concentration of metal ions in the solution.

The linear sweep studies showed that the anodizing curve had the four distinct regions namely active dissolution, passivation, diffusion limited and pitting region similar to characteristic anodizing curves from inorganic acid solution and differed only in positions and current density. Increase in temperature and the addition of water shifted the current density to a higher value and no pitting region was observed due to the change in viscosity and conductivity. Potentiostatic and galvanostatic studies revealed that electropolishing in 1:2 ChCl:EG took place through the formation of a thick viscous liquid film on the surface of the substrate.

The optimal setting for electropolishing of stainless steel with minimum surface roughness ' R_a ' in 1:2 ChCl:EG was approached by using the experimental strategy of Fractional Factorial Design (FFD) coupled with response surface methodology (RMD) and the path of steepest ascent. The effect of different variables i.e. concentration of water, oxalic acid, electropolishing temperature, time and potential were studied. The anodic dissolution variables showed the positive effect on the surface finish. The response surface

contour plot constructed by simultaneously increasing the temperature and time and the path of steepest ascent studies showed that the fitted regression model predicted well the effect of independent variables on the response variable. This was also supported by the linear sweep voltammetry.

3.7 References

- (1) Abbott, A. P.; Capper, G.; McKenzie, K. J.; Glidle, A.; Ryder, K. S. *Physical Chemistry Chemical Physics* **2006**, *8*, 4214-4221.
- (2) Ke Song, Z.; Herman, H. *Wear* **1982**, *80*, 101-113.
- (3) Heathcock, C. J.; Ball, A.; Protheroe, B. E. *Wear* **1981**, *74*, 11-26.
- (4) Okada, T.; Iwai, Y.; Awazu, K. *Wear* **1988**, *124*, 21-31.
- (5) Gately, N. V. H.; Dillich, S. A. *Materials Science and Engineering* **1987**, *90*, 333-338.
- (6) Gately, N. V. H.; Dillich, S. A. *Surface and Coatings Technology* **1988**, *35*, 69-78.
- (7) Matsumura, M.; Oka, Y.; Ebara, R.; Kobayashi, T.; Odohira, T.; Wada, T.; Hatano, M. *Environmentally Assisted Cracking: Science and Engineering*; ASTM STP 1049, ASTM: Philadelphia, **1990**.
- (8) Richman, R. H.; McNaughton, W. P. *Journal of Materials Engineering and Performance* **1997**, *6*, 633-641.
- (9) Sang, K.; Li, Y. *Wear* **1995**, *189*, 20-24.
- (10) Guo, X.; Herman, H. *Cavitation-erosion testing of thermal sprayed Tribaloy (T-400) coatings, in: Thermal Spray Technology: New Ideas & Processes*; ASM International, Materials Park: Ohio, USA, **1989**.
- (11) Frees, N. *Wear* **1983**, *88*, 57-66.
- (12) Vakula, S. I.; Marinin, V. G.; Ostapenko, I. L.; Strel'nitskii, V. E. *Physics and chemistry of materials treatment* **1991**, *25*, 181-185.
- (13) Tomlinson, W.; Talks, M. *Journal of Materials Science* **1991**, *26*, 804-808.
- (14) Giren, B. G. *Surface Engineering* **1998**, *14*, 325-330.
- (15) Draper, C. W. *High Temperature Materials and Processes* **1984**, *6*, 213-224.
- (16) Andrade, L. S.; Xavier, S. C.; Rocha-Filho, R. C.; Bocchi, N.; Biaggio, S. R. *Electrochimica Acta* **2005**, *50*, 2623-2627.
- (17) Tam, S. C.; Loh, N. L.; Mah, C. P. A.; Loh, N. H. *Journal of Materials Processing Technology* **1992**, *35*, 83-91.
- (18) Wilson, J. *Practice and Theory of Electrochemical Machining*; Wiely, **1970**.

- (19) Sautebin, R.; Froidevaux, H.; Landolt, D. *Journal of the Electrochemical Society* **1980**, *127*, 1096-1100.
- (20) Clerc, C.; Datta, M.; Landolt, D. *Electrochimica Acta* **1984**, *29*, 1477-1486.
- (21) Landolt, D. *Electrochimica Acta* **1987**, *32*, 1-11.
- (22) Datta, M.; Landolt, D. *Journal of the Electrochemical Society* **1975**, *122*, 1466-1472.
- (23) Datta, M.; Landolt, D. *Electrochimica Acta* **1980**, *25*, 1255-1262.
- (24) Fedkiw, P. *Journal of the Electrochemical Society* **1980**, *127*, 1304-1308.
- (25) Hryniewicz, T.; Rokicki, R.; Rokosz, K. *Surface and Coatings Technology* **2008**, *202*, 1668-1673.
- (26) Matlosz, M. *Electrochimica Acta* **1995**, *40*, 393-401.
- (27) Wagner, C. *Journal of the Electrochemical Society* **1954**, *101*, 225-228.
- (28) Grimm, R. D.; West, A. C.; Landolt, D. *Journal of the Electrochemical Society* **1992**, *139*, 1622-1629.
- (29) Matlosz, M.; Magaino, S.; Landolt, D. *Journal of the Electrochemical Society* **1994**, *141*, 410-418.
- (30) Yuzhakov, V. V.; Chang, H.-C.; Miller, A. E. *Physical Review B* **1997**, *56*, 12608-12624.
- (31) Bandyopadhyay, S.; Miller, A. E.; Chang, H. C.; Banerjee, G.; Yuzhakov, V.; Yue, D. F.; Ricker, R. E.; Jones, S.; Eastman, J. A.; Baugher, E.; Chandrasekhar, M. *Nanotechnology* **1996**, *7*, 360.
- (32) Lin, C. C.; Hu, C. C. *Electrochimica Acta* **2008**, *53*, 3356-3363.
- (33) H.Figous; Jacquet, P. A. In *French Patent*, **1930**; Vol. 707526.
- (34) Welton, T. *Chemical Reviews* **1999**, *99*, 2071-2083.
- (35) Buzzeo, M. C.; Evans, R. G.; Compton, R. G. *Chemphyschem* **2004**, *5*, 1106-1120.
- (36) Endres, F. *Chemphyschem* **2002**, *3*, 144.
- (37) Abbott, A. P.; McKenzie, K. J. *Physical Chemistry Chemical Physics* **2006**, *8*, 4265-4279.
- (38) Abbott, A. P.; Harris, R. C.; Ryder, K. S. *Journal of Physical Chemistry B* **2007**, *111*, 4910-4913.
- (39) Bockris, J. O. M.; Reddy, A. K. N. *Modern electrochemistry*; Plenum Press, **1998**.
- (40) George J. Janz *Molten salts handbook*; Academic Press: New York, **1967**.
- (41) Abbott, A. P. *Chemphyschem* **2005**, *6*, 2502-2505.

- (42) Abbott, A. P.; Capper, G.; McKenzie, K. J.; Ryder, K. S. *Journal of Electroanalytical Chemistry* **2007**, *599*, 288-294.
- (43) Ghatee, M. H.; Zolghadr, A. R. *Fluid Phase Equilibria* **2008**, *263*, 168-175.
- (44) Freire, M. G.; Carvalho, P. J.; Fernandes, A. M.; Marrucho, I. M.; Queimada, A. n. J.; Coutinho, J. o. A. P. *Journal of Colloid and Interface Science* **2007**, *314*, 621-630.
- (45) Sanchez, L. G.; Espel, J. R.; Onink, F.; Meindersma, G. W.; de Haan, A. B. *Journal of Chemical & Engineering Data* **2009**, *54*, 2803-2812.
- (46) Huddleston, J. G.; Visser, A. E.; Reichert, W. M.; Willauer, H. D.; Broker, G. A.; Rogers, R. D. *Green Chemistry* **2001**, *3*, 156-164.
- (47) Freire, M. G.; Carvalho, P. J.; Fernandes, A. M.; Marrucho, I. M. *Journal of Colloid and Interface Science* **2007**, *314*, 621-630.
- (48) Switzenbaum, M. S.; Veltman, S.; Mericas, D.; Wagoner, B.; Schoenberg, T. *Chemosphere* **2001**, *43*, 1051-1062.
- (49) Abbott, A. P.; Capper, G.; McKenzie, K. J.; Ryder, K. S. *Electrochimica Acta* **2006**, *51*, 4420-4425.
- (50) Riveros, G.; Green, S.; Cortes, A.; Gomez, H.; Marotti, R. E.; Dalchiele, E. A. *Nanotechnology* **2006**, *17*, 561-570.
- (51) Zein El Abedin, S.; Endres, F. *Electrochimica Acta* **2009**, *54*, 5673-5677.
- (52) Nazneen, F.; Galvin, P.; Arrigan, D. M.; Thompson, M.; Benvenuto, P.; Herzog, G. *Journal of Solid State Electrochemistry* **2012**, *16*, 1389-1397.
- (53) Lee, E. S. *The International Journal of Advanced Manufacturing Technology* **2000**, *16*, 591-599.
- (54) Murali, S.; Ramachandra, M.; Murthy, K. S. S.; Raman, K. S. *Materials Characterization* **1997**, *38*, 273-286.
- (55) Magaino, S.; Matlosz, M.; Landolt, D. *Journal of the Electrochemical Society* **1993**, *140*, 1365-1373.
- (56) Ponto, L.; Datta, M.; Landolt, D. *Surface and Coatings Technology* **1987**, *30*, 265-276.
- (57) Huang, C. A.; Lin, W.; Lin, S. C. *Corrosion Science* **2003**, *45*, 2627-2638.
- (58) Hu, C. C.; Bai, A. *Surface and Coatings Technology* **2001**, *137*, 181-187.
- (59) Tsay, P.; Hu, C. C. *Journal of the Electrochemical Society* **2002**, *149*, C492-C497.
- (60) Box, G. E. P.; Hunter, W. G.; Hunter, J. S. *Statistics for Experiments*; John Wiley & Sons: New York, **1978**.

- (61) Montgomery, D. C. *Design and Analysis of Experiments*; 4th ed.; John Wiley & Sons: Singapore, **1997**.
- (62) Hu, C. C.; Tsou, T.W. *Journal of Power Sources* **2003**, *115*, 179-186.

| | | |
|-------------------------------|---|------------|
| Chapter 4 : | Surface texture of Electropolished Stainless Steel | 102 |
| 4.1 | Introduction | 103 |
| | 4.1.1 <i>Types of stainless steel</i> | 107 |
| | 4.1.2 <i>Structure of stainless steel</i> | 108 |
| Results and Discussion | | |
| 4.2 | Nanostructuring of electropolished surface | 109 |
| 4.3 | Surface finish of electropolished surface | 112 |
| | 4.3.1 <i>Surface roughness</i> | 113 |
| | 4.3.1.1 <i>Surface roughness parameters</i> | 114 |
| | 4.3.2 <i>Surface roughness measurement</i> | 117 |
| | 4.3.2.1 <i>Profile (2D) measurements</i> | 118 |
| | 4.3.2.2 <i>Surface (3D) measurements</i> | 119 |
| | 4.3.3 <i>Effect of electropolishing time on surface roughness</i> | 120 |
| | 4.3.4 <i>Surface finish in recycled liquid</i> | 122 |
| | 4.3.5 <i>Amount of material etched</i> | 124 |
| | 4.3.6 <i>Surface roughness measurements by DHM</i> | 126 |
| 4.4 | Corrosion behaviour of austenitic steel | 129 |
| | 4.4.1 <i>Types of corrosion</i> | 128 |
| | 4.4.2 <i>Corrosion resistance measurements</i> | 129 |
| | 4.4.2.1 <i>Open circuit potential (OCP) measurements</i> | 130 |
| | 4.4.2.2 <i>Weight loss measurements</i> | 132 |
| | 4.4.2.3 <i>Potentiodynamic polarization curves</i> | 136 |
| 4.5 | Summary | 142 |
| 4.6 | References | 143 |

4.1 Introduction

In the previous chapter (chapter 3), the fundamental aspects of the electropolishing mechanism of stainless steel in 1:2 ChCl:EG were studied using the electrochemical methods (linear sweep anodizing curves, chronoamperometry and galvanostatic studies) and the optimal setting of the different electropolishing variables like water content, concentration of oxalic acid, electropolishing temperature, time and potential for electropolishing of stainless steel using the fractional factorial design strategies. In this chapter the effect of electropolishing on surface texture (surface overlayer morphology, surface roughness and etch rate) is investigated. The effect of electropolishing on the corrosion behaviour of stainless steel has also been studied using electrochemical and gravimetric methods.

Stainless steels are the most important, diverse and complex family of all steels. Their importance lies in the plentitude of applications ranging from low end applications (cooking utensils, street furniture, cutlery, automotive trims) to very sophisticated ones such as space vehicles^{1,2}. They are also used under very hostile environments of chemicals, oil production and power generation. Their wide spectrum of usage is either for decorative purposes and/or their excellent resistance to corrosion. Their corrosion resistance is due to the spontaneous self healing oxide protective layer on the surface that reduces the rate of corrosion to negligible levels³.

Stainless steels are based on Fe-Cr-C and Fe-Cr-Ni-C systems, sometimes other alloying elements are also present to confer on them special properties. Iron and its alloys can exist in two crystallographic forms (i) body centred cubic (BCC) at temperatures up to 910 °C and above 1400 °C up to melting temperature and iron is called Ferrite (α , δ) (ii) face centred cubic (FCC) between 910 °C – 1400 °C and is called austenite (γ). This phenomenon of change in crystalline structures in response to the temperature change is called ‘Phase transformation’.

In iron metallurgy, the phase transformation is of utmost importance and a large number of microstructures can be produced by controlling the heat treatment with desired mechanical properties. **Figure 4.1** shows the portion of iron- carbon phase diagram which shows the different microstructures formed due to change of the solubility limit of carbon as a function of temperature.

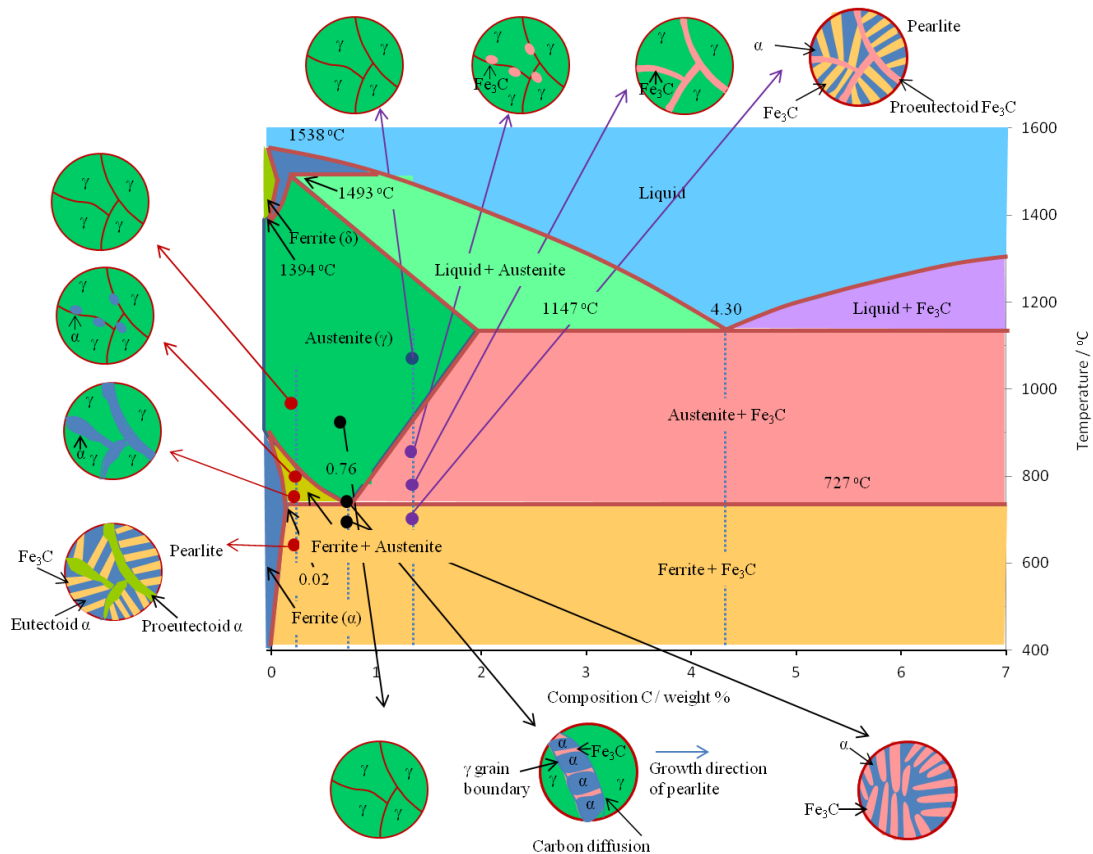


Figure 4.1 : Part of the iron-carbon phase diagram redrawn from the reference⁴

The stainless steel essentially contain iron and chromium which confer to it the corrosion resistance. In addition to these two elements they also contain the other elements

- Nickel (0-25%) - it promotes austenitic stability and reduces the temperature at which austenite can exist.
- Manganese (0-12%) - it also stabilizes the austenite or may be used as substitute for Ni and also increases the strength.
- Molybdenum (0-9%) - it increases the resistance to localized corrosion phenomena such as pitting and crevice corrosion.
- Silicon - it improves the casting properties as well as corrosion resistance in special environments.
- Nitrogen (<0.5%) - it is austenitic stabilizer and also improves the strength and crevice corrosion resistance.

- Copper - improves corrosion resistance in special environments.
- Titanium (<1%) - it reduces the sensitization and is strong carbide former.
- Niobium (<1%) - it also reduces the sensitization and is strong carbide former
- Carbon (< 0.15% except martensitic grades) - it stabilizes the austenite and hardens martensite for cutting edges

In iron alloys relative stability of FCC and BCC is of prime concern and conventionally the major alloying elements (Cr or Ni) are used to quantify the influence on BCC to FCC phase transition. Cr is the BCC stabilizer while Ni is FCC stabilizer, in the absence of C, the maximum limit to stabilize FCC is 13.5 wt% and it increases with the addition of carbon. Other alloying elements also effect the stability of BCC/FCC in one direction or another and accordingly termed as α -stabilizers (BCC stabilizer) or γ -stabilizer (FCC stabilizer). The concept of Cr-equivalent (α -stabilizers) and Ni-equivalent (γ -stabilizers) is widely used to quantify their roles in conjunction with the Schaeffler diagram⁵ **Figure4.2**. This diagram shows limits of the austenitic, ferritic and martensitic phases in relation to the chromium and nickel equivalent after rapid cooling from 1050°C to room temperature and is calculated as follows (all are in wt%).

$$\text{Cr equivalent} = (\text{Cr}) + 2(\text{Si}) + 1.5(\text{Mo}) + 5(\text{V}) + 5.5(\text{Al}) + 1.75(\text{Nb}) + 1.5(\text{Ti}) + 0.75(\text{W})$$

$$\text{Ni equivalent} = (\text{Ni}) + (\text{Co}) + 0.5(\text{Mn}) + 0.3(\text{Cu}) + 25(\text{N}) + 30(\text{C})$$

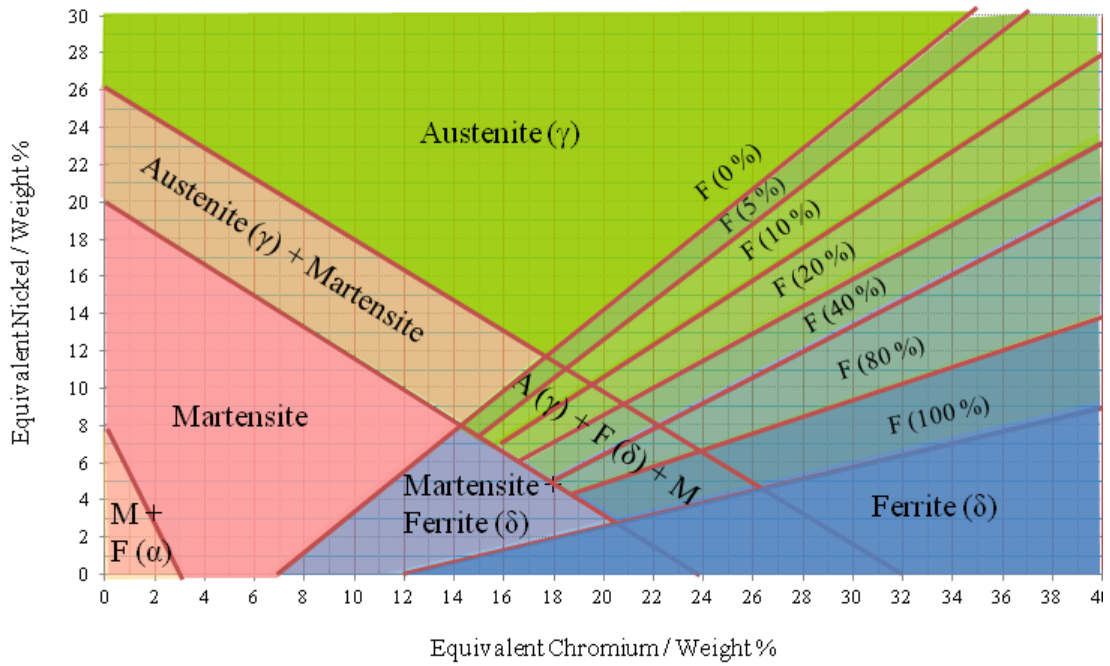


Figure 4.2 : Schaeffler diagram redrawn from reference⁵

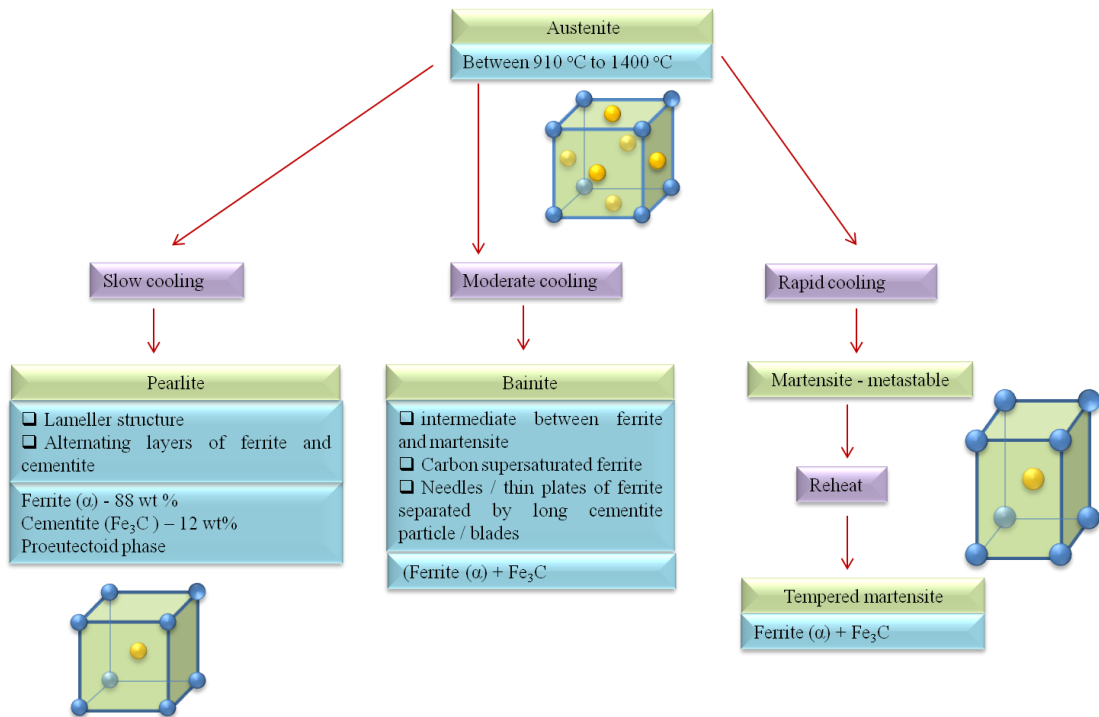


Figure 4.3 : Microstructures of stainless steel as a function of cooling rate

In most grades of stainless steel, alloying elements are present in sufficient amounts which produce second phases mostly carbides, nitrides or intermetallics. These intermediate

phases are in order of cementite, M_2X and M_7C_3 to finally obtain $M_{23}C_6$. The % age and arrangement of carbides/ intermetallics depend on the cooling rate of the austenite iron and is shown in **Figure 4.3**.

4.1.1 Types of stainless steel

On the basis of main microstructures, the stainless steel can be divided into following typical grades and main characteristics and usages of 300 series of stainless steel are shown in **Figure 4.4**.

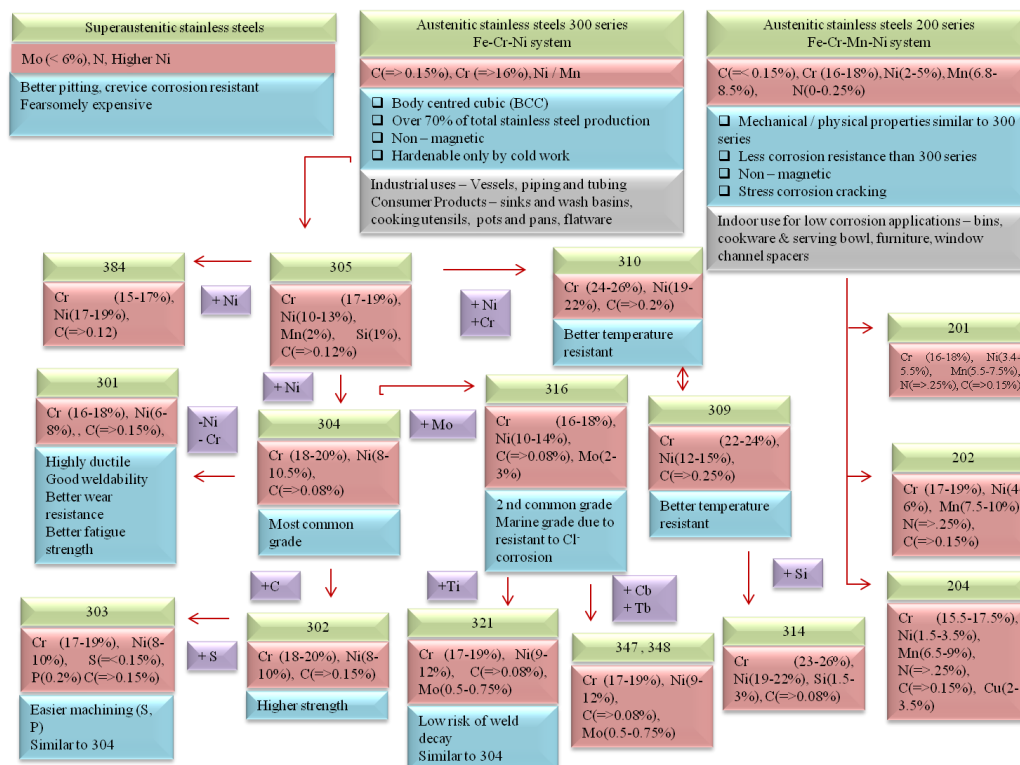


Figure 4.4: Fundamental properties, usages and commercially available grades with compositions⁵ of 300 series stainless steel.

- i. Austenitic chromium-nickel-manganese alloys – AISI type 200 series
- ii. Martensitic stainless steel – AISI type 400 series, containing Cr (12%) and C (0.1%)
- iii. Ferritic stainless steel – AISI type 400 series, high Cr content to stabilizes the ferritic (BCC) structure
- iv. Austenitic stainless steel – AISI type 300 series, contains Cr (≥16%) and Ni (≥ 8%)
- v. Duplex stainless steel – 50/50 ferritic/austenitic microstructure
- vi. Martensitic precipitation hardening alloys - AISI 600 series, Cr (17%), Ni (4%)

vii. Heat resisting chromium alloys – AISI type 500 series

4.1.2 Structure of stainless steel

The steel is a polycrystalline material composed of many grains usually having a diameter of 10-20 μm . The iron atoms arrange themselves regularly either body centred cubic or face centred cubic crystal lattice depending on their type and direction of their arrangement may differ from grain to grain. Lattice defects arise in the grains due to the loss of regularity of the positions of the iron atoms namely; (i) vacancies – point like defects due to missing iron atoms and play important role in the diffusion of atoms (ii) dislocations – linear defects, plastic deformation occurs due to the movement of the dislocations.

Foreign atoms (other than Fe atom) also exist in the grain in one of the two forms; (i) Solid solutions – in the lattice structure of iron either within the spaces between iron atoms (interstitial solid solutions) or replace the iron atoms in the lattice (substitutional solid solutions) (ii) Precipitates – form another crystal structure either within the grain or at the grain boundaries. A schematic presentation of the microstructure of stainless steel is shown in **Figure 4.5**.

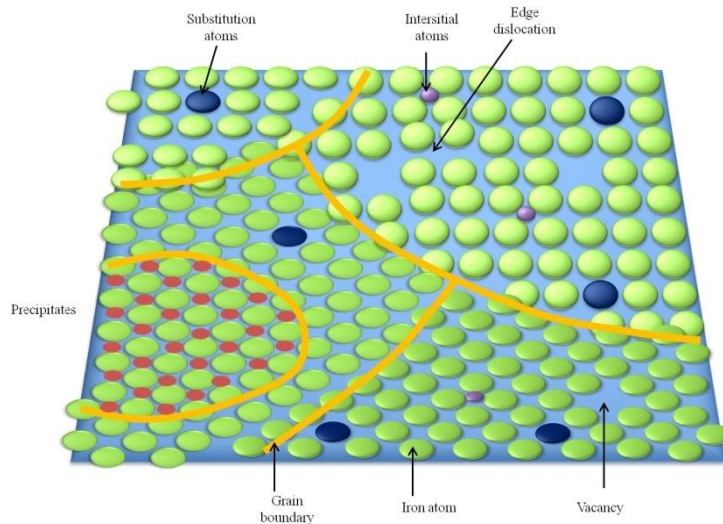


Figure 4.5 : Schematic diagram of microscopic structure of stainless steel

Iron usually assumes the texture that has many grains with specific orientations under some working and heat treatment conditions. A grain boundary has excess energy and reduces it by decreasing its boundary area by the movement of atoms when it becomes

possible. Therefore new small grains are formed which increase toughness and strength. Grains can be generated by transformations or recrystallization. In recrystallization the grain refinement takes place by heating the material beyond its critical strain and the accumulated strain energy is released by diffusion that cause the rearrangement of the atoms and new grains are formed. Grain refinement is achieved by utilizing these mechanisms: (a) annealing (b) normalising (c) quenching (d) tempering. Annealing and normalising are the softening processes and produce soft, low stress and ready for machining steel while quenching and tempering are hardening processes and produce hard and brittle steel.

Stainless steels are the most extensively used Fe-Cr alloys in everyday life ranging from household, construction and high tech applications. Surface condition of stainless steels plays an important role in its applications which is affected by microgeometry and residual stresses / strains arising during fabrication and finishing operations. Most important of them is the surface roughness which greatly influences the performance of machining parts and corrosion resistance of stainless steel. It is very difficult and increases the cost exponentially in manufacturing to decrease surface roughness. High surface quality specifications such as surface smoothness, material cleanliness and corrosion resistance are usually achieved by different surface treatment processes, most widely used and economical of them is electropolishing.

Surface characterization of electrochemically treated surfaces of austenitic stainless steels ss304 and ss316 was carried out by electrochemical and microscopic methods. Surface over layer morphology and surface finish of electropolished samples were investigated using atomic force microscope (AFM), scanning electron microscope (SEM), field emission scanning electron microscope (FE-SEM) and digital holographic microscope (DHM). The effect of electropolishing on corrosion resistance of austenitic stainless steel was conducted using electrochemical methods, open circuit potential measurement (OCP), potentiodynamic polarization curves and gravimetric methods.

4.2 Nanostructuring of electropolished surface

The electropolishing process is widely applied to achieve clean, flat and bright surfaces of pure metals or metallic alloys⁶. Sometimes the electrofinished surfaces may show a particular patterned relief like stripes or quasi periodic arrangements of protrusions or pores are generated under certain physico-chemical conditions. Orientations and

periodicity of such a pattern depend on grain orientations and /or polishing conditions such as applied voltage, the electrolyte concentration and oxidation time⁶. The studies of anodic alumina reveal that the patterns are independent of the orientation of underlying metallic lattice⁷⁻⁹. Anodization of aluminium in perchloric acid-ethanol based electrolyte generates the stripes¹⁰ which change into a hexagonal arrangement of pores in an over layer of amorphous alumina at high voltage (60 V)⁸.

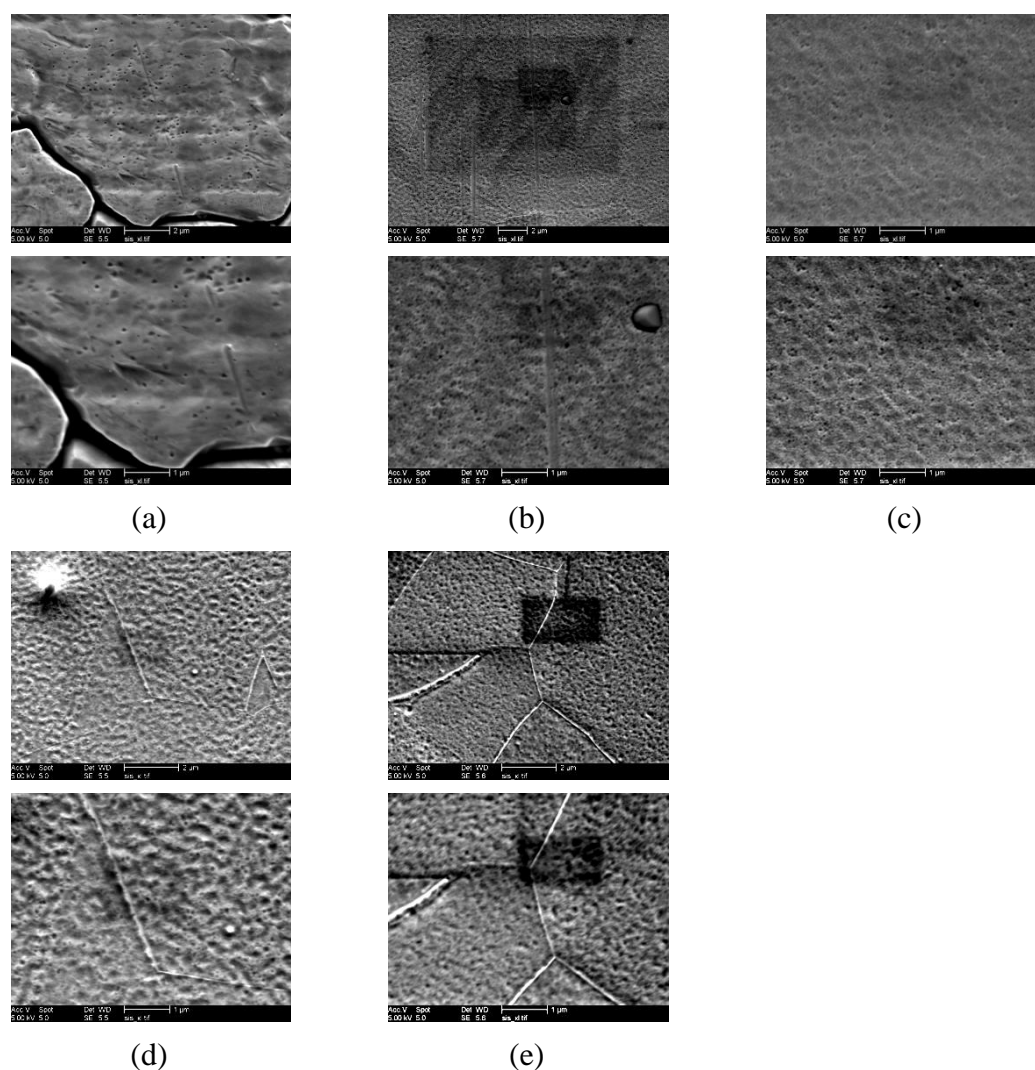


Figure 4.6 : *FE-SEM images showing surface morphology of ss316 electropolished at 6 V for (a) unpolished (b) 5 minutes (c) 10 minutes (d) 20 minutes (e) 30 minutes*

Many studies have revealed the growth of self-organised nanotubes in porous anodic layers under various electrochemical conditions in several metals such as tantalum¹¹, hafnium¹², niobium¹³, tungsten¹⁴ and zirconium¹⁵. Little work has been reported on the surface morphology of electropolished alloy surfaces. Electropolished surface of AISI 316 in

perchloric acid – ethylene glycol monobutylether electrolyte leads to the formation of a quasi-hexagonal arrangement of the porous surface layer¹⁶. Square wave potential pulse polarization in sulphuric acid solution leads to the formation of a porous oxide film¹⁷.

In the present work, primary morphology study of the electropolished surface of ss316 in 1:2 ChCl:EG containing oxalic acid as an additive was conducted and nanostructure was observed using a field emission scanning electron microscope and atomic force microscopy. The ss316 coupons with an exposed area of 2 x 3 cm were electropolished at 6 Volts for varying time lengths of 10, 20 and 30 minutes at 30 °C using a two electrode assembly. The standard pretreatment protocol and washing procedure was adopted.

Figure 4.6 shows FE-SEM images of unpolished and electropolished surfaces, images were obtained at low energy electron beam 5 kV and low current to avoid a charging effect. The images reveal the gradual development of a porous structure with increasing electropolishing time but the pores are of different sizes and are arranged in a random fashion.

Figure 4.7 shows AFM images of ss316 samples which reveal the granular structure of nanometre dimensions of electropolished surfaces and gradual appearance of some pores with increasing electropolishing time as observed in the FE-SEM study. Vagnal et al.¹⁶ showed the platelet structure of the electropolished surface in perchloric acid based electrolyte. This is only a preliminary study of surface morphology of electropolished surface in 1:2 ChCl:EG + oxalic acid solution and a detailed study is required to get complete understanding of the surface over layer behaviour under different electropolishing parameters and different pretreatment methods e.g. mechanical polishing prior to electropolishing as the surface impurities also play an important role in ultimate morphology of the over layer.

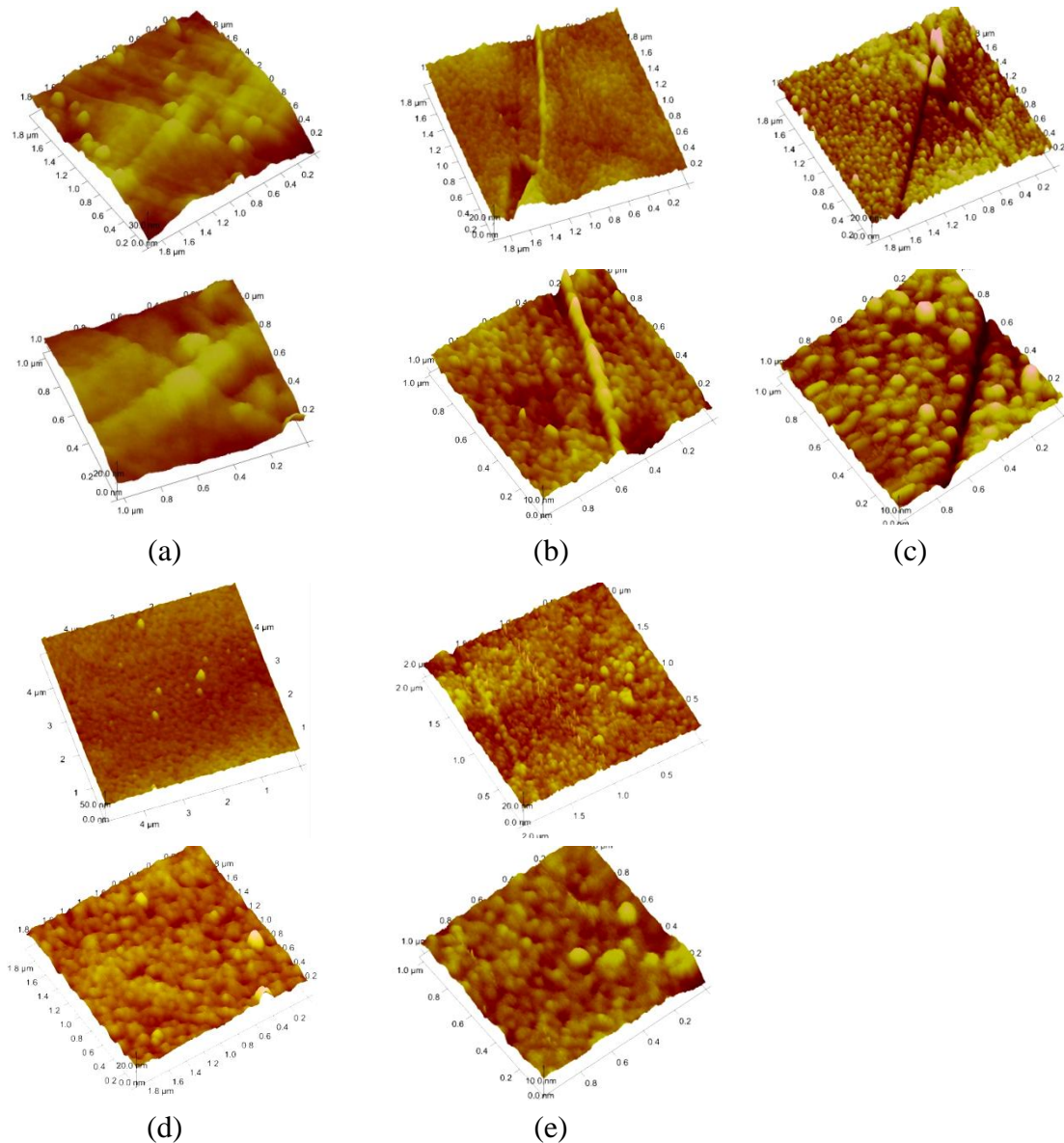


Figure 4.7 : *Atomic force microscope topographic images of ss316 samples electropolished at 6 V for (a) unpolished (b) 5 minutes (c) 10 minutes (d) 20 minutes (e) 30 minutes*

4.3 Surface finish of electropolished surface

The surface texture is the combination of local imperfections on the surface of the engineering part. Roughness, waviness, form (lay) and flaws are the local deviations of a surface from its ideal shape e.g. perfect flat surface, perfect cylindrical shape, perfect spherical shape etc. Surface texture is a key consideration affecting the function and reliability of engineering components and accurate surface texture characterization has become increasingly important in the instrument, computing, data storage, automotive and biomedical industries. Generally the surface texture is determined in terms of

- i. Surface roughness – it is high frequency and short wavelength component of surface texture. It usually results from the production process not from the machining process (if any) like action of cutting tool, chemical action, polishing, lapping and the structure of the material.
- ii. Waviness – it is long wavelength deviations and arises due to machining or external environmental factors like machine or work deflection, vibration, chatter, heat treatment or warping strains.
- iii. Form (lay) – direction of the surface features and is the surface profile ignoring the deviations due to roughness and waviness. These may result from clamping marks or sliding marks and machining guide errors etc.

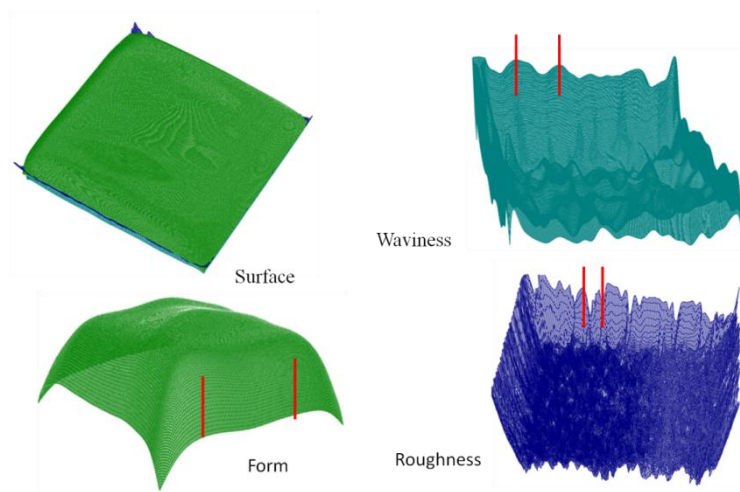


Figure 4.8 : *Surface texture of a typical engineering part*

4.3.1 Surface roughness

Surface finish is typically related to the roughness aspects of the surface and determines the interaction of the object with its environment. Surface finish evaluation is very important for many fundamental problems such as friction, contact deformation, heat and electric current conduction, tightness of contact joints and position accuracy and is a good predictor of the performance of the mechanical component as these irregularities may form nucleation sites for cracks or corrosion.

Surface finish measurement involves three steps

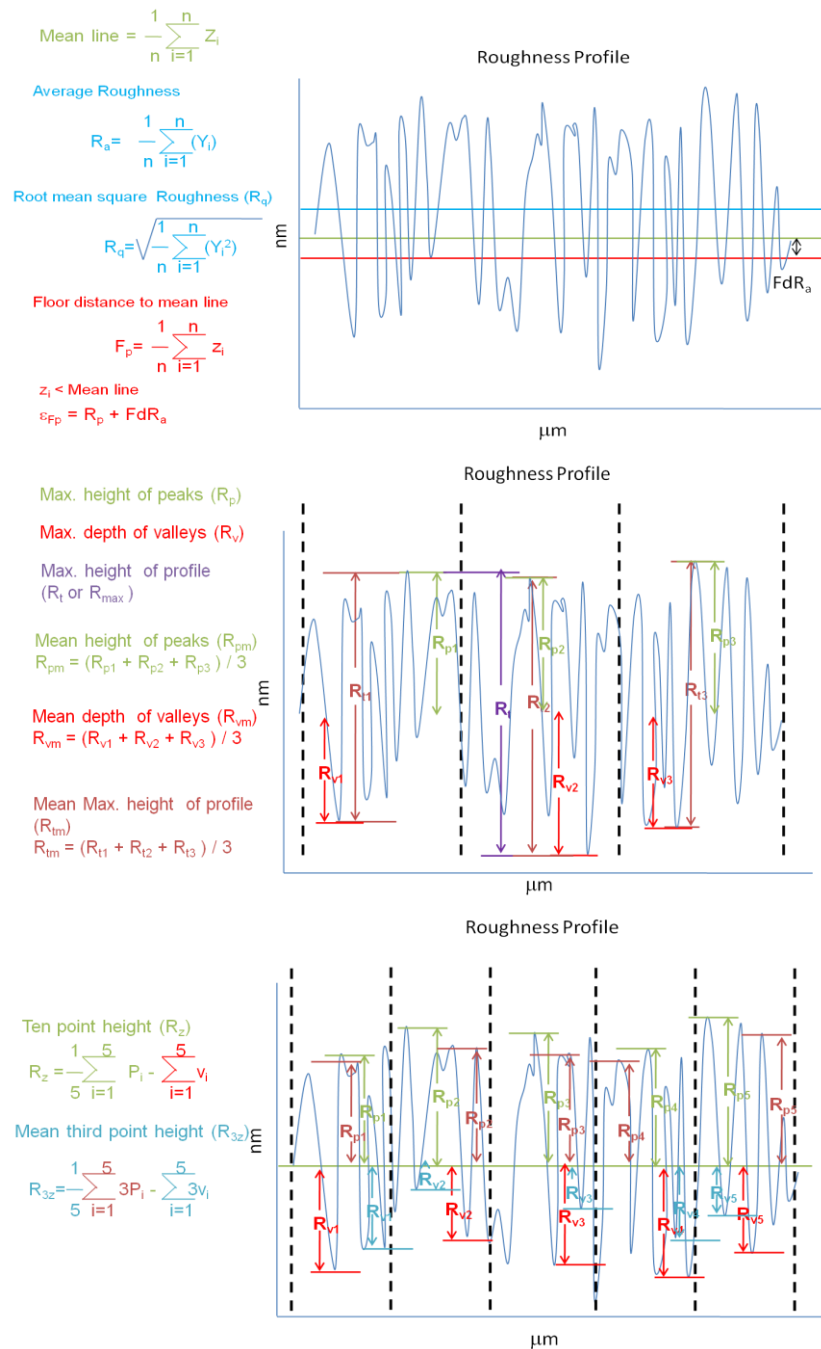
- a) Fitting – it involves the removal of the underlying shape i.e may be tilted surface or nominally curved. This underlying shape is removed by ‘fitting’ of geometric reference and look at the wiggles above and below the reference.
- b) Filtering – roughness is superimposed over waviness as the machine and process induce irregularities simultaneously. These two irregularities are separated by smoothing the primary profile data by applying a ‘filter cutoff wavelength’. In ISO and ASME standards usually a ‘Gaussian’ filter is applied. This smoothing separates the waviness profile and the roughness profile is made up of all of the peaks and valleys above and below the waviness profile.
- c) Analysis – it is the representation of the surface finish in the form of numbers. Surface roughness value can be calculated on a profile (2D) or on a surface (3D). Recently 3D surface topography is gaining more importance in science and engineering applications¹⁸⁻²⁰. The profile parameters are represented by ‘R’ followed by an appropriate subscript while surface parameters are represented by ‘S’ followed by an appropriate subscript. The real surface geometry is so complicated that for accurate description a large number of parameters need to be used.

4.3.1.1 Surface roughness parameters

The surface roughness parameters are categorised into following three groups¹⁸

1. Amplitude parameters – measure the vertical characteristics of the surface deviations. These include Arithmetic average height (R_a), Root mean square roughness (R_q), Ten point height (R_z), Maximum height of peak (R_p), Maximum depth of valleys (R_v), Mean height of peaks (R_{pm}), Mean depth of valleys (R_{vm}), Maximum height of the profile (R_t), Mean of the third point height (R_{3z}), Skewness (R_{sk}), Kurtosis (R_{ku})
2. Spacing parameters – measure the horizontal characteristics of the surface deviations. These include High spot count (HSC), Peak count (p_c), Mean spacing of adjacent local peaks (S), Mean spacing at mean line (S_m)
3. The hybrid parameters – combination of amplitude and spacing parameters. These include Profile slope at mean line (γ), Mean slope of the profile (Δ_a), Bearing area length (t_p) and bearing area curve, Average wavelength (λ_a).

Figure 4.9 shows the definition of some of the important surface roughness parameters^{18,21}.



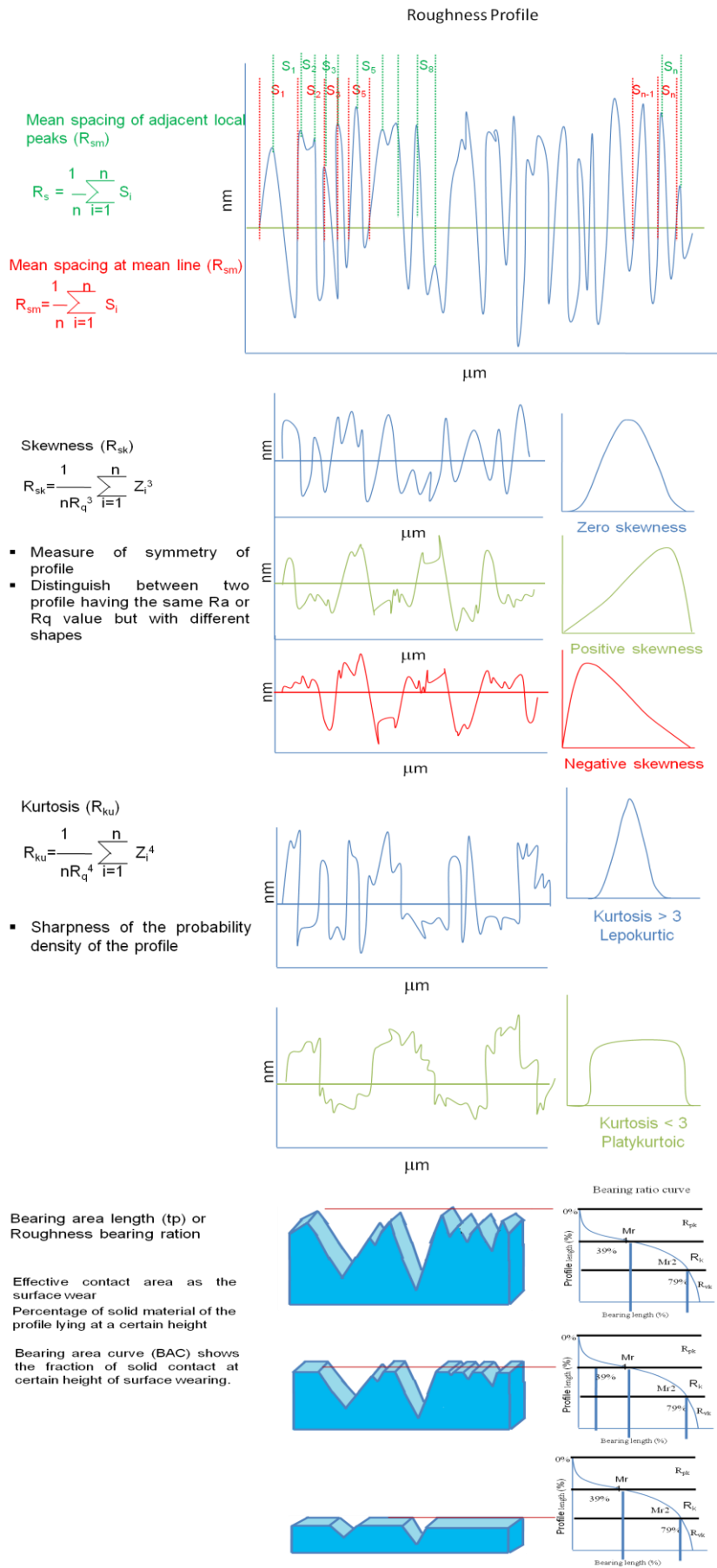


Figure 4.9 : Some of the commonly used surface roughness parameters

4.3.2 Surface roughness measurement

Surface roughness evaluation of stainless steel coupon / plates (ss304) electropolished both potentiostatically and galvanostatically in 1:2 ChCl:EG containing oxalic acid (3% W/V) was carried out by microscopy. Electropolishing of the ss 304 samples was carried out using a two electrode assembly using the power supply. The ss304 coupons having the exposed area of 6 cm² were used as anode while circular carbon mesh (40 cm²) was used as cathode in 300 ml electrolyte at 40°C. The ss304 samples were pre-treated (degreased and pickled) prior to electropolishing. After electropolishing the samples were removed from the electrolyte, rinsed with tap water and washed on an ultrasonic bath at 30°C in deionised water for ten minutes and then dried under air.

The surface roughness measurements were carried out using the Digital Holographic Microscope (DHM) and Atomic Force Microscope (AFM) (**chapter 2**) using the tapping mode. The measurements were carried out at three different places on both unpolished and electropolished surfaces. The profile and surface analysis (40 x 40 µm) were conducted and the mean values of the surface roughness parameters like R_a, R_q, R_z, skewness and kurtosis for profile analysis and S_a, S_q, S_z, skewness and kurtosis for surface analysis are reported.

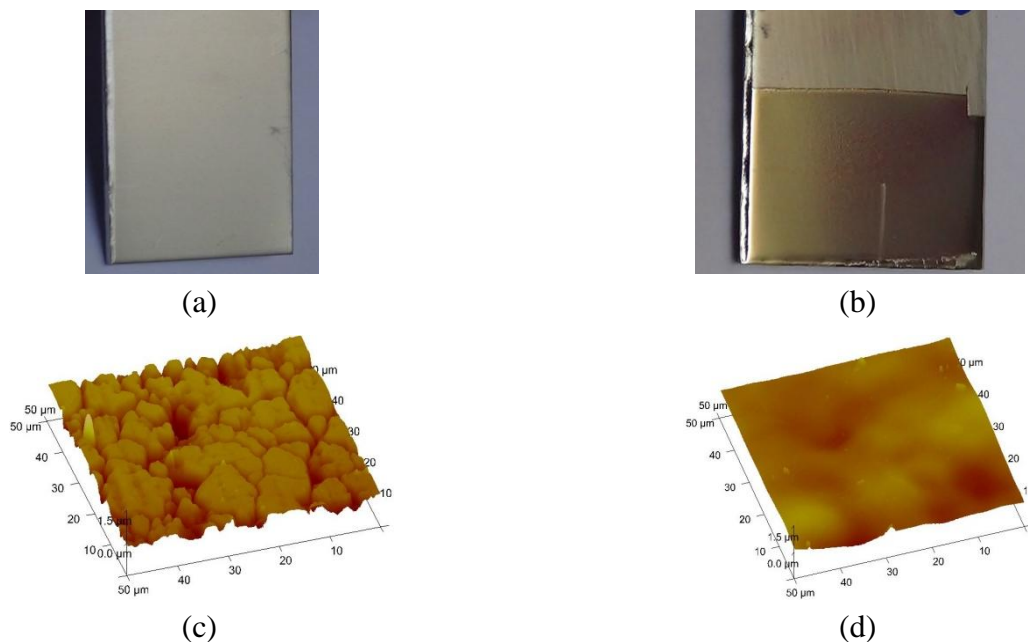


Figure 4.10 : *Comparison of unpolished and electropolished stainless steel (ss304) in deep eutectic solvent (1:2 ChCl:EG) (a) Photograph of the unpolished piece (b) Photograph of electropolished piece (c) AFM image of topography of unpolished stainless steel (d) AFM image of topography of polished stainless steel*

Figure 4.10 shows the topographical images of ss304 samples before and after electropolishing in 1:2 ChCl:EG with oxalic acid as additive. The untreated surface appears dull, rough, presenting irregularities with deep valleys and peaks while the surface electropolished at 6 V for 10 minutes is bright and much smoother.

4.3.2.1 Profile (2D) measurements

Figure 4.11 shows surface roughness profiles of untreated and polished surfaces showing electropolishing has markedly changed the surface finish characteristics. The reported values of surface roughness parameters are obtained by the arithmetic mean of 5 profiles across the entire width of the image (0.1 mm).

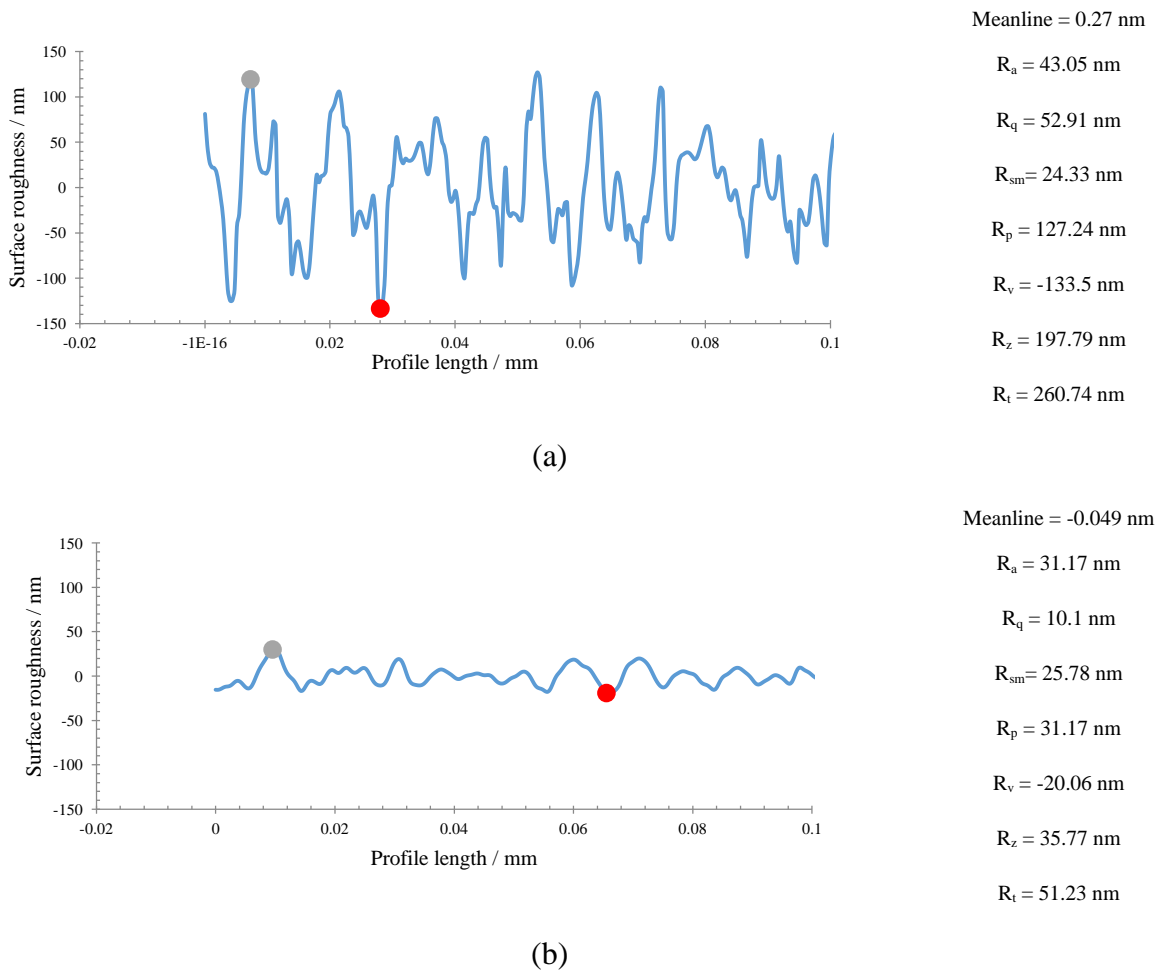


Figure 4.11: Roughness profiles of ss304 samples with common surface roughness parameters (a) unpolished (b) electropolished. Green and red dots show the highest peak and deepest valley on the profile.

4.3.2.2 Surface (3D) measurements

Figure 4.12 shows the comparison of the surface roughness parameters (3D) of electropolished and unpolished samples of ss304 obtained from the arithmetic means of two DHM images of dimension $40\ \mu\text{m} \times 40\ \mu\text{m}$. S_a is the arithmetic average height obtained by the average of absolute deviation of the surface irregularities from the mean line. S_q represents the standard deviation of the distribution of surface heights; it is more sensitive than S_a for large deviation from the mean line. S_p and S_v are the highest peak and deepest valley over the measured surface area respectively. S_t is the vertical distance between the highest peak and the deepest valley and it is also called the profile length. S_z is known as ten point height and is sum of the average of the five highest peaks and five deepest valleys. It is more sensitive than S_a in case of occasional high peaks or deep valleys. All these parameters for electropolished samples have decreased by a factor of roughly 5 as compared to unpolished surface.

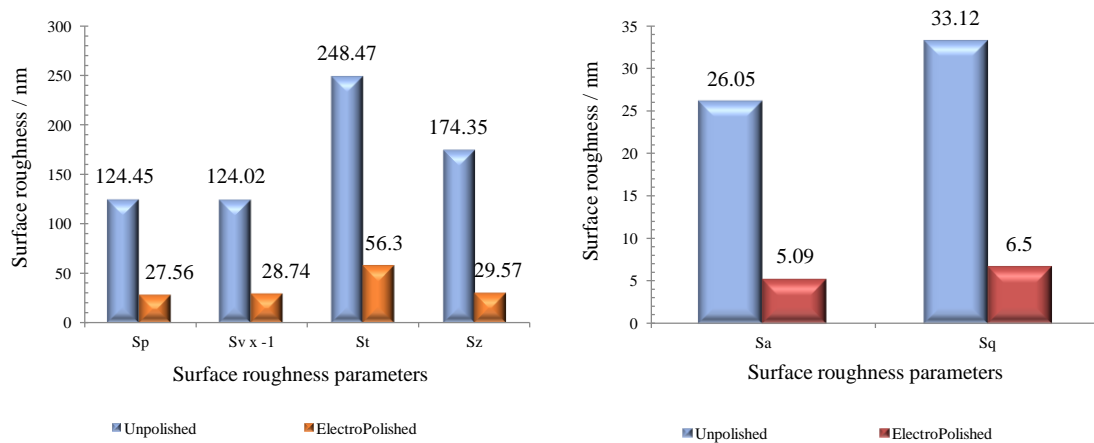


Figure 4.12 : Comparison of surface roughness parameters of unpolished and electropolished samples of ss304 plates.

The profile amplitude probability density functions, skewness (S_{sk}) and kurtosis (S_{ku}), of electropolished surface has changed from -0.44 to 0.31 and 3.27 to 3.64 respectively, indicating that the surface has become slightly rich in peaks and deep valleys have been reduced resulting in the smoothness of the surface.

4.3.3 Effect of electropolishing time on surface roughness

The effect of varying the electropolishing period on surface roughness was studied by conducting electropolishing at 6 V for different lengths of electropolishing time ranging from 10, 20, 30 and 40 minutes on ss304 coupons using the two electrode assembly. In another series of experiments, the electropolishing was carried out at different applied potentials (4, 6, 8 and 10 V) for a time period of 15 minutes. In each case the surface finish was evaluated by atomic force microscope using the Nanoscope version 6.13 over a scanned area of 40 x 40 μm and normalised S_a and S_q values are plotted as a function of electropolishing time (**Figure 4.13 (a)**) and as a function of applied potential (**Figure 4.13 (b)**). Other surface finish parameters, ten point height (S_z), mean maximum peak height (S_{pm}), mean maximum depth (S_{vm}), skewness and kurtosis are tabulated in **Table 4.1** and **Table 4.2**. The surface topographies of these runs are shown in **Figure 4.14**.

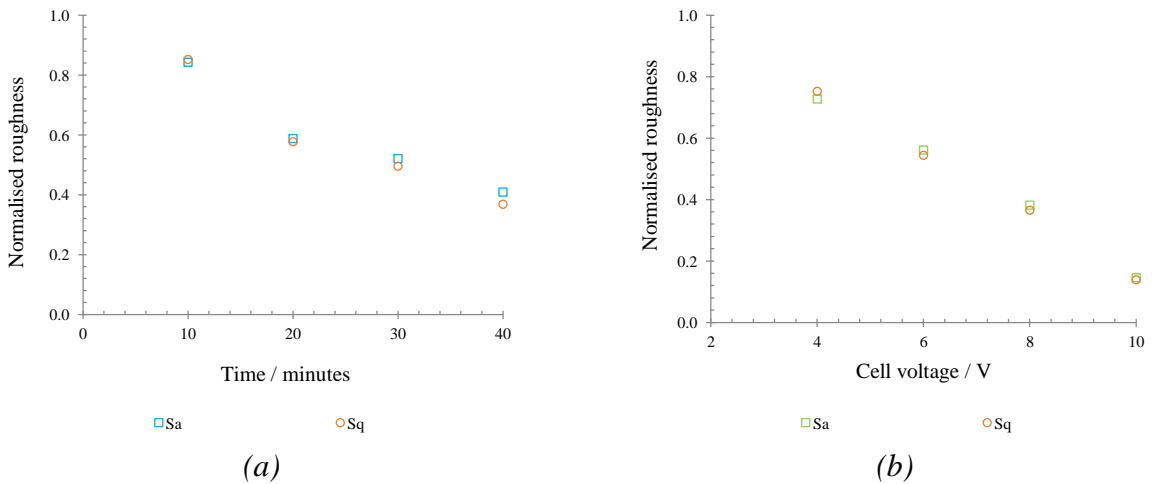


Figure 4.13 : Effect of electropolishing variables on surface finish of ss304
(a) electropolishing time (b) electropolishing voltage

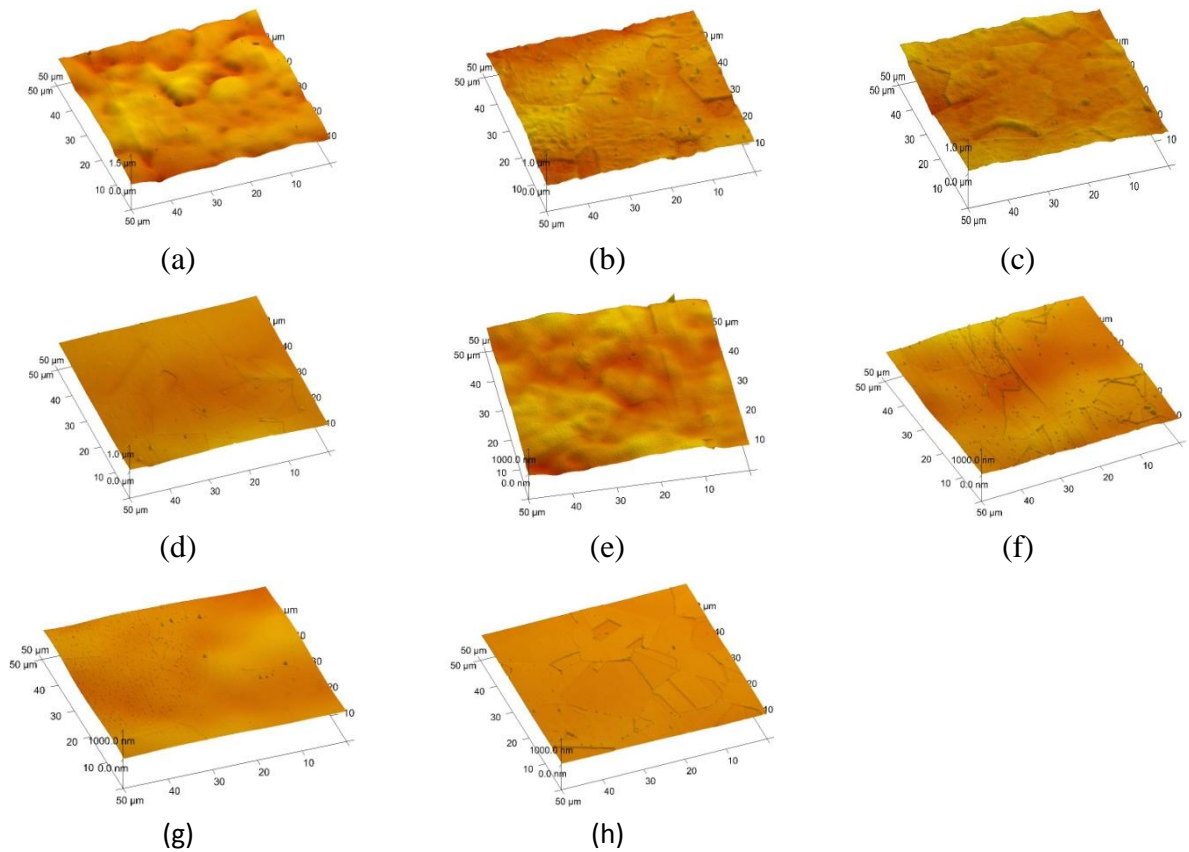


Figure 4.14 : *AFM surface topologies of ss304 coupons electropolished in 1:2 ChCl:EG at different experimental conditions*
 (i) electropolishing time (a) 10 minutes (b) 20 minutes (c) 30 minutes (d) 40 minutes
 (ii) electropolishing voltage (e) 4V (f) 6V (g) 8V (h) 10V

| Table 4.1 : | | <i>Surface roughness parameters of ss304 samples electropolished at 6V for varying length of electropolishing time</i> | | | |
|---------------------------------|--|--|---------------|---------------------|----------|
| Electropolishing Time / minutes | S_z / nm | S_{pm} / nm | S_{vm} / nm | Skewness | Kurtosis |
| Unpolished | 181 | 55 | -121 | -1.35 | 5.75 |
| 10 | 107 | 46.9 | -50 | -0.289 | 3.86 |
| 20 | 69.6 | 30.3 | -33.5 | 0.0952 | 3.17 |
| 30 | 74.1 | 28 | -31.2 | -0.762 | 4.05 |
| 40 | 59 | 21.6 | -28.8 | 0.154 | 2.49 |
| S_z S_{vm} | Ten point height Mean maximum depth | | S_{pm} | Mean maximum height | |

| Table 4.2 : | | <i>Surface finish parameters of ss304 samples electropolished for 15 minutes at different applied potentials</i> | | | |
|-----------------------------------|--|--|----------------------|---------------------|----------|
| Electropolishing Potential / V | S _z / nm | S _{pm} / nm | S _{vm} / nm | Skewness | Kurtosis |
| Unpolished | 164 | 66.5 | -83 | -0.945 | 4.46 |
| 4 | 111 | 32.5 | -45.9 | -0.332 | 3.78 |
| 6 | 96.2 | 48 | -39 | -0.163 | 3.04 |
| 8 | 68.8 | 22.1 | -4.98 | 0.532 | 2.53 |
| 10 | 24.3 | 9.15 | -9.12 | 0.0447 | 3.87 |
| S _z S _{vm} | Ten point height Mean maximum depth | | S _{pm} | Mean maximum height | |

The normalised values for S_a and S_q are used as these values are very sensitive from surface to surface and also show variance in evaluation method and instrument used. The normalised parameter is defined as

$$\text{Normalised roughness} = \frac{\text{Roughness of treated specimen}}{\text{Roughness of untreated specimen}}$$

The surface finish values were found to be a strong function of electropolishing time and cell voltage and in both cases surface roughness decreased linearly. In the case of varying the time, first roughness decreases sharply but later on decreases at a different rate (lower than initial rate) while in case of varying the polishing voltage, the surface roughness decreases at the same rate.

4.3.4 Surface finish in recycled liquid

The electropolishing capacity of the recycled solution (1:2 ChCl:EG) was studied by electropolishing ss304 samples (9.16 cm²) for varying time periods at constant current both in new liquid (1:2 ChCl:EG + oxalic acid) and recycled liquid. The recycled liquid was obtained by first polishing ss316 tube at constant voltage (6 V) for 20 hours in 1:2 ChCl:EG (500 ml), then the spent liquid was recycled using the protocol described in **chapter 3 (section 3.3.4)**.

The electropolishing was carried out in new liquid (300 ml) and recycled liquid (300 ml) at constant current (0.15 A) for time periods ranging from 15, 20, 25 and 30 minutes at 40 °C

using the two electrode assembly. The surface finish was evaluated using the AFM images of an area 40 x 40 μm .

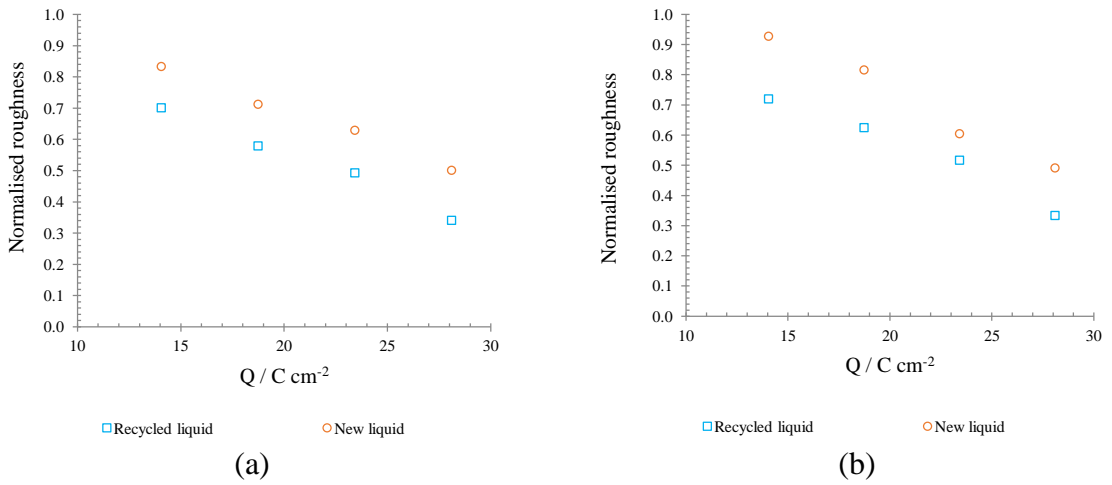


Figure 4.15 : Comparison of surface finish of ss304 plates electropolished in new liquid and recycled liquid

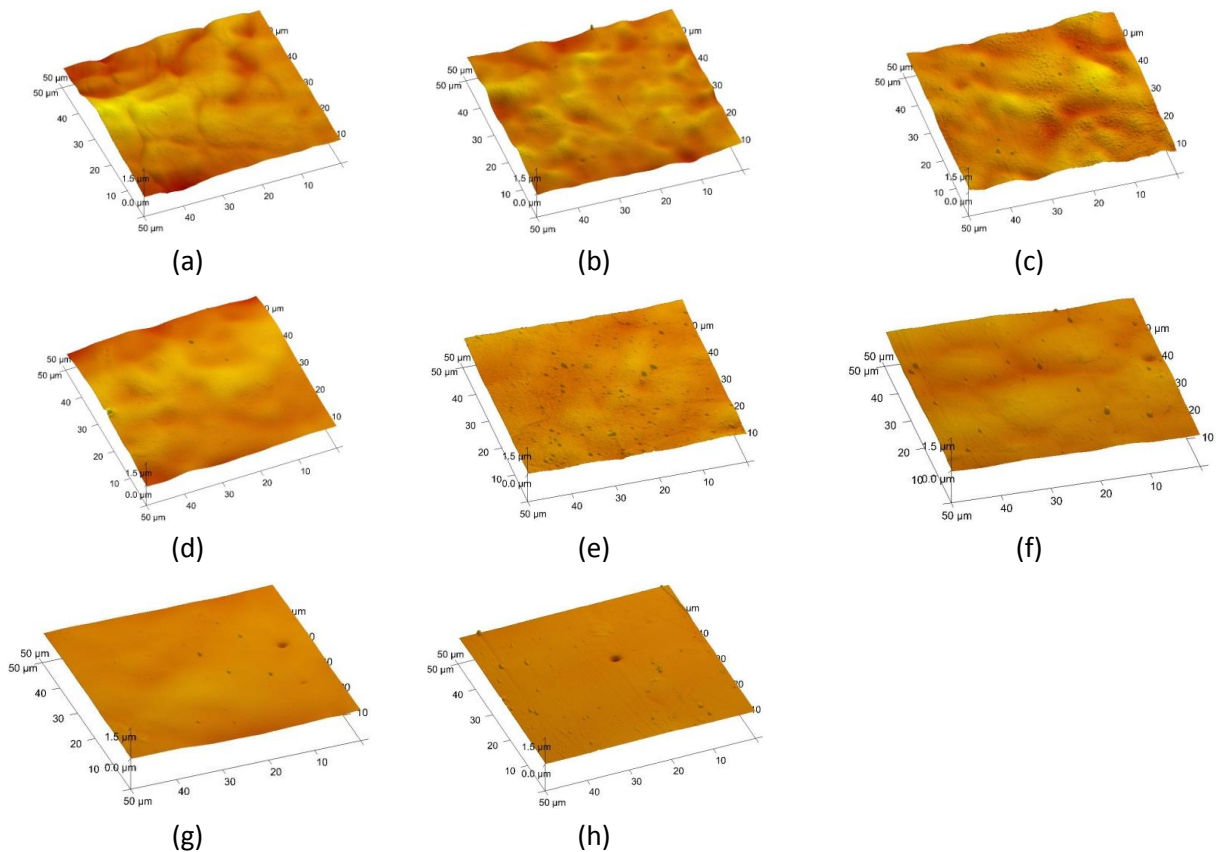


Figure 4.16 : Surface topologies of electropolished ss304 samples (a), (b), (c), (d) in new liquid and (e), (f), (g), (h) in recycled liquid at constant current for varying time 15 minutes, 20 minutes, 25 minutes and 30 minutes respectively.

Figure 4.15 shows normalised roughness parameters (Sa & Sq) as a function of charge passed. The graphs and surface topographical images (**Figure 4.16**) show that the recycled liquid performs equally well as that of new liquid. The slightly lower surface roughness values in recycled liquid may be attributed to the presence of a small amount of water left from the recycling process as studied in chapter 3 (section 3.3.3.3) and a similar study by Abbott et al.²² shows that the presence of small amount of water (10-15%) in 1:2 ChCl:EG gives a better surface finish.

4.3.5 Amount of material etched

The amount of material etched was calculated for the samples of ss304 electropolished in the previous section (new liquid) from the step height at the interface of electropolished and unpolished surfaces using the volume – density - mass relation and plotted against the charge passed (**Figure 4.17 (c)**). **Figure 4.17 (a & b)** shows the step height which was calculated from the AFM images (100 x 100 μm) using Nanoscope version 6.13 software. The reported mean step height was obtained at three places of each image from two images.

The theoretical mass was calculated using Faraday’s law of electrolysis

$$m = \frac{Q}{F} \times \frac{M}{n} \quad (4.1)$$

Where ‘m’ is the mass of substance in grams, ‘Q’ is the charge passed in coulombs, ‘F’ is Faraday’s constant (96,485 C mole⁻¹) and ‘M/n’ is equivalent weight of ss304 (18.99). The equivalent weight of ss304 was calculated using the atomic mass fractions of each alloying element²³

$$W = \frac{1}{\sum_{i=1}^m \frac{x_i z_i}{M_i}} \quad (4.2)$$

Where ‘x_i’ is atomic mass fraction, ‘z_i’ is number of electrons exchanged and ‘M_i’ is the atomic weight. The atomic weight of ss304 was calculated considering Ni = 2, Fe = 3 and Cr = 3.

The theoretical mass is plotted with the actual mass in **Figure 4.17 (c)** and the current efficiency of the process was calculated and found to be 60-70 %.

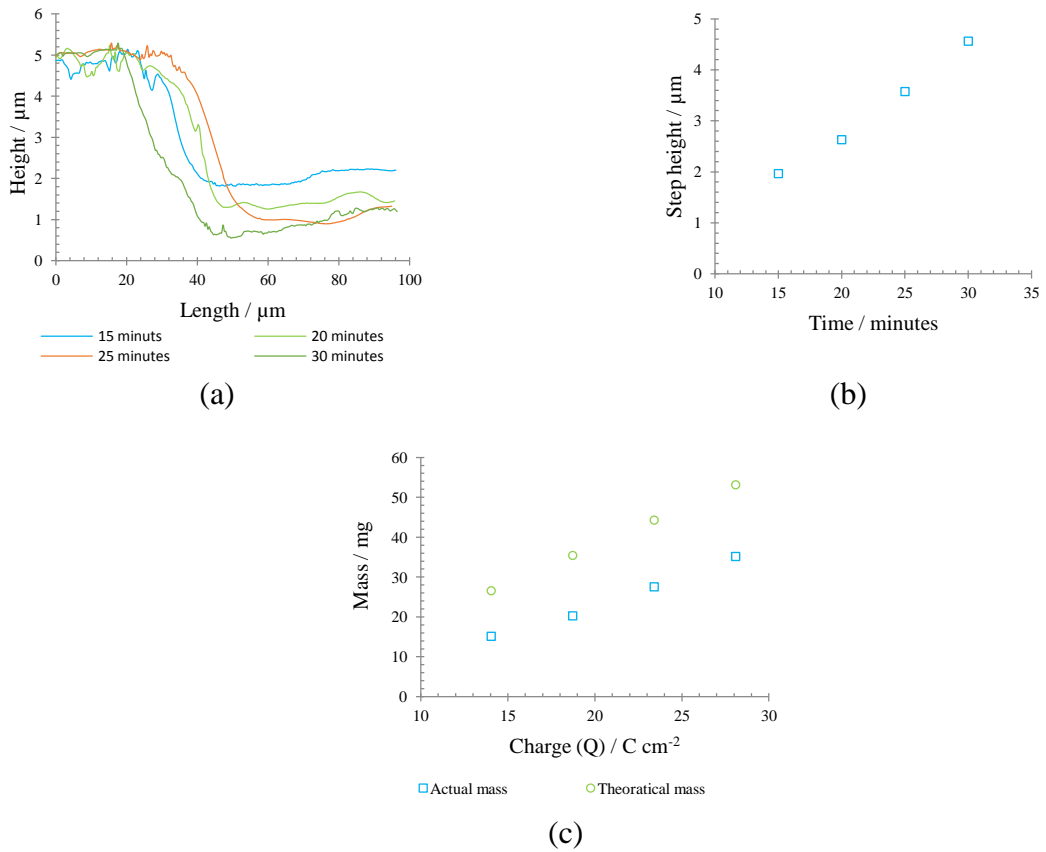


Figure 4.17 : (a) Step height at boundary of unpolished and electropolished ss304 samples of the images of **Figure 4.18** (b) Step height as a function of time (c) amount of material etched as a function of charge passed.

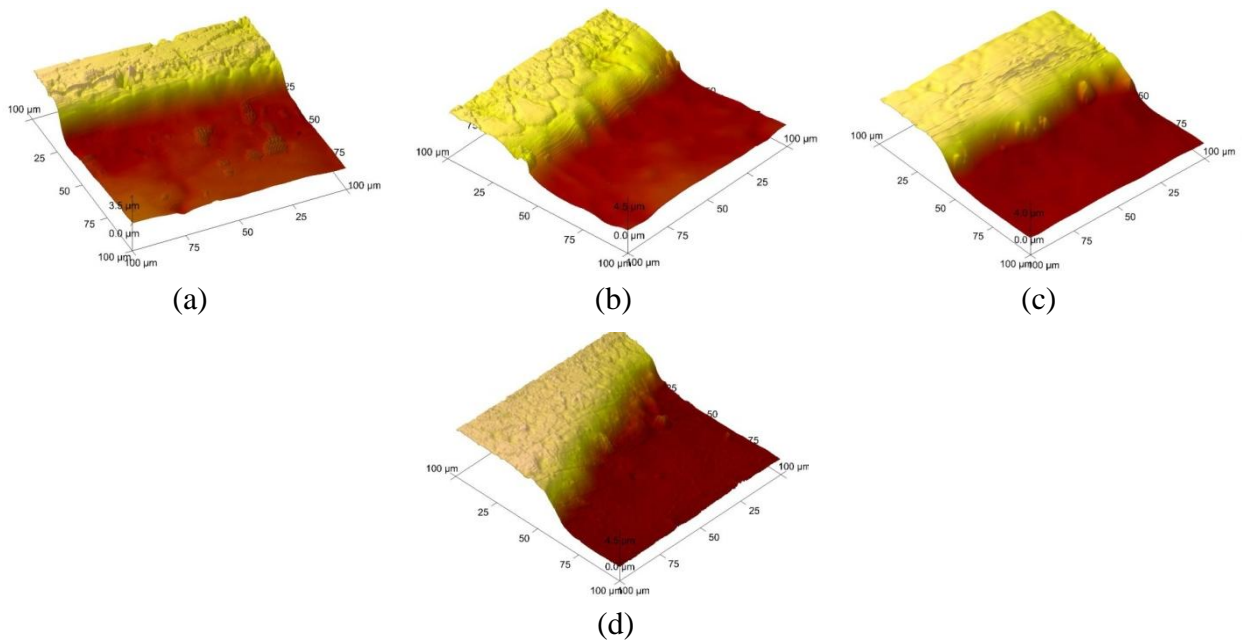


Figure 4.18 : AFM topographical images at interface of the electropolished ss304 coupons in new liquid at constant current (0.15 A) for varying times (a) 15 minutes (b) 20 minutes (c) 25 minutes (d) 30 minutes

4.3.6 Surface roughness measurements by DHM

Typically surface roughness measurements are conducted using a scanned contact stylus probe based instrument consisting of moving stylus, a gauge or transducer, a traverse datum and a processor. As the stylus moves across the surface, the transducer converts this movement into a signal and the processor converts it into numbers and a visual profile. These measurements are sensitive to vibration and it becomes very difficult for small scale roughness – smaller than a few tenths of micrometres as the vibration amplitude is of the same order. The contact mode of operation may damage the surface. The digital holographic microscope provides an ideal alternative as it provides interferometric resolutions and an extremely short acquisition time is used to measure surface roughness²⁴. The strength of DHM lies in the particular use of the so called off-axis configuration which enables it to capture the whole information by a single image acquisition within a few microseconds. The working principle and its salient features for surface roughness measurement are described in **chapter 2 Section 2.10**.

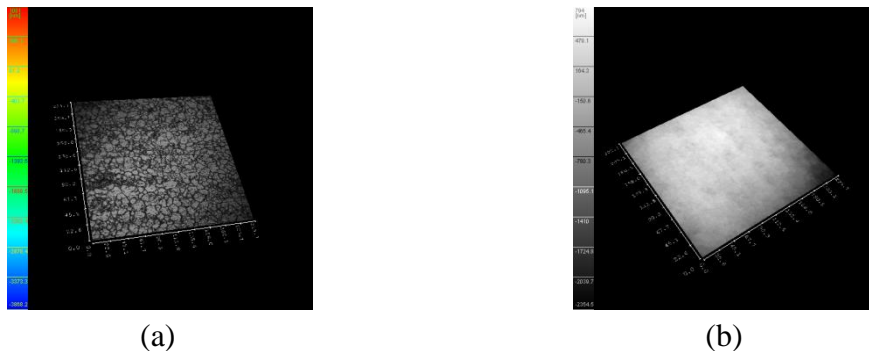


Figure 4.19 : *Digital Holographic microscope images of unpolished ss304 coupon (a) intensity (b) phase*

A comparison of surface roughness measurements using AFM and DHM was carried out. The surface roughness measurements of the electropolished samples in **section 4.3.5** were carried out on an area of 40 μm x 40 μm by Digital Holographic Microscope (DHM 1000 family) operated by Koala Version 4 software and AFM operated by Nanoscope version 6.13.

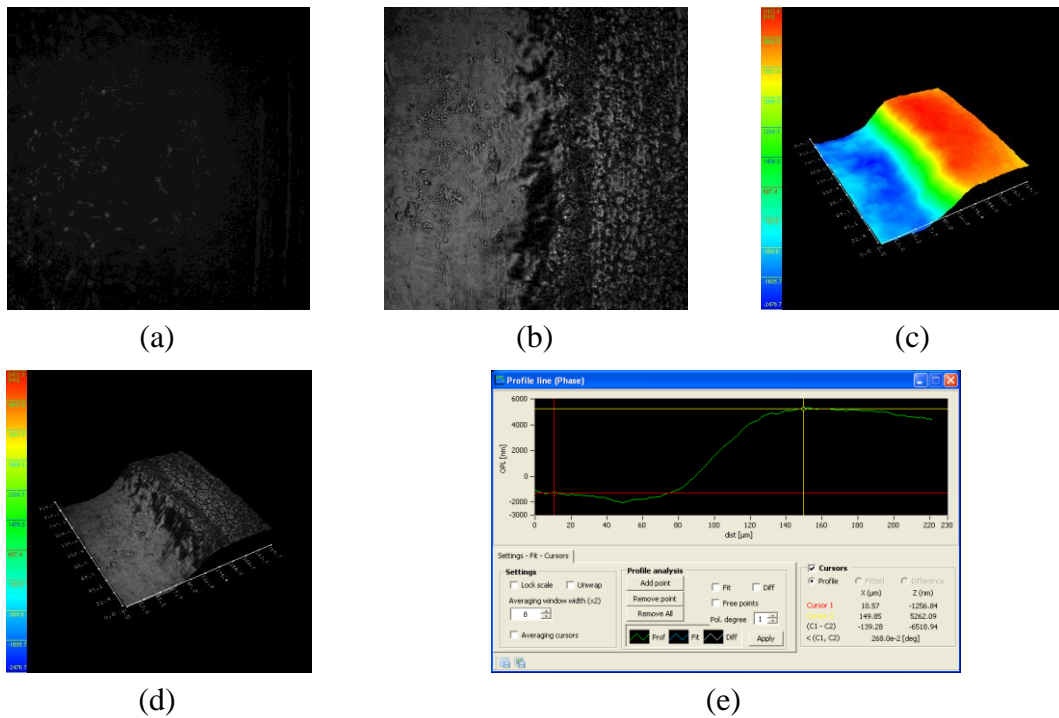


Figure 4.20 : *DHM images at interface of ss304 coupon electropolished at 0.15A for 30 minutes (a) hologram (b) 2D intensity (c) 3D phase (d) 3D intensity (e) profile line*

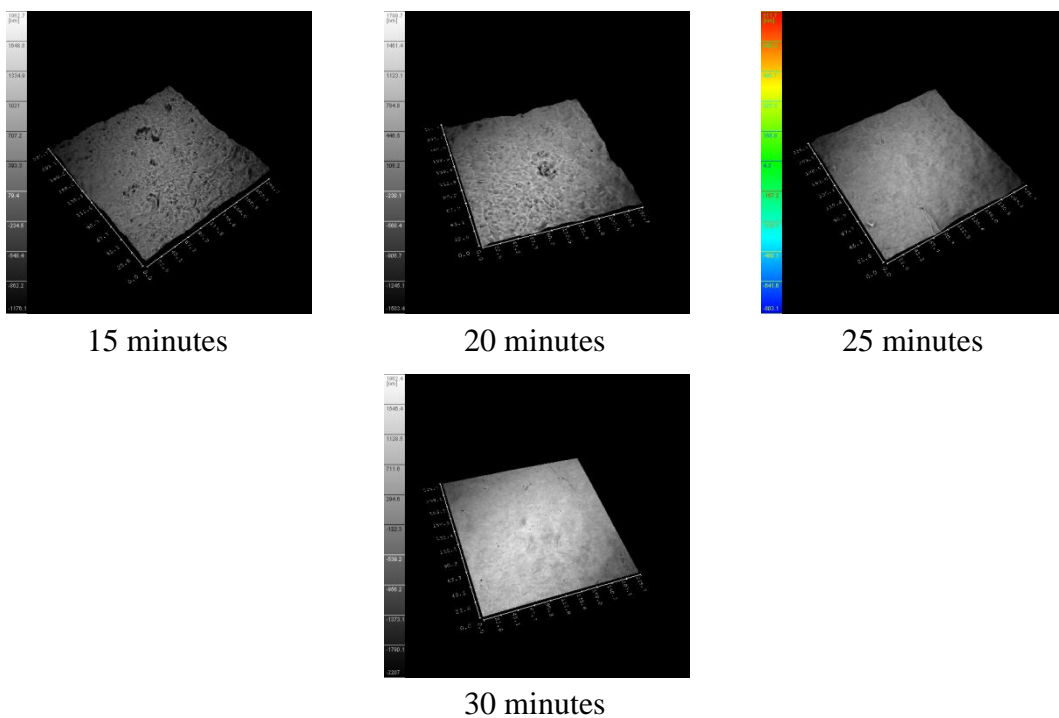


Figure 4.21 : *Intensity images of ss304 electropolished at constant current (0.15 A) for varying time.*

Figure 4.22 shows the comparison of normalised S_a and S_q values as a function of charge passed measured by two instruments and shows that the values obtained agree well with each other.

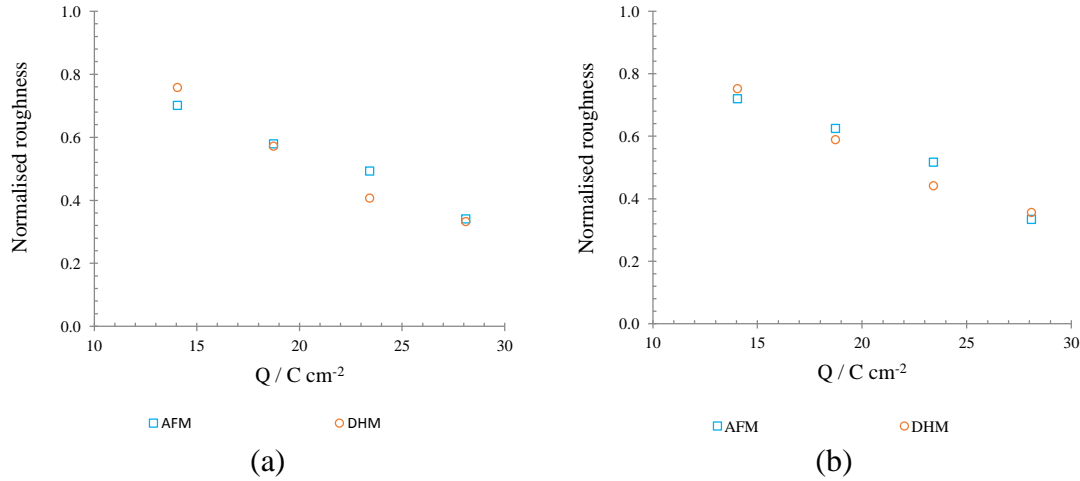


Figure 4.22 : Comparison of surface roughness parameters measured by DHM and AFM (a) arithmetic average height (S_a) (b) Root mean square roughness (S_q)

4.4 Corrosion behaviour of austenitic steel

Stainless steel has the tendency to combat corrosion in thousands of its applications ranging from the monuments to the household usages like sinks etc. This remarkable success of stainless steel is due to the very thin (1-2 nm) self healing passive film principally of chromium oxide on its surface but may contain small amount of other alloying elements as well. Technically to meet the military and aerospace requirements sometimes ‘passivating’ treatment is given to the parts of stainless steel by submerging in nitric acid solution. This treatment removes the impurities from the manufacturing process, oil and grease and the fine metal impurities from the tools used during casting or other processes. This cleanliness promotes the formation of the chromium oxide layer. Under certain circumstances / factors like chemical environment, pH, temperature, equipment design, fabrication methods, surface finish, contamination and maintenance procedures may cause some form of localized corrosion. According to DOD Technical bulletin corrosion detection and prevention, following are the different types of corrosion in stainless steel.

4.4.1 Types of corrosion

Pitting corrosion is highly localized corrosion at individual sites on the surface of metal in media containing halides. It can occur because of minor discontinuities in the passive film, inclusions or defects or dirt and contamination on the surface. Pitting is more likely to occur in stagnant aqueous medium than in the liquid moving with moderate to high velocities.

Uniform corrosion (General corrosion) occurs due to the overall breakdown of the passive film and the entire surface shows a uniform sponge like appearance.

Crevice corrosion occurs at the interface between the corroding metal and other substance which is usually not electrically conductive. It occurs in tight stationary crevices in slow moving solutions or in oxygen restricted crevices like under a bolt head.

Stress corrosion cracking takes place in the presence of chloride ions, tensile stresses (usually residual due to forming or welding) and elevated temperatures. In properly annealed surfaces it is usually transgranular while in poorly annealed or weld effected zones it is intergranular.

Intergranular corrosion occurs in stainless steel that has been exposed to the critical temperature range (425°C to 815°C) during improper annealing, stress relieving or heating during forming and welding. At this temperature chromium carbide is formed at the grain boundaries and the nearby area is depleted in chromium and is more susceptible to attack in acidic media. Corrosion from the surface moves down the grain boundaries to an extent that grains can be detached from the surface.

Galvanic corrosion takes place when two different metals of different electrochemical activity come in contact, a more negative metal in the galvanic series corrodes preferentially to the less negative.

4.4.2 Corrosion resistance measurements

In this section, the corrosion resistance of stainless steel as supplied and after electropolishing in 1:2 ChCl:EG was studied in aerated tap water, aqueous NaCl (3%) and H₂SO₄ (2%). The stainless steel samples were electropolished by controlling the voltage and the electropolishing process was varied by changing the polishing time (5-30 minutes) in 1:2 ChCl:EG + oxalic acid (3%).

The corrosion behaviour of austenitic stainless steels ss304 and ss316 after electropolishing in 1:2 ChCl:EG containing small amount of oxalic acid was carried out using open circuit potential and potentiodynamic polarization in aerated deionized water and aqueous solutions of NaCl (3%) and H₂SO₄ (2%).

The electropolishing of the stainless steels coupons were carried out using a two electrode assembly using PL-P series Thurbly thander at 30°C and the carbon mesh as the counter electrode. The stainless steel samples with an exposed area of 2 cm² were electropolished at 6 V for varying electropolishing times (5 min, 10 min, 20 min and 30 min) in 1:2 ChCl:EG containing the oxalic acid (3%). The electropolished samples were washed in tap water followed by deionized water and then dried under air. The stainless steel samples were degreased and pickled using the standard protocol prior to electropolishing.

The corrosion electrochemical studies were conducted using a potentiaostat (PGSTAT 20 computer controlled) operated by the general purpose electrochemical software (GPES) version 4.9. A three electrode electrochemical cell was used. The unpolished and electropolished stainless steel coupon (1 cm x 0.5 cm x 0.04 cm) with the total exposed area of 0.62 cm² were used as working electrode while a platinum flag and Ag/AgCl electrode (in 3 M KCl) were used as counter and reference electrodes respectively. The potentiodynamic polarization curves were obtained by scanning the potential from - 1.5 V to + 1 V in the forward direction with a scan rate of 2 mV sec⁻¹. The stainless steel coupons were immersed for 30 minutes in the respective electrolyte solutions to allow enough time for potential stabilization prior to start of the scan. The open circuit measurements were also carried out using the potentiostat against the Ag/AgCl electrode for 14 hours in three electrolytes for unpolished and electropolished stainless steel samples with an exposed area of 1 cm² and the measurements were started from the first moment of immersion. Open circuit measurements were also conducted for unpolished stainless steel immersed in 1:2 ChCl:EG with and without oxalic acid as an additive against the silver wire as the quasi reference electrode. All the electrochemical measurements were carried out at 30°C using a thermostated water bath.

4.4.2.1 Open Circuit potential (OCP) measurements

Corrosion of metals takes place through electrochemical reactions at the interface between the metals and an electrolyte solution i.e. anodic (oxidation of metal) and cathodic (reduction of the solution species). Corrosion normally occurs at a rate determined by

equilibrium between these two opposing reactions. The equilibrium potential attained by the system in the absence of electrical connections to the metal is called open circuit potential. OCP measurements indicate the behaviour of the system in the solution. A stable OCP means that the system under study has reached the ‘steady state’ i.e. the corrosion reactions have assumed a constant rate. This steady state varies from system to system, some systems assume this state in few minutes while the others may need several hours.

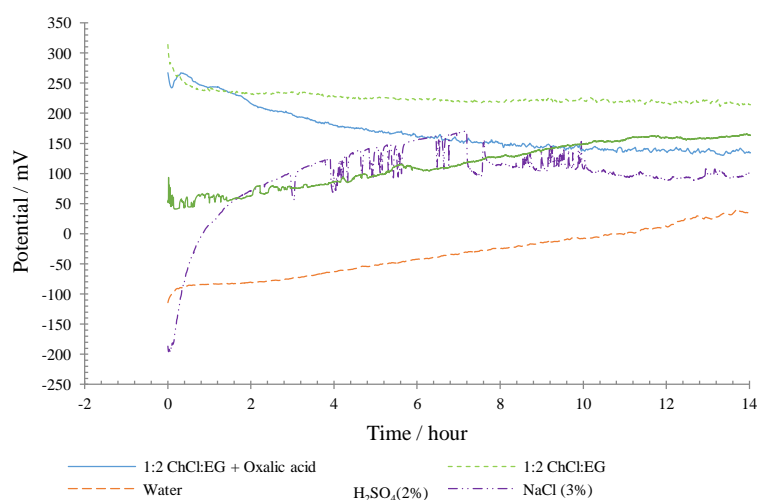


Figure 4.23: Variation of open circuit potential with time for stainless steel ss316 in different solutions

Figure 4.23 shows the OCP measured for ss316 as received from the supplier in different solutions. In 1:2 ChCl:EG, initially potential decreases about 90 mV during the first hour of measurement and then becomes stable at about +230 mV for the rest of measurement. The initial decrease in potential may be attributed to the dissolution of natural oxide passive film on the surface and later on stabilization of the potential indicates some sort of passivation in 1:2 ChCl:EG.

In 1:2 ChCl:EG with oxalic acid (3%) the potential drops initially about 30 mV which may be due to some sort of breakdown of the oxidation layer and then moves in the positive direction and reaches the potential value +270 mV i.e. potential at the time of immersion in the solution may be due to the passivation of the surface as in the 1:2 ChCl:EG solution. After about one hour of immersion the potential starts to move in the cathodic direction at a fast rate up to 9 hours and then stabilizes around +100 mV with a little fluctuation indicating some sort of pitting reaction consistent with high Cl^- concentration for the rest of immersion time.

In aerated water after the initial rapid increase in potential, the potential changes in the anodic direction at a steady rate and no fluctuation in potential is indicative of the absence of pitting reaction. In aqueous NaCl solution, the potential moves in the anodic direction at a fast rate up to the first 4 hours and then fluctuates around +100 mV indicating the initiation of a pitting reaction in the chloride containing environment. After 10 hours of immersion the potential suddenly drops to + 50 mV and stabilizes indicating the steady state of the pitting reaction. In aqueous H₂SO₄ (2%), after the initial rapid decrease due to the dissolution of oxide layer it starts to increase at a steady rate and after 10 hours it becomes stabilized around +100 mV.

Figure 4.24 (a & b) shows the OCP curves for ss316 and ss304 in 3% NaCl solution for unpolished and the electropolished samples at 6 V for different times (5, 10, 20, 30 minutes). The OCP in ss316 is more anodic as compared to ss304 which is due to the presence of Mo in ss316 that enhances its pitting corrosion resistance. The electropolished and unpolished samples of ss316 almost show the same behaviour in NaCl solution but in the case of ss304 the OCP of the electropolished samples is shifted to more cathodic potentials and gradually moves anodically with increasing electropolishing time (i.e longer times increase the corrosion resistance). This suggests some sort of instability of the oxide layer in the electropolished samples. **Figure 4.24 (c & d)** shows the OCP curves of ss316 and ss304 in 2% H₂SO₄ for unpolished and electropolished samples at 6 V for different times. Both grades of stainless steel show similar behaviour in aqueous H₂SO₄.

4.4.2.2 Weight loss measurements

The weight loss of unpolished stainless steel ss304 coupons immersed in 1:2 ChCl:EG and 1:2 ChCl:EG containing 3% oxalic acid for varying time periods 24, 72, 168 and 672 hours are depicted in **Figure 4.27**. Eight ss304 coupons with dimensions (1 cm x 1 cm x 0.04 cm) were degreased in soap in oscillation bath (ultra sonic bath) for 10 minutes followed by washing with deionised water, dried under nitrogen and weighed twice on a precision balance with 4 decimal digits. The weighed coupons were divided into two sets of four and immersed in sample tubes containing 10 ml of 1:2 ChCl:EG and 1:2 ChCl:EG containing oxalic acid respectively. The sample tubes were closed with lid and placed in the oven at 40°C. After the specified time period the coupons were taken out

and washed in deionized water in an ultrasonic bath for 10 minutes, rinsed with acetone, dried under nitrogen and weighed.

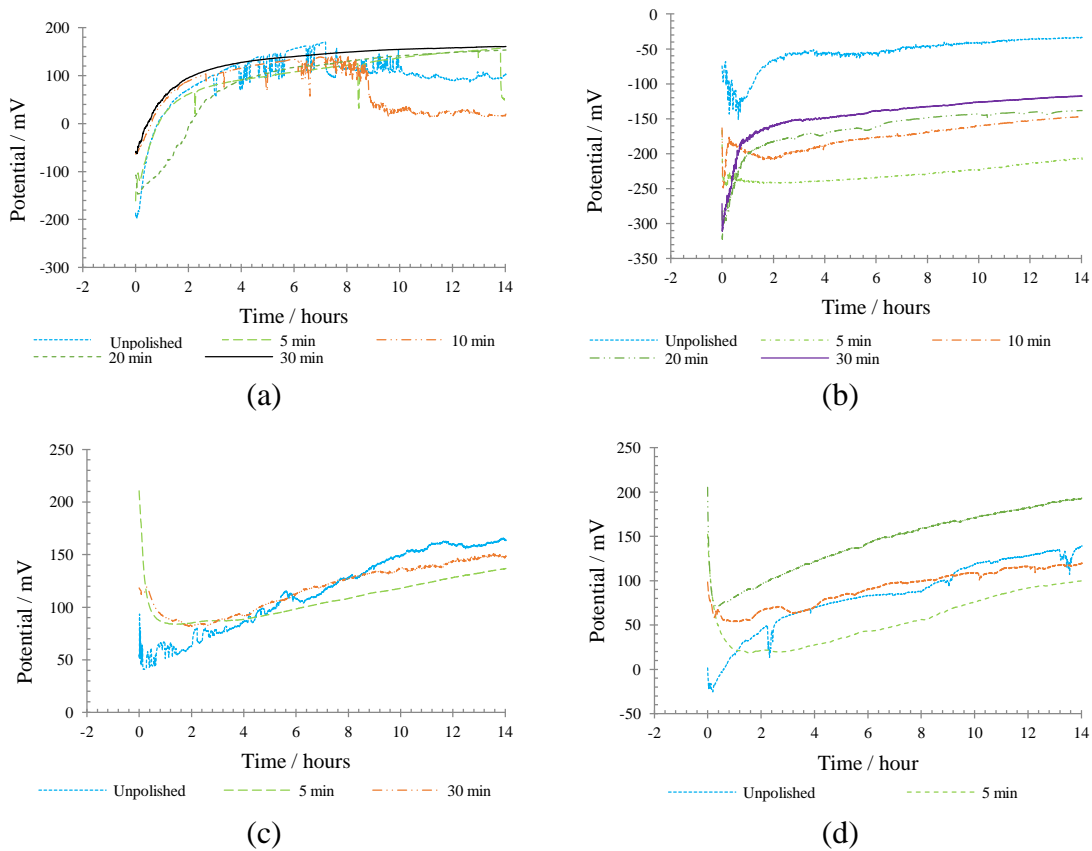


Figure 4.24 : *Open circuit potential variations as a function of time for unpolished and electropolished samples for varying time (a) ss316 in NaCl (3%) (b) ss304 in NaCl (3%) (c) ss316 in H₂SO₄(2%) (d) ss304 in H₂SO₄ (2%)*

Atomic force microscopic and scanning electron microscopic studies of the surface topography of these coupons reveal that the samples immersed in 1:2 ChCl:EG containing oxalic acid show uniform corrosion - a dissolution around the grain boundaries is observed during the first 24 hours of immersion and continues for the rest of test. The samples immersed for 672 hours in 1:2 ChCl:EG showed some pitting while other samples did not show any pitting. The AFM and SEM surface topography of these samples is shown in **Figure 4.25 and 4.26**.

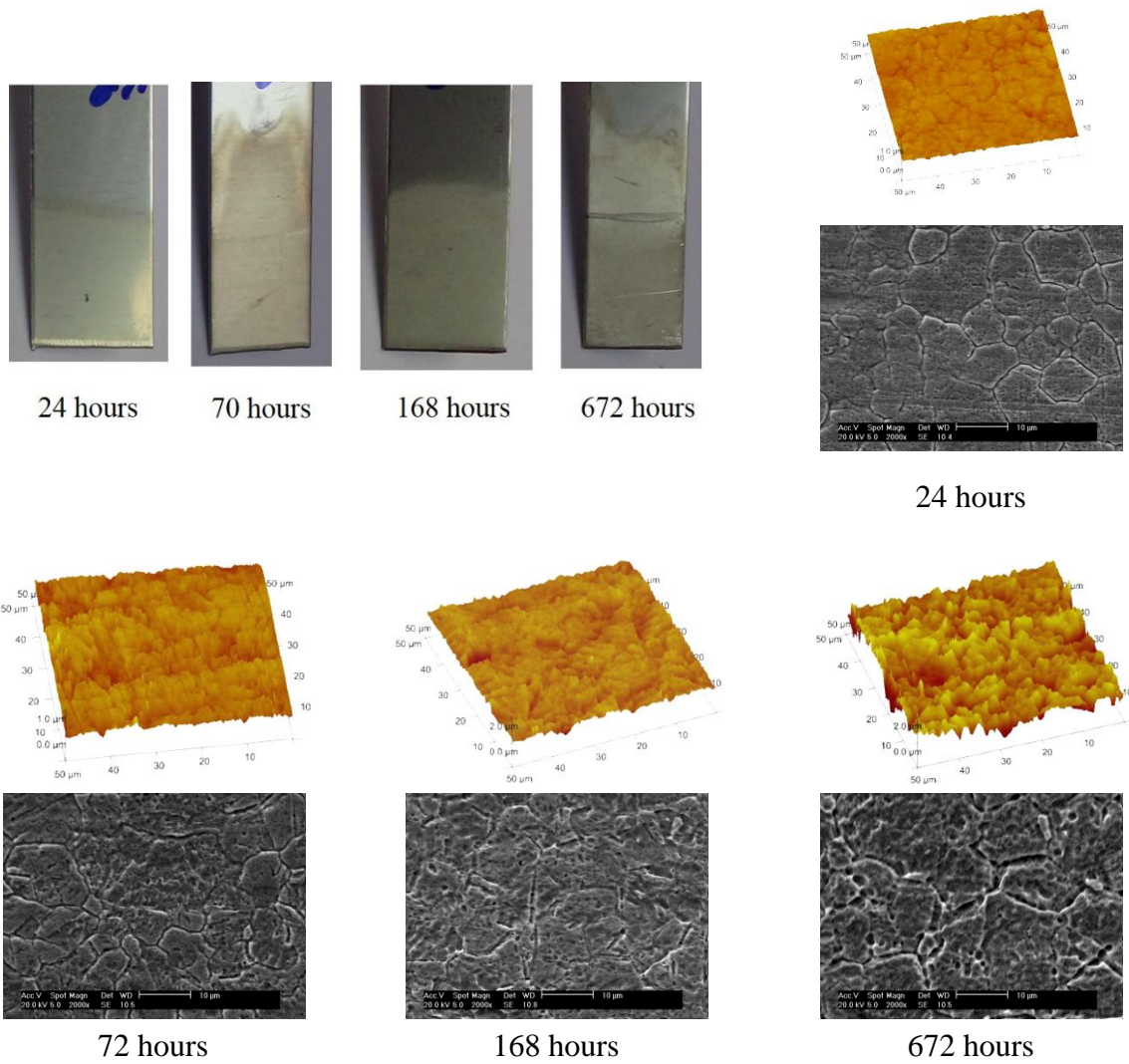


Figure 4.25 : Topographical images of ss304 coupons immersed in 1:2 ChCl:EG containing oxalic acid (3% w/v)

The weight loss per unit area and the corrosion rate was calculated using **equations 4.3 and 4.4**²⁵

$$\Delta m = \frac{m_1 - m_2}{A} \quad (4.3)$$

$$K_{corr} = k \left(\frac{\Delta m}{DA t} \right) \quad (4.4)$$

Where ‘m₁’ and ‘m₂’ are weights before and after immersion in solution in grams and ‘A’ is the exposed area of the coupon (cm²), ‘D’ is the density of ss304 (8.01 g cm⁻³), ‘t’ is time of immersion in hours, ‘k’ is the constant that defines the unit of the corrosion rate (k = 8.76x10⁴ for the mmpy) and ‘K_{corr}’ is the corrosion rate.

The weight loss data and the corrosion rate are shown in **Figure 4.27**. No weight loss was observed for the samples immersed in 1:2 ChCl:EG during the experimental time period while there was a gradual weight loss for the samples immersed in 1:2 ChCl:EG containing oxalic acid. The corrosion rate of ss304 samples increases with the immersion time which indicates the absence of formation of secondary passive layer in the immersion solution or the deposition of the corrosion products on the surface.

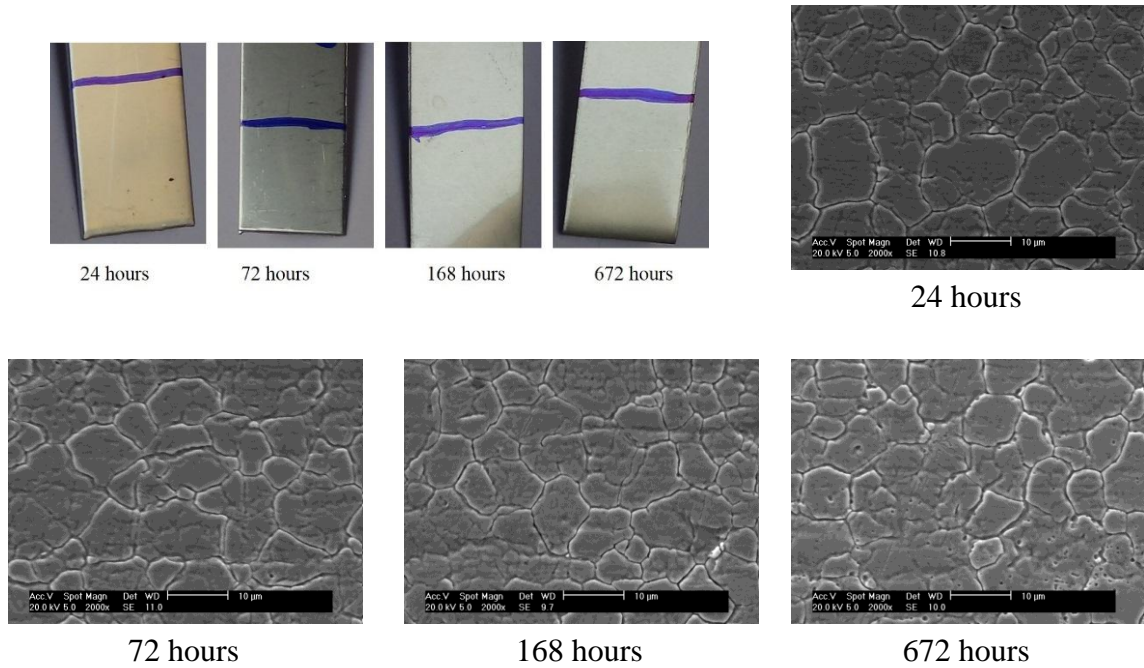


Figure 4.26 : SEM and AFM topographical images of ss304 samples immersed in 1:2 ChCl:EG for varying time lengths

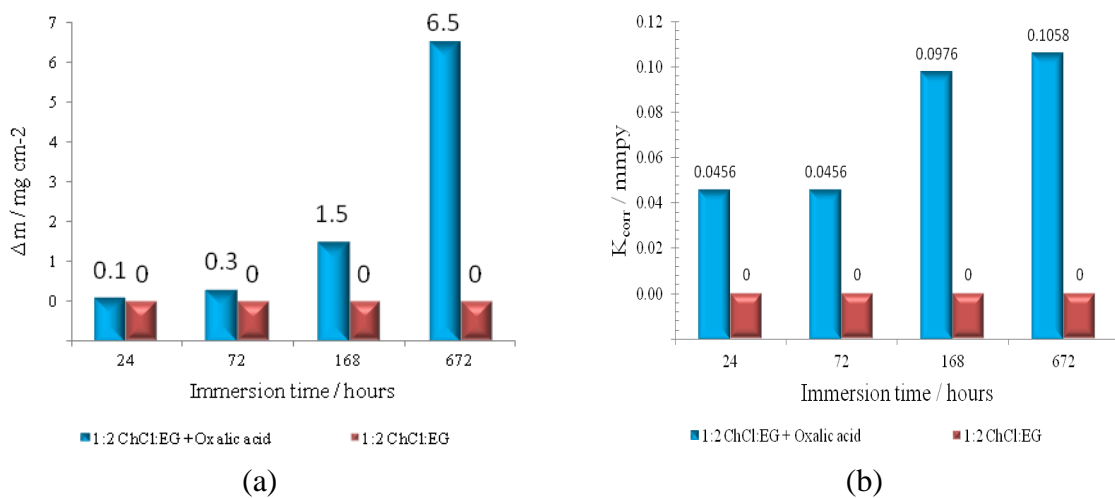


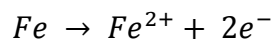
Figure 4.27 : (a) Weight loss (b) corrosion rate of ss304 samples immersed in 1:2 ChCl:EG and 1:2 ChCl:EG with oxalic acid as a function of time.

4.4.2.3 Potentiodynamic polarization curves

The characteristics of potentiodynamic anodic polarization curves provide an insight into the corrosion behaviour of alloys. Potentiodynamic polarization experiments were conducted to quantitatively evaluate the effect of electropolishing on the corrosion behaviour of stainless steel in NaCl (3%), H₂SO₄ (2%) and aerated tap water. The measured potentiodynamic curves of unpolished and electropolished samples of ss304 against Ag / AgCl after immersion for 30 minutes are shown in **Figure 4.28**.

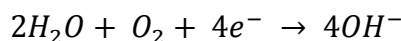
The polarization curves of ss304 in sulphuric acid display a similar trend with a small active – passive transition (**Figure 4.28 (a)**). The corrosion potential of the electropolished samples slightly shifts to more negative value with slight increment in the passive region with electropolishing time. The polarization curves obtained in NaCl (3%) do not show noticeable active – passive transition but the pitting resistance increase with the electropolishing of the samples (**Figure 4.28 (b)**). **Figure 4.28 (c)** shows the polarization curves measured in aerated tap water. They describe similar corrosion behaviour with active passive transition. The corrosion potential of the electropolished samples slightly shifts to positive potential and shows more corrosion resistance than the unpolished sample. The corrosion potential of ss304 shifts in cathodic direction from sulphuric acid, sodium chloride and aerated tap water while the passive regions of ss304 in increasing order in these solutions are aerated tap water > sulphuric acid > sodium chloride.

It is generally believed that the anodic reaction during corrosion of steel is the dissolution of iron

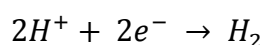


The cathodic reaction is sensitive to the reaction environment

In aerated near neutral pH solutions the cathodic reaction is oxygen reduction^{26,27}



While in acidic solution, the predominant cathodic reaction is hydrogen ion reduction²⁵



The corrosion current densities are estimated from log current versus potential plots (Tafel plot). The corrosion reactions (anodic and cathodic) are kinetically controlled at metal surface and obey the Tafel equation²⁸

$$I = I_0 e^{\frac{2.3(E-E^0)}{\beta}} \quad (4.5)$$

Where ‘I’ is the current resulting from the reaction, ‘I₀’ is reaction dependent constant called the exchange current, ‘E’ is the electrode potential, ‘E⁰’ is the equilibrium potential (constant for a given reaction) and ‘β’ is the reaction’s Tafel constant (constant for a reaction and has units of volts/decade).

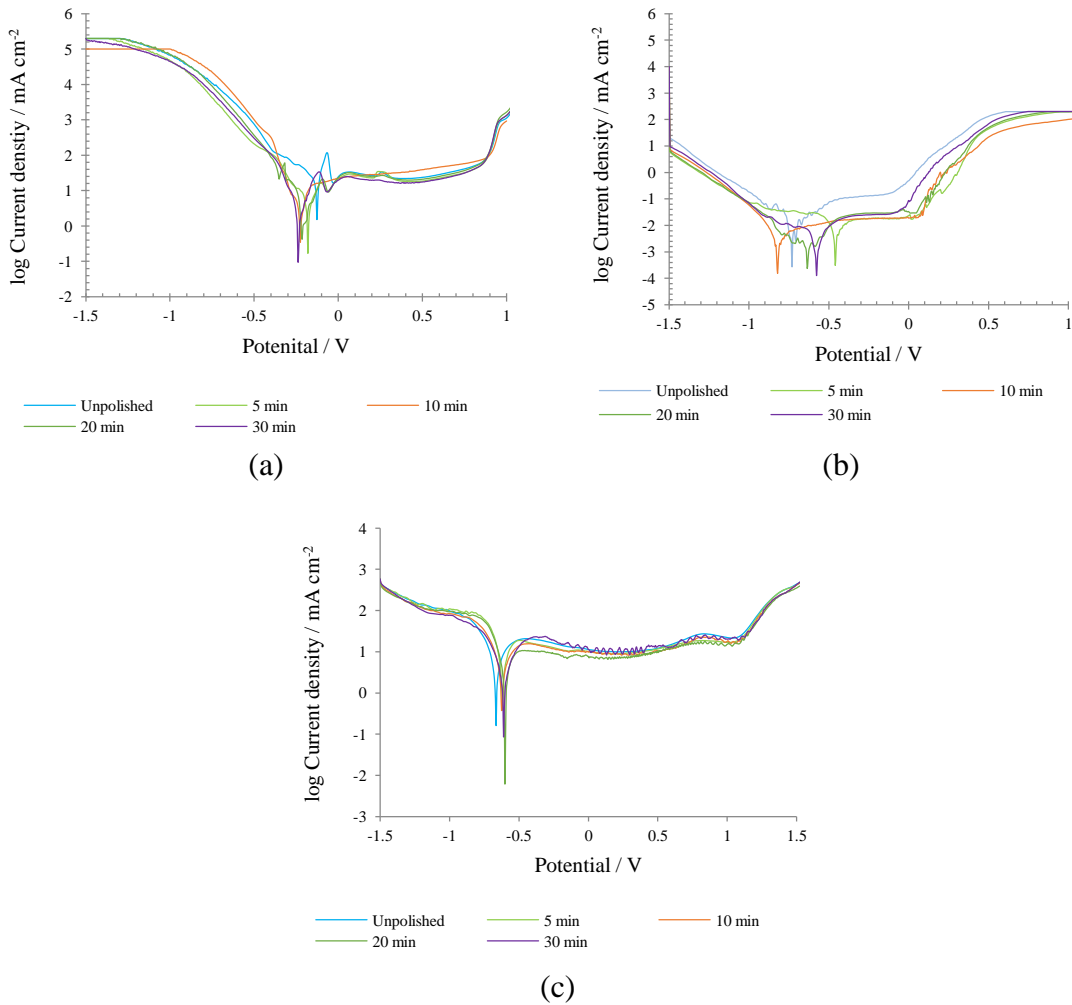


Figure 4.28: Polarization curves of ss304 in (a) H₂SO₄ (2%) (b) NaCl (3%) (c) aerated tap water

In corrosion process two reactions i.e. anodic and cathodic are taking place together so total current of the process is given by the ‘Butler Volmer’ equation²⁸

$$I = I_a + I_c \quad (4.6)$$

$$I = I_{corr} \left(e^{\frac{2.3(E-E_{oc})}{\beta_a}} - e^{\frac{2.3(E-E_{oc})}{\beta_c}} \right) \quad (4.7)$$

Where ‘I’ is the measured current in amperes, ‘I_{corr}’ is the corrosion current in amperes, ‘E’ is the electrode potential’ ‘E_{oc}’ is the corrosion potential in volts, ‘β_a’ is the anodic Tafel constant in volts/decade and ‘β_c’ is the cathodic Tafel constant in volts/decade.

Near ‘E_{oc}’ both anodic and cathodic exponential terms contribute to the total current and as the potential is swept away on either side of ‘E_{oc}’, one exponential term predominates and other term can be ignored. Kinetically controlled systems show a linear relationship between log current and potential on either side of ‘E_{oc}’ but in practice systems do not behave ideally due to the following complications (a) concentration polarization (b) oxide formation (c) other effects that alter the surface (d) mixed control processes (e) potential drop due to solution resistance.

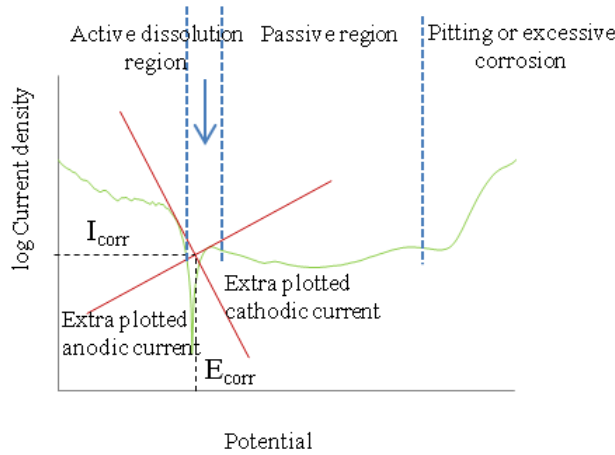


Figure 4.29 : Schematic representation of Tafel analysis and the different regions in potentiodynamic anodic polarization curve

The Tafel analysis is carried out by extrapolating the linear portions of a log current versus potential plots back to their intersection. The value of the current density and potential are the corrosion current density and corrosion potential respectively. In real systems, many

factors influence the linearity and it practically becomes difficult to find the linear region. This problem is overcome by sophisticated numerical fit to Butler Volmer equation of the experimental curve using the GPES v4.9 software.

The corrosion rate is calculated using **equation 4.8**²⁹

$$\text{Corrosion rate (mmpy)} = 0.0033 \times \frac{e}{\rho} I_{corr} \quad (4.8)$$

Where 'e' is the equivalent weight and calculated equivalent weight is 25.12 grams / equivalent and is calculated using **equation 4.2** and 'ρ' is the theoretical density determined using inverse rule of mixture and is 8.01 g/cm³.

The passivation efficiency (PE%) was calculated using **equation 4.9**²⁵

$$PE\% = \frac{j_{corr} - j_{corr}^0}{j_{corr}} \times 100 \quad (4.9)$$

j_{corr} and j_{corr}^0 are the corrosion current densities of unpolished and polished samples respectively.

Figure 4.30 shows the comparison of corrosion rate, passivation efficiency and corrosion current densities of the untreated and electropolished ss304 coupons. The electropolished ss304 has low corrosion rate and corrosion current densities as compared to unpolished samples and furthermore these are the function of the electropolishing time. Materials with a corrosion rate less than 0.02 mm per year are considered to be outstanding in relative corrosion resistance^{23,30} and the samples electropolished for 30 minutes have values very close to this.

Figure 4.30(d) shows the relative variation in mass fractions of chromium and iron as function of electropolishing period lengths obtained from EDAX analysis. The graph shows the enrichment of chromium in the surface layer which may passivate the surface and hence results in the increase of corrosion resistance of the electropolished samples and a similar effect of surface chromium enrichment on corrosion resistance has been reported previously^{26,31,32}.

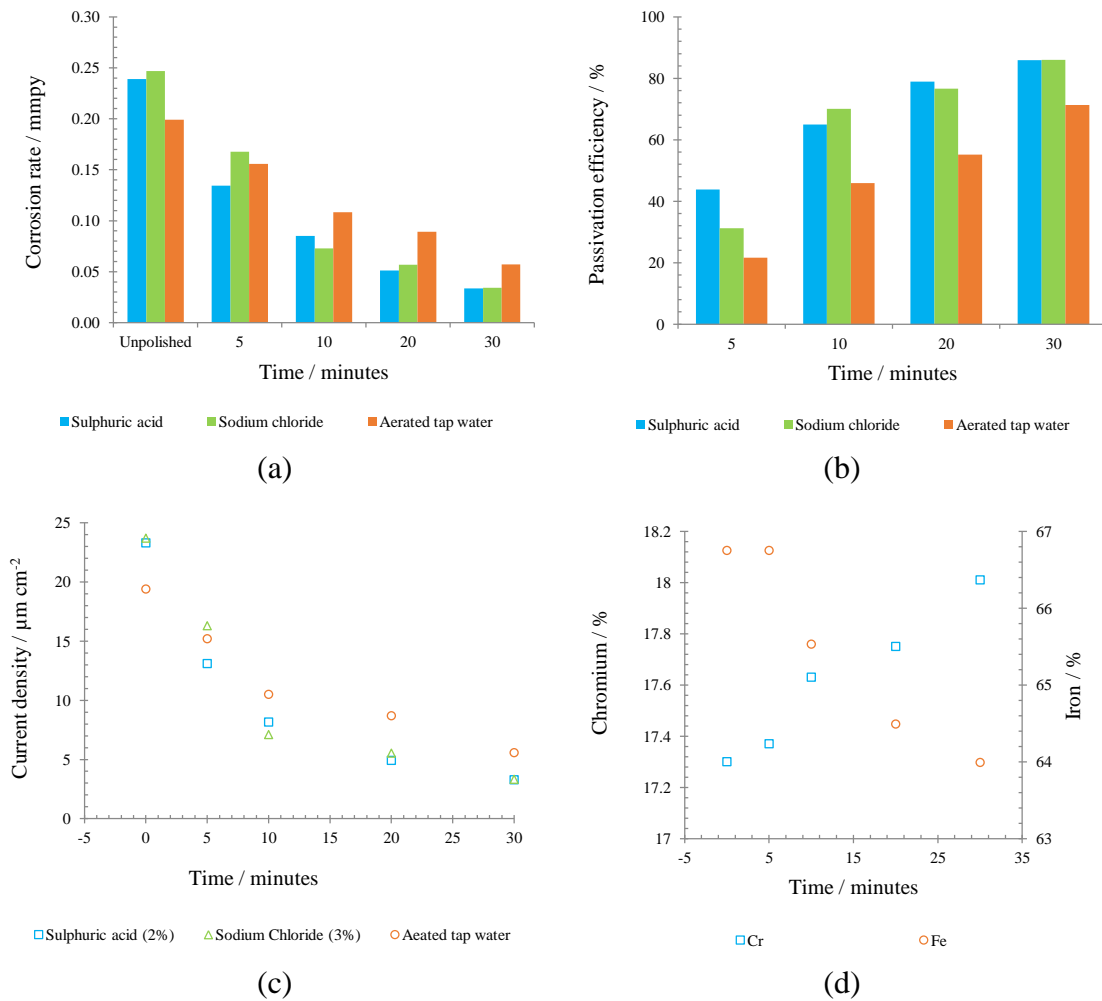


Figure 4.30 : (a) corrosion rate of untreated and electropolished ss304 (b) comparison of % age passivation efficiency (c) variation of the corrosion current density (d) variation of relative mass fraction of Iron and chromium in the samples as a function of electropolishing time

Figure 4.31 shows scanning electron microscope images of ss304 samples obtained at potential in the pitting/excessive corrosion region of the potentiodynamic polarization curves. **Figure 4.31** shows the images of unpolished ss304 in H_2SO_4 (2%). Corrosion in sulphuric acid is uniform or general type and takes place around the grain boundaries. Corrosion in NaCl (3%) is localized resulting in pitting and **Figure 4.32 (a-h)** depict the images of unpolished and electropolished (5, 10, 20 and 30 minutes) samples obtained in the pitting region of polarization curve. The images show that pitting corrosion resistance of ss304 increases with the electropolishing time. Deep and large pits and excessive dissolution along the edges was observed in untreated samples while size of the pits and dissolution along the edges successively decrease with increasing the electropolishing time

and no dissolution around the edges were observed in samples electropolished at 6 V for 20 and 30 minutes.

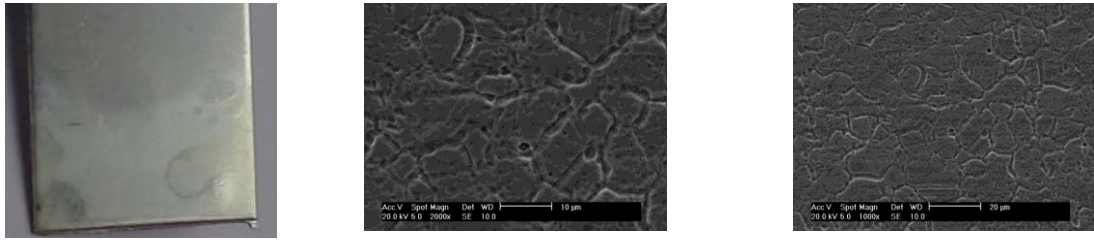


Figure 4.31 : *Corrosion of unpolished ss304 in H_2SO_4 (2%) showing the dissolution along the grain boundaries (uniform corrosion).*

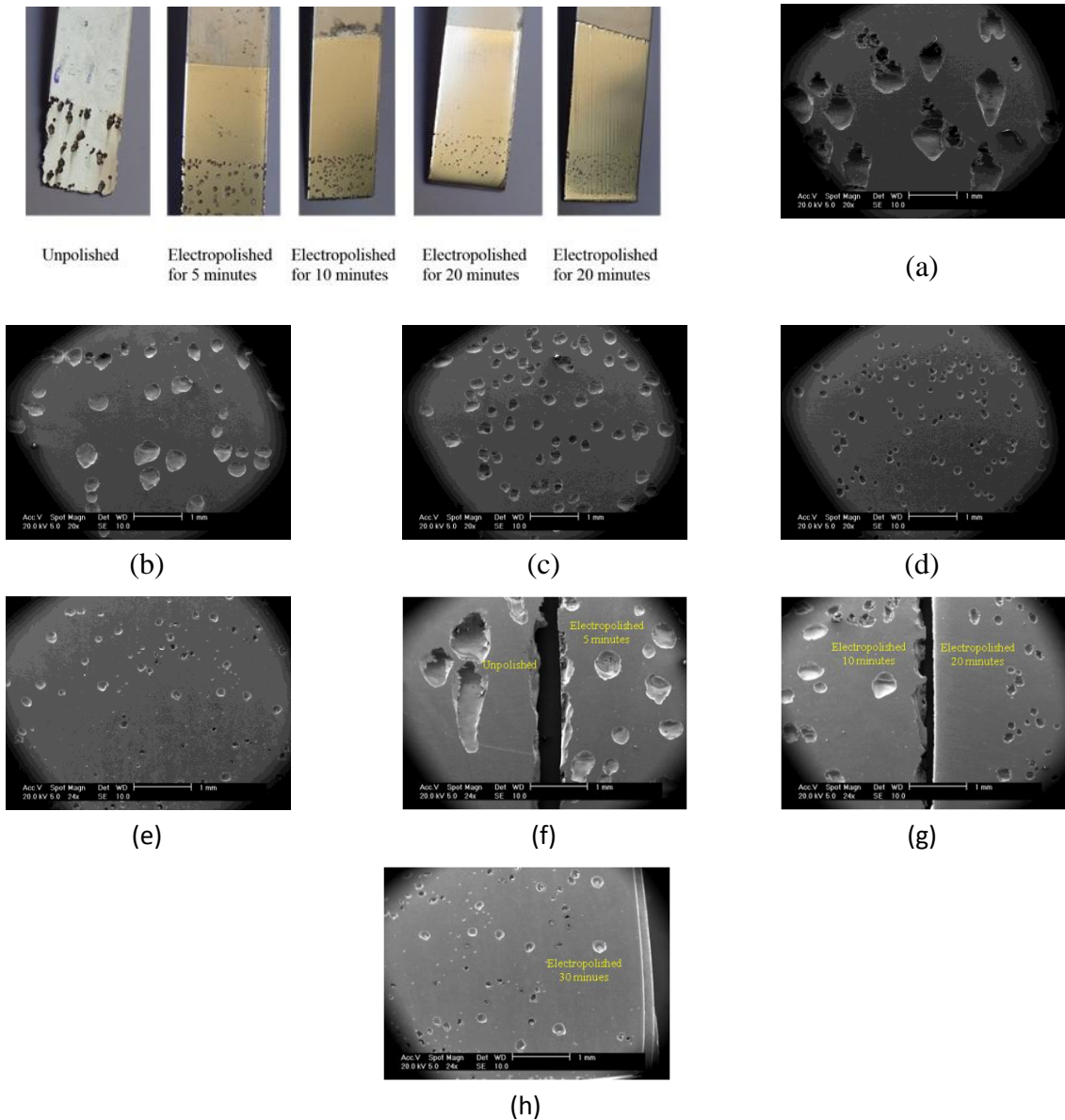


Figure 4.32 : *Pitting corrosion of ss304 samples in $NaCl$ (3%), untreated and electropolished at 6 V for different periods (a) unpolished (b) 5 minutes (c) 10 minutes (d) 20 minutes (e) 30 minutes. (f–h) images of the above samples showing dissolution along edges*

4.5 Summary

Electropolishing is the surface modification phenomenon widely used for the improvement of the surface characteristics of stainless steel. It influences the surface characteristics by changing the stability of the passivation oxide layer which in turn influences the surface energy by providing the hydrophilicity to a material³³ and surface potential by preventing the release of electrons. The stability of the natural surface oxide layer in stainless steel is not very high and the possibility of changing this feature exists.

A preliminary nanoscale morphology of the over layer of electropolished surface of ss316 in 1:2 ChCl:EG electrolyte bath was studied using AFM and FE-SEM. The micrographs revealed granular surface morphology consisting of nanoscaled hemispherical grains and contained some pores which develop with increasing the electropolishing time.

The surface roughness studies were carried out using AFM and DHM. The surface roughness parameters S_a , S_q , skewness, kurtosis, mean maximum height, mean maximum depth were investigated. Normalised values of mean surface roughness (S_a) and mean square root roughness (S_q) were reported as these values are very sensitive to samples, method and instruments used for measurement. Surface roughness was found to be the strong function of electropolishing time and it decreased with increasing electropolishing time. A new technique, digital holographic microscopy (DHM) which is based on the interferometric principle, was also used for surface roughness measurements and results were compared with AFM measurements. Both measurements agreed well with each other.

In the last section, the corrosion behaviour of electropolished austenitic stainless steel in aerated tap water, sulphate, chloride containing aqueous media, 1:2 ChCl:EG and 1:2 ChCl:EG containing oxalic acid (3%) was investigated using electrochemical methods, open circuit potential measurement, potentiodynamic polarization curves and a gravimetric method. Potentiodynamic polarization curves showed that electropolishing of stainless steel improves the general or pitting corrosion of samples and about 70-80% passivation efficiency was achieved at an electropolishing time of 30 minutes. This increase in passivation efficiency may be attributed to decrease in surface roughness³⁴ and the enrichment of chromium in the surface layer²⁵. Gravimetric studies of untreated samples in 1:2 ChCl:EG and 1:2 ChCl:EG with oxalic acid showed that oxalic acid in 1:2 ChCl:EG had more adverse effect on the corrosion behaviour of austenitic stainless steel.

4.6 References

- (1) Lula, R. A. *Stainless steel*; American Society for Metals, **1986**.
- (2) Beddoes, J.; Parr, J. G. *Introduction to Stainless Steels*; 3rd ed.; ASM International, Materials Park: Ohio, USA, **1999**.
- (3) Newman, R. C. *Nature* **2002**, *415*, 743-744.
- (4) Rack, P.; University of Tennessee, Dept. of Materials Science and Engineering, <http://web.utk.edu/~prack/MSE%20300/FeC.pdf>, Access date 16/11/2012.
- (5) McGuire, M. F. *Stainless Steels for Design Engineers*; A S M International, Incorporated, **2008**.
- (6) Martin, F.; Del Frari, D.; Cousty, J.; Bataillon, C. *Electrochimica Acta* **2009**, *54*, 3086-3091.
- (7) Masuda, H.; Fukuda, K. *Science* **1995**, *268*, 1466-1468.
- (8) Yuzhakov, V. V.; Chang, H. C.; Miller, A. E. *Physical Review B* **1997**, *56*, 12608-12624.
- (9) Li, A. P.; Muller, F.; Birner, A.; Nielsch, K.; Gosele, U. *Journal of Applied Physics* **1998**, *84*, 6023-6026.
- (10) Jessensky, O.; Muller, F.; Gosele, U. *Applied Physics Letters* **1998**, *72*, 1173-1175.
- (11) Sieber, I.; Kannan, B.; Schmuki, P. *Electrochemical and Solid-State Letters* **2005**, *8*, J10-J12.
- (12) Tsuchiya, H.; Schmuki, P. *Electrochemistry Communications* **2005**, *7*, 49-52.
- (13) Sieber, I.; Hildebrand, H.; Friedrich, A.; Schmuki, P. *Electrochemistry Communications* **2005**, *7*, 97-100.
- (14) Tsuchiya, H.; Macak, J. M.; Sieber, I.; Taveira, L.; Ghicov, A.; Sirotna, K.; Schmuki, P. *Electrochemistry Communications* **2005**, *7*, 295-298.
- (15) Tsuchiya, H.; Macak, J. M.; Sieber, I.; Schmuki, P. *Small* **2005**, *1*, 722-725.
- (16) Vignal, V.; Roux, J. C.; Flandrois, S.; Fevrier, A. *Corrosion Science* **2000**, *42*, 1041-1053.
- (17) Fujimoto, S.; Tsujino, K.; Shibata, T. *Electrochimica Acta* **2001**, *47*, 543-551.
- (18) Gadelmawla, E. S.; Koura, M. M.; Maksoud, T. M. A.; Elewa, I. M.; Soliman, H. H. *Journal of Materials Processing Technology* **2002**, *123*, 133-145.
- (19) Teague, E. C.; Scire, F. E.; Baker, S. M.; Jensen, S. W. *Wear* **1982**, *83*, 1-12.
- (20) Pancewicz, T.; Mruk, I. *Wear* **1996**, *199*, 127-131.

- (21) Young, P. L.; Brackbill, T. P.; Kandlikar, S. G. *Heat Transfer Engineering* **2009**, *30*, 78-90.
- (22) Abbott, A. P.; Capper, G.; McKenzie, K. J.; Glidle, A.; Ryder, K. S. *Physical Chemistry Chemical Physics* **2006**, *8*, 4214-4221.
- (23) Arenas, M. F.; R.G.Reddy *Journal of Mining and Metallurgy* **2003**, *39(1-2)B*, 81-91.
- (24) *DHM 1000 Family - User Operating Manual*; Lyncee tec.
- (25) Sherif, E. S. M. *International Journal of Electrochemical Science* **2011**, *39*, 2286-2298.
- (26) Sherif, E. S. M.; Potgieter, J. H.; Comins, J. D.; Cornish, L.; Olubambi, P. A.; Machio, C. N. *Corrosion Science* **2009**, *51*, 1364-1371.
- (27) Sherif, E. S. M. *Applied Surface Science* **2006**, *252*, 8615-8623.
- (28) Uhlig, H. H. *Corrosion and Corrosion control*; 3rd ed.; John Wiley and Sons: New York, **1985**.
- (29) Sedriks, A. J. *Corrosion of Stainless Steel*; Second ed.; John Wiley: New York, **1996**.
- (30) Jones, D. A. *Principles and Prevention of Corrosion*; 2nd ed.; Prentice Hall, Inc.: Upper Saddle River, NJ, **1996**.
- (31) Sherif, E. S.; Potgieter, J. H.; Comins, J. D.; Cornish, L.; Olubambi, P. A.; Machio, C. N. *Journal of Applied Electrochemistry* **2009**, *39*, 1385-1392.
- (32) Wolff, I. M.; Iorio, L. E.; Rumpf, T.; Scheers, P. V. T.; Potgieter, J. H. *Materials Science and Engineering: A* **1998**, *241*, 264-276.
- (33) Hryniewicz, T.; Rokosz, K.; Rokick, R. *Metal Finishing* **2006**, *104*, 26-33.
- (34) Lee, S. J.; Lai, J. J. *Journal of Materials Processing Technology* **2003**, *140*, 206-210.

| | | |
|-------------------------------|---|------------|
| Chapter 5 : | Electrofinishing of nickel based superalloy | 145 |
| 5.1 | Introduction | 146 |
| | 5.1.1 <i>Superalloys</i> | 147 |
| | 5.1.2 <i>Nickel based superalloys</i> | 150 |
| | 5.1.2.1 <i>Microstructure of nickel based superalloys</i> | 151 |
| | 5.1.3 <i>Processing of superalloys</i> | 154 |
| | 5.1.4 <i>Applications of nickel based superalloys</i> | 156 |
| Results and Discussion | | |
| 5.2 | Surface morphology of CMSX-4 | 157 |
| | 5.2.1 <i>Topography of unpolished CMSX-4</i> | 157 |
| | 5.2.2 <i>Surface morphology of electropolished CMSX-4</i> | 158 |
| | 5.2.2.1 <i>Controlled potential electropolishing</i> | 159 |
| | 5.2.2.2 <i>Galvanostatically electropolished</i> | 161 |
| 5.3 | Surface roughness of electropolished CMSX-4 | 163 |
| | 5.3.1 <i>Surface roughness of potentiostatically electropolished CMSX-4</i> | 164 |
| | 5.3.2 <i>Surface roughness of galvanostatically electropolished CMSX-4</i> | 167 |
| 5.4 | Material etch rate of CMSX-4 | 168 |
| | 5.4.1 <i>Extended time scale electropolishing</i> | 169 |
| | 5.4.2 <i>Anodic dissolution rate</i> | 171 |
| 5.5 | Surface composition | 175 |
| 5.6 | Summary | 177 |
| 5.7 | References | 178 |

5.1 Introduction

In the previous chapters, the electropolishing of austenitic stainless steel was studied in the novel choline chloride based deep eutectic solvent, 1:2 ChCl:EG. In this chapter, the electropolishing of nickel based cast single crystal superalloy CMSX-4 used for aerospace turbine blade in ethaline has been studied. Modern aerospace engines and land based power generation turbines have certain sections in which components functions under extreme mechanical / thermal stresses. Aerospace turbine blades (combustion sections of the engine) work at temperature which is about 200 -300 °C higher than the melting point of the fabricated alloy metals. Therefore these components have rigorous specifications of melting point, strength, creep and thermal expansion. For this purpose a range of superalloys have been developed to combat harsh operational environments. The alloy chemistry and innovative processing routes i.e. migration from equiaxed to directional and single crystal solidification have evolved during the last forty years. The single crystal investment casting improves the strength and durability of the turbine blades and eliminates the grain boundaries in adjacent crystallites thus reducing the instances of crack propagation, fracture and subsequent failure¹⁻⁵.

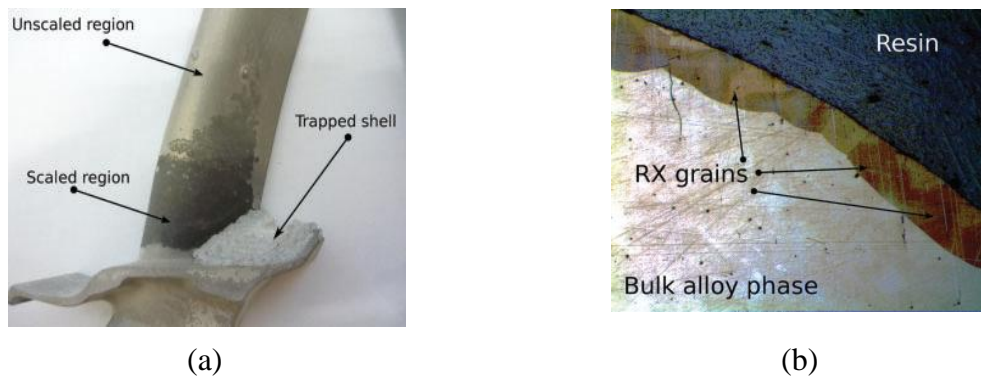


Figure 5.1 : (a) Blade aerofoil close to root block showing scaled and unscaled regions as well as some residual mould shell⁷ (b) As cast 10 mm test bar (CMSX4 alloy) grit blasted, then mounted in resin and sectioned. The grain contrast is enhanced for optical analysis using a ferric chloride (FeCl₃) etch⁷

The casting of single crystal components is carried out in a ceramic mould. During solidification some of the mould metals separate due to differential thermal contraction and these metals deposit as oxide on the surface of the blade as a thin layer, usually across the aerofoil under the shoulder of turbine blade and is referred as 'surface scale' due to its

texture. **Figure 5.1 (a)** shows the typical surface scale on the turbine blade. The causes of the formation of these scales in Ni-based superalloys are not well documented and recently Brewster et al.⁶ tried to describe the mechanism of their formation.

As cast turbine components are subjected to rigorous heat treatment to homogenise the as cast microstructure and obtain the optimum γ' morphology. The static components such as nozzle guide vanes (NGV's) are visually inspected to check the metallurgical integrity of the components i.e. grain defects. The presence of surface scale have significant subsequent processing issues like identification of defects (microstructure assessment) and surface incipient melting in these areas. Mechanical polishing (blasting, grinding and machining) cannot be done prior to heat treatment because it may results in surface recrystallization and the formation of grain structure⁷ as shown in **Figure 5.1 (b)**. Chemical etching and electrolytic electropolishing in aqueous bath are the possible alternative processes for the removal of the surface scales. These processes require the aggressive oxidising environments using toxic reagents and the mixture of strong inorganic acids (phosphoric acid, sulphuric acid or nitric acid etc.) and are under serious pressure due to their adverse environmental impacts. Moreover the conventional electrolytic etches often cause the pitting and uneven dissolution in the unscaled surface regions of the blade⁷. Therefore an ionic liquid electrolyte based on choline chloride (deep eutectic solvent) is tested for the removal of the surface scales of the nickel based superalloys which has been studied for electropolishing of different grades of 300 series stainless steel in **chapter 3**. The deep eutectic solvents have also been successfully used for a number of electrofinishing processes described in **chapter 1 section1.6**. These liquids are benign to environment, cheap, and require no registration.

5.1.1 Superalloys

Super alloys are an unusual class of metallic materials that can withstand challenging and harsh environments such as high temperatures, high stresses, extreme corrosive and oxidation conditions. They have good corrosion, oxidation, creep and rupture resistance at high temperatures. They have an austenitic fcc structure which confers them the following properties such as (i) better mechanical properties (ii) higher modulus (iii) higher solubility of alloying elements (iv) systems of gliding plane.

They have been developed for specific, specialized properties and applications and are widely used in aircraft engines, power generation turbines, rocket engines, nuclear power

and chemical processing plants. They can tolerate average temperatures of 1050 °C with occasional excursions to temperature as high as 1200 °C where most of the material (90%) gets melted or soften.

There are three main classes of superalloys :

- i. Nickel based superalloys – they are the most complex class of superalloys and widely used in the hottest parts. They have high fcc matrix phase stability which may be further strengthened by many direct or indirect means. Currently they constitute about 40-50% of the total weight of an air craft engine and extensively used in the combustor and turbine sections of engine where elevated temperatures are maintained during the operation.
- ii. Iron – nickel based superalloys – they have austenitic fcc matrix based on Fe and Ni (at least 25 %). They are cheaper as a part of Ni is replaced with Fe but they cannot be used at as high a temperature as that of Ni based alloys. Their strength is due to the presence of primarily ordered intermetallics (γ' Ni₃Al, γ'' Ni₃Nb).
- iii. Cobalt based superalloys – they have superior hot corrosion and thermal fatigue strength at temperatures between 980°C to 1100°C. They have fcc matrix which is stabilized by alloying with Ni. They have a lower strength at intermediate temperatures due to the absence of γ' phase and are sometimes preferentially used instead of Ni based alloys at the temperature 750°C.

The main alloying elements of superalloys belong to 8th group of the periodic table and contain 10+ alloying elements to modify their properties. **Table 5.1** shows the different alloying elements along with their role in superalloys. **Figure 5.2** shows the typical composition of three types of superalloys along with some common examples of wrought and casting superalloys.

| Table 5.1 : | Alloying elements and their role in superalloys⁹ | | |
|--|--|--------------------------|--------------------------|
| Effect | Type of superalloys | | |
| | Iron – Nickel base | Co base | Nickel base |
| γ former : (partition to γ matrix) Solid solution strengtheners | Cr, Mo | Nb, Cr, Mo, Ni, W, Ta | Co, Cr, Fe, Mo, W, Ta |
| Fcc matrix stabilizers | C, W, Ni | Ni | |
| γ' former : partition to γ' precipitates | Al, Ti, Ni | | Al, Ti |
| Carbide Forms : grain boundary strengthening | | | |
| MC type | Ti | Ti, Ta, Nb | W, Ta, Ti, Mo, Nb |
| M ₇ C ₃ type | | Cr | Cr |
| M ₂₃ C ₆ type | Cr | Cr | Cr, Mo, W |
| M ₆ C type | Mo | Mo, W | Mo, W |
| Carbonitrides : M(CN) type | C, N | C, N | C, N |
| Grain boundary refiners : segregate to grain boundaries | B | B, Zr | B, Zr, C, Hf |
| Hardening precipitates and/or intermetallics | Al, Ti, Nb | Al, Mo, Ti, W, Ta | Al, Ti, Nb |
| Oxidation resistance | Cr | Al, Cr, Ta | Al, Cr, Ta, Ce |
| Hot corrosion resistance | Cr | Cr | Cr, Co, Si, La, Th |

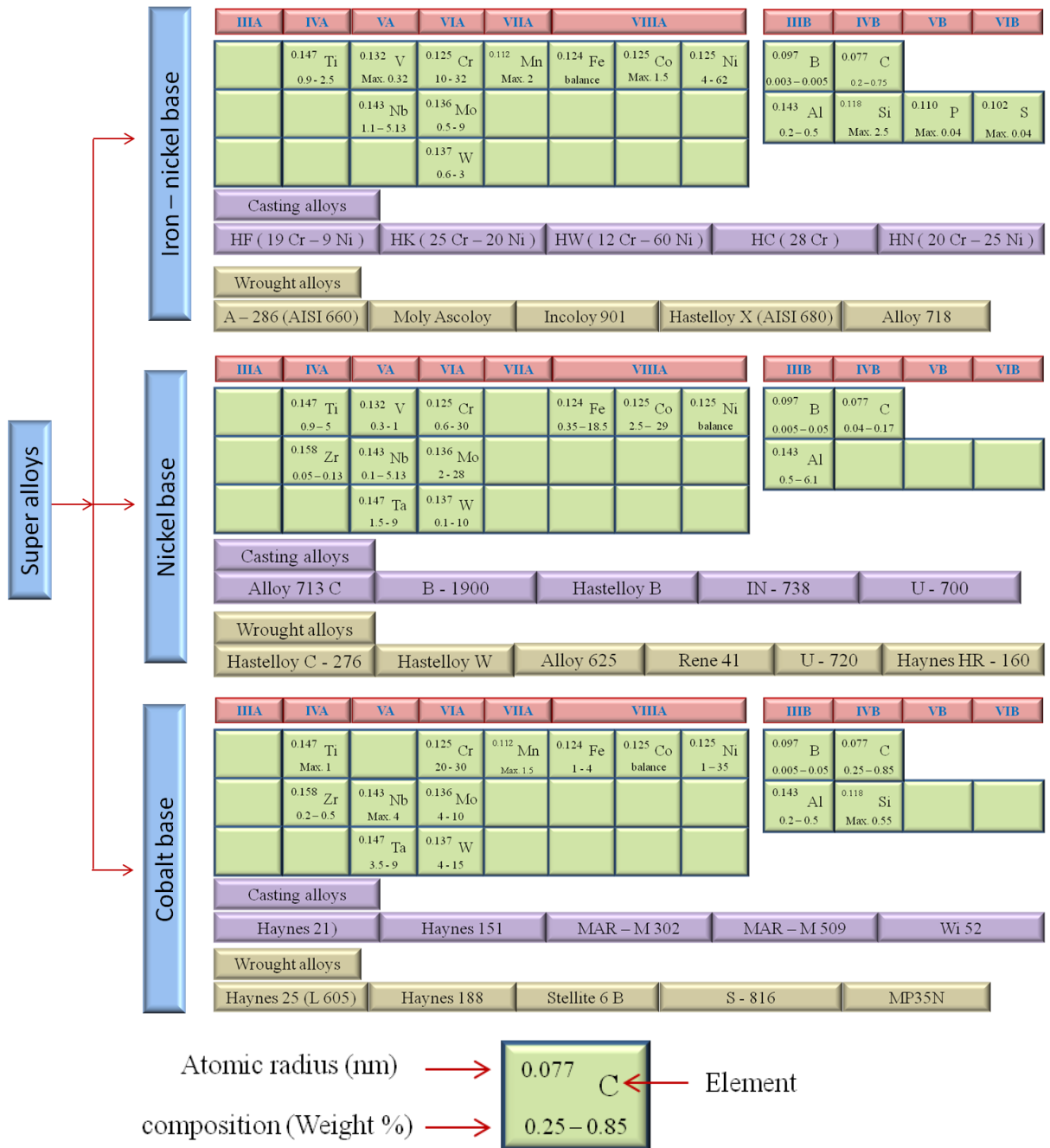


Figure 5.2 : Different types of superalloys along with their typical composition and some common examples of each type¹⁰.

5.1.2 Nickel based superalloys

Nickel superalloys are the most complex and predominately used at higher temperatures in the range 750°C to 980°C and some of the nickel based superalloys along with their composition are shown in **Figure 5.3**. They are preferred over cobalt based and iron-nickel

based superalloys at temperature close to the melting temperature of the materials. The high temperature strength is attributed to very stable γ' ordered fcc precipitates.

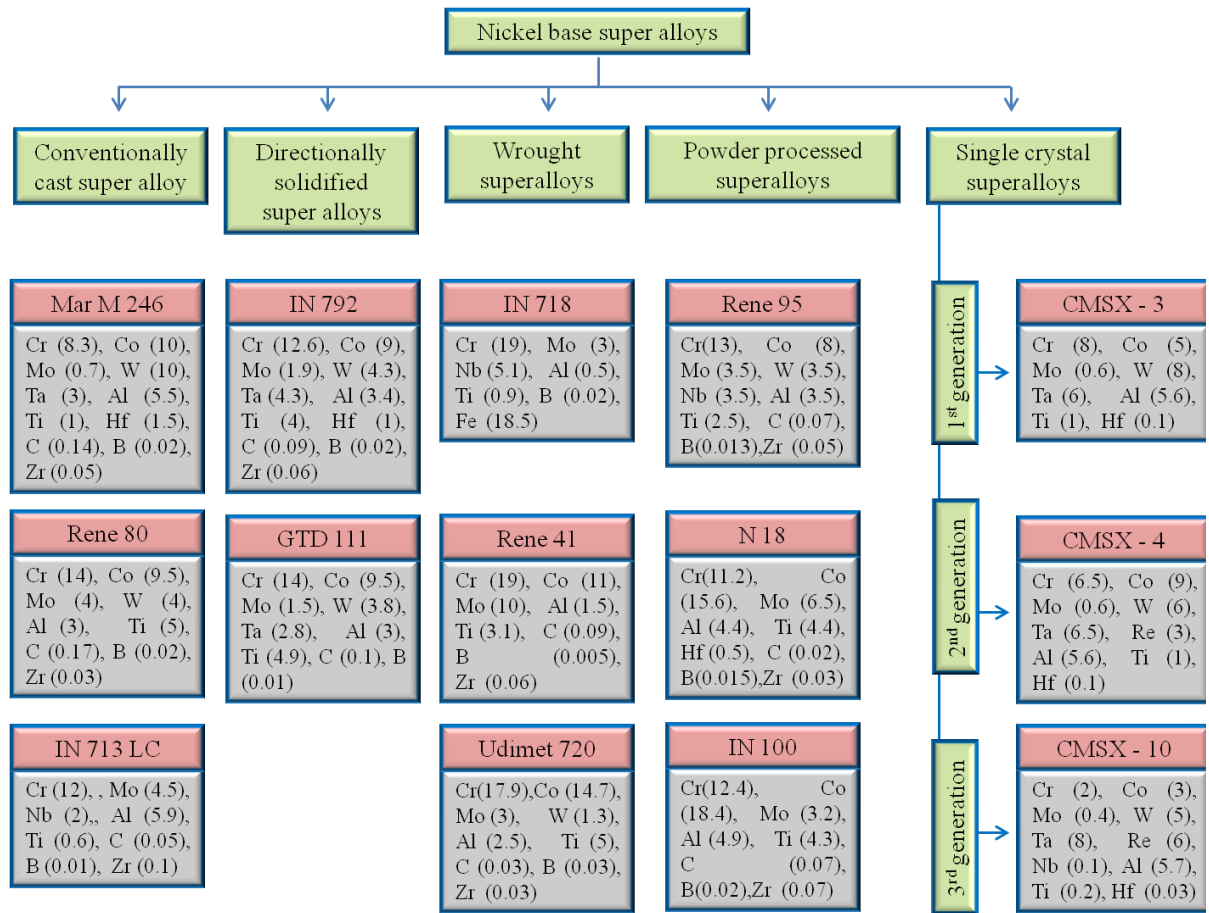


Figure 5.3 : Different types and compositions of some of commercial Ni based superalloys⁹

5.1.2.1 Microstructure of nickel based superalloys

There are four major phases present in nickel based superalloys

- i. Gamma (γ) phase
- ii. Gamma prime (γ') phase
- iii. carbides
- iv. Topologically close packed phases
 - (i) Gamma phase

This is continuous, non-magnetic nickel based phase which forms the matrix. It has a fcc structure and contains most of the solid solution elements mainly belonging to Group V,

VI and VII such as cobalt, iron, chromium, molybdenum and tungsten due to the nearly filled 3d electronic shell that allows alloying with these elements.

(ii) Gamma prime (γ') phase

This consists of Ni_3Al , Ti and has a fcc structure which precipitates coherently with the austenitic gamma matrix. Elements niobium, tantalum and chromium segregate in γ' phase. It has face centred cubic (fcc) structure with nickel atoms at the face centres and aluminium or titanium atoms at the cube corners. This ordered L1_2 crystal structure gives elevated temperature strength and excellent creep resistance. In modern alloys the volume fraction of γ' precipitates is about 70%.

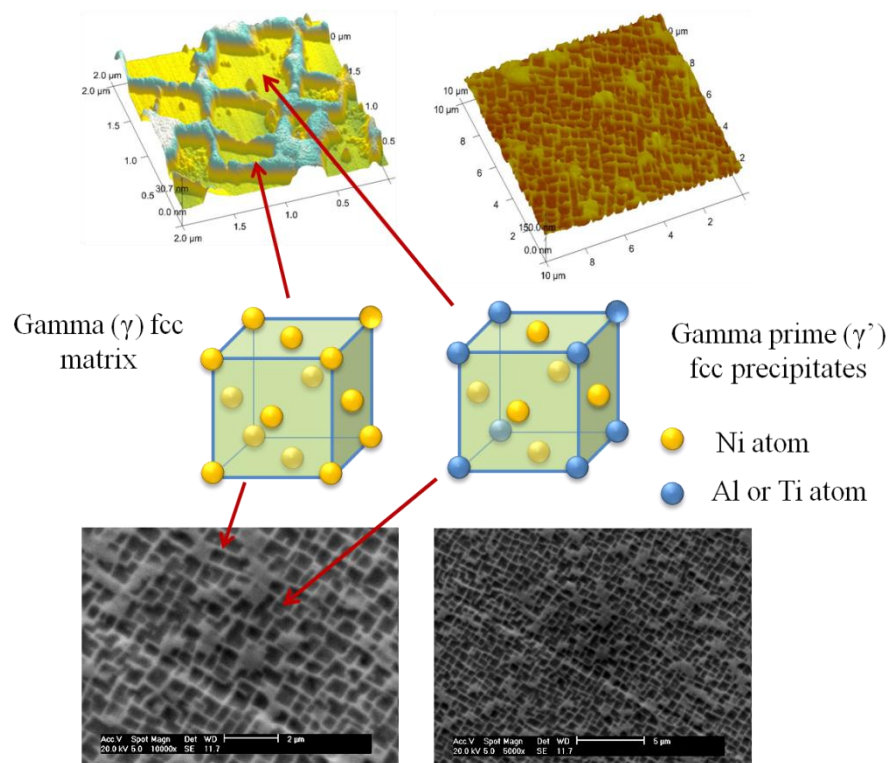


Figure 5.4 : *Microstructure of the nickel based superalloys(CMSX-4)*

γ and γ' phases are in equilibrium and have very unusual crystallographic relationship. Both phases are face centred cubic with almost identical lattice dimensions and also similar orientation, so these two phases are almost coherent and are shown in **Figure 5.4**. Due to this coherence allows γ' precipitates homogeneously throughout the matrix (γ phase). The gamma prime adopts such morphology which minimize the interfacial energy which depends on the mismatch between matrix / precipitates (γ / γ'). If the mismatch is smaller

then γ' precipitates are larger in size and the preferred morphology is cubic or plates while in case of large mismatch, the γ' precipitates are small in size and have spherical shape.

(iii) Carbides

The added carbon (0.02 – 0.2%) combines with reactive elements like Ti, Ta, Hf and Nb to form metal carbides (MC). These carbides decompose to produce other carbides such as $M_{23}C_6$ and /or M_6C . All the carbides have a fcc crystal structure and increase the rupture strength at high temperature.

(iv) Topologically close packed phases

These are undesirable plate like, or needle like, brittle phases formed during the heat treatment and the common forms are σ , μ and Laves and are shown in **Figure 5.5**. TCPs have close packed atoms in layers with relatively large interatomic distances one below the other and characteristic topology is produced when larger atoms are sandwiched between layers. These phases lowered the rupture strength and ductility due to tie up of γ and γ' strengthening elements.

σ phase – this is hard plate like and the most undesirable phase. It shortened creep rupture life. It has the composition of type $(Cr, Mo)_x (Ni, Co)_y$ and possesses 30 atoms per cell and structure is similar to $M_{23}C_6$.

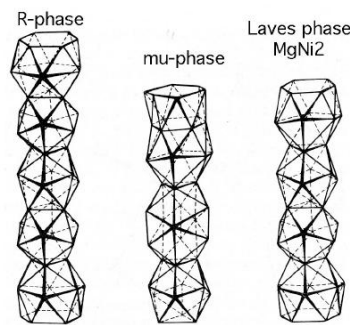


Figure 5.5 : *Topologically close packed phases¹¹*

μ phase – it has the similar composition as that of σ phase with majority of Mo and Co. it possesses 13 atoms per cell and the structure similar to M_6C .

Laves phase – it has composition of type AB_2 such as $(MoCo_2$ and $TaCo_2)$. It has a negative impact on tensile ductility and creep properties at room temperature.

5.1.3 Processing of superalloys

A base alloy ingot is produced by melting the raw material through vacuum induction melting (VIM). VIM is preferred over electric arc furnace (air / slag) due to its effectiveness in removing the traces of low melting contaminants. Prior to adding γ' forming elements (Ti, Al and Hf) after the removal of impurities, the melt is deoxidised by carbon boil. After attaining the desired composition, alloy is solidified to ingot.

The ingots are converted to the desired components by one of three major routes (**Figure 5.6**) involving remelting or consolidation depending on the final application of the components.

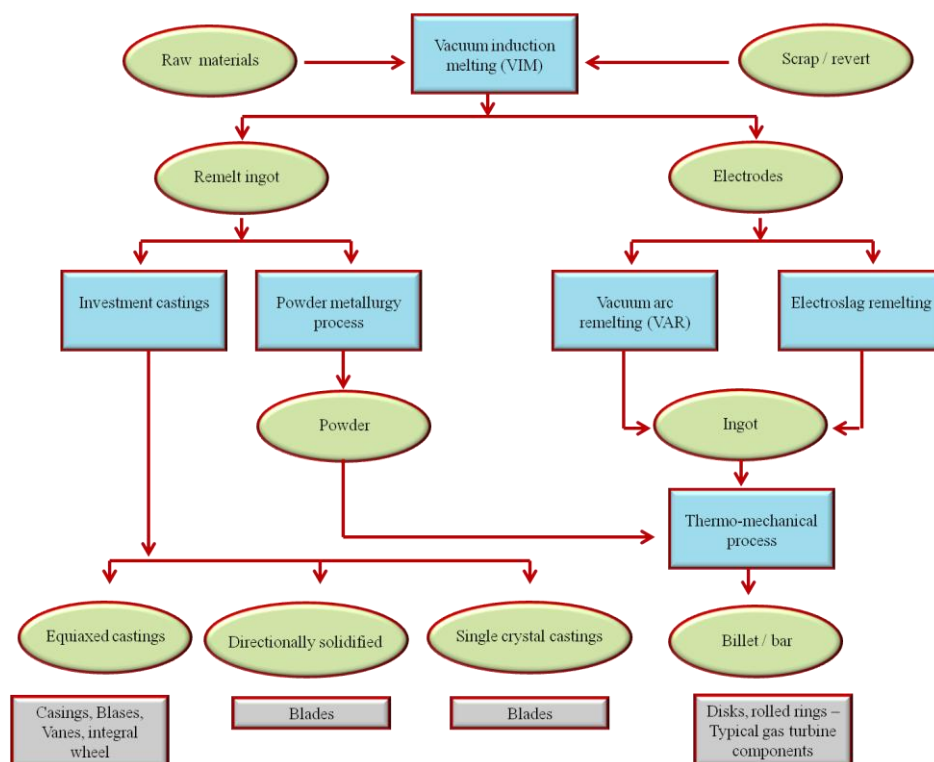


Figure 5.6 : Traditional processes used to produce components from superalloys⁹

Investment casting – it is primary casting process for complex shaped components. A single use ceramic mould is progressively built up around a wax pattern. A thermal cycle is used to remove the wax and the mould is filled with remelted superalloy in the preheated

vacuum chamber. The cooled component is removed by shattering the mould with vibrations.

The final structure of the material is sensitive to the thermal conditions applied during the solidification of the castings and may be classified into (i) equiaxed (cooled uniformly throughout their volume). (ii) columnar or single crystal casting (these are removed from the hot zone to a cold zone at the controlled rate). These final structures are shown in **Figure 5.7**.

Directionally solidify alloys – Creep resistance is linked with the grain boundaries and can be increased with orienting the grain boundaries parallel to applied stress (columnar grain) or by removing the grain boundaries entirely (single crystal grains). The columnar grain or single crystal grain can be produced by withdrawing the mould downward through a radiation baffle at moderate thermal gradients and the grain growth takes place along the applied stress. The two major defects that arise in directionally solidifying alloys are freckle chains and misoriented grains^{9,12}.



Figure 5.7 : *Different types of blades¹¹*

Wrought alloys – the superalloy ingots are subjected to secondary remelting of VIM ingots to produce secondary ingots or powder. Secondary melting removes the defects like macrosegregation or large shrinkage cavities produced during VIM solidification. The removal of these defects is necessary for high temperature properties of Ni based superalloys as these are sensitive to microstructural variations, chemical inhomogeneities and inclusions.

Powder metallurgy alloys – The segregation of solid solution elements (Ti, W, Mo, Ta and Nb) and their low ductility strength make the ingot susceptible to cracking as thermally induced stresses evolve during cooling. These melt related defects can be overcome by using the powder processing routes due to rapid solidification of the fine powders. Powders are collected into steel cans which are then evacuated under vacuum and sealed. The cans are hot isotatically pressed (HIP) or extruded to consolidate the powder.

Deformation processing – the superalloy ingots are converted to useful components by commonly used hot working processes such as forging and cogging. These processes refine the microstructure to yield isotropic properties and attain a net shape component.

5.1.4 Applications of Nickel base superalloys

The major applications of nickel based superalloy is in gas turbines, about 50% of the modern jet engine is composed of nickel based superalloys. The applications of superalloys are categorized as follows.

1. Air craft gas turbines – disks, combustion chambers, bolts, casings, shafts, exhaust systems, cases, blades, vanes, burner cans, afterburners, thrust reversers and are shown in **Figure 5.8**.

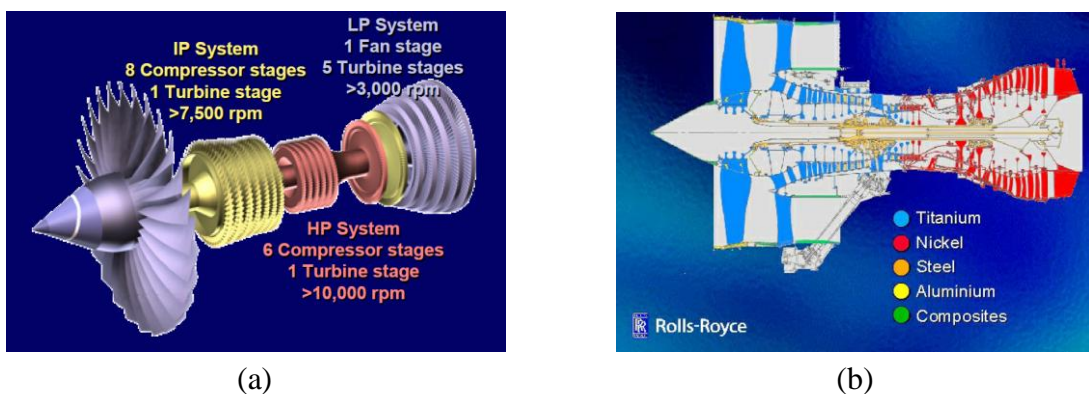


Figure 5.8 : Multiple shafts –Trent 95,000 lbs thrust (b) Materials of the gas turbine

2. Steam turbine power plants – bolts, blades, stack gas reheaters
3. Reciprocating engines – turbochargers, exhaust valves, hot plugs, valve seat inserts.
4. Space vehicles – aerodynamically heated sinks, rocket engine parts.
5. Nuclear power systems – control rod drive mechanisms, valve stems, springs, ducting.
6. Coal gasification and liquefaction systems – heat exchangers, re-heaters, piping.

7. Metal processing – hot work tools and dies, casting dies.

This chapter focuses on the electrolytic polishing of the second generation single crystal nickel based superalloy (CMSX-4) in deep eutectic solvents based on choline chloride and ethylene glycol (hydrogen bond donor) both at controlled voltage and current. The effect of electropolishing on surface texture (surface topography and surface roughness) had been studied using microscopic techniques like Atomic Force Microscope (AFM), Scanning Electron Microscope (SEM) and Digital Holographic Microscope (DHM). The etch rate of the material as a function of electropolishing variables such as electropolishing voltage, current density and time was studied.

5.2 Surface morphology of CMSX-4

5.2.1 Topography of unpolished CMSX-4

CMSX-4 is a cast second generation single crystal nickel based superalloy developed for use in aeroturbine applications by Cannon Muskegon Corporation and produced by investment casting process. It can withstand high homologous temperature ($> 0.7 T_M$) and has excellent creep resistance and stress rupture life. The surface topography of the blade samples as received from Rolls-Royce was studied using the atomic force microscope and scanning electron microscope and the topographical images are shown in **Figure 5.9**. The sections of the blades were mounted in resins. The topography shows the cubic holes of γ' phase and the raised γ phase. The high volume fraction (60 – 80 %) ordered FCC (crystal structure $L1_2$) cuboidal precipitates (γ') mainly consisting of Ni_3Al are uniformly distributed in disordered FCC matrix (γ). The quantitative evaluations of two phases was conducted by line scan (section analysis) of three AFM images ($5 \mu m \times 5 \mu m$) at randomly selected places and in total 30 precipitates were investigated. The average size of γ' precipitates is about ~ 600 nm and the depth is approximately 22 nm from γ phase.

| Table 5.2 : | | <i>Nominal composition of CMSX-4 (Weight percent)</i> | | | | | |
|--------------------|------|---|------|------|------|------|---------|
| Al | Cr | Co | Mo | W | Ta | Re | Ni |
| 5.5 | 1.79 | 3.42 | 0.84 | 6.86 | 5.77 | 7.86 | balance |

The nominal composition of CMSX-4 superalloy is shown in **Table 5.2**. The reported average values were obtained by EDAX analysis of six samples by bombarding the

electronic beam of 20 keV for a period of 60 seconds. The alloy has a density of 8.70 Kg cm^{-3} and has a total refractory content of about 22 % weight including 8 weight % of Re to provide the creep resistance.

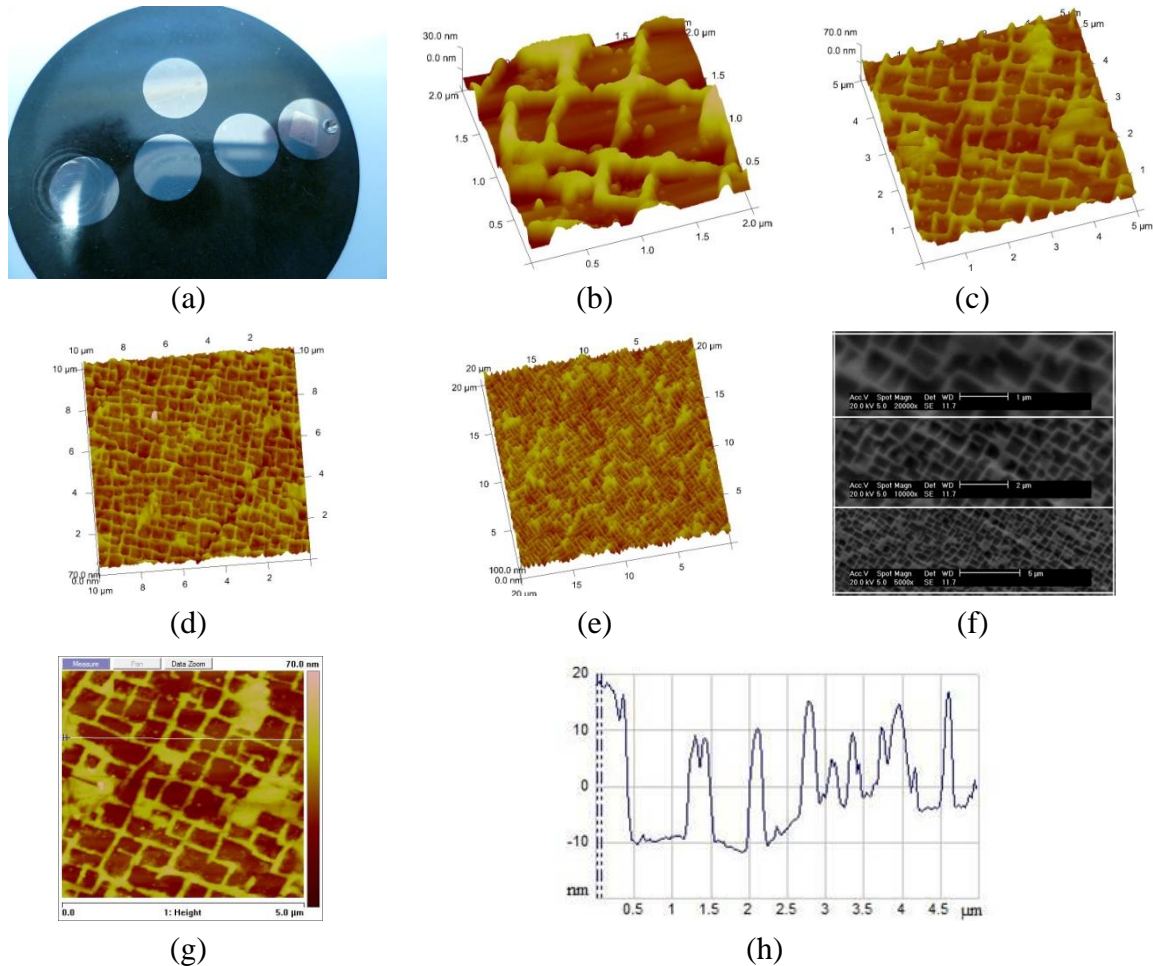


Figure 5.9 : *Topographical images of unpolished CMSX-4 sample (a) sections of the samples mounted on resin (b – e) AFM images, (f) SEM images (g – h) line scan of AFM image*

5.2.2 Surface morphology of electropolished CMSX-4

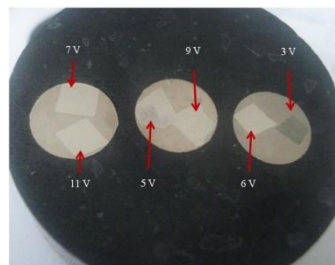
The CMSX-4 samples were electropolished in ethaline containing oxalic acid (3%) at controlled current and voltage to study the effect of electropolishing on the surface topography. The circular CMSX-4 samples sectioned and mechanically polished were mounted into bakelite and were electropolished using Thurbly thandar (TTi) power supply using a two electrode assembly. First holes were drilled into the resin from the reverse of the sample upto the samples. The holes were threaded to fix the bolt for electric connections as shown in **Figure 5.10**.



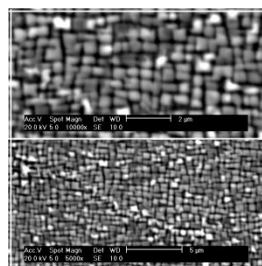
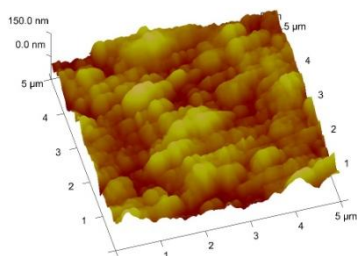
Figure 5.10 : Pictures of the CMSX-4 samples mounted into resin prepared for electropolishing by drilling holes on the backside in the resin upto the samples and bolt fixed for electric connections

An area (0.16 cm^2) of the samples was exposed for electropolishing while rest of the surface was masked with electric tape. The masked samples were dipped upside down into the container containing the electrolyte consisting of ethaline + oxalic acid (3%). A carbon mesh (5 cm x 15 cm) folded into a cylinder was used as the counter electrode. The electropolishing was conducted at controlled voltage of 3 V, 5 V, 6 V, 7 V, 9 V and 11V. Similarly the electropolishing was conducted at constant current densities of 10 mA cm^{-2} , 20 mA cm^{-2} , 30 mA cm^{-2} , 40 mA cm^{-2} and 50 mA cm^{-2} .

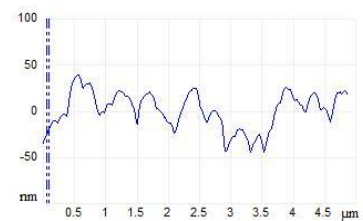
5.2.2.1 Controlled potential electropolishing



(a)



(b)



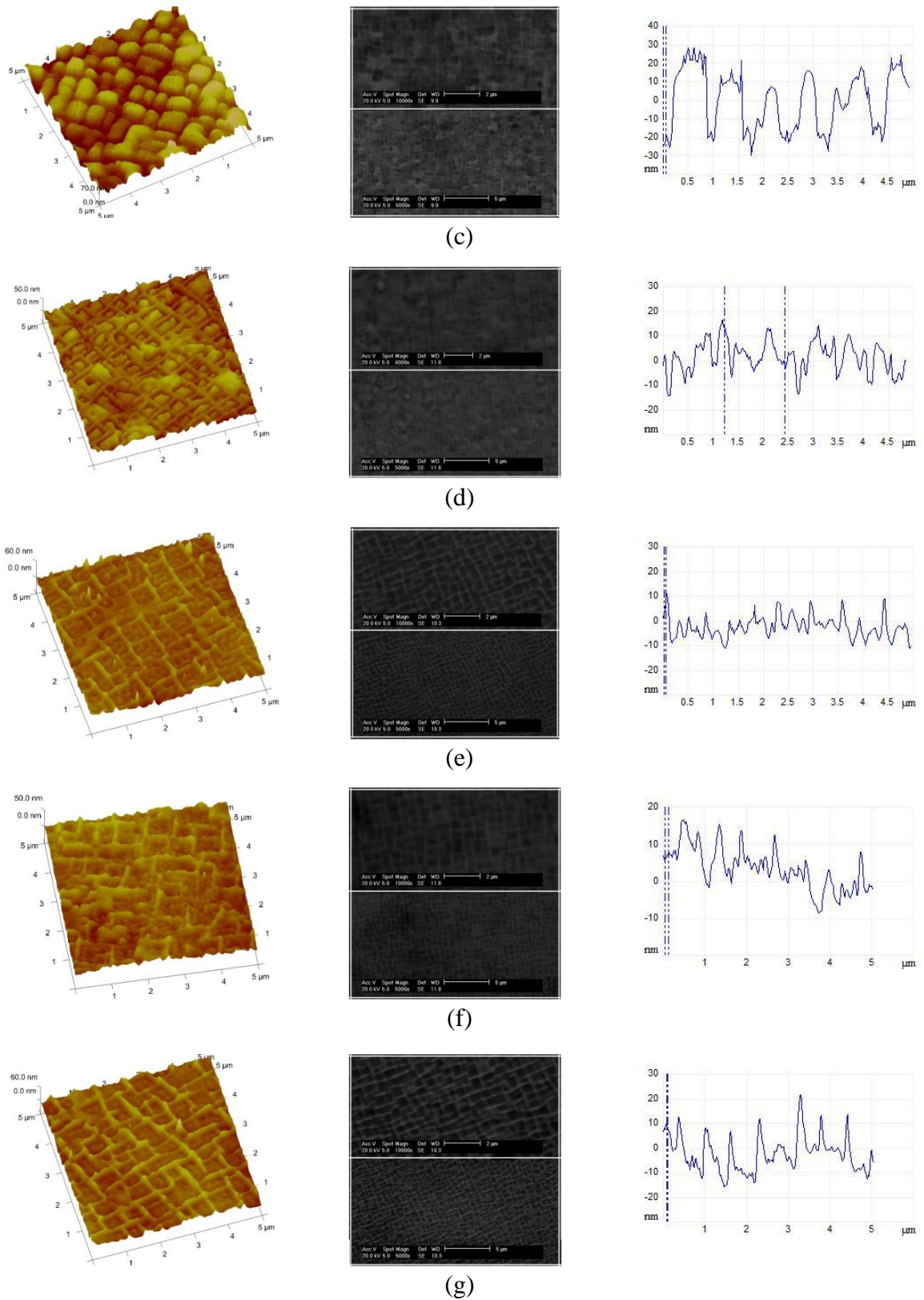


Figure 5.11 : *AFM and SEM topography of electropolished CMSX-4 samples at controlled potential (a) photograph of electropolished samaples (b) 3 V (c) 5 V (d) 6 V (e) 7 V (f)9 V (g) 11 V*

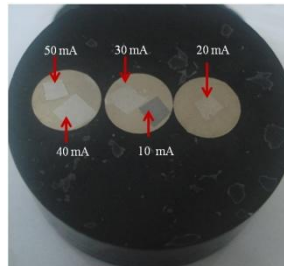
The surface morphologies of the electropolished samples at constant voltage were imaged using the atomic force and scanning electron microscopes and are shown in **Figure 5.11**. The line scans (sections) of two AFM images obtained from two different places were used for analysis of the two phases (γ and γ'). The dissolution of the two phases was found to be a function of the electropolishing potential.

The electropolishing of CMSX-4 samples at 3 V results in the preferential dissolution of the γ phase which results in the disappearance of the waffle like appearance of surface and there is no distinction between the two phases (γ & γ'). Topographical images of the surface electropolished at 5V show the inverted morphology that is the ditches of gamma phase with an average depth of 23.58 nm and the raised cubic (average size ~585.88 nm) gamma prime phase indicating the preferential dissolution of gamma phase. The surface morphology of the electrochemically polished surface at controlled voltage of 6V reveals the start of the dissolution of gamma prime precipitates at the periphery of the precipitates which results in a decrease in size and the average size of the cubic precipitates was found to be 353.27 nm. The γ phase also dissolved and it levels with the γ' phase. The electropolished samples at voltages of 7 V, 9 V and 11 V show the waffle like topography similar to the unpolished surface indicating the comparable rate of dissolution of both the phases. The average size of the cubical precipitates slightly increased, that may be due to the thinning of the gamma phase and also the depth of the γ' cubes decreased slightly compared to the unpolished surfaces. The average size of the gamma prime phase for samples electropolished at 7 V, 9 V and 11 V are 652.14, 669.1, 622.83 nm respectively while the average depth is 12.36, 13.14 and 15.25 nm respectively.

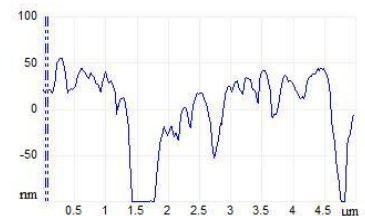
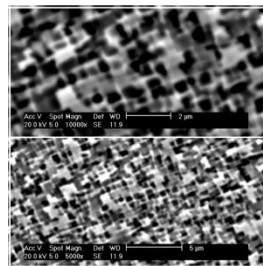
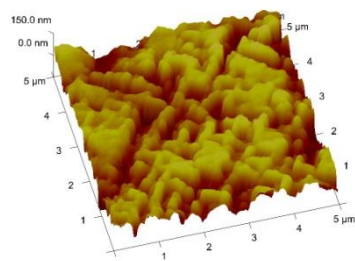
5.2.2.2 Galvanostatically electropolished

The surface morphologies of CMSX-4 samples electropolished at constant current densities of 10 mA cm⁻², 20 mA cm⁻², 30 mA cm⁻², 40 mA cm⁻² and 50 mA cm⁻² are shown in **Figure 5.12**. The samples electropolished at 10 mA cm⁻² showed localized polishing of the surface which results in pitting due to the low current density. The surface topography of the samples electropolished at 20 mA cm⁻² show the disappearance of the raised gamma matrix indicating the dissolution of the gamma phase while the size of the gamma prime phase is 610.88 nm which is approximately same as that of the unpolished surface indicating little or no dissolution of this phase. The sample electropolished at 30 mA cm⁻² and 40 mA cm⁻² showed the trenches of average depth of 32.75 nm and 40.86 nm of

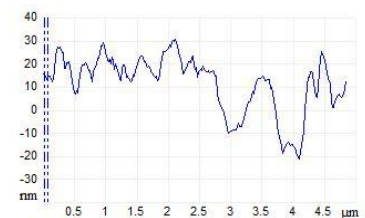
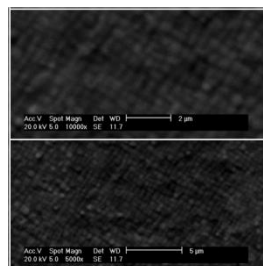
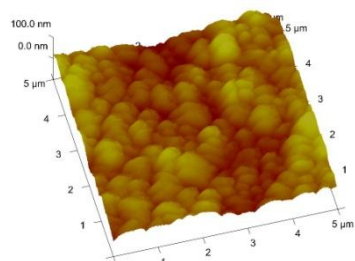
gamma phase around the cubical gamma prime precipitates having average size of 587.64 and 568.57 nm showing the preferential dissolution of the gamma phase rather than the gamma prime phase. The samples electropolished at 50 mA cm⁻² had similar trenches with an average depth of 45.70 nm for the γ phase. The cubical gamma prime precipitates decreased in size (526.36 nm) indicating the dissolution at the periphery of the precipitates and becoming spheroidal in appearance.



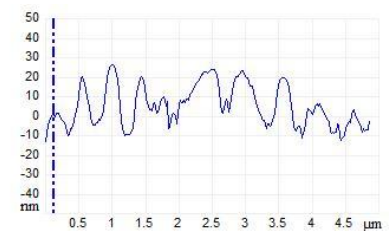
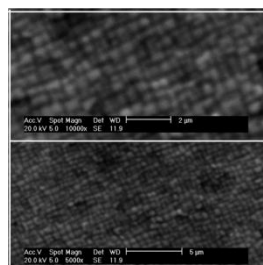
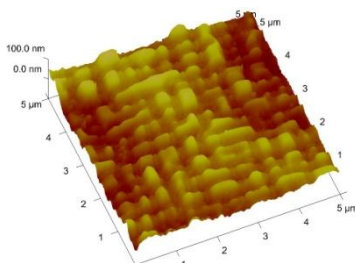
Photograph of galvanostatically electropolished samples



10 mA



20 mA



30 mA

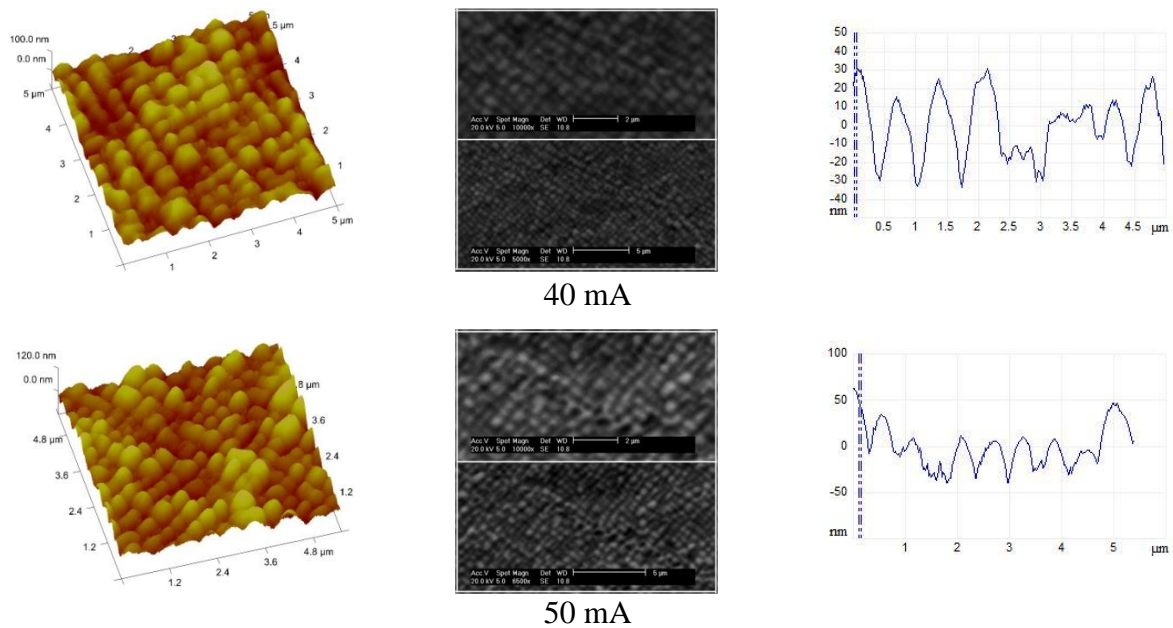


Figure 5.12 : Surface topography (AFM & SEM) of CMSX-4 samples at controlled current of 10 mA, 20 mA, 30 mA, 40 mA and 50 mA

5.3 Surface roughness of electropolished CMSX-4

A combination of local imperfection such as surface roughness, waviness, form and flaws constitute the surface texture which is a key consideration / factor for proper function and reliability of engineering components (end products). Surface roughness is a high frequency and short wavelength component of surface texture and determines the interaction of the object with its environment. The evaluation of surface roughness is of key importance for many fundamental problems like friction, contact deformation, tightness of contact joints, corrosion and the performance of the mechanical components as these irregularities may form nucleation sites for crack or corrosion.

There are different parameters for the judgement of surface roughness depending on the application of the component/s and they are mainly divided into three groups (i) Amplitude parameters – measure vertical characteristics of surface imperfections (ii) Spacing parameters – measures horizontal characteristics of surface deviations (iii) Hybrid parameters – combination of amplitude and spacing parameters. The detail description of these parameters is given in **chapter 4 (section 4.3.1)**.

Surface roughness measurements were conducted on second generation single crystal nickel based superalloy electropolished in section 5.2 in ethaline containing oxalic acid (3% W/V) using digital holographic microscope (DHM) and atomic force microscope

(AFM) in tapping mode. The 3-D surface roughness measurements were carried out on the sections of $40\ \mu\text{m} \times 40\ \mu\text{m}$ and $80\ \mu\text{m} \times 80\ \mu\text{m}$ of AFM and DHM images respectively. The values of surface roughness parameters reported are the arithmetic average of images obtained at two different places.

5.3.1 Surface roughness of potentiostatically electropolished CMSX-4

The AFM and DHM topographic images of unpolished and electropolished surfaces are presented in Figure 5. 13. Figure 5.14 (a) shows the 2-D surface roughness profiles of the electropolished samples while Figure 5.14 (b & c) present the S_a and S_q values as a function of electropolished voltage obtained by AFM and DHM using Nanoscope version 6.13 and Koala version 4 softwares respectively for potentiostatically electropolished samples.

S_a is the arithmetic average height obtained by the average of absolute deviation of the surface from the mean line while S_q represents the standard deviation of the distribution of surface heights. S_{pm} and S_{vm} are mean height of peaks and mean depth of valleys over the measured surface area respectively. S_z is known as the ten point height and is the sum of the average of the five highest peaks and five deepest valleys. Skewness is the measure of symmetry of the profile i.e either more peaks or valleys in the profile and kurtosis define the sharpness of the probability of distribution. The values of roughness parameters of the potentiostatically electropolished samples are tabulated in **Table 5.3**.

The surface roughness values of sample electropolished at 3V had markedly increased which may be attributed to the localized non-uniform dissolution. The lowest S_a and S_q values were obtained for samples electropolished at 6V due to the disappearance of raised gamma phase and levelling of the gamma prime phase. The samples electropolished at 7V, 9V and 11V had S_a and S_q values slightly less than the unpolished surface with the same waffle like surface morphology with slightly less raised gamma phase as compared to the unpolished surface. The surface roughness measurements are in accordance with the observations in the previous sections.

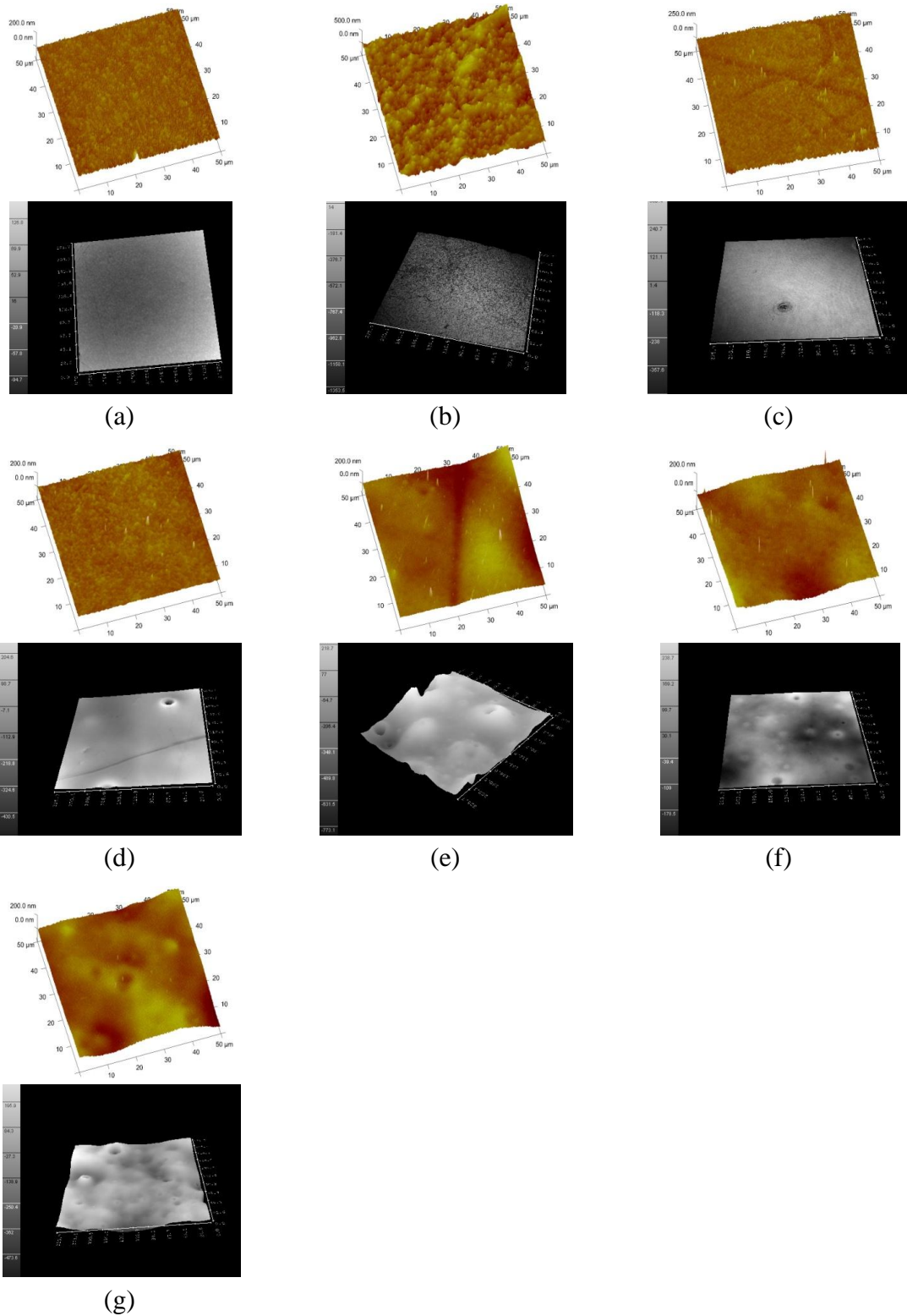
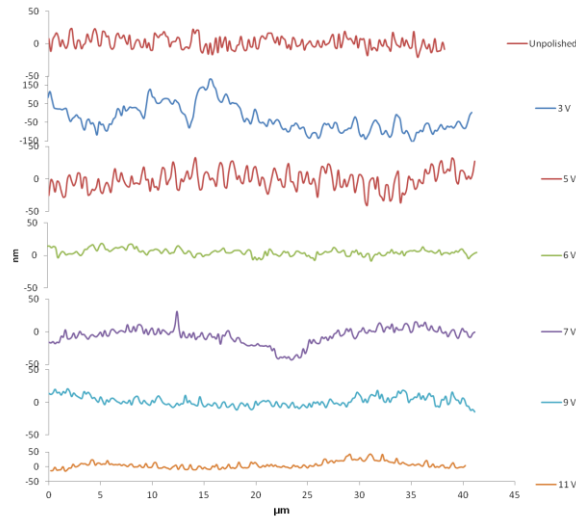
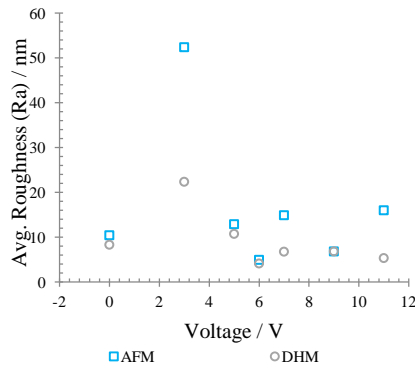


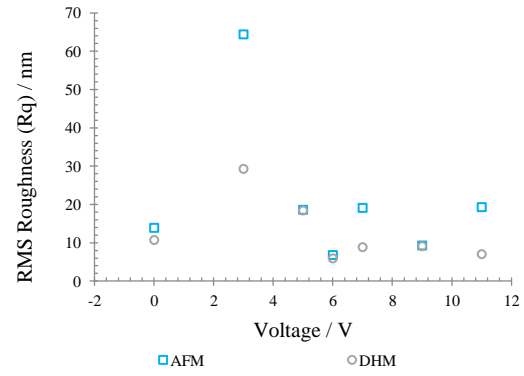
Figure 5.13 : *AFM and DHM Phase images showing surface morphologies of potentiostatically electropolished samples of CMSX-4 at (a) unpolished, (b) 3 V, (c) 5 V, (d) 6 V, (e) 7 V, (f) 9 V and (g) 11 V respectively.*



(a)



(b)



(c)

Figure 5.14 : (a) 2-D surface roughness profiles (b & c) 3-D surface roughness parameters (S_a & S_q) obtained from images presented in **Figure 5.11**.

| Table 5.3 : | | <i>Surface roughness parameters of CMSX-4 for samples electropolished at controlled potential.</i> | | | | | | | |
|--|-------|--|-------|--------|--|--------|----------|----------|----------|
| Voltage (V) | S_q | S_a | S_z | S_p | S_{pm} | S_v | S_{vm} | S_{sk} | S_{Ku} |
| 0 | 13.90 | 10.43 | 27.90 | 188.13 | 11.33 | -72.83 | -13.27 | 2.12 | 50.33 |
| 3 | 64.4 | 52.4 | 130 | 291 | 55.8 | -191 | -56.1 | 0.278 | 2.86 |
| 5 | 18.6 | 12.9 | 35.9 | 407 | 16.2 | -60 | -14.4 | 4.14 | 65.5 |
| 6 | 6.8 | 4.94 | 11.2 | 119 | 5.39 | -22.8 | -5.57 | 2.43 | 33.3 |
| 7 | 19.1 | 14.9 | 26.4 | 204 | 9.59 | -57 | -8.82 | 0.408 | 5 |
| 9 | 9.28 | 6.82 | 13.7 | 214 | 6.38 | -37.7 | -4.71 | 0.66 | 21 |
| 11 | 19.3 | 16 | 22.2 | 105 | 9.21 | -59.2 | -10.1 | -0.015 | 2.4 |
| S_a = Average roughness | | S_q = Root mean square roughness | | | S_p = Maximum height of peak | | | | |
| S_{pm} = Mean maximum height of peak | | S_v = Maximum depth of valley | | | S_{vm} = Mean maximum depth of valleys | | | | |
| S_{sk} = Skewness | | S_{ku} = Kurtosis | | | | | | | |

5.3.2 Surface roughness of galvanostatically electropolished CMSX-4

Figure 5.15 & **Figure 5.16** shows the topographical images of electropolished samples and the surface roughness profile and average roughness (S_a & S_q) plotted as a function of electropolishing current densities respectively. The surface roughness parameters S_z , S_{pm} , S_{vm} , S_{sku} and S_{kur} for the samples of **Figure 5.15** are tabulated in **Table 5.4**.

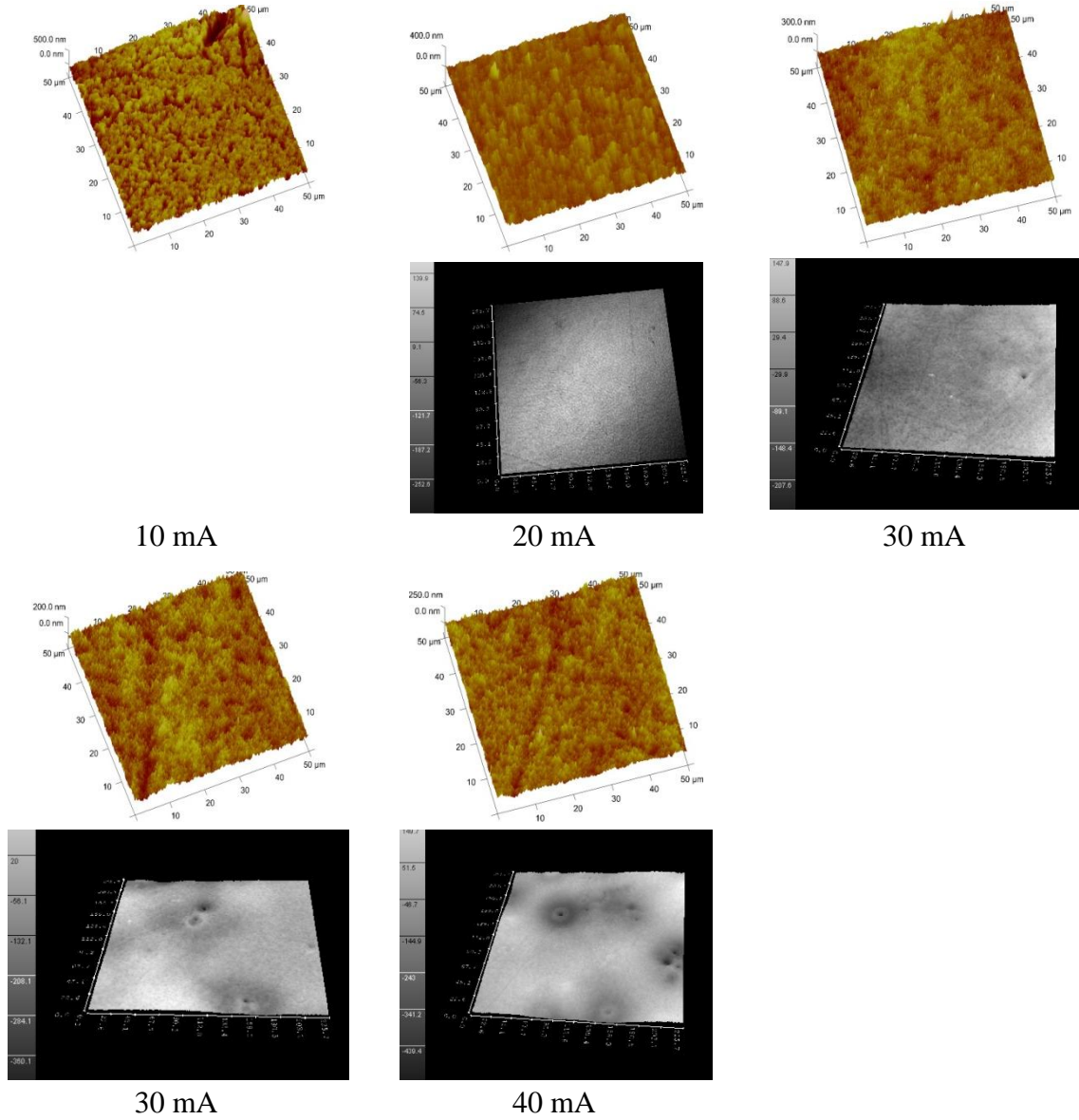


Figure 5.15 : Surface texture of CMSX-4 samples electropolished at constant current density (10, 20, 30, 40 and 50 mA-cm⁻²) AFM and DHM phase images. The DHM image for sample electropolished at 10 mA - cm⁻² is missing due to its dull appearance.

A close inspection of the surface roughness parameters in **Table 5.4** shows an increase in surface roughness of the samples electropolished at controlled current. The very high S_a and S_q values of samples electropolished at 10 mA cm⁻² may be attributed to non uniform

electropolishing due to low current density resulting in pitting. The larger surface roughness values of samples electropolished at 20, 30, 40 and 50 mA cm⁻² are due to the preferential dissolution of gamma phase which results in trenches which grow deeper with increasing current density. The trend in S_{vm} and S_{sk} values with increasing current densities are according to observations in the previous section.

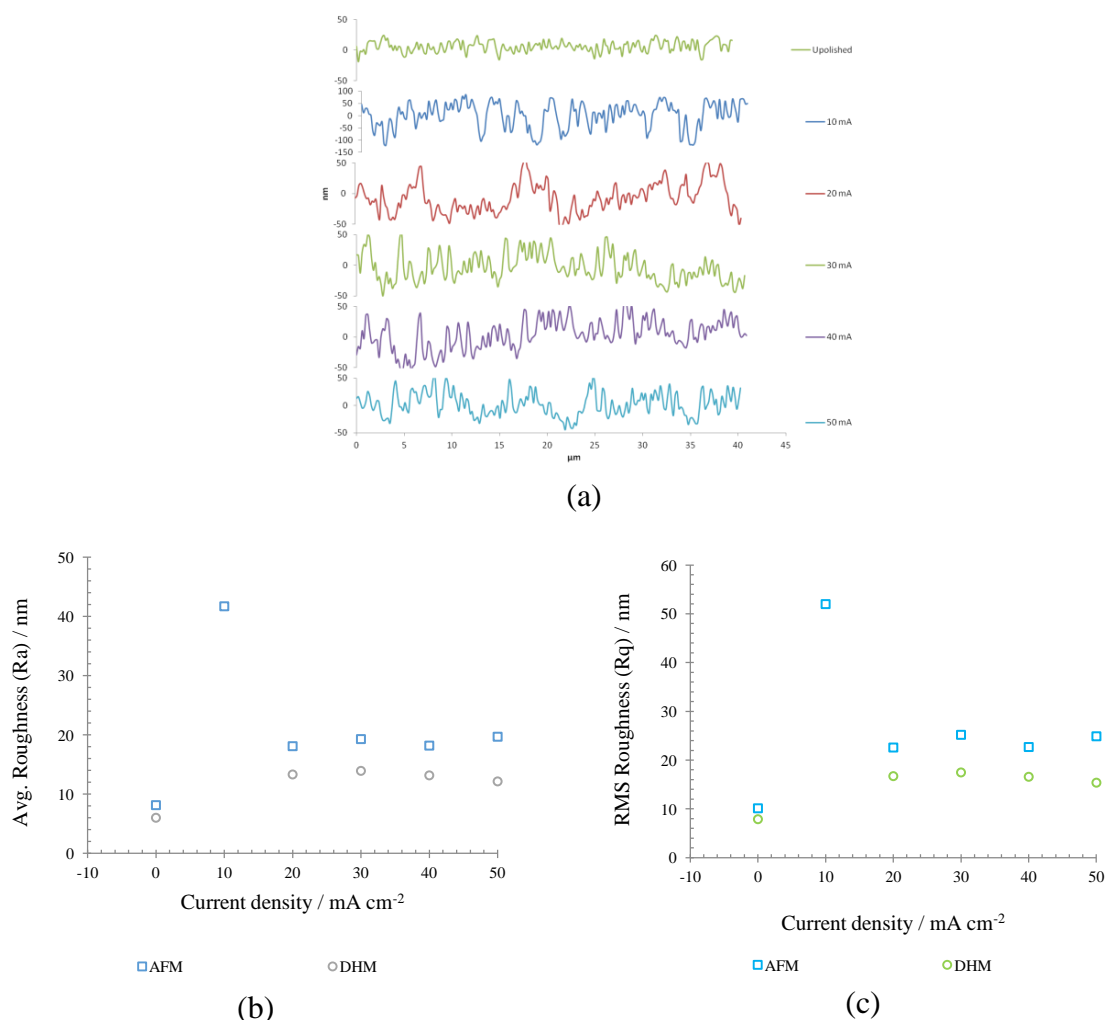


Figure 5.16 : (a) 2D surface roughness profiles (b & c) S_a & S_q values plotted against current densities of CMSX-4 samples galvanostatically electropolished at 10, 20, 30, 40 and 50 mA cm⁻².

5.4 Material etch rate

The material removed during electropolishing depends on a number of factors like liquid formulation i.e. metal ion solubility, electropolishing bath conditions such as temperature, electropolishing time and electrochemical regime like applied potential and current density. In this section, the quantitative estimation of the material etched as a function of

electropolishing time, applied voltage, current density and composition of the electrolyte bath was studied.

| Table 5.4 : | | <i>Surface roughness parameters of CMSX-4 for samples electropolished at controlled current.</i> | | | | | | | |
|---|----------------|--|----------------|---|-----------------|----------------|-----------------|-----------------|-----------------|
| Current density / (mA cm ⁻²) | S _q | S _a | S _z | S _p | S _{pm} | S _v | S _{vm} | S _{sk} | S _{Ku} |
| 0 | 10.14 | 8.16 | 20.63 | 79.67 | 9.60 | -38.23 | -9.08 | 0.16 | 3.52 |
| 10 | 52 | 41.7 | 94.8 | 106 | 43.3 | -192 | -51 | -0.793 | 3.05 |
| 20 | 22.6 | 18.1 | 39.2 | 101 | 19.8 | -67.6 | -16.8 | 0.365 | 2.99 |
| 30 | 25.2 | 19.3 | 49.3 | 386 | 21.7 | -117 | -17.8 | 0.828 | 10.5 |
| 40 | 22.7 | 18.2 | 50 | 98.4 | 18.4 | -79.9 | -18.8 | 0.212 | 2.9 |
| 50 | 24.9 | 19.7 | 52 | 204 | 20.9 | -78.7 | -19.5 | 0.334 | 3.76 |
| S _a = Average roughness | | S _q = Root mean square roughness | | S _p = Maximum height of peak | | | | | |
| S _{pm} = Mean maximum height of peak | | S _v = Maximum depth of valley | | S _{vm} = Mean maximum depth of valleys | | | | | |
| S _{sk} = Skewness | | S _{ku} = Kurtosis | | | | | | | |

5.4.1 Extended time scale electropolishing

The capacity for metal ion solubility in choline based electrolyte ethanline was studied by performing the long time scale electropolishing of nickel based superalloy CMSX-10N for 16 hours at a controlled current of 200 mA. The experiment was performed in 500 ml 1:2 ChCl:EG using a two electrodes assembly (carbon mesh as counter electrode) with CMSX-10N blade piece as anode. The CMSX-10N blade piece was degreased in degreasing solution composed of soap and organic solvent before starting the polishing. The experiments were stopped after every hour and the anode was taken out, washed with water, air dried and weighed. The same piece was further electropolished in the same solution without degreasing and every time the solution was stirred for five minutes prior to the start of the new experiment. **Figure 5.17 (a)** shows the unpolished and electropolished blade piece, the unpolished piece has a dull and rough appearance and scale marks from the casting mould while the electropolished piece has a bright, smooth and shining appearance with no scale marks on its surface. **Figure 5.17 (b)** shows the cross section of unpolished and polished surfaces, the amount of surface etched is 1.10 mm and 0.553 mm from thick reverse and front thin side respectively.

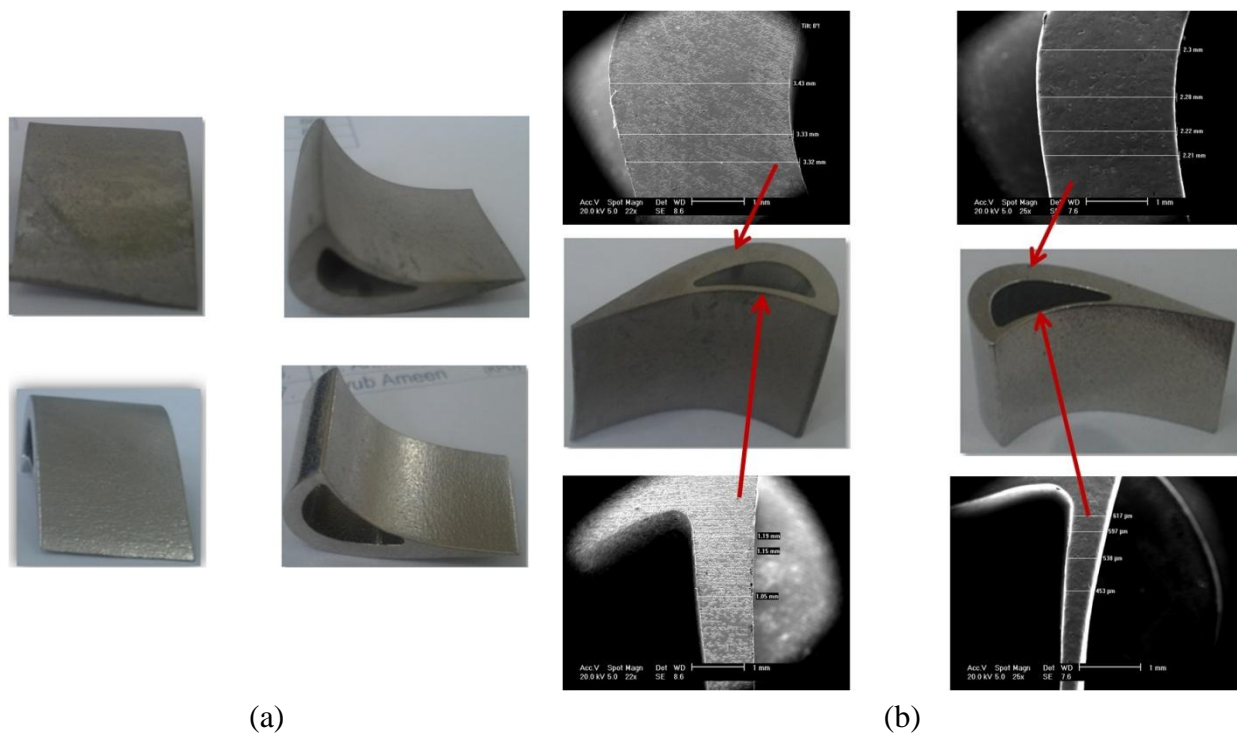


Figure 5.17 : (a) Piece of CMSX-10N blade; (top) unpolished (bottom) electropolished at 6 V for 16 hours (b) SEM images of cross section of piece in (a)

The ethaline solution turns green from colorless due to NiCl_2 . **Figure 5.18 (c)** shows the variation of potential as a function of the electropolishing time, the voltage increases from 5.50 V to 7.10 V during the course of the experiment. This increase in potential may be attributed to the increase in resistance of the mobility (diffusion) of the dissolving ions from the vicinity of dissolving metal to the bulk of electrolyte as a result of increase in the concentration of the metal ions in the solution. The weight loss for galvanostatic extended time scale electropolishing is plotted against time and charge passed and is found to be the linear function of time and charge passed (**Figure 5.18 (a & b)**). This shows that the choline based electrolyte has a good polishing capacity for an extended time.

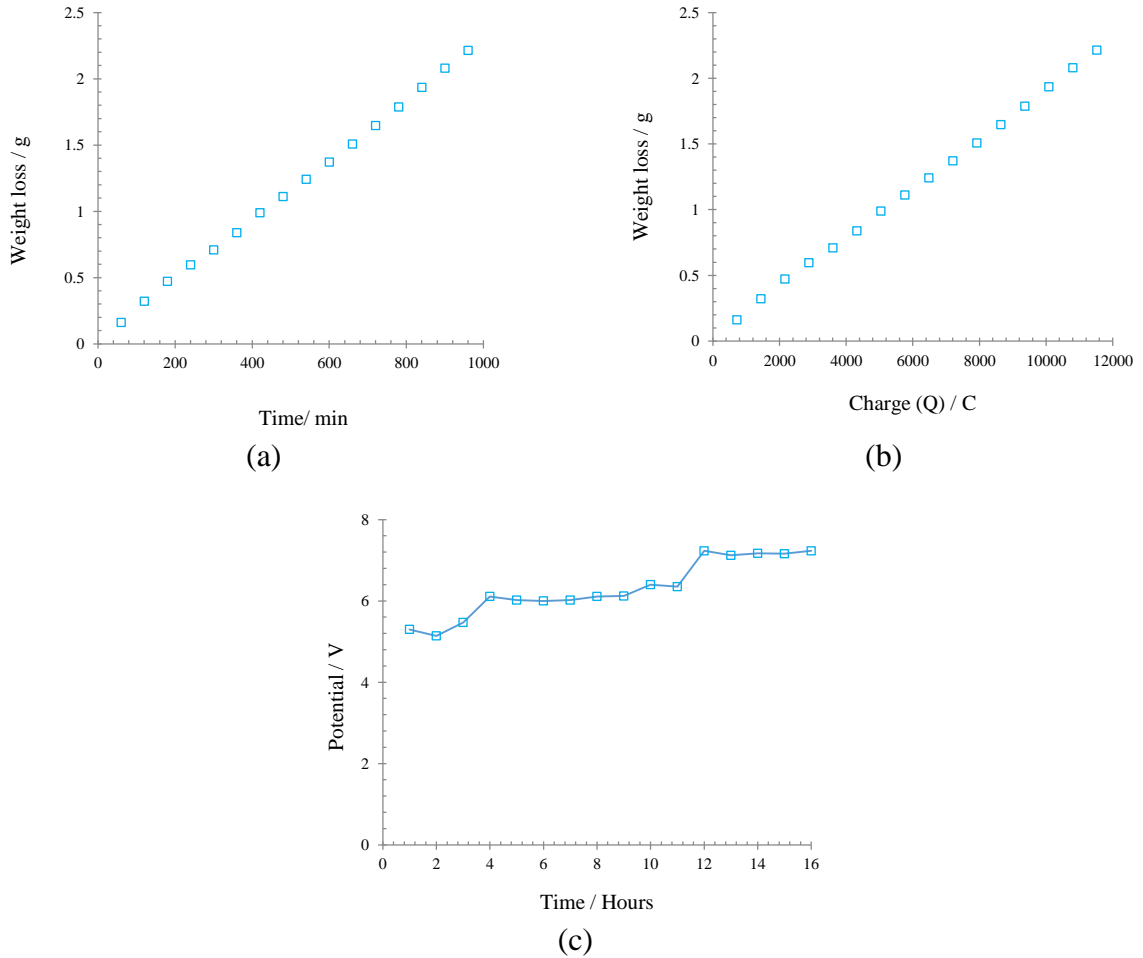


Figure 5.18 : *Plot of weight loss of nickel based superalloy as a function of (a) electropolishing time (b) charge passed for extended time scale electropolishing experiment (c) variation of potential as a function of electropolishing time*

5.4.2 Anodic dissolution rate

The anodic dissolution rate for electropolished samples in section 5.2 was determined as a function of applied potential and current density from the step height at the interface of electropolished and unpolished surfaces. The etch depth was determined by surface profiling techniques namely atomic force microscope (AFM) and digital holographic microscope (DHM). **Figure 5.19 & Figure 5.20** show the SEM and AFM images at the interface of unpolished and electropolished surfaces both at controlled potential and current respectively.

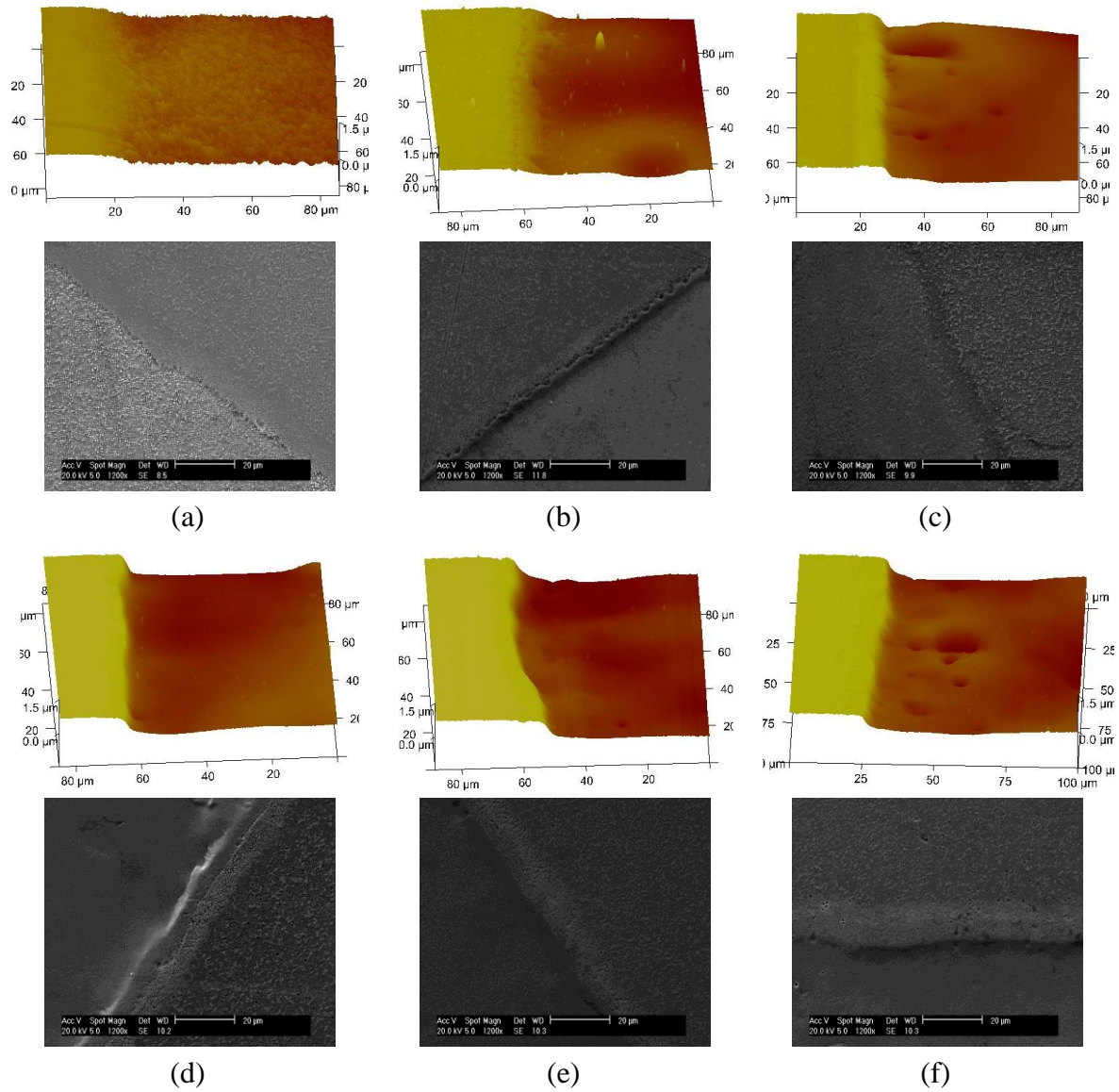


Figure 5.19 : *Atomic force microscope (AFM) and scanning electron microscope (SEM) topographic images across polished and unpolished surface of potentiostatically electropolished samples at (a) 3 V, (b) 5 V, (c) 6 V, (d) 7 V, (e) 9 V, (f) 11 V.*

2-D profiles of the images in **Figure 5.19** and **Figure 5.20** across the masked surface obtained from AFM images (80 μm x 80 μm) are shown in **Figure 5.21 (a & b)**. The amount of material dissolved was calculated using the volume-density-mass relationship **equation 5.1** and the etch volume is calculated from the mean etch depth calculated from two AFM and DHM images and electropolished area (0.16 cm²).

$$m = d \times v \quad (5.1)$$

Where 'm' is the mass, 'd' is the density of the material (CMSX-4¹³ = 8.90 g cm⁻³) and 'v' is the etch volume.

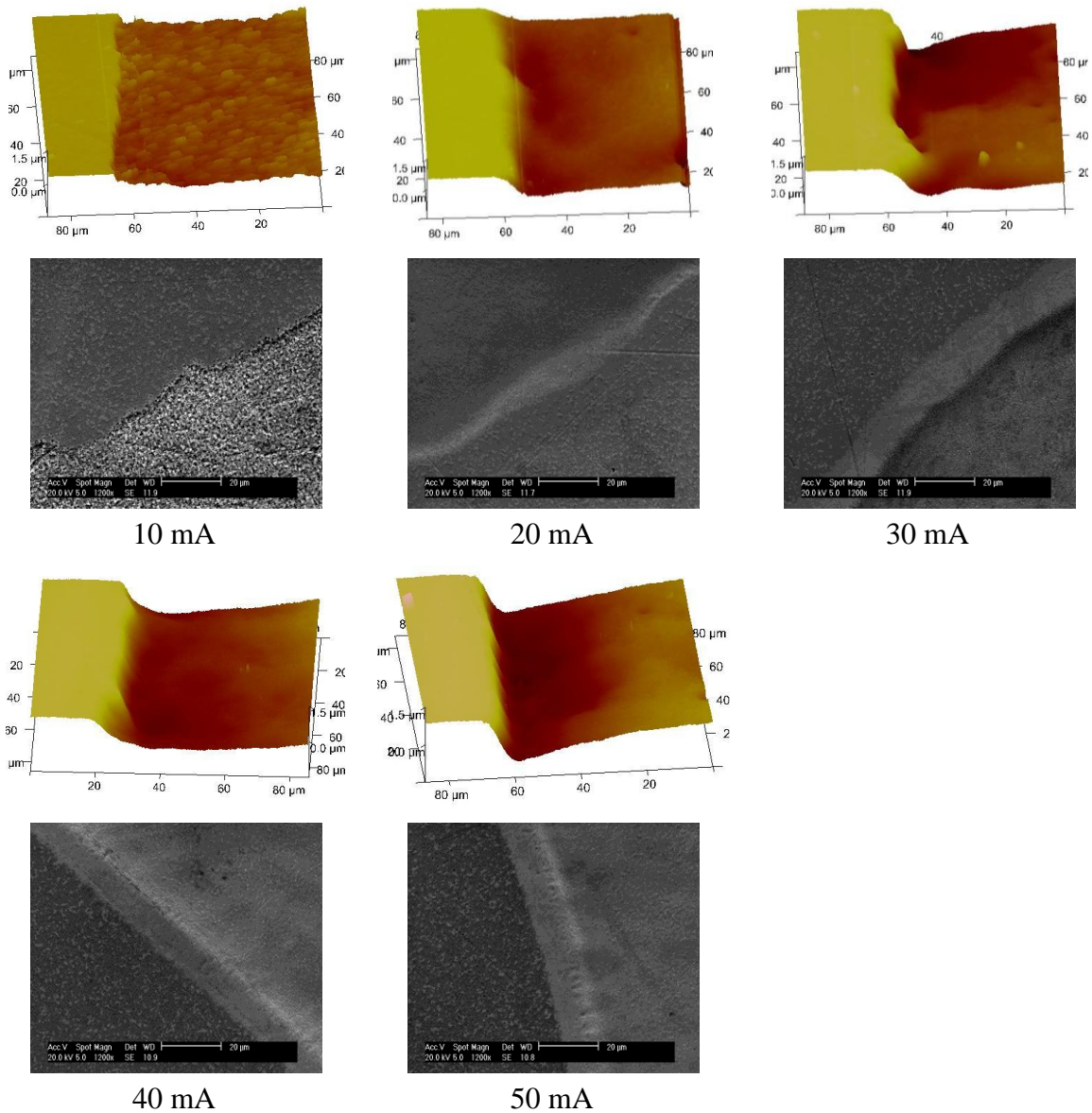


Figure 5.20 : *AFM and SEM topographic images across polished and unpolished surface of galvanostatically electropolished samples at 10, 20, 30, 40 and 50 mA - cm⁻².*

The metal dissolution rate is plotted against applied potential and current density is shown in **Figure 5.21 (e & f)** and is found to be a linear function of applied potential and current density.

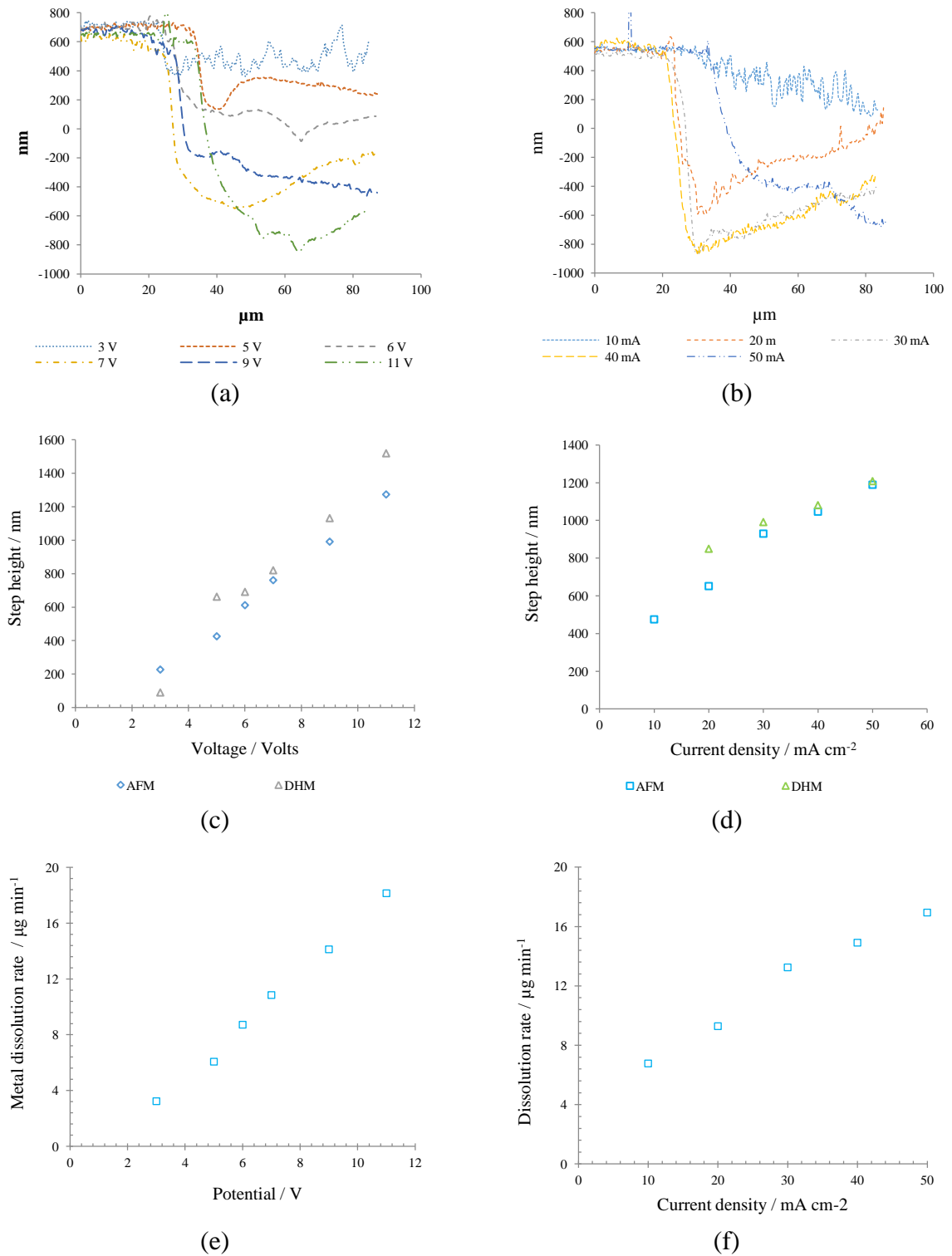


Figure 5.21 : (a & b) 2-D profile of step height across unpolished and polished surface (c & d) Step height as a function of applied potential and current density (e & f) metal dissolution rate as a function of applied potential and current density.

5.5 Surface composition

Ni based alloy samples (1 cm²) were cut from a casting and examined using XPS. XPS data were acquired using the Scienta ESCA300 instrument at the NCESS, Daresbury laboratory UK, a facility using monochromated Al K_α (1486.7 eV) radiation, with a slit width of 0.8 mm and a take off angle of 90°. Samples were subjected to Ar ion etching by filling the sample preparation chamber of the Scienta instrument with Ar gas to a pressure of approximately 2 x 10⁻⁶ torr. The sample was then exposed to the Ar ion beam for a time period of typically several minutes using an accelerator voltage of 5 kV resulting in a beam current of ~200 mA.

One of the samples was examined in the spectrometer with no further sample preparation whilst the other was electropolished in 1:2 ChCl:EG (oxalic acid) for 20 mins at 5.8 V. The XPS spectra were acquired for both samples first as a broad survey spectrum and then at high resolution in the binding energy regions corresponding to Ni(2p) and the refractory metal elements characterizing this alloy, Re, W and Ta (4f).

Apparent from early measurements was the fact that the qualitative appearance of the spectra was strongly dependent on the history of the sample. This is exemplified in **Figure 5.22** which shows the survey spectra for the polished sample initially, (a) as removed from the electrolyte (after rinsing and drying), and then subsequently after 20 mins etch with Ar ion plasma in the instrument, (b), and then after a further 20 mins Ar ion etch (c). Initially the spectrum is very poorly defined and even the principal component of the alloy (Ni) is barely visible above the noise level. After subsequent etching, the metals are exposed and the spectrum becomes very much clearer and well defined. This observation is probably caused by a layer of native oxide that forms immediately after the sample is exposed to air, following electropolishing. The layer of oxide is, apparently, sufficient to block photo-electrons from the metal substrate resulting in very low signal levels. The fact that the appearance of subsequent spectra, after Ar ion etch, changes with etch time which makes it very difficult to interpret quantitative evaluations (integrals) of signal intensity because the extent of etch time is subjective.

As a consequence of the observation (above) there is little value in integral comparisons of the Ni and refractory metal regions before and after electropolishing. On the other hand qualitative comparison of Ni(2p) **Figure 5.23 (a)** and refractory metal regions (4f) **Figure 5.23 (b)** of unpolished and polished samples (under the same experimental

conditions and with otherwise identical histories) show clearly that the signal intensity is increased after electropolishing. This is almost certainly the result of two factors; (i) electropolishing reduces the level of residual surface oxide on the casting, (ii) electropolishing reduces surface roughness. Both of these factors will result in higher photoelectron yield (more signal) in the electropolished samples.

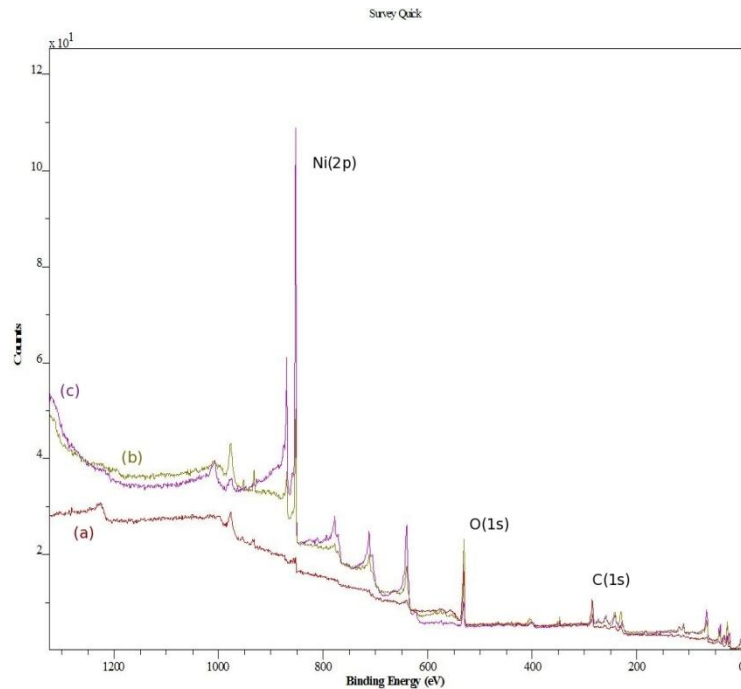


Figure 5.22 : XPS spectra of electropolished samples of Ni based superalloys of casting blade obtained by (a) without etching with Ar ion plasma (b) after etching for 20 minutes with Ar ion plasma (c) after etching for 40 minutes with Ar ion plasma.

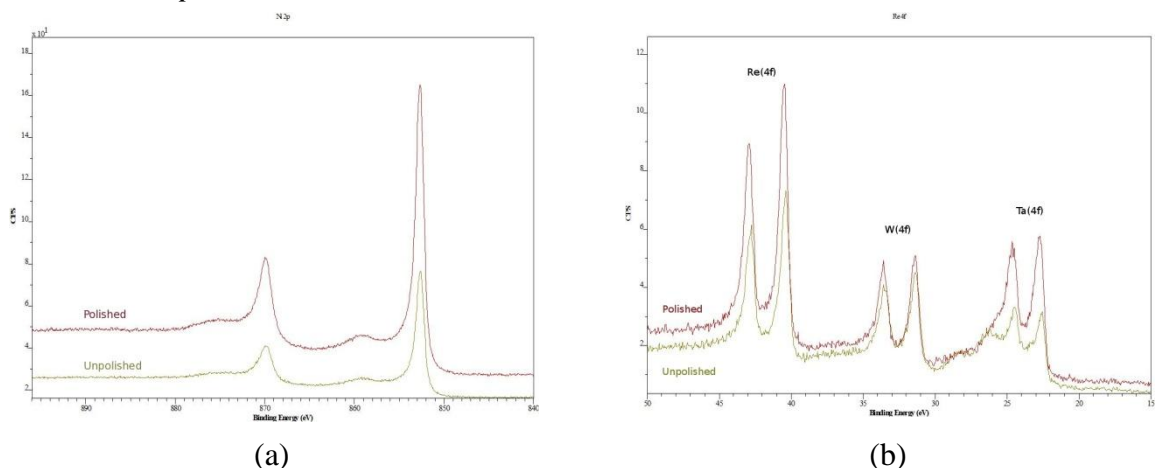


Figure 5.23 : Comparison of XPS spectra of unpolished and electropolished samples (1 cm^2) of Ni based alloys cut from the casting blade (a) expanded in the Ni(2p) region (b) expanded in the refractory metals region.

5.6 Summary

Nickel based superalloys are used extensively to accommodate the ever higher temperature in the high efficiency turbine engine. These components are produced as castings from ingot or powder metallurgy preforms and may be equiaxed or columnar grained or may be single crystal. The differential thermal contraction during solidification process may result in separation of some mould metals that form the oxide layer on the surface known as casting scales. These scales are undesirable and must be removed. Electropolishing is the best option to remove them and at the same time the microstructure of nickel based superalloy is important to withstand the drastic conditions like high temperature and stress. The electropolishing of second generation single crystal nickel based superalloy CMSX-4 in choline chloride based deep eutectic solvent was conducted to study its effect on microstructure and surface texture.

The surface morphology of the CMSX-4 electropolished at controlled potential and current was studied using the SEM and AFM. In the case of potentiostatic electropolishing, the dissolution was found to be a strong function of applied voltage. At low voltage 3 V, 5 V and 6 V the preferential dissolution of gamma phase was observed resulting in deep trenches of gamma phase while at high voltage 7 V, 9 V and 11 V the two phases gamma and gamma prime dissolved at a comparative rates preserving the same waffle like surface. In case of controlled current polishing at current densities of 10, 20, 30, 40 and 50 mA cm⁻², the preferential dissolution of gamma phase took place resulting in deep ditches of gamma phase which grew deeper with increasing current density and only some evidence of dissolution of gamma prime phase was observed at 50 mA cm⁻².

The surface roughness measurements of electropolished surfaces was conducted using AFM and DHM and the surface roughness parameters like average roughness (S_a), root mean square roughness (s_q), mean depth of valleys (S_{vm}), mean height of peaks (S_{pm}), Skewness and kurtosis were measured. Surface roughness was found to be the function of the electrochemical regime i.e applied potential and current density. The increase in surface roughness was observed that may be attributed to preferential dissolution of gamma phase at controlled current and low electropolishing potential. The surface roughness at high electropolishing potential 7, 9 and 11 V was comparable with the unpolished surface due to the same waffle appearance.

The capacity of the electropolishing electrolyte based on choline chloride was studied by conducting extended time scale experiments and the material etch rate was determined. The study revealed a good polishing capacity after 16 hours of electropolishing. In the last section, surface composition was studied using XPS.

5.7 References

- (1) Brewster, G.; Dong, H. B.; Green, N. R.; DSouza, N. *Metallurgical and Materials Transactions B* **2008**, *39*, 87-93.
- (2) Pang, H. T.; Dong, H. B.; Beanland, R.; Stone, H. J.; Rae, C. M. F.; Midgley, P. A.; Brewster, G.; DSouza, N. *Metallurgical and Materials Transactions A* **2009**, *40*, 1660-1669.
- (3) Dai, H. J.; Dong, H. B.; DSouza, N.; Gebelin, J. C.; Reed, R. C. *Metallurgical and Materials Transactions A*, **2011**, *42*, 3439-3446.
- (4) Dai, H. J.; DSouza, N.; Dong, H. B. *Metallurgical and Materials Transactions A*, **2011**, *42*, 3430-3438.
- (5) Giamei, A. F.; Anton, D. L. *Metallurgical Transactions A* **1985**, *16*, 1997-2005.
- (6) Brewster, G.; DSouza, N.; Ryder, K. S.; Simmonds, S.; Dong, H. B. *Metallurgical and Materials Transactions A*, **2012**, *43*, 1288-1302.
- (7) Abbott, A. P.; Dsouza, N.; Withey, P.; Ryder, K. S. *Transactions of the Institute of Metal Finishing* **2012**, *90*.
- (8) Simmonds, S.; Souza, N. D.; Ryder, K. S.; Dong, H. *IOP Conference Series: Materials Science and Engineering*, **2011**, *27*, 012038.
- (9) Pollock, T. M.; Tin, S. *Journal of Propulsion and Power Research* **2006**, *22*, 361.
- (10) Vander Voort, G. F. *Metallography Principles and Practice*, ASM International, **1984**.
- (11) Glage, A., *Universita Degli studi di Trento*, **2007**.
- (12) J.K., T.; T, C. *Superalloys, Supercomposites and superceramics*; Academic Press: New York, **1988**.
- (13) Appleton, M., MChem thesis, University of Leicester, **2012**.

| | | |
|--------------------|--|------------|
| Chapter 6 : | Summary and Future Directions | 179 |
| 6.1 | Summary | 180 |
| | <i>6.1.1 Electropolishing of austenitic steel in deep eutectic solvent</i> | 180 |
| | <i>6.1.2 Surface texture of electropolished stainless steel</i> | 181 |
| | <i>6.1.3 Electropolishing of nickel based superalloys</i> | 182 |
| 6.2 | Future Directions | 182 |
| 6.3 | References | 184 |

6.1 Summary

Electropolishing is the economical and the most widely used surface finishing process for stainless steel. It is the controlled dissolution of metal surface (20-40 μm) to optimize the corrosion resistance by reducing the surface roughness and eliminates all micro-cracks and internal crevices. The electropolishing of various grades of stainless steel approximately account for 95% of all metal processed today. The mechanical surface finishing processes using abrasives or cutting distort the metal surface with lots of scratches and strains.

The present electropolishing baths are based on concentrated sulphuric acid and phosphoric acid and viscosity improvers like glycerol. These baths are under tremendous pressure because of their highly corrosive nature, strong negative impact on the environment and poor current efficiency due to the extensive gassing. Over the last 20 years, low temperature molten salts 'ionic liquids' have been gaining considerable interest in electrochemical and synthetic applications¹⁻⁴ due to their unique electrochemical properties but the research is at its infancy and is a subject of considerable investigation.

In the present thesis, electropolishing of 300 series stainless steel (ss316 and ss304) was carried out to gain insight into the mechanism of electropolishing in choline chloride and hydrogen bond donor deep eutectic solvents. A systemic study of electropolishing of stainless steel was conducted to develop understanding of the mechanism and optimization of electropolishing process on the following lines

- Process optimization using electrochemical techniques and experimental design strategies.
- Life cycle studies to define and quantify the process control and management parameters including recycling and reuse.
- Surface texture measurements of electropolished surface using microscopic techniques; atomic force microscope (AFM), scanning electron microscope (SEM) and digital holographic microscope (DHM)

6.1.1 Electropolishing of autenitic steel in deep eutectic solvents

The physical properties of 1:2 ChCl:EG like viscosity, surface tension and conductivity showed the strong dependence on temperature and large value of surface entropy is the indicative of high level of surface organization attributed to the strong hydrogen bonding. Life cycle study of 1:2 ChCl:EG at 40 °C at controlled potential and current for extended

time scale of 16 hours indicated that electrolyte history has no effect on the quality of electropolishing and recycled liquid behaved like the virgin liquid.

Electrochemical techniques linear sweep anodizing curves, potentiostatic and galvanostatic revealed that the electropolishing of stainless steel in 1:2 ChCl:EG take place through the formation of thick viscous liquid film on the substrate surface and the anodizing curve had four distinct regions namely active dissolution, passivation, diffusion limited and pitting regions similar to the electropolishing in inorganic acid solution. Fractional factorial design (FFD) coupled with response surface methodology (RMD) and the path of steepest ascent showed that electropolishing variables like concentration of water, oxalic acid, electropolishing temperature, time and potential had the positive effect on the response variable 'surface roughness' i.e. optimal setting for minimum value.

6.1.2 Surface texture of electropolished stainless steel

Electropolishing influence the stability of the surface passive oxide layer and hence changing the surface energy by providing the hydrophilicity to material and surface potential by preventing the release of electrons. Micrographs of over layer of electropolished ss316 obtained by Atomic force microscope and field emission scanning electron microscope revealed the granular surface morphology composed of nanoscaled hemispherical grains and contained some pores which developed with the electropolishing time.

Effect of electropolishing on surface roughness of stainless steel was studied using the atomic force microscope (AFM) and digital holographic microscope (DHM). Normalised values of average surface roughness (S_a) and mean square root roughness (S_q) were used to avoid the effect of method and instrument used for measurements and was found to be the strong function of electropolishing time. The surface roughness values obtained by AFM and DHM agrees well with each other, therefore DHM can be used to measure surface roughness which offer fast, non-destructive and non-contact mode of measurement in contrast to using the scanning probe microscope or profilometer techniques that suffer from limitations such as slow scan rate, precise control of the movement of tip or sometimes smearing of surface due to moving tip.

The corrosion behaviour of electropolished stainless steel was studied in tap water, sulphate and chloride environments. Open circuit potential measurements and potentiodynamic polarization curves revealed the better corrosion resistance of

electropolished stainless steel and passivation efficiency increased about 70-80% after electropolishing for 30 minutes in 1:2 ChCl:EG containing oxalic acid as an additive.

6.1.3 Electropolishing of nickel based superalloys

Superalloys are developed to withstand the challenging and harsh environment such as high temperature, high stress, extreme corrosive and oxidation conditions. Nickel based single crystal second generation superalloy CMSX-4 is used aerospace turbine blades. During casting some of the mould's metals segregate and form the oxide layer on the surface known as scales. The electropolishing of CMSX-4 was conducted to remove the scales both at constant potential and current.

Micrographs obtained by Atomic force microscope and scanning electron microscope revealed the waffle like morphology consisting of cuboid gamma prime phase and matrix of gamma phase. The dissolution of these phases was found to be the function of applied potential. At low potential (3 V, 5 V 6V) the gamma phase dissolved preferentially resulting in deep ditches while at higher potentials (7 V, 9 V and 11 V) both the phases dissolved at comparative rates and retaining the same waffle appearance of unpolished surface. At controlled current densities the dissolution of gamma phase was observed.

Surface roughness parameters average surface roughness (Sa), mean square root roughness (Sq), mean depth of valleys (Svm), mean height of peaks (Spm), skewness and kurtosis were measured using the atomic force microscope and digital holographic microscope. Increase in surface roughness was observed at low applied potential and constant current densities due to preferential dissolution of one phase i.e. gamma phase while at high electropolishing potentials the surface roughness is comparable to unpolished surface with same waffle like appearance. The extended scale electropolishing experiments at constant current revealed the good electropolishing capacity of 1:2ChCl:EG even after the electropolishing of 16 hours.

6.2 Future Directions

The electropolished surface of pure metals and metallic alloys show particular patterns such as stripes and hexagonal networks. The mechanism of the formation of the particular pattern depends on the electropolishing variables and the electrolytes used. Orientation and periodicity of the pattern is dependent on the grains orientation. A preliminary study of the surface overlayer of electropolished workpiece in 1:2ChCl:EG has revealed the nanoscaled

hemispherical grains containing pores. A detailed study of the correlation of the electropolishing variables such as electropolishing temperature, time and composition of electrolyte can be carried out to investigate their effect on the surface morphology.

The amount of material etched in electropolishing was determined by measuring the step height at the interface of electropolished and unpolished surface using the atomic force microscope (AFM) which suffers from the limitation of maximum step height of 8 μm . A different analytical techniques such digital holographic microscope (DHM) and scanning optical microscopy may be used to measure the step height at the boundary for the samples electropolished for longer time periods as these techniques do not use the probe tips. **Figure 6.1** features an image of scanning optical microscopes of a CMSX-4 workpiece electropolished for 30 minutes showing the representation and information available use the scanning optical microscope.

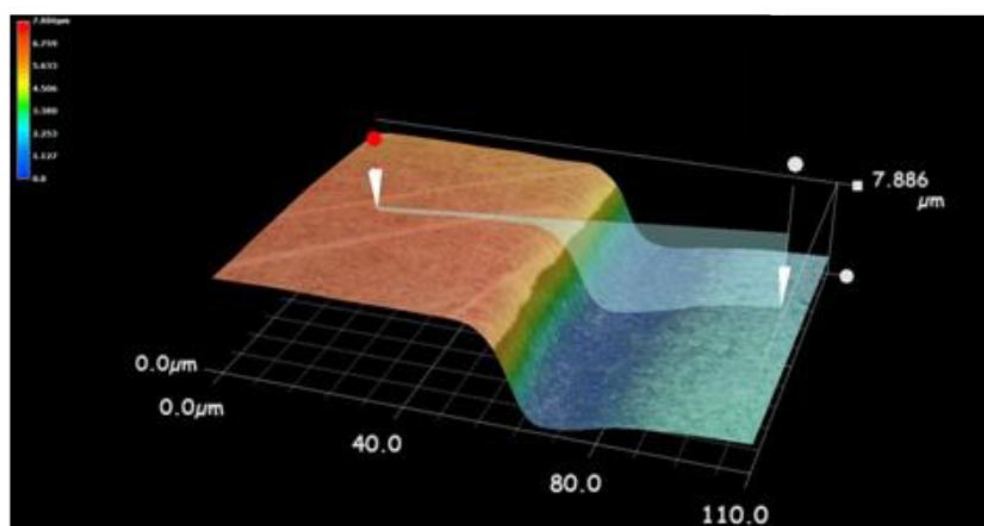


Figure 6.1: An image obtained by optical scanning microscope at the interface of electropolished and unpolished surface⁵.

The spectrum of electropolishing in 1:2 ChCl:EG may also of extended to other metals and alloys. For example aerospace gas turbine also use the titanium alloys in blades in moderate temperature regions. These alloys may be electropolished in high quality as CMSX-4 in deep eutectic solvents.

6.3 References

1. P. Wasserscheid and T. Welton, *Ionic liquid in synthesis*, Wiley VCH, Weinheim, **2003**.
2. P. Wasserscheid and W. Keim, *Angewandte Chemie International Edition*, **2000**, **39**, 3772-3789.
3. F. Endres, *ChemPhysChem*, **2002**, **3**, 144-154.
4. H. Ohno, *Electrochemical aspects of ionic liquids*, Hoboken, N.J. : Wiley-Interscience, **2005**.
5. M. Appleton, MChem thesis, University of Leicester, **2012**.